

T  
F191-91  
SIN

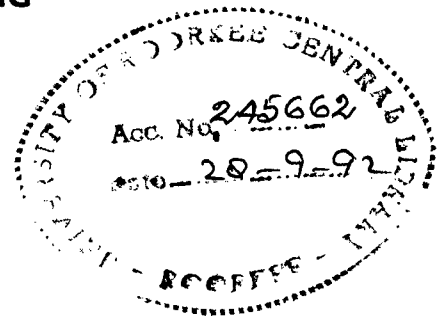
**STUDIES ON THE MICROSTRUCTURE, MECHANICAL  
PROPERTIES AND WEAR BEHAVIOUR OF SQUEEZE CAST  
Al-Al<sub>2</sub>O<sub>3</sub>-MgO PARTICULATE MMCs**

**A THESIS**

submitted in fulfilment of the  
requirements for the award of the degree  
of  
**DOCTOR OF PHILOSOPHY**  
in  
**METALLURGICAL ENGINEERING**

By

**JAGPAL SINGH**



**DEPARTMENT OF METALLURGICAL ENGINEERING  
UNIVERSITY OF ROORKEE  
ROORKEE-247 667 (INDIA)**

**MARCH, 1991**

CANDIDATE'S DECLARATION


I hereby certify that the work which is being presented in the thesis entitled **STUDIES ON THE MICROSTRUCTURE, MECHANICAL PROPERTIES AND WEAR BEHAVIOUR OF SQUEEZE CAST Al-Al<sub>2</sub>O<sub>3</sub>-MgO PARTICULATE MMCs** in fulfilment of the requirement for the award of the Degree of Doctor of Philosophy, submitted in the Department of Metallurgical Engineering of the University is an authentic record of my own work carried out during a period from 16th May, 1986 to 26th March, 1991 under the supervision of Prof. S.K. Goel, Prof. V.N.S. Mathur and Prof. M.L. Kapoor.


The matter embodied in this thesis has not been submitted by me for the award of any other degree.

  
( JAGPAL SINGH )

This is to certify that the above statement made by the candidate is correct to the best of our knowledge.

  
(DR. S.K. GOEL )  
PROFESSOR

Signature of Supervisor(s)  
  
(DR. V.N.S. MATHUR)  
PROFESSOR

  
(DR. M.L. KAPOOR)  
PROFESSOR AND HEAD

Department of Metallurgical Engineering  
University of Roorkee  
Roorkee - 247 667 (INDIA)

The Ph.D. viva-voce examination of Sri JAGPAL SINGH, Research Scholar has been held on.....

Signature of Guide(s)

Signature of External Examiners

(Prof.S.K.Goel) (Prof.V.N.S.Mathur)

(Prof. M.L. Kapoor)

**ACKNOWLEDGEMENT**

I wish to express my deep sense of gratitude and appreciation of my thesis Supervisors Dr. S.K. Goel, Dr. V.N.S. Mathur and Dr. M.L. Kapoor for their painstaking efforts, support and guidance during the course of present investigation. But for their constant encouragement throughout the course of present investigation and at difficult times particularly, the present work would have not been possible.

My sincere and grateful thanks are also due to Professor M.L. Kapoor, present Head of the Deptt. and to Prof. D.B. Goel and Prof. A.K. Patwardhan, the previous Heads of the Department, for providing laboratory facilities to me during the course of the present investigation.

My special and grateful thanks are due to Professor S.N. Tewari, Prof. & Head, and Professor V.V.P. Kutumba Rao of the Department of Metallurgical Engineering, Institute of Technology, Banaras Hindu University, Varanasi, for providing Instron facilities for carrying out elevated temperature tensile tests of the composites. The hydrogen content of composites was analysed at Mishra Dhatu Nigam Ltd. (MIDHANI), Hyderabad. For this, my most grateful thanks are due to Dr. K.K. Sinha, Managing Director, MIDHANI and to Sri P. Mukherjee, Engineer, S.C. Laboratory of MIDHANI for carrying out the above analysis and for making the results available to me just in time. This was indeed a very timely help and I have really no words to express my gratitude to Dr. Sinha and Sri Mukherjee for this assistance. My grateful

thanks are also due to Sri T. Anil Kumar, M.E. student, for all the trouble he took in contacting HAL and MIDHANI for the hydrogen analysis of my composite samples. My special and very grateful thanks are due to Prof. E.S. Dwarakadasa of the Deptt. of Metallurgy, Indian Institute of Science, Bangalore, for his help in arranging the above analysis of hydrogen content of composite samples. But for his timely help, the above work could not have been possible. Also, I would like to express my sincere thanks to Dr. Kailash Chandra, Director, USIC, University of Roorkee, and Mrs. Rekha Sharma, SLT, for helping me with the SEM study of tensile fracture surfaces and worn surfaces of composite specimens. My special thanks are due to Prof. A.K. Jain and Mrs. Amita, Scientist 'B' for helping me with the analysis of reacted layer around  $Al_2O_3$  particles using JEOL EPMA facility at USIC, University of Roorkee.

I would like to express my sincere thanks to the staff of various laboratories of Metallurgical Engineering Department, especially to S/Sri B.P. Sharma, J.P. Sharma, Raj Kumar Sharma, S.P. Kush, S.K. Seth, S.C. Kaushik, Mam Chand, Balesh Kumar and Vidya for the help rendered at various stages of my experimental work. My special thanks are due to Sri S.K. Seth for helping me with the preparation of numerous photomicrographs. I would like to acknowledge with thanks the assistance rendered by Sri M.C. Vaish in the preparation of neat sketches and many drawings. My special thanks are due to Miss Vijay Laxmi for a neat and flawless typing of the manuscript of my thesis.



I wish to express my gratitude to the authorities of University Grants Commission, Govt. of India, for providing me with financial assistance during the course of this investigation.

Last but not the least, I take this opportunity to express my deep sense of gratitude towards my wife, my relatives & parents and friends who have shown tremendous patience and keen interest in my work and have contributed directly and indirectly towards this achievement.

Dated: 26th March, 1991

  
( JAGPAL SINGH )

## PREFACE

The present thesis comprises of mainly five chapters. Chapter - 1, Introduction, outlines the achievements and problems associated with the fabrication of cast particulate MMCs through the liquid metallurgy route. The major problem of considerable amount of porosity in the cast structure, which seriously deteriorates the performance of composites in tension, has been pin-pointed and emphasized. It has been reasoned in this chapter, as to how the process of squeeze-casting can be a possible means of overcoming this problem satisfactorily. This chapter also details out the entire scope of present investigation.

Chapter - 2 deals mainly with a comprehensive study of different composite systems, role of squeeze casting operation in improving the performance levels of different alloys & composite systems, and, the wear behaviour of aluminium alloys and different composite systems under mainly dry sliding conditions. The objective of this study was to critically examine the findings of other workers and identify the information gaps. This chapter is divided into three major sections. The first section is devoted to a discussion of the characteristics of different composite systems.

In the beginning, the composite systems are classified into different categories and then a major discussion on the Metal Matrix Composites (MMCs) is taken-up. Again in this sub-section, major emphasis is laid on the kinds of cast particulate composites, liquid metallurgy route of their fabrication, and, problems associated with vortex liquid metallurgy route of their preparation

in particular. The second major section deals mainly with the squeeze casting process. In this section are discussed various operating steps, control parameters and the theoretical aspects related with the influence of squeeze pressure on the phase diagrams of different alloy systems. Considerable amount of work done by different workers on the influence of squeeze pressure on the properties of different alloy systems and composites has been critically analysed in this section. The third major section of this chapter is devoted to a study of the fundamental aspects of wear. This section includes a discussion on the types of wear, techniques of measuring wear and an account of recent investigations into the wear behaviour of aluminium alloys and composites. A critical appraisal of various aspects mentioned above finally leads to the formulation of a specific strategy to be followed in the present investigation.

Chapter - 3 deals with various experimental techniques adopted in the present investigation. Starting from the preparation of  $\text{Al}_2\text{O}_3$  and submicron MgO ceramic powders with respect to the dehydroxylation of their surfaces, their blending and the development of 'modified MgO coating technique' is explained. What different parameters are required to be controlled during the creation of vortex and the preparation of the stirred slurry are then explained. Process parameters and their limits are then set out for the gravity chill casting and squeeze casting of the stirred slurry. This chapter details out various techniques employed for the characterisation of cast particulate composites in respect of  $\%V_f$  retention of  $\text{Al}_2\text{O}_3$ , density, mean dendritic arm

spacing, Vicker's hardness and microhardness and tensile property evaluation upto 300°C (573K). This chapter also details out the techniques adopted for evaluation of the wear behaviour of above composites under dry sliding conditions.

Chapter - 4 is devoted to a critical examination of the results of present study. The strategy adopted is that the entire set of results are first divided into three main sections dealing with three specific aspects. The first section deals with the preparation and initial characterisation of gravity chill cast and squeezed Al-Al<sub>2</sub>O<sub>3</sub>-MgO and Al-MgO particulate composites. The second section deals with the mechanical property evaluation of above composites upto 300°C (573K). This section also deals with a detailed SEM examination of the tensile fracture surfaces of different composites. This study was undertaken with a specific objective of establishing the nature and mode of fracture in case of gravity chill cast and squeezed Al-Al<sub>2</sub>O<sub>3</sub>-MgO particulate composites. The third major section of this chapter is devoted to a study of the wear behaviour of above composites under dry sliding conditions. The major objective of this study was to ascertain as to how the squeeze pressure influences the wear behaviour of Al-Al<sub>2</sub>O<sub>3</sub>-MgO particulate MMCs. The common strategy adopted in this chapter is that the results are presented first and summarised and then these results are discussed also in the same sub-section. Like this, the entire set of results are fully compartmentalised.

In chapter - 5, the conclusions arising from the above investigation are listed systematically. The later part of this

chapter is devoted to a listing of suggestions for future studies.

In the Appendix, some Xerox copies of research publications emanating from the present investigation are presented.

List of research papers emanating from present thesis  
(Published and accepted for publication)

by

Jagpal Singh, S.K. Goel, V.N.S. Mathur and M.L. Kapoor

1. "Initial Experiences with squeeze casting of Al-Al<sub>2</sub>O<sub>3</sub>-MgO Particulate Composites prepared by Modified MgO Coating Technique", Proc. Seminar on "Science and Technology of Composites, Adhesives and Sealants", Sept. 28-30, 1989, Bangalore (India), pp. 439-447.
2. "Studies on the behaviour of Squeeze-Cast Al-Al<sub>2</sub>O<sub>3</sub>-MgO Particulate Composites Prepared by Modified MgO Coating Technique", ASM International Conference on "Advances in Composite Materials", Jan. 15-18, 1990, Bombay (India) (In Press).
3. "Role of Squeeze Casting Technique in Achieving Improved Property Performance Levels of Al-Al<sub>2</sub>O<sub>3</sub>-MgO Cast Particulate Composites", 94th Casting Congress, AFS, April 21-24, 1990, Detroit, MI, USA. AFS Transactions, 98, (1990), 115-122.
4. "Elevated Temperature Tensile Properties of Squeeze Cast Al-Al<sub>2</sub>O<sub>3</sub>-MgO Particulate MMCs upto 573 K", Journal of Material Science, U.K. (1990). (Accepted)
5. "Optical and SEM Observations of Porosity in Gravity and Squeeze Cast Al-Al<sub>2</sub>O<sub>3</sub>-MgO Particulate Composites", Indian Foundry Journal Vol. XXXVI, No.12, Dec. 1990, 17-23. This paper was also presented in National Seminar on "Alloy Design and Development", March 10-11, 1989, Roorkee (India).

6. "Mechanical Property Evaluation of Al-Al<sub>2</sub>O<sub>3</sub>-MgO Particulate MMCs upto 300 C (573 K) Solidified under Pressure between 80 and 140 MPa" Int. Conf. on Aluminium (INCAL-91), Bangalore, (India), Feb. 6-8, (1991). (Accepted)
7. "Development & Characterisation of high quality Al-Al<sub>2</sub>O<sub>3</sub>-MgO Squeeze Cast Particulate MMCs for Elevated Temperature Application upto 573 K", the First Metallurgical Symposium of Iran, (F-MSI), Shahid Chamran University, Ahuag, Iran, March 5-15, (1991). (Accepted)
8. "Adhesive Wear Behaviour of Squeeze Cast Al-Al<sub>2</sub>O<sub>3</sub>-MgO Particulate MMCs under Dry Sliding Conditions", AFS Casting Congress - 1991, May 5-9, 1991, Birmingham, AL, USA. (Accepted)

## LIST OF ABBREVIATIONS

- $\%V_f$  - Percent volume fraction of  $Al_2O_3$  particles retained in the matrix.
- G - Temperature gradient.
- m - Slope of eutectic liquidus line.
- $C_o$  - Concentration of impurity atom.
- h - Partition coefficient
- $\lambda$  - Mean free matrix path
- $D_p$  - Interparticle separation
- $V_p$  - Volume concentration of particles
- Gm - Matrix shear modulus
- b - Burger's Vector
- $\tau_i$  - Stress required to bow the dislocation about the dispersion
- $\sigma$  - Yield strength
- $\gamma_{sv}$  - Interfacial force acting between solid-vapour
- $\gamma_{sl}$  - Interfacial force acting between solid-liquid
- $\gamma_{lv}$  - Interfacial force acting between liquid-vapour
- $\theta$  - Contact angle
- $W_{sl}$  - Work of adhesion of a solid to a liquid
- $W_{ss}$  - Work of adhesion at the interface when the system has cooled
- $f(\Delta\alpha)$  - A function dependent upon the difference between thermal expansion coefficient of matrix and reinforcing materials
- $\beta_{so}$  - Equilibrium spreading pressure of the vapour on the solid surface.
- p - Vapour pressure
- $\epsilon_v$  - Surface concentration of the adsorbed vapour
- $T_m$  - Melting point



- $V_2$  - Specific volume of liquid phase
- $V_1$  - Specific volume of solid phase
- $\Delta T$  - Rise in the melting point
- $\Delta P$  - Increase in squeeze pressure
- $N_A$  - Number of particles/mm<sup>2</sup>
- $N_V$  - Number of particles/mm<sup>3</sup>
- $HM_{5gm}$  - Microhardness at 5 gm load
- $HM_{10 gm}$  - Microhardness at 10 gm load
- $HV_5$  - Vicker's hardness at 5 kg load
- $HV_{30}$  - Vicker's hardness at 30 kg load
- Composite No.1 - Gravity chill cast composite
- Composite No.2 - Squeezed composite at 80 MPa and ambient die temperature
- Composite No.3 - Squeezed composite at 140 MPa and ambient die temperature

## LIST OF TABLES

| Table No. | Title   | Page No. |
|-----------|---|----------|
| 2.1       | Representative Metal-matrix Composite Materials. (Ref.7)  | .. 17    |
| 2.2       | Ceramic Fibres Available for Squeeze Casting of Aluminium MMC Components. (Ref.7)   | .. 20    |
| 2.3       | Typical Chemical Analysis of Ceramic Fibres. (Ref.7)  | .. 22    |
| 2.4       | Typical Physical Properties of Various Fibres. (Ref.7)  | .. 23    |
| 2.5       | Tensile Data for Squeeze-cast Material Compared with Properties of Chill Casting. (Ref.108)   | .. 93    |
| 2.6       | Squeeze Cast Properties of 356 Aluminium Alloy. (Ref.83)  | .. 97    |
| 2.7       | Comparative Properties of CDA 377 Forging Brass. (Ref.92)   | .. 101   |
| 2.8       | Comparative Properties of CDA 624 Aluminium Bronze. (Ref.92)  | .. 101   |
| 2.9       | Comparison of AISI 1345 and Squeeze Casting Composite Properties. (Ref.7)   | .. 127   |
| 3.1       | Sieve Classification of Al <sub>2</sub> O <sub>3</sub> Powder   | .. 135   |
| 3.2       | Variable Parameters and their Ranges Employed During Wear Experiments.  | .. 164   |
| 4.1       | Characteristics of Composites Prepared by 'Modified MgO Coating' Technique using Varying Amounts of Metallic Mg for Plunging.   | .. 174   |
| 4.2       | Some Characteristics of Gravity Chill Cast and Squeezed Commercially Pure Aluminium and Al-Al <sub>2</sub> O <sub>3</sub> -MgO Particulate Composites.  | .. 192   |
| 4.3       | Point Analysis for %MgO Content at Different Locations of the Composite   | .. 201   |
| 4.4       | Mean Vicker's Hardness (HV <sub>5</sub> ) and Mean Microhardness (HM <sub>5gm</sub> ) of Gravity Chill Cast and Squeezed Commercially Pure Aluminium and Al-Al <sub>2</sub> O <sub>3</sub> -MgO Particulate Composites. | .. 206   |

| Table No. | Title  | Page No. |
|-----------|--|----------|
| 4.5       | Characterisation of Al-MgO Composites Prepared with and Without Mg Plunging.   | .. 211   |
| 4.6       | Tensile Properties of Gravity Chill Cast and Squeezed Commercially Pure Aluminium and Al-Al <sub>2</sub> O <sub>3</sub> -MgO Particulate Composites at Ambient Test Temperature. | .. 217   |
| 4.7       | Tensile Properties of Gravity Chill Cast and Squeezed Commercially Pure Aluminium and Al-Al <sub>2</sub> O <sub>3</sub> -MgO Particulate Composites at 100°C Test Temperature.   | .. 225   |
| 4.8       | Tensile Properties of Gravity Chill Cast and Squeezed Commercially Pure Aluminium and Al-Al <sub>2</sub> O <sub>3</sub> -MgO Particulate Composites at 200°C Test Temperature.   | .. 226   |
| 4.9       | Tensile Properties of Gravity Chill Cast and Squeezed Commercially Pure Aluminium and Al-Al <sub>2</sub> O <sub>3</sub> -MgO Particulate Composites at 300°C Test Temperature.   | .. 227   |
| 4.10      | Wear Data of Composite Nos. 1,2 and 3.   | .. 255   |

## LIST OF FIGURES

| Fig.No. | Title   | Page No. |
|---------|---|----------|
| 2.1     | Schematic representation of the stress-strain curves of a brittle fibre, a metal matrix and composite (somewhere in the dashed region depending on the volume fraction of fibres). (Ref.1)  | .. 8     |
| 2.2     | Formation of a lammelar structure (and phases) in a unidirectional solidification of a eutectic. The solidification front is perpendicular to the direction of growth (direction of arrows). $T_L$ , $T_E$ and $T_S$ are the temperature of the liquid (L), the solidification front and the solid, respectively. (Ref.1) | .. 34    |
| 2.3     | Sequence of dislocation movement passing through a dispersoid net (Ref.2).  | .. 36    |
| 2.4     | Relationship between dispersoid volume fraction and mean free matrix path for dispersion-strengthened composite materials of different dispersoid size (Ref.2).   | .. 38    |
| 2.5     | Schematic diagram showing fluidization and injection technique. (Ref.58)  | .. 47    |
| 2.6     | Plot of a weight percentage of alumina retained in the castings vs. the weight percentage of the magnesium present as an alloying element in pure aluminium for both manual and mechanical stirring. (Ref.58)   | .. 49    |
| 2.7     | Plot of weight percentage of alumina retained in the castings vs. the weight percentage of the magnesium present as an alloying element in F-22 alloys for both manual and mechanical stirring. (Ref.58)  | .. 50    |
| 2.8     | Plot of weight percentage alumina retained vs. the amount of freshly added magnesium for F-22 alloy and pure aluminium at hand and mechanical stirring. (Ref.58)  | .. 51    |
| 2.9     | Plot of weight percentage of alumina retained vs. the time elapsed for addition of alumina particles to the melt. (Ref.58)  | .. 52    |

| Fig.No. | Title   | Page No. |
|---------|---|----------|
| 2.10    | Schematic diagram of a liquid drop resting on a solid surface showing the interfacial forces and contact angle at point A. (Ref.14)   | .. 59    |
| 2.11    | Steps in producing a squeeze casting, (a) molten metal poured into die, (b) punch activated, (c) pressure applied to molten metal, and, (d) casting ejected. (Ref.89)   | .. 70    |
| 2.12    | Schematic representation of squeeze casting modes. (A) squeeze casting, (B) extrusion casting, and, (C) indirect pressure solidification. (Ref.89)  | .. 72    |
| 2.13    | (a) A rapid cooling rate combined with pressure application causes deviation (dashed line) from equilibrium conditions (solid line) in the Al-Si equilibrium diagram (Ref.89). (b) a rapid cooling rate combined with pressure application causes deviation (dashed line) from equilibrium conditions (solid line) in the Mg-Al equilibrium diagram. (Ref.89) | .. 81    |
| 2.14    | Comparative fatigue performance for alloy 6061-T <sub>6</sub> , wrought and squeeze-formed. (Ref.91)  | .. 95    |
| 3.1     | Schematic diagram showing eccentrically mounted blender for the preparation of MgO coated Al <sub>2</sub> O <sub>3</sub> powder.  | .. 137   |
| 3.2     | Schematic diagram showing the experimental set-up for preparing the stirred slurry.   | .. 139   |
| 3.3     | Schematic diagram showing (a) the squeeze casting arrangement and (b) the plan of placement of thermocouples (No.1,2 and 3) in the side walls of die to precisely monitor the temperature of die just prior to pouring the stirred slurry in the cavity.  | .. 145   |
| 3.4     | Schematic representation of the strategy adopted for MgO analysis at different locations of the matrix and Al <sub>2</sub> O <sub>3</sub> particle.   | .. 153   |
| 3.5     | Schematic diagram of tensile specimen (dimensions in mm).   | .. 156   |
| 3.6     | 2 KW.Kanthal resistance wound furnace shown with the tensile specimen gripped within the chamber of the furnace. Above arrangement employed for the determination of tensile properties of composites at elevated temperatures upto 300°C (573K).   | .. 158   |

| Fig.No. | Title  | Page No. |
|---------|--|----------|
| 3.7     | Schematic diagram of the pin-on-disc wear testing rig.   | .. 160   |
| 3.8     | Schematic representation of oblique polishing of worn wear pin specimen for subsurface damage study.   | .. 168   |
| 4.1     | (a) SEM picture of some Al <sub>2</sub> O <sub>3</sub> particles showing their morphology, (b) details of a single Al <sub>2</sub> O <sub>3</sub> particle showing an assemblage of crystallites.  | .. 177   |
| 4.2     | SEM pictures showing MgO coated Al <sub>2</sub> O <sub>3</sub> particles. (a) a single MgO coated Al <sub>2</sub> O <sub>3</sub> particle, (b) a single crystallite of Al <sub>2</sub> O <sub>3</sub> particle coated with sub-micron MgO particles.   | .. 178   |
| 4.3     | Optical pictures showing typical characteristics observed in gravity chill cast composite. Locations showing typical problems are marked by arrows. (a) coagulation of Al <sub>2</sub> O <sub>3</sub> particles occurring in many locations, (b) occurrence of porosity in the matrix in general and close to particle matrix interface in many locations, (c) and (d) same as in case of (b), (e) unfed interdendritic regions, and, (f) same as (b) above.   | .. 183   |
| 4.4     | SEM pictures of polished specimen, showing typical characteristics of gravity chill cast composites. (a) and (b) SEM pictures of polished specimens showing MgO coating around Al <sub>2</sub> O <sub>3</sub> particle. Note that part of the coating has been erased during polishing. Also, the coating can be seen to be intact on comparatively smaller Al <sub>2</sub> O <sub>3</sub> particle, (c) picture shows coagulation of Al <sub>2</sub> O <sub>3</sub> particles forming a chain-like structure, (d) SEM picture showing the presence of micro voids at particle/matrix interface.             | .. 184   |
| 4.5     | Optical and SEM pictures depicting the characteristics of squeeze cast composites. (a) Optical picture showing a uniform distribution of Al <sub>2</sub> O <sub>3</sub> particles in the matrix, (b) SEM picture showing the retention of Al <sub>2</sub> O <sub>3</sub> particles in the matrix, (c) optical picture showing that Al <sub>2</sub> O <sub>3</sub> particle is nicely bonded with the base matrix, (d), and, (e) optical picture showing that particle matrix interface is continuous and free from the presence of voids, and, (f) optical picture showing the presence of some second phase | .. 189   |

| Fig.No. | Title   | Page No. |
|---------|---|----------|
|         | constituents in the matrix. Also, this picture shows good bonding of $Al_2O_3$ particle with the matrix.  |          |
| 4.6     | Optical pictures showing the presence of considerable quantity of second phase constituents in the matrix owing to the presence of iron and silicon as chief impurities in commercial purity aluminium. | .. 190   |
| 4.7     | Percent increment in density of composites shown as a function of the squeeze pressure applied.   | .. 193   |
| 4.8     | Variation in mean dendritic arm spacing of composite obtained at three different die temperatures shown as a function of the squeeze pressure applied.  | .. 194   |
| 4.9     | SEM picture of the $Al_2O_3$ particle examined by Jeol JXA 8600 M EPMA.   | .. 202   |
| 4.10    | Line analysis for Al and Mg obtained by Jeol EPMA across the $Al_2O_3$ particle shown in Fig.4.9.   | .. 203   |
| 4.11    | Vicker's hardness of composites obtained at three die temperatures shown as a function of the squeeze pressure applied.   | .. 207   |
| 4.12    | Microhardness of the base matrix obtained at three different die temperatures shown as a function of the squeeze pressure applied.  | .. 208   |
| 4.13    | Influence of the extent of dispersion of sub-micron MgO particles and the degree of squeeze pressure applied on the microhardness ( $HM_{5gm}$ ) of Al-MgO composites.                                  | .. 212   |
| 4.14    | Vicker's hardness of Al-MgO composites shown as a function of the amount of sub-micron MgO particles dispersed and the degree of squeeze pressure applied.  | .. 213   |
| 4.15    | UTS of Al-MgO composites as influenced by the amount of sub-micron MgO particles dispersed and the extent of squeeze pressure applied.  | .. 214   |
| 4.16    | A typical engineering stress vs. strain curve obtained in different cases of gravity chill cast and squeezed composites and commercially pure aluminium.  | .. 218   |

| Fig.No. | Title  | Page No. |
|---------|--|----------|
| 4.17    | UTS and 0.2% offset Y.S. data of composites at different die temperatures shown as a function of the squeeze pressure applied.   | .. 219   |
| 4.18    | Percent elongation of composites shown as a function of the squeeze pressure and the die temperature.  | .. 220   |
| 4.19    | UTS of gravity chill-cast and squeezed composites shown as a function of the test temperatures. Squeezed composites prepared at three die temperatures: (0) ambient, (x) 100°C, (●) 200°C.   | .. 228   |
| 4.20    | 0.2% offset Y.S. of gravity chill-cast and squeezed composites shown as a function of the test temperatures. Squeezed composites prepared at three die temperatures: (0) ambient, (x) 100°C, (●) 200°C.  | .. 229   |
| 4.21    | Percent elongation of squeezed composites obtained at ambient and 200°C test temperatures shown as a function of the degree of squeeze pressure applied at three die temperatures: (0) ambient, (x) 100°C, (●) 200°C.  | .. 230   |
| 4.22    | Percent elongation of squeezed composites obtained at 100 and 300°C test temperatures shown as a function of the degree of squeeze pressure applied at three die temperatures: (0) ambient, (x) 100°C, (●) 200°C.  | .. 231   |
| 4.23    | Percent drop in UTS obtained in (▽) commercially pure aluminium, (□) gravity chill-cast and (0, Δ, x, ●) squeezed composites (ambient die temperature) shown as a function of the three test temperatures, and at (0) 80 MPa, (Δ) 100 MPa, (x) 120 MPa, (●) 140 MPa.             | .. 235   |
| 4.24    | Percent drop in 0.2% offset Y.S. obtained in (▽) commercially pure aluminium, (□) gravity chill cast and (0, Δ, x, ●) squeezed composites (ambient die temperature) shown as a function of the three test temperature, and at (0) 80 MPa, (Δ) 100 MPa, (x) 120 MPa, (●) 140 MPa. | .. 236   |
| 4.25    | Histogram showing percent UTS retained by composite Nos.1,2 and 3 upto 300°C test temperature.   | .. 238   |
| 4.26    | Histogram showing 0.2% offset yield strength retained by composite Nos.1,2 and 3 upto 300°C test temperature.  | .. 239   |



| Fig.No. | Title   | Page No. |
|---------|---|----------|
| 4.27    | Relationship between YS/UTS ratio and the three different test temperatures obtained for ( $\nabla$ ) commercially pure aluminium, ( $\square$ ) gravity chill-cast and ( $\circ$ , $\Delta$ , $x$ , $\bullet$ ) squeezed composites (ambient die temperature), at ( $\circ$ ) 80 MPa. ( $\Delta$ ) 100 MPa, ( $x$ ) 120 MPa, ( $\bullet$ ) 140 MPa.  | .. 242   |
| 4.28    | SEM pictures of the tensile fractured surfaces of gravity chill cast composite. (a) showing the presence of large sized voids pulled and enlarged under tension, (b) showing typical brittle fracture features. Note one MgO coated $Al_2O_3$ particle sitting at the base of the void. This particle is apparently loosely bonded to the matrix, (c) and (d) showing the presence of interdendritic solidification contraction areas. Note the dendritic arms jetting out into the void space from the opposite solidification fronts.   | .. 244   |
| 4.29    | SEM pictures of the tensile fractured surfaces of the composite squeezed at 140 MPa and ambient die temperature. (a) and (b) showing the presence of deep dimples characteristics of a ductile fracture, (c) showing the chisel-point separation of intervening matrix between two adjoining dimples typical of a ductile fracture.   | .. 247   |
| 4.30    | Fractographs of the composite with 5 wt.% total ( $Al_2O_3$ +MgO) powder mixture stirred in the melt and squeezed at 115 MPa and ambient die temperature. (a) SEM picture showing fairly good ductile fracture feature. Note one large $Al_2O_3$ particle sitting at the base of the crater where partial particle/matrix decohesion has occurred at the location marked by an arrow, (b) SEM picture showing typical ductile fracture features depicting the presence of a large number of deep dimples. In addition to many smaller dimples, a relatively larger dimple is seen in the centre of the fractograph. | .. 248   |
| 4.31    | Scanning Electron Micrographs of the tensile fracture surfaces of the composite squeezed at 140 MPa and ambient die temperature and (a) pulled in tension at 100°C (373K) and (b,c and d) pulled in tension at 300°C (573K). (a) Note particle/matrix decohesion almost along 3/4th surface area of the $Al_2O_3$ particle marked by an arrow, (b), (c) and (d) typical ductile fracture features showing relatively larger average size of dimples than what is obtained at ambient temperature.   | .. 252   |

| Fig.No. | Title  | Page No. |
|---------|--|----------|
| 4.32    | Wear rate plotted as a function of bearing load (gms) for composite No.1 (gravity chill cast) (x), composite No.2 (squeezed at 80 MPa, and ambient die temperature) (0), and composite No.3 (●), at a sliding speed of $9.4 \text{ m.sec}^{-1} \cdot 10^{-2}$ , sliding distance 508.5 m.  | .. 257   |
| 4.33    | Wear rate plotted as a function of bearing load (gms) for composite No.1 (gravity chill cast) (x), composite No.2 (squeezed at 80 MPa, and ambient die temperature) (0), and composite No.3 (●), at a sliding speed of $14.1 \text{ m.sec}^{-1} \cdot 10^{-2}$ , sliding distance 508.5 m.   | .. 258   |
| 4.34    | Wear rate plotted as a function of bearing load (gms) for composite No.1, (gravity chill cast) (x), composite No.2 (squeezed at 80 MPa, ambient die temperature) (0), composite No.3 (squeezed at 140 MPa, ambient die temperature) (●), at a sliding speed of $18.8 \text{ m.sec}^{-1} \cdot 10^{-2}$ , sliding distance 508.5 m. | .. 259   |
| 4.35    | Variation in the adhesive wear rates of binary aluminium-silicon alloys as a function of bearing load. (Ref.124)   | .. 261   |
| 4.36    | Wear rate vs. load in the matrix alloy and composites containing 3.5, 15 and 20wt% bauxite particles. (Ref.157)  | .. 262   |
| 4.37    | Effect of normal load and volume fraction of fibre on the wear rate of $\text{Al}_2\text{O}_3/6061$ composite (velocity = $1 \text{ m.sec}^{-1}$ ). (Ref.88)   | .. 263   |
| 4.38    | Wear rate of composite No.1 (x), 2(0) and 3(0) shown as a function of sliding speed at three different bearing loads of 500 gms. (————), 1000 gms. (-----) and 1500 gms. (——.—). Track length = 500 m in each case.  | .. 266   |
| 4.39    | Effect of sliding speed on the wear rate in Al-22wt%Si (0) and pure aluminium (●) (bearing pressure, 13 KPa, sliding circle diameter, 180 mm; dry sliding on a steel surface of hardness 30 HRC). (Ref.126)  | .. 268   |
| 4.40    | Wear loss vs. surface speed characteristics for base alloy (0), low graphite composite (x) and high graphite composites (●); (sliding distance, $8 \times 10^3 \text{ m}$ : bearing pressure, $0.08 \text{ kgf.mm}^{-2}$ ). (Ref.143)  | .. 269   |

| Fig.No. | Title  | Page No. |
|---------|--|----------|
| 4.41    | Effect of sliding speed and volume fraction of fibre on the wear rate of $Al_2O_3/6061$ composite (load = 4.9 N). (Ref.88)   | .. 270   |
| 4.42    | Temperature at a distance of 3mm from the rubbing surface on Al-16%Si-1%Cu alloy: ●-2 kgf; ○-8 kgf; ▲- 12 kgf; △- 18 kgf. (Ref.182)  | .. 271   |
| 4.43    | Temperature vs. sliding distance characteristics at two speeds $4.17 \text{ m.sec}^{-1}$ (□, ■, x) and $8.5 \text{ m.sec}^{-1}$ (○, ●, △): □, ○, base alloy; x, △, low graphite composite; ■, ●, high graphite composite. (Ref.143)  | .. 272   |
| 4.44    | Weight loss (mg) plotted as a function of the sliding distance(m) for composite No.1(x), composite No.2(○) and composite No.3(●) at a sliding speed of $9.4 \times 10^{-2} \text{ m.sec}^{-1}$ and three different bearing loads namely: 500 gms (—), 1000 gms. (----) and 1500 gms.(-.-).     | .. 274   |
| 4.45    | Weight loss (mg) plotted as a function of the sliding distance (m) for composite No.1(x), composite No.2(○) and composite No.3(●) at a sliding speed of $14.1 \times 10^{-2} \text{ m.sec}^{-1}$ and three different bearing loads namely: 500 gms.(—), 1000 gms. (----) and 1500 gms. (-.-).  | .. 275   |
| 4.46    | Weight loss (mg) plotted as a function of the sliding distance (m) for composite No.1(x), composite No.2(○), and composite No.3(●) at a sliding speed of $18.8 \times 10^{-2} \text{ m.sec}^{-1}$ and three different bearing loads namely: 500 gms. (—), 1000 gms. (---) and 1500 gms. (-.-). | .. 276   |
| 4.47    | Comparison of the wear behaviour of composites containing SiC and $Al_2O_3$ particles. (Ref.62)  | .. 279   |
| 4.48    | Wear weight loss vs. sliding distance of the matrix, Al-18 Si alloy and B8G (8wt% bauxite and 3wt% uncoated graphite dispersed in Al-12Si-1.4Cu-1.3Mg a base alloy) composite. (Ref.157)   | .. 280   |
| 4.49    | Wear progressive curves of ceramic fibre-reinforced aluminium alloy composites (load=4.9 N, speed = $1 \text{ m.sec}^{-1}$ ). (Ref.88)   | .. 281   |
| 4.50    | Wear rate shown as a function of the degree of squeeze pressure applied during the fabrication of composites under three different conditions  | .. 284   |

| Fig.No. | Title   | Page No. |
|---------|---|----------|
|         | of wear; ( $\Delta$ ) - Load=500gms, sliding speed=9.4 m.sec <sup>-1</sup> .10 <sup>-2</sup> , track length=169.5 m. ( $\square$ ) - Load=1000gms, sliding speed=14.1 m.sec <sup>-1</sup> .10 <sup>-2</sup> , track length=508.8 m. ( $\blacksquare$ ) - Load=1500gms, sliding speed=18.8 m.sec <sup>-1</sup> .10 <sup>-2</sup> , track length=1017 m.  |          |
| 4.51    | SEM pictures of the worn surface of composite No.1 under 500 gm bearing load, 18.8 m.sec <sup>-1</sup> .10 <sup>-2</sup> sliding speed and 1017 m track length. (a) and (b) show typical scoring marks, grooves and worn patches adhering to the worn surface, (c) and (d) showing grooved worn surface littered with fragmented fine debris material. Note numerous wide and deep tracks occurring in the displaced material on the ridge of grooves. Some of these cracks are marked by arrows.   | .. 292   |
| 4.52    | SEM pictures showing the details of the worn surface. (a) patches of matrix material scooped out from the grooves undergoing fragmentation through the process of cracks formation. Some of these cracks are marked by arrows, (b) SEM picture showing the special features of cracks emanating from the surface of grooves to the displaced materials on the edges of these grooves. Also, numerous cracks (marked by arrows) can be seen developing into the displaced material on both the edges of the grooves, (c) and (d) SEM pictures showing similar features as mentioned above. | .. 293   |
| 4.53    | SEM pictures showing the fracture and removal of matrix material close to the edge of the wear pin. (a) Note the partially sheared material still adhering to the edge of the wear pin because of excellent ductility of composite material, (b) Note typical scoring marks on the individual sheared and partially fragmented pieces. Numerous cracks can be seen developing in these fragmented pieces.   | .. 294   |
| 4.54    | Optical pictures showing the morphology of smeared material onto the surface of counter face steel disc. Material in these seizure patches can be seen to be in a state of complete fragmentation. Fine debris particles are filled into the grooves of the counterface steel disc and can be seen coagulated.  | .. 298   |

| Fig.No. | Title   | Page No. |
|---------|---|----------|
| 4.55    | SEM pictures of debris material produced during wear experiments. (a) showing the presence of laminates, foils and thin long chips in the aggregate debris material, (b) a foil kind of debris material undergoing further fragmentation, (c) a laminate also undergoing further fragmentation along its lower surface. A number of smaller and approximately spherical debris pieces can also be seen in the picture. These particles appear to be the result of coagulation of several smaller particles into a single nearly spherical aggregates.   | .. 300   |
| 4.56    | SEIs of some other typical debris particles. (a) showing a thin long chip in the process of severe fragmentation. Note the presence of several deep cracks all along the length of this chip, (b) a laminate in the process of further fragmentation, (c) a rare thin foil laminate. Presence of fine cracks in the central region of this foil can be seen. In some instances these cracks can be seen developing from the central region to the periphery of these foils.   | .. 301   |
| 4.57    | (a) and (b) optical pictures showing the microstructures of oblique section exhibiting the presence of river delta pattern of cracks in the work hardened region immediately below the worn surfaces. A dark portion in the extreme left corner region shows the edge of the grooved worn surface. It can be seen that these cracks finally dissipate into the worn surface mentioned above. It is also noteworthy that dispersed $Al_2O_3$ particles are firmly bonded to the base matrix, (c) SEM picture showing grooved wear track and scooped out matrix material on the ridges of these grooves and $Al_2O_3$ particles firmly bonded and still present on the grooved track and not dislodged. | .. 304   |
| 4.58    | Microhardness ( $HM_{10gms.}$ ) plotted as a function of the depth of subsurface region immediately below the worn surface. (x) - composite No.1, the depth of work hardened region is approx. 250 $\mu m$ , (O) - composite No.2, depth of work hardened region is 200 $\mu m$ , and (●) composite No.3, depth of work hardened region, approx. 125 $\mu m$ .  | .. 305   |

## C O N T E N T S

| CHAPTER   | PAGE NO. |
|---|----------|
| CANDIDATE'S DECLARATION   | .. 1     |
| ACKNOWLEDGEMENT   | .. ii    |
| PREFACE   | .. v     |
| LIST OF PUBLICATIONS  | .. ix    |
| ABBREVIATIONS   | .. xi    |
| LIST OF TABLES  | .. xiii  |
| LIST OF FIGURES   | .. xv    |
| 1. INTRODUCTION   | .. 1     |
| 2. A COMPREHENSIVE STUDY OF COMPOSITE SYSTEMS,<br>SQUEEZE CASTING AND WEAR OF Al ALLOYS AND<br>COMPOSITES |          |
| 2.1 Composite Systems : General   | .. 7     |
| 2.1.1 Definition of Composites  | .. 9     |
| 2.1.2 Composite Systems other than MMCs   | .. 10    |
| 2.1.2.1 Ceramic Systems   | .. 11    |
| 2.1.2.2 Glass Systems   | .. 11    |
| 2.1.2.3 Thermoplastic Systems   | .. 12    |
| 2.1.2.4 Elastomer Systems   | .. 13    |
| 2.1.2.5 Concrete Systems  | .. 14    |
| 2.1.2.6 Asphalt Systems   | .. 14    |
| 2.1.3 Metal Matrix Composites (MMCs)  | .. 14    |
| 2.1.3.1 Introduction  | .. 14    |
| 2.1.3.2 Kinds of MMCs   | .. 18    |
| (a) Fibre Reinforced<br>Composites  | .. 18    |

|         |  |       |
|---------|--|-------|
|         | (b) Laminar Composites   | .. 27 |
|         | (c) Flake Composites   | .. 29 |
|         | (d) Filled Composites  | .. 30 |
|         | (e) In-situ Grown<br>Composites  | .. 30 |
|         | (f) Dispersion Strengthened<br>Composites  | .. 35 |
|         | (g) Particulate Composites   | .. 40 |
| 2.1.4   | Developments in Cast Particulate<br>Composites                                   | .. 43 |
| 2.1.4.1 | Introduction   | .. 43 |
| 2.1.4.2 | Types of Cast Particulate<br>Composites  | .. 44 |
| 2.1.4.3 | Liquid Metallurgy<br>Techniques of Preparing<br>Particulate Composites           | .. 45 |
|         | (a) Fluidization and<br>Injection Technique                                      | .. 45 |
|         | (b) Vortex Technique   | .. 46 |
|         | (c) Pellet Technique   | .. 54 |
|         | (d) Infiltration Technique   | .. 55 |
| 2.1.4.4 | Problems of Vortex Liquid<br>Metallurgy Route and the<br>Controlling Parameters. | .. 56 |
|         | (a) Wettability  | .. 57 |
|         | (b) Particle Matrix Bonding  | .. 61 |
|         | (c) Vortex Formation   | .. 63 |
|         | (d) Segregation and Floccu-<br>lation of Dispersoids                             | .. 65 |
|         | (e) Porosity in the Composites<br>Produced by Vortex Methods                     | .. 65 |
| 2.2     | Squeeze Casting Process  | .. 67 |

|         |   |        |
|---------|---|--------|
| 2.2.1   | Introduction  | .. 67  |
| 2.2.2   | Squeeze Casting Process   | .. 69  |
| 2.2.2.1 | Special Merits  | .. 73  |
| 2.2.2.2 | Comparison of Squeeze Casting with Alternative Metal Forming Techniques | .. 75  |
| 2.2.3   | Theoretical Aspects of the Effects of Squeeze Pressure                  | .. 77  |
| 2.2.3.1 | Reduction of Porosity   | .. 77  |
| 2.2.3.2 | Effect on Equilibrium Diagram and Structure                             | .. 78  |
| 2.2.4   | Process Parameters  | .. 82  |
| 2.2.4.1 | Metal Casting Temperature   | .. 82  |
| 2.2.4.2 | Tooling Temperature   | .. 83  |
| 2.2.4.3 | Melt Quality and Quantity   | .. 84  |
| 2.2.4.4 | Dia Coating/Lubricant   | .. 85  |
| 2.2.4.5 | Temperature for Pressure Application                                    | .. 86  |
| 2.2.4.6 | Specific Pressure Level and Duration                                    | .. 86  |
| 2.2.4.7 | Press Speed   | .. 88  |
| 2.2.5   | Die Material and Configuration  | .. 88  |
| 2.2.6   | Application of Squeeze Casting Technique                                | .. 90  |
| 2.2.6.1 | General   | .. 90  |
| 2.2.6.2 | Squeeze Casting of Metals and alloys                                    | .. 92  |
| 2.2.6.3 | Squeeze Casting of Composite Systems                                    | .. 102 |
| 2.3     | Wear  | .. 113 |
| 2.3.1   | Introduction  | .. 113 |



|           |   |        |
|-----------|---|--------|
| 2.3.2     | Definition of and Parameters Controlling Wear   | .. 114 |
| 2.3.3     | Type of Wear  | .. 115 |
| 2.3.3.1   | Adhesive Wear   | .. 115 |
| 2.3.3.2   | Abrasive Wear   | .. 116 |
| 2.3.3.3   | Corrosive Wear  | .. 116 |
| 2.3.3.4   | Surface Fatigue Wear  | .. 116 |
| 2.3.3.5   | Other Forms of Wear   | .. 117 |
| 2.3.4     | Techniques of Measuring Wear  | .. 117 |
| 2.3.5     | Some Recent Investigations Into the Wear Behaviour of Aluminium Alloys and Composites | .. 119 |
| 2.3.5.1   | Al-Si System  | .. 119 |
| 2.3.5.2   | Al-Pb System  | .. 122 |
| 2.3.5.3   | Al-Graphite Particulate Composites  | .. 123 |
| 2.3.5.4   | Al-Mica Particulate Composites  | .. 124 |
| 2.3.5.5   | Al-Fibre Reinforced Composites  | .. 125 |
| 2.3.5.6   | Al-Ceramic Particle Composites  | .. 128 |
| 2.4       | Summary and Strategy for Present Investigation  | .. 129 |
| <b>3.</b> | <b>EXPERIMENTAL PROCEDURE</b>   | .. 133 |
| 3.1       | Introduction  | .. 133 |
| 3.2       | Specifications of Raw Materials   | .. 134 |
| 3.3       | Blending and Dehydroxylation of Ceramic Powders                                       | .. 136 |
| 3.4       | Experimental Set-up Employed for the Preparation of the Stirred Slurry                | .. 136 |
| 3.5       | Preparation of the Stirred Slurry: Process Details                                    | .. 140 |
| 3.5.1     | Development of modified 'MgO Coating' Technique                                       | .. 140 |

|         |  |        |
|---------|--|--------|
| 3.5.2   | Process Control During Vortex Formation  | .. 142 |
| 3.5.3   | Preparation of Al-MgO Composites   | .. 143 |
| 3.6     | Squeeze Casting (liquid forging) and Gravity Chill Casting of the Stirred Slurry                           | .. 144 |
| 3.7     | Optical and SEM Examination  | .. 147 |
| 3.7.1   | Topography Study of Coated and Uncoated Al <sub>2</sub> O <sub>3</sub> Particles and Sub-micron MgO Powder | .. 147 |
| 3.7.2   | Examination of Polished Surfaces of Composite Specimens  | .. 147 |
| 3.7.2.1 | Preparation of Metallographic Specimens  | .. 147 |
| 3.7.2.2 | Quantitative Metallography   | .. 149 |
| 3.8     | EPMA Examination of the Reacted Layer Around Al <sub>2</sub> O <sub>3</sub> Particles                      | .. 151 |
| 3.9     | Measurements of Density  | .. 152 |
| 3.10    | Mechanical Property Evaluation   | .. 154 |
| 3.10.1  | Vicker's Hardness and Microhardness Measurements   | .. 154 |
| 3.10.2  | Tensile Property Evaluation Upto 300°C (573K)  | .. 155 |
| 3.11    | SEM Examination of Tensile Fracture Surfaces   | .. 157 |
| 3.12    | Evaluation of Wear Behaviour under Dry Sliding Conditions  | .. 159 |
| 3.12.1  | Fabrication of the Wear Testing Rig  | .. 159 |
| 3.12.2  | Selection of Composites for Wear Studies   | .. 161 |
| 3.12.3  | Wear Test Procedure and Parameters   | .. 163 |
| 3.12.4  | SEM Examination of the Worn Surface  | .. 166 |
| 3.12.5  | Examination of Sub-surface Damage  | .. 167 |
| 3.12.6  | Examination of the Wear Debris   | .. 170 |

|         |   |        |
|---------|---|--------|
| 4.      | RESULTS AND DISCUSSION  | .. 172 |
| 4.1     | Introduction  | .. 172 |
| 4.2     | Preparation and Initial Characterisation of Gravity Chill Cast and Squeezed Al-Al <sub>2</sub> O <sub>3</sub> -MgO and Al-MgO Particulate Composites. | .. 172 |
| 4.2.1   | Role of Modified 'MgO Coating' Technique in the Preparation of Composites.  | .. 172 |
| 4.2.2   | Optical and SEM Examination of the Cast Structure   | .. 182 |
| 4.2.2.1 | Gravity Chill Cast Composites   | .. 182 |
| 4.2.2.2 | Squeeze Cast Composites   | .. 188 |
| 4.2.3   | Influence of Squeeze Pressure on %V <sub>f</sub> Retention of Al <sub>2</sub> O <sub>3</sub> , Density and Mean Dendritic Arm Spacings of Composites  | .. 191 |
| 4.2.4   | Particle/Matrix Bonding: Examination of the Reacted Layer Around Al <sub>2</sub> O <sub>3</sub> Particles by the EPMA                                 | .. 199 |
| 4.3     | Mechanical Property Evaluation  | .. 205 |
| 4.3.1   | Vicker's Hardness and Microhardness of Composites   | .. 205 |
| 4.3.2   | Studies on Al-MgO Composites:Dispersion Strengthening Effect of Sub-micron MgO Particles  | .. 209 |
| 4.3.3   | Tensile Properties upto 300°C(573K)   | .. 216 |
| 4.3.3.1 | General   | .. 216 |
| 4.3.3.2 | Ambient Temperature Tensile Properties  | .. 216 |
| 4.3.3.3 | Elevated Temperature Tensile Properties   | .. 223 |
| 4.3.4   | SEM Examination of Tensile Fracture Surfaces  | .. 241 |
| 4.3.4.1 | Features of Gravity Chill Cast Composites   | .. 243 |
| 4.3.4.2 | Features of Squeezed Composites   | .. 246 |

|  |        |
|--|--------|
| a) Fracture Features at Ambient Test Temperature                           | .. 246 |
| b) Fracture Features at Elevated Test Temperature                          | .. 251 |
| 4.4 Wear Behaviour of Composite Nos 1,2 and 3 Under Dry Sliding Conditions | .. 254 |
| 4.4.1 General  | .. 254 |
| 4.4.2 Bearing Load-Wear Rate Relationships                                 | .. 256 |
| 4.4.3 Effect of Sliding Speed on Wear Behaviour                            | .. 265 |
| 4.4.4 Effect of Sliding Distance on the Weight Loss During Wear            | .. 273 |
| 4.4.5 Influence of Squeeze Pressure on the Wear Behaviour                  | .. 283 |
| 4.4.6 Texture of Worn Surface and the Debris Material                      | .. 291 |
| 4.4.7 Sub-surface Damage   | .. 303 |
| <br>   |        |
| 5. <b>SUMMARY OF CONCLUSIONS AND SUGGESTIONS FOR FUTURE STUDIES</b>        | .. 309 |
| 5.1 Conclusions  | .. 309 |
| 5.2 Suggestions for Future Studies   | .. 317 |
| <b>REFERENCES</b>  | .. 320 |
| <b>APPENDIX</b>  | .. 339 |

## CHAPTER - 1

## INTRODUCTION

The scientific and technological interest in cast particulate composites has grown world wide in recent years. It is because of the ease with which reinforcing non-metal or ceramic particles/continuous or broken fibres can be introduced into a variety of metal matrices using foundry techniques. It is also well established that the fabrication of cast particulate composites using the foundry route is much less energy intensive compared to P/M route. Using this technique, a wide variety of ceramic particles such as  $\text{Al}_2\text{O}_3$ ,  $\text{ZrO}_2$ , Illite clay, mica, graphite, shell-char, SiC,  $\text{Al}_2\text{O}_3+\text{MgO}$  etc. have been introduced successfully in aluminium and magnesium alloy base matrices. Depending upon the reinforcing constituent, the cast product can be put to specific end applications. For example, Al- $\text{Al}_2\text{O}_3$  and Al- $\text{Al}_2\text{O}_3$ -MgO cast particulate composites have been found to retain over 90% of their ambient yield strength at 300°C test temperature. Besides, these composites have been found to display excellent adhesive cum abrasive wear resistance under dry sliding conditions compared to pure aluminium. As such, this class of composites can be put to specific end applications requiring retention of strength at elevated temperatures upto 300°C (573K) or requiring superior wear resistance compared to ordinary aluminium and magnesium base alloys at ambient temperature. Also, these composites offer special advantage in terms of superior strength/weight ratio as against ferrous alloys for many critical

engineering applications.

But the fabrication of cast particulate composites is associated with numerous problems such as poor wettability of dispersoid particles for the liquid melt, segregation and non-uniform distribution of these particles in the matrix, presence of considerable amount of total porosity in the cast structure and coarse grained structure of the matrix. Although several of these problems have been solved so far, but the problem of porosity still remains to be tackled. One of the important aspects that influence the mechanical properties of cast particulate composites very adversely is the presence of considerable amount of porosity in the cast structure. This total porosity basically consists of gas porosity plus unfed interdendritic regions. In many instances, these voids may be interconnected presenting a serious amount of discontinuity in the cast structure. Under these circumstances, not only that the matrix is considerably weakened but also the dispersoid particles, though present in the matrix but loosely bonded, are not able to perform their function of reinforcing the base matrix. As such, the total porosity present in the cast structure, brings about a serious deterioration in the performance of such composites. And the coarse grained structure of the base matrix adds another difficulty in the performance of such composites.

The present work is concerned with the question of achieving a cast structure relatively free from total porosity. Another objective set for the present investigation was to achieve

a densified and grain refined structure in the cast composite. Given that these objectives are achieved, the performance of ordinary gravity chill cast Al-Al<sub>2</sub>O<sub>3</sub>-MgO composite developed earlier could be expected to be greatly improved. Earlier investigations had revealed that the performance of above class of composites is fairly good with respect to their tensile properties upto 250°C (523K). In order to improve the performance of above composites further, it was planned to squeeze cast (or liquid forge) the stirred slurry in the pressure range of 80 to 140 MPa using three die temperatures namely ambient, 100 and 200°C. Using this technique, a composite matrix with relatively greater grain refinement and a higher degree of densification could be expected to be produced.

The present investigation, therefore, is devoted to a study of the influence of squeeze pressure and die temperature on the properties of resulting Al-Al<sub>2</sub>O<sub>3</sub>-MgO squeeze cast composites. The properties investigated in the present work include: an examination of the morphology of distribution of Al<sub>2</sub>O<sub>3</sub> particles retained in the matrix, density, Vicker's hardness and microhardness and average size of dendritic arm spacing leading to the initial characterisation of squeezed composites; ambient and elevated temperature tensile properties upto 300°C (573K) and wear behaviour of three typical composites under dry sliding conditions.

The present study also deals with the development of modified 'MgO coating' technique, with the help of which, a stirred slurry was produced using vortex liquid metallurgy route.

This stirred slurry was later squeezed in the pressure range of 80 to 140 MPa using alloy cast iron dies as mentioned above. The present study was also concerned with the role of submicron MgO particles in stiffening the base matrix of Al-Al<sub>2</sub>O<sub>3</sub>-MgO particulate MMCs. An experimental verification of the hypothesis proposed in an earlier study was obtained in the present work. It was confirmed experimentally that the submicron MgO particles do cause dispersion strengthening of the base matrix of above composites.

A basic study relating to the probable chemical nature of the reacted layer around Al<sub>2</sub>O<sub>3</sub> particles was also undertaken with the help of Jeol EPMA. It was shown that MgO forms an essential constituent of this reacted layer & that this layer could be a MgAl<sub>2</sub>O<sub>4</sub> spinel.

Solidifying the stirred slurry in the pressure range of 80 to 140 MPa would be expected to bring about an overall improvement in the tensile behaviour of Al-Al<sub>2</sub>O<sub>3</sub>-MgO particulate MMCs as a highly refined and densified matrix with near zero porosity level is obtained upon squeezing. The present study deals with a detailed examination of the tensile behaviour of squeezed Al-Al<sub>2</sub>O<sub>3</sub>-MgO particulate MMCs upto 300°C (573K). It was found that the tensile properties of above composites uniformly improve as the degree of squeeze pressure applied is systematically raised in steps. Progressively increasing squeeze pressure improves not only the UTS but also the ductility of the composites simultaneously. But increasing the die temperature (at a given level of squeeze pressure) uniformly deteriorates the



properties of above composites. The best tensile properties are displayed by a composite squeezed at 140 MPa and ambient die temperature (the highest squeeze pressure employed in the present work). This particular composite also displays best performance upto 300°C (573K) test temperature. Interestingly, this composite retains 72% of its ambient UTS value and 94% of its ambient Y.S. value at 300°C (573K) test temperature. The performance of this composite is observed to be nearly twice as good as the performance of ordinary gravity chill cast composite at the above test temperature.

An initial effort has been made in the present work to examine the wear behaviour of three typical composites under dry sliding conditions using a standard Pin-on-disc wear testing rig. The three different composites selected for the study represent three different extreme conditions of composite fabrication. Composite No.1 selected for the study represents gravity chill cast condition, while composite Nos.2 and 3 represent two extreme conditions of squeeze pressures employed in the present work. Composite No.2 represents the minimum squeeze pressure (80 MPa, ambient die temperature), while composite No.3 represents the highest squeeze pressure (140 MPa, ambient die temperature) employed for composite fabrication. Three different bearing loads namely 500, 1000 and 1500 gms and three different sliding speeds namely 9.4, 14.1 and 18.8 m.sec<sup>-1</sup>.10<sup>-2</sup> were employed and the wear rates in terms of kg.km<sup>-1</sup>.10<sup>-6</sup> were determined for the three composites at ½, 1 and 1½ hr intervals of wear runs. Thus, in all 81 experiments were conducted for the three composites. An

analysis of wear data reveals that a) composite No.3 displays the highest wear resistance compared to composite No.2 and 1 under all conditions of dry sliding wear and b) the overbearing factor influencing the wear of composite No.3 is the bearing load. It was also shown through an examination of polished oblique sections that minimum amount of subsurface damage occurs in case of composite No.3 as compared with the damage seen in composite No.2 and 1. A comparatively superior wear resistance of composite No.3 is attributed to its matrix characteristics namely, highest hardness, maximum grain refinement and highest level of densification and a continuous matrix with minimum level of porosity in the cast structure.

It was concluded from present studies that the process of squeeze casting greatly improves the overall characteristics of Al-Al<sub>2</sub>O<sub>3</sub>-MgO particulate MMCs. However, there is a considerable scope of improving the properties of these composites still further. For this purpose, it is suggested that the squeeze pressure should be taken to still higher levels such as 160 to 240 MPa. Also, the %V<sub>f</sub> retention of Al<sub>2</sub>O<sub>3</sub> should be raised from the existing level of 12/13 to 20/22%. At the same time, the matrix of the composite should be changed from the existing commercially pure aluminium to a high strength heat-treatable aluminium alloy such as 2014, 2024, 201, 206, 356 etc.

## CHAPTER 2

### A COMPREHENSIVE STUDY OF COMPOSITE SYSTEMS, SQUEEZE CASTING AND WEAR BEHAVIOUR OF ALUMINIUM ALLOYS AND COMPOSITES

#### 2.1 COMPOSITE SYSTEMS : GENERAL

Several engineering and scientific applications of materials, demand combination of physical and/or mechanical properties, that are not easily attainable in metallic materials inspite of use of a variety of mechanical and/or heat-treatment or alloying, to influence their structural features and hence properties. Composite materials, consisting of a properly controlled dispersed reinforcing phase in a base matrix, have therefore been developed to meet demands of some of these new applications, specially those involving use of components either at elevated temperatures or under severe adverse environmental condition or those requiring high strength/weight ratio of components used or a combination of high strength, high toughness and high wear resistance. Typical improvement in properties of composite material is schematically represented in Fig.2.1, after Piatti [1], showing a schematic stress-strain curve for a brittle-fibre, metal matrix and a composite having both. For these composite materials both the base matrix as also the reinforcing dispersed phase can be either metallic or non metallic in nature depending upon the service requirements.

Discussions in this section is essentially devoted to a detailed study of metal-matrix composite systems (MMCs). An

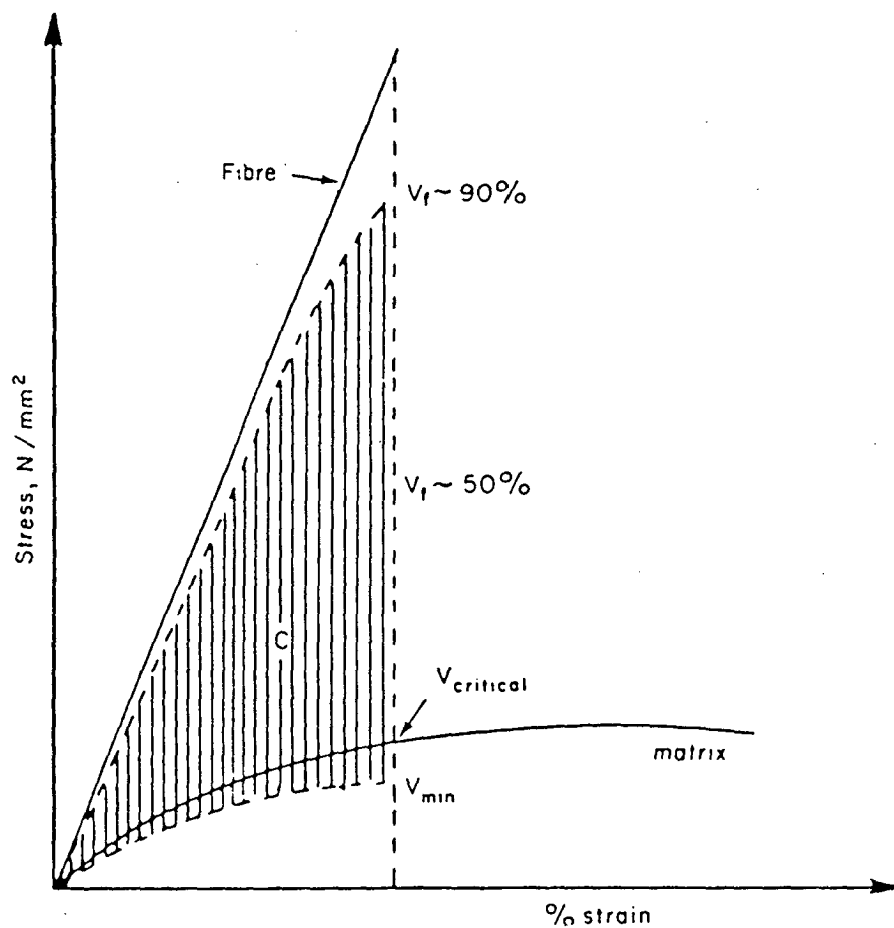


**FIG.2.1** Schematic representation of the stress-strain curves of a brittle fibre, a metal matrix and composite (somewhere in the dashed region depending on the volume fraction of fibres). (Ref.1)

effort has been made to review different systems developed so far and highlight briefly the scientific achievements in each case. The approach adopted is to discuss critically the following aspects for each type of composite studied,

- a) Fabrication technique and associated problems.
- b) Reinforcing constituent and interface bonding
- c) Characterisation
- d) Possible applications

#### 2.1.1 DEFINITION OF COMPOSITE

Composite systems have been defined in a number of ways by different workers. Some of the important definitions are outlined below:

In a statement, after Piatti [1], Javitz defined composite as, "multifunctional materials systems that provide characteristics not obtainable from any discrete material, which are cohesive structures made by physically combining two or more compatible materials, differing in composition and characteristics and sometimes in form".

Berghezan, after Piatti [1], has defined composites as "compound materials which differ from alloys by the fact that individual components retain their characteristics but are so incorporated into the composite as to take advantage only of their attributes and not of their shortcomings, in order to obtain an improved material".

In another statement, after Piatti [1], quoting the design philosophy of composites, Berghezan defined composites as, "The fibre reinforced composites are only those heterogeneous materials, which are prepared by association and bonding in a single structure of materials possessing quite different properties and when these are complementary give a composite material possessing additional and/or superior properties to the individual components either alone or mixed together".

Broutman and Krock [2] have outlined the basic characteristics of composite materials as follows:

- (i) The composite material must be man made.
- (ii) The composite material must be a combination of at least two chemically distinct materials with a distinct interface separating the components.
- (iii) The separate materials forming the composites must be combined three dimensionally.
- (iv) The composite material should be created to obtain properties which would not be achieved by any of the components acting alone.

#### 2.1.2 COMPOSITE SYSTEMS OTHER THAN MMCs

Brief discussion on properties and applications of different composite systems, not involving metal-matrix composites (MMCs) and classified based on the type of matrix involved, is presented in this section.

### 2.1.2.1 CERAMIC SYSTEMS

A number of ceramic composite systems [3] such as ceramic-pore system, ceramic-glass system, ceramic-ceramic system, ceramic-metal system have been developed for specific end applications. However, applications of these systems involve static rather than dynamic operating conditions, basically because of inherent brittleness and the resulting low impact strength of ceramics. A large proportion of current research is directed towards the development of tougher basic ceramic materials, and to the design of composite systems in which the ceramic component is either reinforcing a metal or protected by a metal from surface damage. These composites find a number of applications, viz. porcelain for high voltage insulation components, in valves inserts for rocket nozzles, ram jet engine, space vehicles etc.

### 2.1.2.2 GLASS SYSTEM

In this class of composites [3], involving use of several reinforcing phases, the glass-resin composites are by far the most important one. The properties of resulting composite are a function of the relative quantities and types of glass and resin, the orientation of the fibre-reinforcements in the resin matrix, the environmental conditions under which the composite is used in respect of the temperature, surrounding medium, stress and time, and, the conditions under which the composite was manufactured in respect of humidity, moulding temperature, technique etc. Almost any two-dimensional directional fibre orientation can be designed

into such composite laminates. Such composites find extensive application in industries where a high strength/weight ratio is required and also where complex shapes of limited number are called for.

### 2.1.2.3 THERMOPLASTIC SYSTEMS

Thermoplastics are used widely as the continuous phase in composite materials. Amongst the thermoplastic composites, three types namely those using 'polyethylene', 'polystyrene', and 'styrene - acrylonitrile copolymer' are widely used. The first of these represents one of the major types of commercial thermoplastic which is crystalline, opaque and ductile in nature. The latter two represent a second major type of thermoplastic which is generally transparent, rigid, brittle and glassy.

Thermoplastic system may further be classified [3] into following three sub-systems:

- (i) Thermoplastic-rubber systems or the rubber-modified polymers.
- (ii) Thermoplastic-solid filler systems or the polymers containing rigid fillers.
- (iii) Thermoplastic-gas systems or the foams.

Polymers containing rigid fillers are used in application formerly employing bronze. The material is made by combining 65% of a chlorinated polymer with 20% calcium metasilicate and 15%



graphite. The combination of polyethylene and lead powder leads to a material which is an effective radiation shield against both neutrons, which are stopped by the large concentration of hydrogen atoms in the polyethylene, and gamma rays, which are stopped by lead. Lead-filled Vinyls have been used for sound insulation of a gas-turbine powered hydro-foil passenger craft. Small, robust pressure transducers have been made from polymers filled with carbon black.

#### 2.1.2.4 ELASTOMER SYSTEMS

In contrast with the ordered and rigid crystalline arrangement of atoms in metals, elastomers are 'Coherent elastic solids' composed of a tangled mass of kinked, twisted and intertwined chain-like molecules [3]. The basic element of an elastomer is the monomer i.e. the link in the chain which determines the chemical character of the material and its resistance to oil, ozone, solvents and chemicals. Addition of inert materials, dispersed in the elastometric mass prior to curing, can increase strength and hardness or resistance to deformation, usually with a reduction in elasticity and resilience. The various reinforcing materials used in this system include, (i) Carbon Black, (ii) Inorganic fillers-clay, magnesium carbonate, zinc oxide, iron oxide, precipitated calcium carbonate, finely divided calcium silicate etc., (iii) Inert fillers-barytes, diatomaceous earth, talc, lithopone etc., (iv) Organic fillers-organic reinforcing agents include such materials as

phenolic-amino and high-styrene resins, cyclised-rubber and lignin.

#### 2.1.2.5 CONCRETE SYSTEMS

Concrete is a mixture of naturally occurring gravels or crushed rock materials called aggregates bonded together by some form of cement. The cements used for concrete belong to the calcareous group of cements, and, a concrete mixture of sand and cement is called mortar. The cheapest of all cements, the 'Portland cement', is manufactured from CaO, occurring in nature in the form of chalk or limestone, and silica and alumina occurring as clay or shale.

#### 2.1.2.6 ASPHALT SYSTEMS

For all practical purposes, asphaltic bitumen is preponderantly applied in the form of heterophase systems with bitumen as the continuous phase. Investigations of bituminous heterophase systems have usually been directed especially towards the mechanical properties of mixtures with high concentrations of widely-graded mineral aggregate in connection with their extensive use as a road-building material.

#### 2.1.3 METAL-MATRIX COMPOSITES (MMCs)

##### 2.1.3.1 INTRODUCTION

FRP-composites are not suitable for elevated temperature applications. For applications involving high levels of stresses and strains, abrasive and elevated temperature conditions,

metal-matrix composites (MMCs) are the best choice. In recent times, Al-and Mg-based composites prepared by using reinforcements of either fibres of graphite,  $Al_2O_3$ , SiC, or particulates of SiC, TiB, TiC,  $B_4C$  etc. have been fabricated to the potential candidates for a number of components for static-and rotating-engine components and frames of aircrafts and other space-and defence-applications. Even Ti and super-alloys based composites are being thought of for future applications. Satyanarayana [4] has reported that the use of composite materials in aerospace industries has brought about a saving of about \$200-300\$ per kg. Laminated BV/Al composites seem to be the future materials, to meet the exacting demands of aerospace industries such as low density, high strength, fuel economy, low operating-and maintenance-costs and shorter inspection periods.

The basic characteristics expected of metal-matrix composites (MMCs) such as high strength at ambient temperatures, excellent retention of strength at elevated temperatures, fairly-reasonable ductility, high modulus of elasticity, excellent wear resistance, high stiffness etc. are obtained by a suitable selection of the 'base-matrix' and the 'reinforcing-material' and also by a proper selection of fabrication technique. Comparatively inexpensive dispersoid particles such as glass and zircon-sands, when dispersed in aluminium, can confer improved wear-resistance on the Al-alloy which can be substituted for heavier ferrous alloys in wear-resistant applications. The friction and bearing characteristics of Al-alloys may be improved

by incorporating graphite, thus providing, for example, a cheaper alternative to aluminium-tin bearing alloys. Clegg [5] has pointed out that improvement in tensile properties especially at elevated temperatures may be obtained by incorporating ceramic fibres and dispersoid particles within Al-alloys.

A significant portion of the work done in the field of metal-matrix composites deals with discontinuous second-phase particles that are uniformly distributed in an alloy-matrix. Oxides, carbides, silicides, borides and other non-metallic dispersoid systems have shown some degree of promise in wear and strengthening. Various metals are being attempted as matrices. These are listed in Table-2.1. Of these, aluminium is a commonly used metal followed by Mg, Ti and super-alloys. Super-alloys, steels, titanium, Mg, Cu, titanium aluminide and refractory metals-all are being used as matrix materials for composites requiring specific property-combinations. Margaret [6] has pointed out that iron composites reduce weight and improve strength for aerospace components, copper-based composites provide ductility for super-conductors, high thermal conductivity for high heat-flow applications such as rocket engines and tolerable properties for electronic applications, and, the refractory metal-based composites provide the strength and fatigue life required for space-based nuclear power systems and toughness for wear and corrosion applications.

Initially MMCs were thought of as materials to overcome

**TABLE - 2.1**  
**REPRESENTATIVE METAL-MATRIX COMPOSITE MATERIALS\***

| Matrix              | Fibre           | Potential Applications                             |
|---------------------|-----------------|--|
| Aluminium           | Graphite        | Satellite, missile, and helicopter structures      |
| Magnesium           | -do-            | Space and satellite structures                     |
| Lead                | -do-            | Storage battery plates                             |
| Copper              | -do-            | Electrical contacts and bearings                   |
| Aluminium           | Boron           | Compressor blades and structural supports          |
| Magnesium           | -do-            | Antenna structures                                 |
| Titanium            | -do-            | Jet engine fan blades                              |
| Aluminium           | Borsic          | Jet engine fan blades                              |
| Titanium            | -do-            | High-temperature structures and fan blades         |
| Aluminium           | Alumina(FP)     | Superconductor restraints in fusion power reactors |
| Lead                | -do-            | Storage battery plates                             |
| Magnesium           | -do-            | Helicopter transmission structures                 |
| Aluminium           | Silicon Carbide | High-temperature structures                        |
| Titanium            | -do-            | High-temperature structures                        |
| Superalloy(Co-base) | -do-            | High-temperature engine components                 |
| Superalloy          | Molybdenum      | High-temperature engine components                 |
| Superalloy          | Tungsten        | High-temperature engine components                 |

\* abstracted from Ref.[7].

serious limitations of FRPs for their use in aerospace industry, viz. working at high temperature. Hence some reinforcements such as boron, carbon and graphite fibres used in FRPs were utilised earlier. However, with emphasis coming on high performance at lower cost, alternative reinforcements have been developed alongwith new fabrications processes. Reinforcements can be either continuous fibres or discontinuous fibres, whiskers and particulates. Satyanarayana [4] has suggested that continuous fibres of graphite and silicon carbide are expected to be the most common reinforcing fibres followed by those of  $Al_2O_3$ , carbon and boron; whiskers of SiC, and  $Al_2O_3$ , and, the least-expensive particulates of SiC,  $Al_2O_3$ , TiC, TiB and  $B_4C$ .

#### 2.1.3.2 KINDS OF MMCs

Metal-Matrix composites can be divided into seven general categories depending upon their structural constituents, viz. (a) Fibre Composites, (b) Laminar Composites, (c) Flake Composites, (d) Filled Composites, (e) In-situ grown Composites, (f) Dispersion Strengthened Composites, and, (g) Particulate Composites.

These will be briefly discussed in the following sub-sections.

##### (a) FIBRE-REINFORCED COMPOSITES

Fibre-reinforced composites present a new class of materials that offers another choice for selection and new

solutions to the machine designer for a high performance machine such as the internal combustion engines, industrial robots, turbo-machinery, variable speed rotary compressors etc. The choice of fibres has to be made in terms of, (i) the desired mechanical, physical and chemical properties, and, (ii) the environmental condition encountered during service, e.g. for a high-temperature composite material, fibres which preserve their strength at high temperature and a metal-matrix which possesses a very good oxidation resistance are needed.

Problems associated with the incorporation of the fibres into the matrix are listed below:

- (i) Introduction of the fibres in the matrix, without any mechanical damage,
- (ii) The perfect alignment and uniform distribution of the fibres, and, finally,
- (iii) The most important and also the most difficult problem to be solved is that of the bonding of the matrix to the fibres.

A variety of ceramic fibres and metal matrices have been employed in actual practice for the fabrication of fibre reinforced MMCs. Details of these are presented in a consolidated form in Tables-2.1 and 2.2. In a recent publication, by Verma [7], the manufacturing procedure and typical characteristics of alumina-silica fibres have been reported. One composition of

TABLE - 2.2

CERAMIC FIBRES AVAILABLE FOR SQUEEZE CASTING OF ALUMINIUM MMC COMPONENTS\*

| Trade Name                              | Composition, Vol%                                    |
|---|--|
| Saffil                                  | 95Al <sub>2</sub> O <sub>3</sub> -5SiO <sub>2</sub>  |
| Kaowool 17C                             | 81Al <sub>2</sub> O <sub>3</sub> -19SiO <sub>2</sub> |
| Kaowool 3000                            | 65Al <sub>2</sub> O <sub>3</sub> -35SiO <sub>2</sub> |
| Kaowool 2600                            | 50Al <sub>2</sub> O <sub>3</sub> -50SiO <sub>2</sub> |
| Fibremax                                | 72Al <sub>2</sub> O <sub>3</sub> -27SiO <sub>2</sub> |
| Fibrefrac                               | 50Al <sub>2</sub> O <sub>3</sub> -50SiO <sub>2</sub> |
| FP/Fibres                               | 99% Al <sub>2</sub> O <sub>3</sub>                   |
| Durocel/SiC<br>(Foamed Ceramic Preform) | 99.9% $\beta$ -SiC                                   |

\* abstracted from Ref.[7]



these fibres industrially known as 'fibrefax' conformed to 48%  $\text{Al}_2\text{O}_3$  and 52%  $\text{SiO}_2$  while the other composition contain 72%  $\text{Al}_2\text{O}_3$  and 27%  $\text{SiO}_2$ . Typical chemical analysis of these ceramic fibres is presented in Table-2,3 and the typical physical and mechanical properties of these fibres are listed in Table- 2.4. Todate, a number of high specific strength ceramic fibres have been developed such as Boron fibres, (prepared by CVD technique), carbon fibres, SiC fibres (PCS-Nicolan, CVD-AVCO process),  $\text{Al}_2\text{O}_3$  fibre, and, the whiskers of SiC,  $\text{Si}_3\text{N}_4$ , and  $\text{TiO}_2$ . Fibre-reinforced composites prepared from these materials result in high specific strength, heat resistance, excellent high temperature stability and superior abrasion resistance.

Fibre reinforced MMCs have already offered excellent performance in several applications limited to industrial use. These composites offer considerable weight saving, high strength at moderate temperature, wear resistance, thermal stability and durability in vacuum and in atomic oxygen environments. Typical examples of these applications include, bolts in special duty applications, direct injection diesel piston, connecting rods, fan blades, impeller of jet engine, gun tube, missile guidance system, helicopter transmission housing, centrifugal rotating drum, space station truss, skinnig machine parts, power semi conductor devices, etc. [8]. Ceramic fibres available for the manufacture of Al-based MMCs components are listed in Table- 2.2[9].

Satyanarayana [4] has pointed out that Niobium and Niobium-1%Zr composites reinforced with tungston alloy filaments

TABLE - 2.3

## TYPICAL CHEMICAL ANALYSIS OF CERAMIC FIBRES\*

| Material                       | Fiberfrax<br>Amorphous<br>Ceramic<br>Fibre | Fibrefrax Polycrystall-<br>ine Ceramic Fibre |
|--------------------------------|--|--|
| Al <sub>2</sub> O <sub>3</sub> | 49.2%                                      | 72.0%  |
| SiO <sub>2</sub>               | 50.5                                       | 27.0   |
| Na <sub>2</sub> O              | 0.2  | 0.10   |
| Fe <sub>2</sub> O <sub>3</sub> | 0.06                                       | 0.02   |
| TiO <sub>2</sub>               | 0.02                                       | 0.001  |
| Leachable<br>chlorides         | <10 ppm                                    | <10 ppm                                      |

\* abstracted from Ref.[7].

TABLE - 2.4

## TYPICAL PHYSICAL PROPERTIES OF VARIOUS FIBRES\*

| Property   | Fibrefax   | Fibremax<br>(Mullite) | Carbon<br>Fibres | Silicon<br>Carbide<br>Whiskers |
|--|------------|-----------------------|------------------|--------------------------------|
| Tensile<br>Strength,ksi<br>(MPa)                   | 250(1725)  | 120(830)              | 550(3800)        | 1200<br>(8300)                 |
| Young's<br>Modulus,msi<br>(GPa)                    | 15(105)    | 22(150)               | 33(230)          | 80(550)                        |
| Density,lb/in <sup>3</sup><br>(g/cm <sup>3</sup> ) | 0.10(2.7)  | 0.11(3.0)             | 0.06(1.8)        | 0.11(3.1)                      |
| Continuous<br>use Limit in<br>Air,°F(°C)           | 2300(1260) | 3000(1650)            | 600(315)         | 2550(1400)                     |
| Fibre Dia-<br>meter,mils(μm)                       | 0.10(2.5)  | 0.12(3.0)             | 0.28(7.0)        | 0.01(.3)                       |
| Fibre Length,<br>mils (μm)                         | 30(762)    | 30(762)               | Continuous       | 4.9(125)                       |

\* abstracted from Ref.[7].

provide the high temperature capability required for such systems to operate at their highest efficiency. Similarly Fe-Cr-Al-Y superalloy reinforced with tungsten fibres of W-Re-Hf-C exhibits, the best combination of high temperature strength, ductility, low strain rate hardening, oxidation resistance and corrosion resistance, whereas, thin walled graphite fibre-Mg tubes exhibiting zero coefficient of thermal expansion, a modulus approaching  $345 \text{ GN/m}^2$  and a density of  $1900 \text{ kg/m}^3$  are intended for aerospace applications where dimensional stability is critical, such as mirror mounts and antenna sub-structures for space platforms. Another composite developed at NASA, [4] consisting of 10 Vol% tungsten filaments in a copper alloy matrix provides 90% increase in strength with a loss in thermal conductivity of only 4% compared with currently used monolithic copper wall. Graphite/copper composites [4] having tailorable properties are useful for high temperature application in air and provide excellent mechanical characteristics as well as high electrical and thermal conductivity. Applications include impellers, space power systems, missile components and tribological systems which run at high temperatures where there is a possibility of failure of liquid lubricants. Iron based alloy with SiC or  $\text{B}_4\text{C}$  coated boron fibres composites [4] also exhibit superior stress-rupture strengths at  $871^\circ\text{C}$  to those of the strongest cast super alloys used in jet engine components.

Verma [7] has pointed out that amongst the various methods to fabricate fibre reinforced composites the liquid metal

infiltration process is most commonly used. It consists of the injection and subsequent solidification of liquid metal within the interstitial spaces of a fibre preform. The fibrous preform is an important step in making fibre reinforced composites by this technique. Preform are made in near net shapes. Preforms are designed to provide the needed performance at the lowest fibre concentration in order to minimise costs. Preform compositions, fibre volume, fibre type, and degree of fibre orientation are all essential to good metal matrix parts using this technique. Equally important is control of the preheating of the preform in order to avoid freezing of the liquid on the surface of the preform. Fukunaga [9] showed that this could result in incomplete infiltration in the final cast composite and also that the main parameters to be controlled in this process are molten metal temperature just before contact with the fibre preform, preform temperature, die temperature and its temperature gradient, applied pressure and plunger speed. A unique technique has been developed to minimize the direct contact between continuous fibres by S.Towata et al. [10,11] in which whiskers or particulates are distributed among continuous fibres. In their report they also revealed that additional reinforcement were extremely efficient in improving the strength of composites fabricated by liquid metal infiltration process.

A number of other liquid metallurgy techniques have been developed to incorporate fibres of different kinds into the metal base matrix. Mehrabian et al. [12,13] employed compocasting

technique for the dispersion of Duponts FP1- $\alpha$ -Al<sub>2</sub>O<sub>3</sub> fibres of 20 $\pm$ 5  $\mu$ m dia in Al-4 wt.%Mg melt. The temperature of the melt is set about 50 K above its liquidus temperature and kept there throughout the compocasting cycle. Fibres of about 6mm length are then fed into the melt through a vibrating hopper. Graphite stirrer blade positioned just below the surface of the melt is employed for stirring. After only a short period of time the fibres are completely wetted and suspended into the melt. The stirring speed is so chosen that most of the fibres are drawn into the melt through the vortex. The composites so produced contain discontinuous fibres which are randomly oriented in 3 dimensions. In order to align fibres in 2 dimensions, called 'plainer-random alignment', the composite was remelted and squeezed using a 200 ton hydraulic press. By this process, modulus of elasticity was improved by 50% and UTS was improved by 40% at a 23%V<sub>f</sub> level of FP 1- $\alpha$ -Al<sub>2</sub>O<sub>3</sub> fibres. SEM studies of the fractured surfaces showed that the failure of this composite occurs through the matrix and not at the interface. Auger electron spectroscopy and electron diffraction studies revealed that discrete MgAl<sub>2</sub>O<sub>4</sub> crystals are formed on the surface of the Al<sub>2</sub>O<sub>3</sub> fibres exposed to sufficiently well agitated Al-Mg melt [13,14,15]. The problem of wettability of dispersoid phases such as fibres and particulates have been discussed in detail by Banergy [14] and Mortensen [15] in their extensive reviews.

Das, Clegg and Zantout [16,17,18] employed normal 'Vortex' liquid metallurgy technique for the incorporation of

$\text{Al}_2\text{O}_3$  fibres in Al-3.75% Mg alloy and SiC fibres in Al and Zn based alloys. In one study, they dispersed SiC fibres (Nicalon-R) of dia 10-15  $\mu\text{m}$  and  $\text{Al}_2\text{O}_3$  fibre (Saffil-RF grade) of 3  $\mu\text{m}$  dia in Al-4.5%Cu melt [18]. In all these cases, a random distribution of fibres is obtained. In all their studies, they have attempted to squeeze the stirred slurry upto 140 MPa with attendant improvement in the mechanical properties. But because of the random orientation of the fibres, the improvement in the properties was not upto the expectations. In their EPMA studies involving  $\delta\text{-Al}_2\text{O}_3$  fibre, added to Al-3.75%Mg alloy, it was shown that Mg concentration around alumina fibre is not obtained. Also, the formation of a reaction product of the kind reported by Mehrabian et.al. [12,13] i.e.  $\text{Mg Al}_2\text{O}_4$  is not detected by these workers. The squeeze composites fabricated by these workers displayed good elevated temperature properties in addition to good fatigue life.

(b) **LAMINAR COMPOSITES**

A laminar or layered composite [3,19,20] consists of two or more different layers bonded together. The layers can differ in material, form and/or orientation. The main types of laminar composites include, (i) metal-metal laminates, (ii) metal-organic laminates, (iii) metal-inorganic laminates, (iv) organic-organic laminates, (v) organic-inorganic laminates, and, (vi) inorganic-inorganic laminates. Due to their relative importance, only laminated metal composites will now be briefly discussed.

A laminated-metal composite consists of two or more

layers or laminae of different metals completely bonded to each other so as to yield a composite material whose properties differ from and are more desirable than those of its constituents. By careful selection of these layers, laminated-metal composites may be designed to have outstanding properties such as resistance to wear, corrosion and impact or thermal or electrical characteristics, besides lower costs, good appearance and formability. Metal-laminate composites are manufactured by various techniques such as roll-bonding, co-extrusion, explosive welding and brazing.

There are three basic functional categories of metal-laminate composites, viz: (i) laminates, whose face is primarily decorative, (ii) laminates, whose face provides one or more important surface properties and whose base makes the laminate cheaper only or stronger than the equivalent face material alone, and, (iii) laminates that provide special bulk properties, or properties resulting from a chemical reaction between the laminate-face and the base.

There are two major classes of laminates based on the method of their fabrication, namely, (i) the precoated-metals and, (ii) the clad-metals. In precoated metal, the face is formed by building-up the second constituent on a substrate to form a thin, essentially continuous film. The face of a clad-metal is usually considerably thicker than that of a precoated-metal. Cladding thickness generally ranges from 2.5-2.0% of total laminate thickness depending on the application. However, this proportion may be as high as 90% in some special cases.



A great variety of common metals have been employed for the preparation of laminated-metal composites. A few common examples include, (i) copper-clad stainless-steel as an excellent roofing material, (ii) cupro-nickel cladding on copper as a corrosion-resistant, low cost, attractive appearance material for coinage, (iii) stainless steel-clad carbon steel, (iv) seamless-clad nuclear fuel elements, (v) mild steel solder laminates, (vi) stainless steel-aluminium laminates, (vii) Uranium Zirconium alloy-clad with Zircaloy-2 with Zn-1.5, Fe-0.1, Ni-0.05, Cr-0.1, etc. Typical applications of laminated metal composites include aircraft structure, anodes for aluminium potlines, roofing and wiring, copper-clad aluminium wire, chemical process-equipments, clad-metal bullet proof jackets, coinage, dual hardness armour plates, marine structures, nuclear reactor fuel-elements, thermostats etc.

(c) **FLAKE COMPOSITES**

A flake composite [3,20] consists of flakes held together by an interface binder or incorporated into the matrix. Being flat, flakes can be tightly packed to provide a high percentage of reinforcing material for a given cross sectional area.

Overlapping and touching metal flakes provide electrical conductivity through the composites. With non-conductive flakes such as mica or glass, it is possible to obtain good dielectric properties as well as resistance to heat. By selecting proper flake material and by controlling flake shape and orientation, a number of useful properties can be obtained from flake composites.

A limited number of materials are used in flake composites. Most flakes are of aluminium, silver, mica or glass and therefore, most metal flake composites consist of aluminium and silver flakes.

**(d) FILLED COMPOSITES**

Filled composites [3,20] consist of a continuous three dimensional structural matrix infiltrated or impregnated with a second phase filler material. The matrix may be an ordered honey comb, a group of cells, or a random sponge like network of open pores. In most filled composites, the matrix provides the framework and the filler provides the desired functional properties.

Most filled composites in use today consist of a matrix having random network of open passages of pores, that lend themselves to filling, for example, cast-metal or powder-metal parts, ceramics, carbides, graphite and foams. The open network of a sponge-like structure can be filled with a wide variety of materials such as metals, plastics, lubricants etc. Impregnants can serve several specific functions for example it may provide better bearing properties, or it may make metals pressure-tight, or it may make a metal honeycomb structure filled with ceramics resistant to high heat-fluxes etc.

**(e) IN-SITU GROWN COMPOSITES**

Among the various methods for producing fibre reinforced

composite materials that have been prepared and/or invented, perhaps the most elegant, as well as easiest to apply, is that in which the fibres are grown in-situ, i.e., the fibres are developed inside the matrix which is itself automatically formed during solidification of certain molten, multi-component systems. The suitable systems to work with are eutectics, in which the various phases precipitate simultaneously and thus grow side by side forming a regular alternate structure of either fibres or lamellae embedded in the matrix. This method is the only one which in addition to producing an ideal structure, automatically fulfills the two requirements most difficult to realize by all other methods, namely good bonding between the fibres and matrix, and the growth of whiskers in very long or continuous lengths. Kovacova [21] has emphasized that this latter aspect, contrasts with the very limited short length, only few millimeters, when they are prepared separately.

For technological applications of unidirectionally solidified composites, priority is now given to multi-component systems rather than to binary alloys. The main advantage of this lies in the possibility of producing a wider variety of alloys of different compositions and having larger amounts of the reinforcing phase. However, successful application of such multi-component systems requires meeting more strict specifications in the selection of alloys and in selecting their solidification parameters. A Golden Rule to be observed in selection of the appropriate alloying element is that it must not

induce or help to form any primary phases in unwanted shapes such as the dendritic shapes. Another important condition is that the solidification interface must be planer. Lawson [22] has emphasized that if this is not observed, then a cellular structure could form due to the deterioration of such a non-planer interface, resulting in a corresponding rapid deterioration of the mechanical properties not only at elevated temperatures but also at normal or room temperatures. Formation of primary phases can be suppressed by choosing the mono-variant type of alloys from a binary to a ternary eutectic system, possessing the required equilibrium diagram. The planar solidification interface can be secured using Tiller's formal analysis of constitutional under-cooling [23]. It is given by the following relationship (expressed in units of  $^{\circ}\text{C}\cdot\text{sec}\cdot\text{mm}^{-2}$ ) :

$$\left(\frac{G}{R}\right)^* = \frac{-m}{D} \frac{1-k}{k} \cdot C_o \quad \dots\dots\dots (2.1)$$

where,  $G$ , is the temperature gradient,  $R$  is the solidification rate,  $m$ , the slope of the eutectic liquidus line,  $D$ , the liquid diffusion coefficient of the impurity atom,  $k$ , the partition-coefficient of the impurity atom, and,  $C_o$ , its concentration.  $\left(\frac{G}{R}\right)^*$  is the critical value of ratio  $\left(\frac{G}{R}\right)$  for plane-front solidification. When  $\left(\frac{G}{R}\right)$  is less than that given by Eq.(2.1), cells or dendrites of the new or solidified phase form. For in-situ grown composites to occur,  $\left(\frac{G}{R}\right)$  ratio must be greater than that given by the above equation. Piatti [1] has pointed out that, under strictly controlled plane-front solidification

conditions, the solid-liquid interface moves at a constant velocity through the entire length of the ingot, and the two phases  $\alpha$  &  $\beta$  formed at the interface will follow the solidification front movement leading to the lamellar morphology with the single lamellar oriented along the direction of heat extraction, as shown in Fig.2.2, which is self-explanatory.

Unidirectional solidified turbine blades, with columnar dendritic structure have now come of age. Careful control in processing is required to obtain the directional solidification, but there is the practical advantages that only relatively low ratios of thermal gradient to growth rate ( $\frac{G}{R}$ ) are required. Directionally solidified eutectic-like 'in-situ composites' have great potential for achieving higher temperature and as pointed out by Lemkey [24] are envisaged as the next generation high-temperature gas-turbine blade materials. However, these materials have the disadvantage, from their processing stand-point of requiring high values of ( $\frac{G}{R}$ ) during solidification. A third, as yet relatively unexploited, intermediate structure, grown at ( $\frac{G}{R}$ ) ratios between the above two extremes, is emerging as a possible 'compromise high temperature material'. Dunn and Farag [25,26] have suggested that these intermediate, 'cellular in-situ composites' are attractive since they may offer much of the mechanical property advantage of the true in-situ composite and yet require lower ( $\frac{G}{R}$ ) ratios in casting and hence offer processing economies.

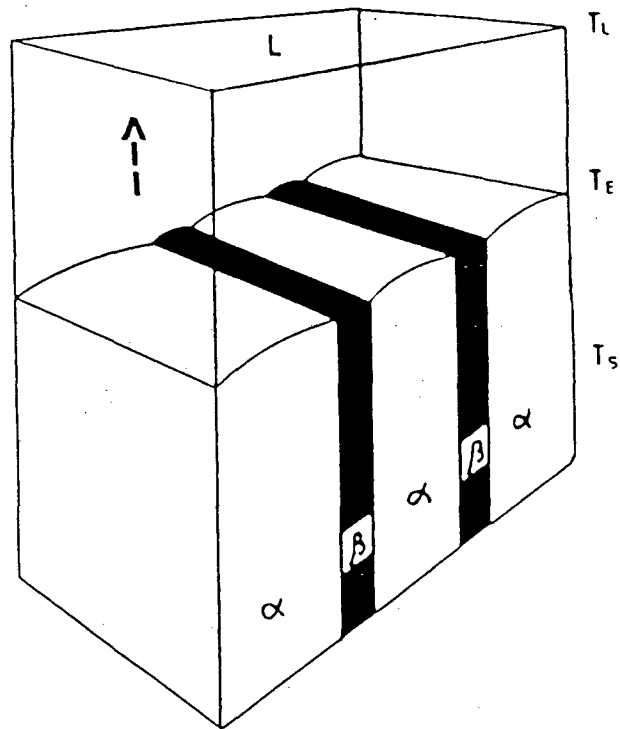


FIG.2.2 Formation of a lamellar structure ( $\alpha$  and  $\beta$  phases) in a unidirectional solidification of a eutectic. The solidification front is perpendicular to the direction of growth (direction of arrows).  $T_L$ ,  $T_E$  and  $T_S$  are the temperature of the liquid (L), the solidification front and the solid, respectively (Ref.1).

## (f) DISPERSION STRENGTHENED COMPOSITES

In dispersion strengthened composite materials, the matrix is the major load-bearing constituent. The fine dispersion is present to impede the motion of metal matrix-dislocations. The prime variables in determining the effectiveness of a dispersion are the mean free matrix path,  $\lambda$ , between particles in the dispersion and the interparticle separation,  $D_p$ . According to Broutman [2] these parameters are related to the particle diameters,  $d$ , and volume concentration of particles,  $V_p$ , by the following expressions,

$$\lambda = (2 d/3V_p) (1-V_p) \dots\dots\dots (2.2)$$

$$D_p = (2 d^2/3V_p) (1-V_p) \dots\dots\dots (2.3)$$

For a matrix-dislocation to pass through a dispersion of fine particles, the applied stress must be sufficient to bend the dislocation into a semi-circular loop. The smallest radius of curvature,  $R$ , to which a dislocation can be bent under the influence of an internal stress field  $\tau_i$ , is,

$$R = G_m b/2 \tau_i \dots\dots\dots (2.4)$$

where,  $G_m$ , is the matrix shear modulus, and,  $b$ , is the Burger's vector. Hence for the dispersion of interparticle spacing,  $D_p$ , the stress required to bow the dislocation about the dispersion is,

$$\tau_i = G_m b/D_p \dots\dots\dots (2.5)$$

since, as shown in Fig.2.3, representing sequence of dislocation movement passing through the dispersoid net with increasing stress values,  $D_p = 2R$ . Once the stress is large enough to create a radius

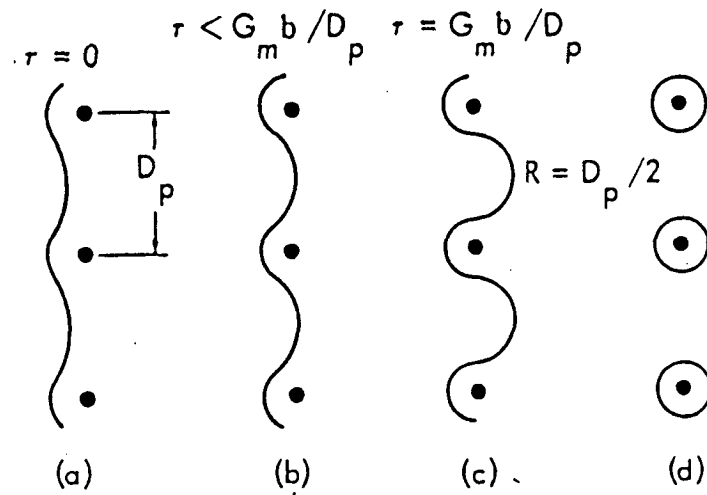


FIG. 2.3 Sequence of dislocation movement passing through a dispersoid net (Ref.2).



$R = \frac{D_p}{2}$ , the dislocation loop can be expanded without the need for any further stress-increase.

Variation of mean free matrix path,  $\lambda$ , and volume fraction,  $V_p$ , inter-related by Eq.(2.2), are plotted in Fig.2.4 for dispersoid particle diameters,  $d$ , of 0.01, 0.1 and 1.0  $\mu\text{m}$ . Typical ranges for these parameters in dispersion-strengthened composite-materials lie between the limits indicated, viz,  $\lambda = 0.3$  to 0.01  $\mu\text{m}$ ;  $D_p = 0.3$  to 0.01  $\mu\text{m}$ ;  $V_p = 0.01$  to 0.15, and,  $d = < 0.1$   $\mu\text{m}$ .

The sequence of stress induced dislocation bowing, with an increase in stress, referred to above, is also depicted in Fig.2.3. It will be observed, that as the applied stress is increased from  $\tau = 0$  to  $\tau = G_m b/D_p$ , the dislocation line progressively bows further until, at stage C, it can move through the particles without any further stress increase. Since the dislocation line cannot be bent to a zero radius, a loop of slipped area is left about the dispersed particles after the dislocation line has moved through them,

The relationship between the 'scale of dispersion' and the 'yield strength' was first proposed by Gensamer [27] on the basis of his studies on carbon steels tempered to produce various carbide dispersions, as represented by following expression;

$$\sigma = - A \log \lambda + B \quad \dots\dots\dots (2.6)$$

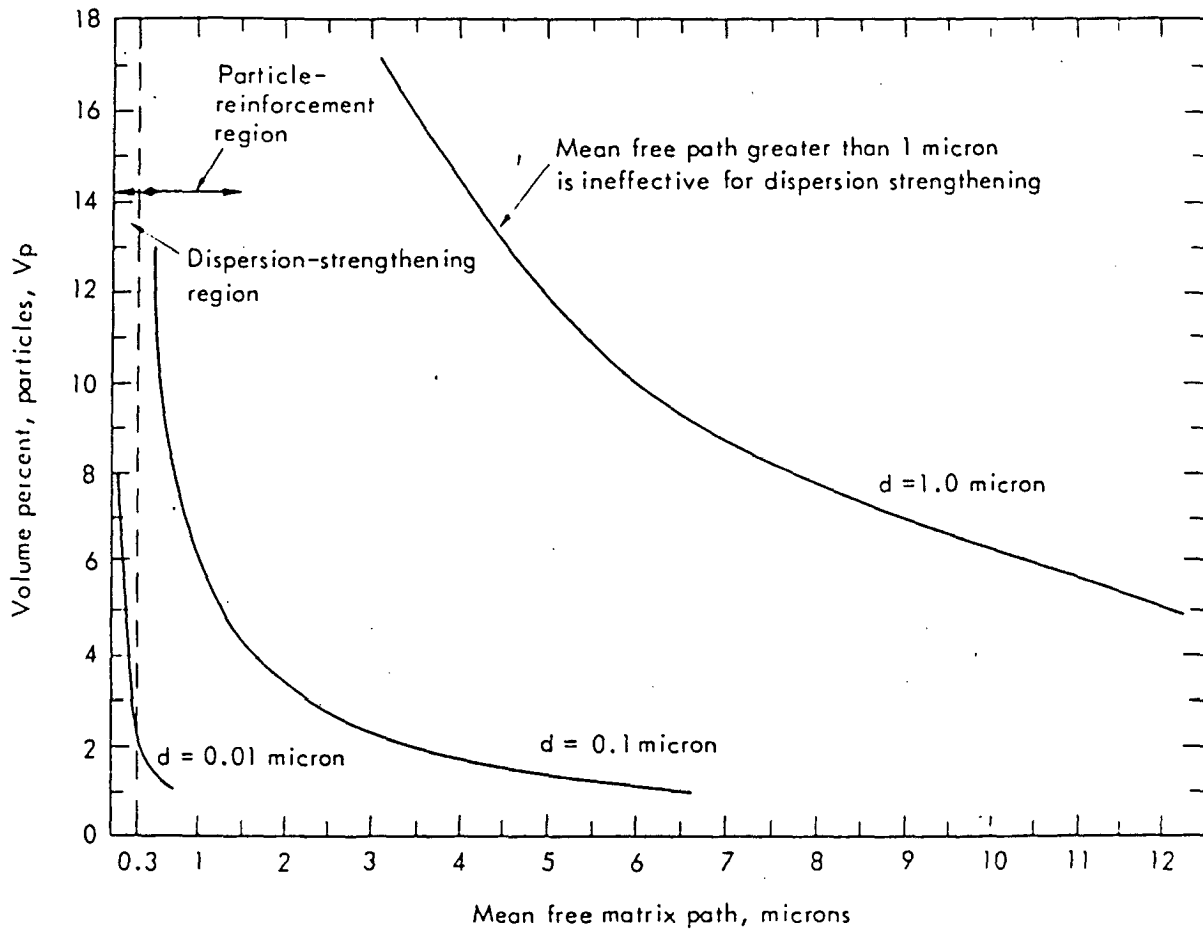


FIG. 2.4 Relationship between dispersoid volume fraction and mean free matrix path for dispersion-strengthened composite materials of different dispersoid size. (Ref.2)

where,  $\sigma$ , is the yield strength,  $\lambda$ , is the mean free path, and, A & B are constants, characteristic of the matrix system under study.

Other workers, viz, Ansell and Lenel [28] have also concluded that the yield strength,  $\sigma$ , of tempered steel should be described in terms of the inter-particle spacing, as expressed by following relationship,

$$\sigma = \frac{K}{D_p} \quad \dots\dots\dots (2.7)$$

where,  $D_p$ , is the interparticle spacing and K is a constant.

The primary advantage of dispersion-strengthened materials, however, is not their ability to improve the room temperature yield strength or work hardening rate of elemental or alloy matrices but their ability to maintain this increased yield strength and the resulting increase in creep resistance over a wide range of temperature, upto almost 80% of the melting point of the matrix. As a matter of fact, the effectiveness of the dispersion is determined by its insensitivity of increase in temperature, distinguishing dispersion-hardened composites from precipitation-hardened alloys, since the latter weaken as a result of ageing, caused by increasing temperatures. The aforesaid dispersion in the dispersion-hardened materials is made from oxides, carbides and/or boride particles.

Various commercial and experimental techniques available for the preparation of dispersion-strengthened alloy systems include the following:

(A) Commercial processes: (i) Surface oxidation, (ii) Internal oxidation, (iii) Reduction processes, (a) Du Pout Co precipitation technique, (b) DS Nickel process, and,

(B) Experimental processes: (i) Mechanical mixing, (ii) Salt decomposition, (iii) Reduction processes.

(g) **PARTICULATE COMPOSITES**

In particulate composites, the second-phase particles having a length/diameter ratio of approximately unity are dispersed in the base-matrix to result in its strengthening. The particulate composites differ from dispersion-strengthened materials by the larger size of the dispersoids exceeding  $1.0 \mu\text{m}$  with their volume concentrations as high as 30%. Unlike dispersion-strengthened materials, where the matrix acts as the only load-bearing constituent and the strength of the matrix is increased in proportion to the effectiveness of the dispersoid to act as a barrier to the motion of matrix dislocations, in the particle-reinforced composite, the matrix and the dispersed-particles both share the load. Because of the non-directionality of the mechanical properties and also the ease of fabrication into various shapes [29-33], the particulate

composites have attracted widespread attention for a variety of applications. In the conventional dispersion-strengthening alloys prepared by casting methods, the dispersion of second-phase (amount, size and shape) in the matrix is governed by thermodynamic considerations. Hence opportunities for strengthening of alloys by dispersion of second-phase is restricted. In particulate composite materials, however, it is easily possible to control the amount and morphology of the second-phase particles to much greater extents by choosing suitable manufacturing techniques and operating parameters. The range of attainable properties is therefore much wider in case of the particulate composites.

The production of metal-based particulate composites has been tried from two principal approaches, one is the Powder-Metallurgy and the other is by Foundry Technique. Mechanical mixing [34-35] of two comminuted phases by means of mixing and blending in ball mills, colloid mills or blenders followed by compactions, sintering or hot pressing and consolidation by metal-working such as hot rolling, forging and especially extrusion are the powder metallurgical approach for introducing fine-or-coarser-particles in the matrix of a particle strengthened component. In spite of the simplicity of this process the technique has some inherent problems [36] of inferior dispersion or distribution due to adherence and clustering or agglomeration depending on the size and the physical nature of the particles.

In a comparative study [37] between powder metallurgy and other competitive processes for the mass production of structural parts it has been observed that the powder metallurgy process is economically preferable for components weighing 20 to 200 gms. From the view point of energy consumption, the advantage of powder metallurgical process over other competitive processes is doubtful [37]. A comparison of the potential and the limitations of sintering and foundry technology reveals [38] that for manufacturing of complex precision parts with high dimensional accuracy, the foundry technique is more advantageous than powder metallurgy, specially when die-casting can be employed.

Fabrication of metal base composites by foundry technique has been pursued over a decade now. This is a more direct and simpler process than other energy intensive techniques for making isotropic composite materials by homogeneous dispersion of short fibres or particles in molten metals or alloys [39]. Several variations have been applied in Foundry Technique for the production of particulate composites such as Vortex method, blowing of reducible oxide and high melting point materials in molten aluminium, infiltration method, blowing of oxygen in molten aluminium. Out of these processes the Vortex method has drawn a considerable attention since the process offers a reasonable extent of control over the incorporation of particles in the composite and application of the process for making various size of products are comparatively easier in this method.

## 2.1.4 DEVELOPMENTS IN CAST PARTICULATE COMPOSITES

### 2.1.4.1 INTRODUCTION

During the past few years, there has been a search for alternative techniques of producing particulate-composites, as the conventional powder-metallurgy techniques have proved to be very energy intensive. The chunk materials available from extraction processes have to be disintegrated into powders by the application of energy and then the powders of different constituents have to be mixed, pressed and sintered with a further expenditure of energy. Pressing of powders put a natural limit to the size of product because uniform compacting will not be possible otherwise and thus a degradation of product quality is inevitable beyond a practical size limit. It is because of these reasons that powder-metallurgical products are prohibitively expensive. Recently, 'Liquid-Metallurgy Techniques' [40-60] have been investigated intensively and tried as a viable alternative to conventional P/M techniques for the production of particulate-composites.

In 'Liquid-Metallurgy Techniques', basically, refractory particles such as graphite, alumina, magnesium oxide, silicon carbide,  $TiO_2$ ,  $ZrO_2$ , Illite clay, mica etc. are introduced into liquid melt prior to solidification. The liquid melt with dispersed particles is then frozen fast to produce cast particulate composites.

#### 2.1.4.2 TYPES OF CAST PARTICULATE COMPOSITE

Generally, there has been interest in Al-Al<sub>2</sub>O<sub>3</sub>, Al-Al<sub>2</sub>O<sub>3</sub>-MgO and Al-graphite systems. The choice of aluminium as base-matrix is firstly because of its industrial significance due to high strength to weight ratio and secondly because of ease of handling and fabrication due to its low melting point.

The Al-Al<sub>2</sub>O<sub>3</sub> and Al-Al<sub>2</sub>O<sub>3</sub>-MgO systems [47-49] are important for their application as structural material at elevated temperatures due to their high strength and improved creep resistance as seen in SAP materials.

The Al-graphite system is important, since it finds potential application as piston material in all aluminium engines and as bearing materials.

Besides pure aluminium, a number of aluminium-base alloys such as Al-13%Si, Al-4.2% Si-3.2%Cu-0.2%Mg-0.6%Mn, Al-0.2% Si-4.5% Cu-0.2%Fe, Al-7.2% Si-0.2% Cu-0.2%Fe, Al-0.76% Si-2.5% Cu-0.6% Fe-0.76% Ni-0.5% Mn-0.5% Zn etc. have been employed to prepare particulate composites. A recent study by Rohatgi et.al. [31] has shown that Tin-graphite particulate composites can be used in bearings or as bearing alloys or even as a master alloy to disperse graphite in the matrix of other alloys through the 'Liquid Metallurgy Technique'. Many of the aforementioned Al-base alloys have also been employed for the fabrication of particulate composites in heat-treated condition.



As a variation of the standard 'Liquid Metallurgy Techniques', Mehrabian and co-workers [12], employed compocasting technique for the dispersion of broken  $\alpha$ -Alumina fibres of about 15 to 25  $\mu\text{m}$  dia and about 3 mm length. The stirred slurry obtained upon compocasting was then squeezed using forging dies and ceramic filters. A similar attempt has been made by Clegg and co-workers [17], but in this work SiC fibres of about 10-15  $\mu\text{m}$  dia and 3 mm length were stirred in superheated Al-4.5%Cu alloy and then squeeze-cast at 140 MPa. This class of composites viz. the compocast product also display excellent elevated temperature properties [12,17].

#### 2.1.4.3 LIQUID METALLURGY TECHNIQUES OF PREPARING PARTICULATE COMPOSITES

Several processes involving introduction of particles like graphite, alumina, magnesium-oxide, silicon carbide etc. in aluminium-base alloy melts to produce cast-particulate MMCs have recently been developed. These may be classified as under:

- (a) Fluidization and Injection technique
- (b) Vortex technique using an impeller
- (c) Pellet method
- (d) Infiltration technique

##### (a) FLUIDIZATION AND INJECTION TECHNIQUE

In an earlier attempt, Badia and Rohatgi [50] tried to inject graphite particles into molten aluminium bath using a

nitrogen-gun, as shown in Fig.2.5. In this gun, the particles are fluidized by nitrogen gas and are injected into the molten metal through the graphite nozzle. However, the kinetic energy imparted to the particles by the gas was not sufficient for its transfer into liquid under the gas pressures used in their experiments. Interestingly, when the surface of graphite particles was coated with nickel, they displayed good wettability for liquid aluminium and therefore it was found possible to make a suspension under similar gas pressures. Wettability was, therefore, found to be the main problem in case of all types of dispersoids such as alumina, silicon carbide etc. Therefore, as a matter of general practice, Rohatgi et.al. [43,59] coated graphite, alumina and silicon carbide particles with either nickel or copper in their later experiments. Badia, Rohatgi and Ray [50,58] found that if the liquid melt is superheated to-about  $1200^{\circ}\text{C}$ , the wettability is considerably improved. They further reported that the inclination of graphite nozzle with the liquid, bath also influences the degree of particle transfer into the bath.

(b) **VORTEX TECHNIQUE**

Badia, Rohatgi and co-workers [53-58,60] developed this technique of producing cast-particulate composites. This method involved stirring the alloy melts using an impeller, and, then introducing nickel-or copper-coated graphite, or nickel-coated alumina particles at the centre of the vortex produced by stirring. Copper was coated onto graphite particles using cementation technique [50] and nickel was coated onto graphite particles using carbonyl process [56].

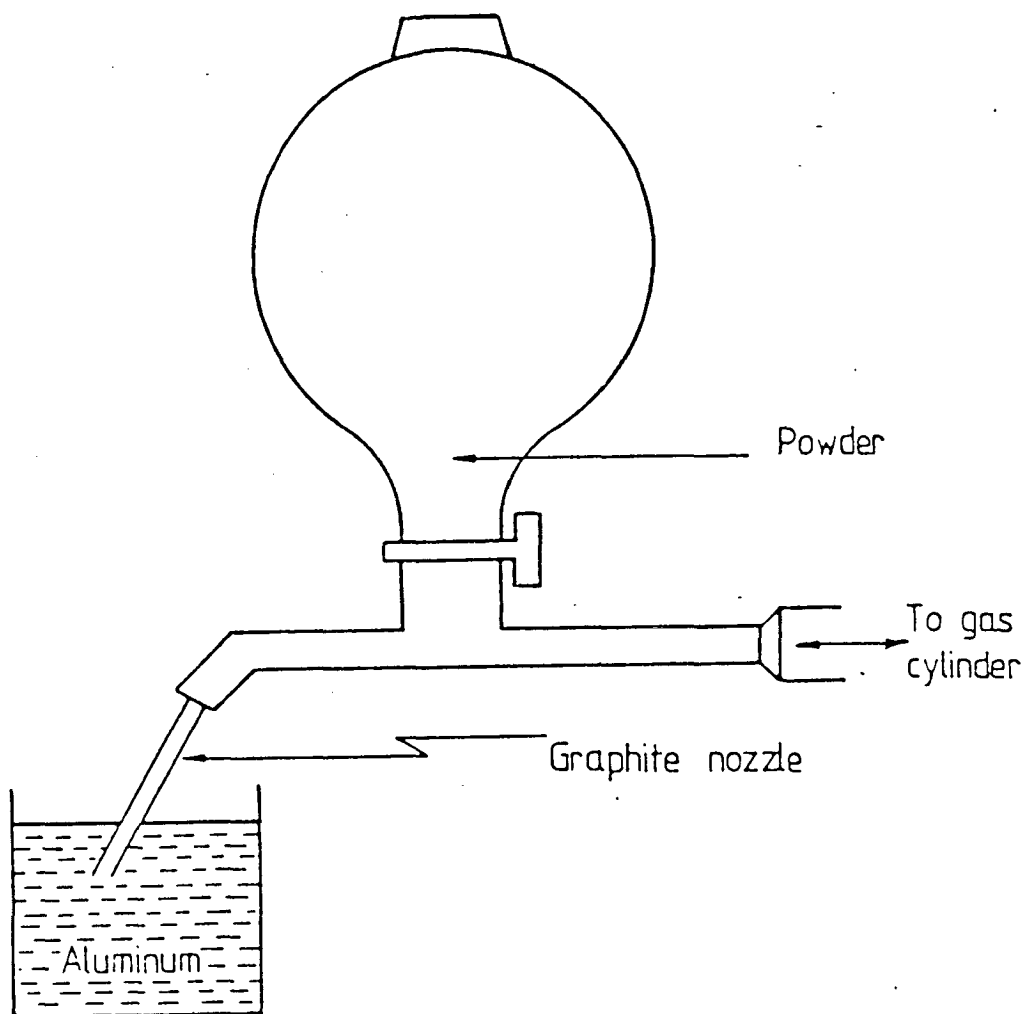


FIG.2.5 Schematic diagram showing fluidization and injection technique. (Ref.58)

In another variation, Pai, Rohatgi and Ray [57,58] employed fresh magnesium metal additions to liquid aluminium bath prior to the addition of uncoated alumina particles in an effort to overcome wettability problems. In some of their experiments, fresh magnesium pieces of about one cm. cube size were first added in the centre of the vortex and then alumina particles were added soon after. In all these experiments, three kg. melts of either pure aluminium or F-22 aluminium alloy of composition 2.9% Cu, 2.5% Si, 0.7% Ni, 0.5% Mn, 0.5% Zn, 0.6% Fe, balance aluminium, were used. In all the cases, the melt temperature was kept between  $750^{\circ}\text{C}$  and  $790^{\circ}\text{C}$  during the addition of  $\text{Al}_2\text{O}_3$  particles, and, the casting temperature was maintained at around  $720^{\circ}\text{C}$ .

These workers investigated the influence of various parameters such as, (a) the presence of residual magnesium present in the melt as an alloying element, (b) fresh magnesium additions just prior to alumina additions, (c) time elapsed between magnesium plunging and alumina additions, and, (d) solidification pattern of the casting, on the extent of retention of uncoated alumina particles and their distribution in the cast Al- $\text{Al}_2\text{O}_3$  particulate composite. Some of their interesting results are shown in Figs.2.6-2.9. From these studies, therefore, they concluded that freshly added magnesium leads to higher alumina retention in castings as compared with that when it is present as an alloying element in the same amount, at all magnesium contents and at all speeds of stirring. However, increase of stirring speeds, from, approximately 50-60 rpm in manual stirring to,

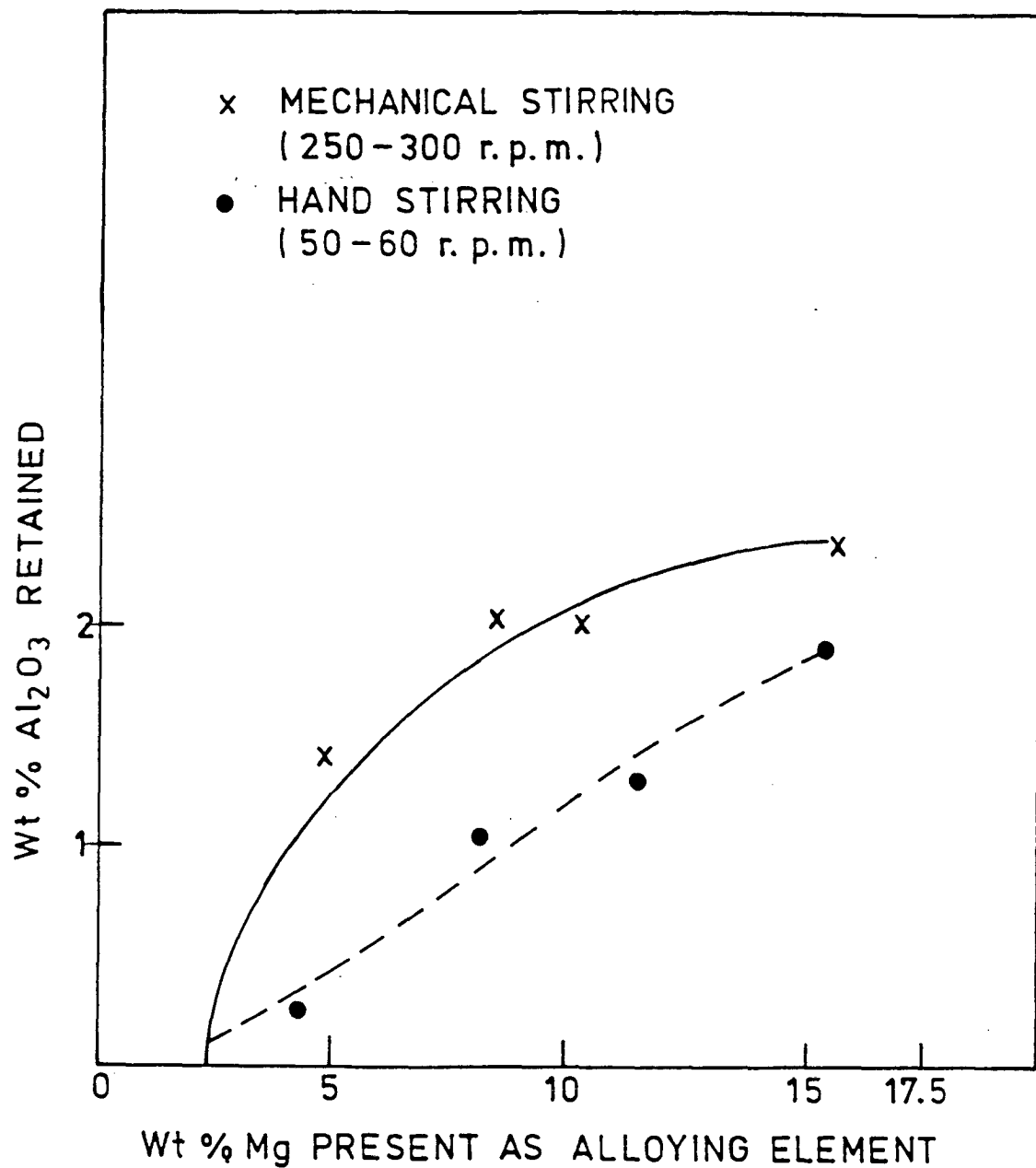


FIG.2.6 Plot of a weight percentage of alumina retained in the castings vs. the weight percentage of the magnesium present as an alloying element in pure aluminium for both manual and mechanical stirring.(Ref.58)

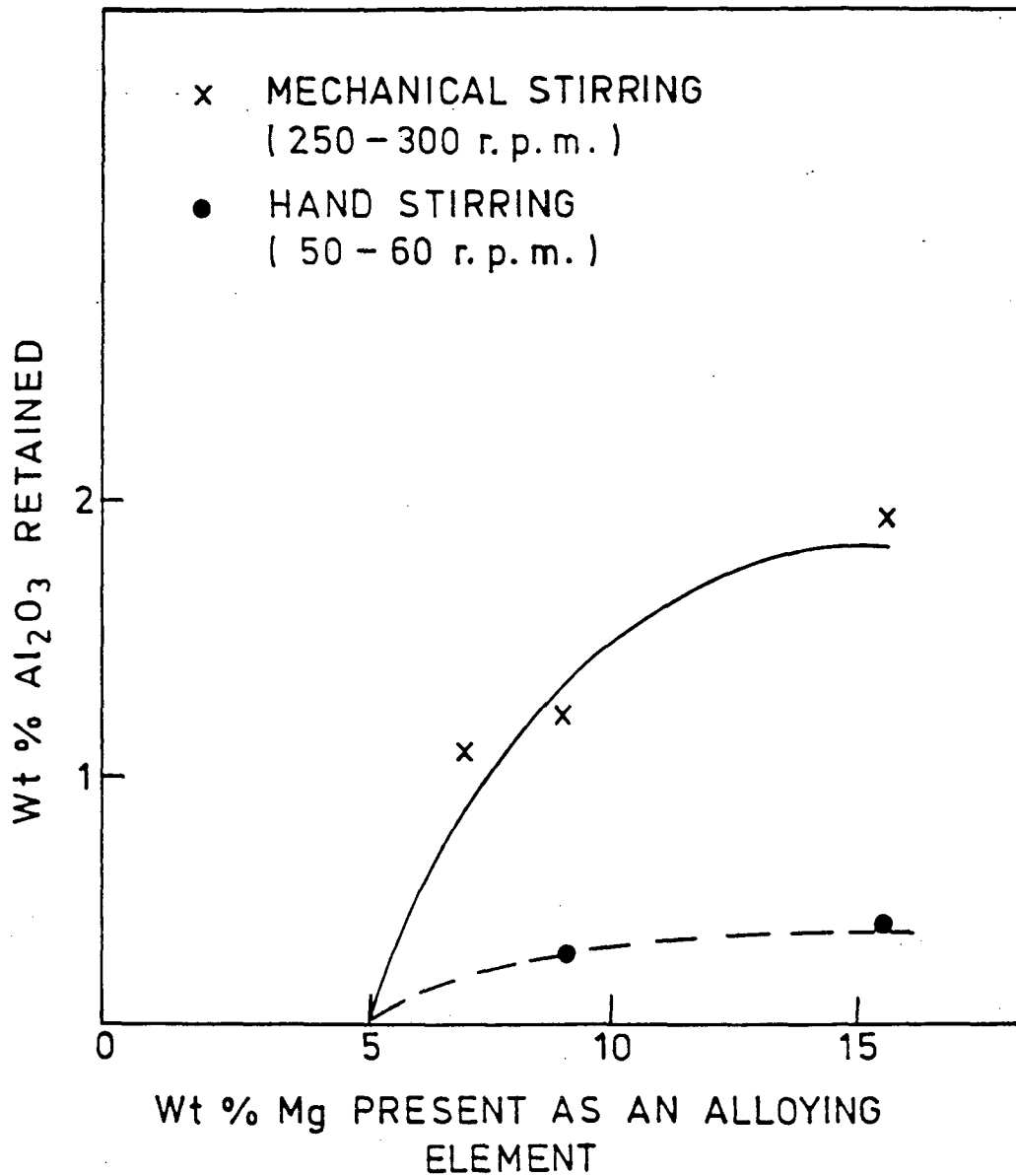
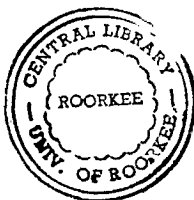


FIG.2.7 Plot of weight percentage of alumina retained in the castings vs. the weight percentage of the magnesium present as an alloying element in F-22 alloys for both manual and mechanical stirring. (Ref.58)



245662

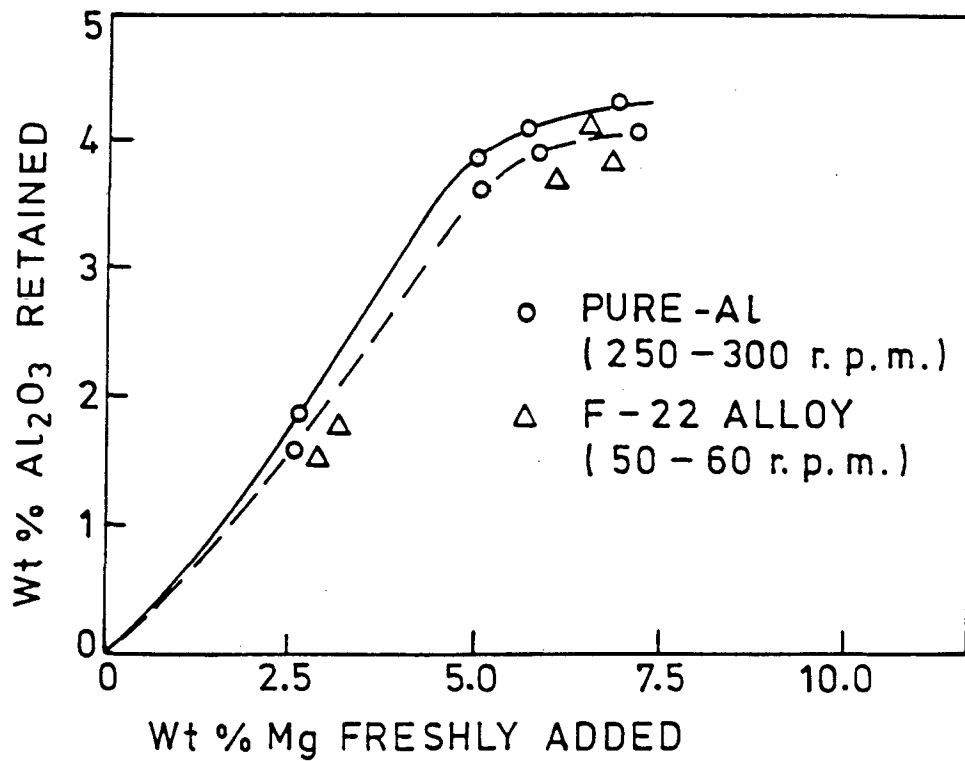


FIG.2.8 Plot of weight percentage of alumina retained vs. the amount of freshly added magnesium for F-22 alloy and pure aluminium at hand and mechanical stirring. (Ref.58)

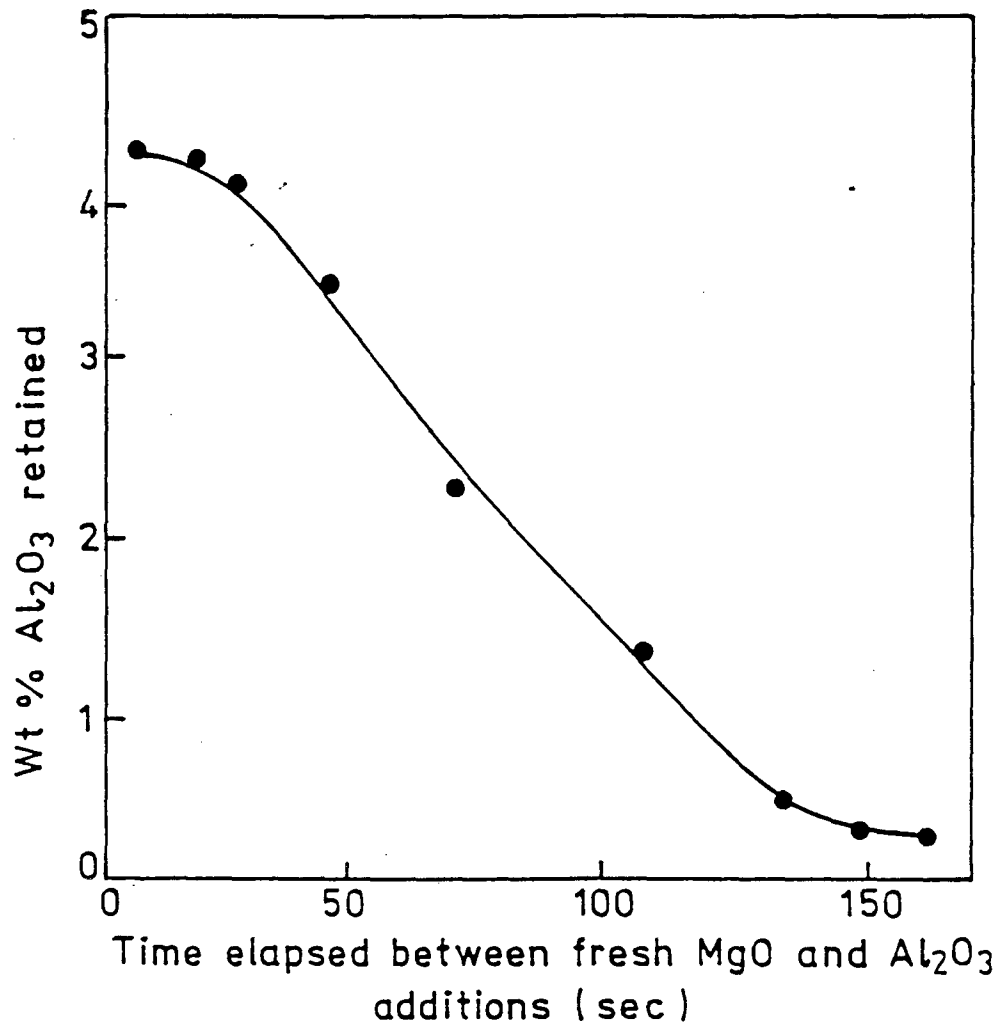
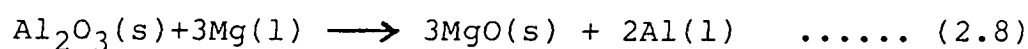


FIG.2.9 Plot of weight percentage of alumina retained vs. the time elapsed for addition of alumina particles to the melt. (Ref.58)



approximately 250-300 rpm in mechanical stirring, largely improved the extent of retention of alumina particles both in case of pure aluminium as well as in the F-22 alloy melts containing freshly added magnesium.

An important contribution of this research [57,58] was to show that the presence of magnesium, either by way of prior alloying or by fresh additions of magnesium to liquid aluminium melts, acts in two ways. Firstly, the presence of magnesium decreases the contact angle between alumina and liquid aluminium melt, thereby considerably improving their wettability and secondly, magnesium has the capability of chemically altering the substrate of alumina particles according to the following reaction, thereby improving the wettability:



$$(\Delta G^\circ = -30,290 + 3.02T \log T + 11.37 T), T \text{ in K} \quad \dots\dots (2.9)$$

and therefore at 1000K,  $\Delta G^\circ = -32.6 \text{ k.cal.}$

The surface of alumina particles therefore can be reduced by magnesium at 1000 K to form MgO(s) and Al(l). This MgO, as pointed by McCoy et.al. [61], shows good wettability for liquid aluminium. As a result, chemically altered alumina particles, particularly on the surface, show good wettability towards liquid aluminium and are, therefore, retained in the melt. It was also pointed out by Pai, Rohatgi and Ray [57,58] that in extreme cases, when the magnesium added was as high as 14.5%, some of the alumina

particles were completely transformed to MgO. Almost similar observations have been recorded by Mehrabian et.al. [12,13,62] during the fabrication of aluminium -  $\alpha$  -Al<sub>2</sub>O<sub>3</sub> fibre composites using compocasting technique. Using the sophisticated Augur and electron diffraction techniques, they demonstrated that discrete crystals of MgAl<sub>2</sub>O<sub>4</sub> spinel are present on the fibre surface.

(c) **PELLET TECHNIQUE**

This technique was developed by Pai and Rohatgi [59] for the preparation of aluminium-graphite particulate composites. In this process, copper-or nickel-coated graphite particles are mixed with aluminium powder and then the mixture is pressed into the desired shape of pellets. These pellets are plunged into liquid aluminium-alloy melts prior to the hand-stirring of melt, followed by casting. The variables examined were the optimum size and amount of aluminium powder, the pressure applied to make the pellet, and the size of the coated graphite particles. A number of aluminium-base alloys such as Al-Si-Fe, Al-Si-Cu-Mg-Mn etc detailed in sub-section 2.5.2 were employed for the preparation of particulate composites using pellet technique.

The investigations [59] revealed that for the most efficient recovery of graphite particles in the cast-particulate composite, the pellet should be made from a mixture of 67 wt.% of 80  $\mu$ m copper-or nickel-coated graphite powder and 33 wt.% of 400  $\mu$ m size aluminium powder, and the pellet should be compacted at a pressure of 2 to 5 kg.mm<sup>-2</sup>. They [59] also found that graphite

particles were generally present in inter-dendritic regions and that the inter-particle distance varied from 100 to 1000  $\mu\text{m}$ . Their results also indicated that graphite containing copper bearing alloys respond to solutionizing and ageing treatment. This would permit production of alloys with a range of strengths and ductilities to suit any desired application.

Additions of copper-coated graphite particles were found to decrease the tensile strength and ductility of all as-cast aluminium-base alloy composites.

#### (d) INFILTRATION TECHNIQUE

The infiltration technique has already been employed extensively for the preparation of fibre-composites. However, Rohatgi and co-workers [43] made use of vacuum infiltration technique probably for the first time for the production of particulate-composites using nickel-and copper-coated graphite powders. Their basic idea was to prepare tin/graphite particulate composites for use as bearings or bearing alloys. This composite could also be used as a master alloy for dispersing graphite in the matrix of other alloys through any liquid metallurgy technique. For example, they suggested that tin/graphite alloys can be dispersed in aluminium alloy melts to make an aluminium/tin/graphite composite for bearing applications. Graphite, being a solid lubricant, could reduce the requirement of tin, which is an expensive and scarce metal, in aluminium/tin bearing alloys.

Their results [43] confirmed that metal-coated ceramic particles could be successfully used to make particulate composites by infiltration of liquid metals. The metal coatings can be very useful in providing the wetting between the liquid alloys and ceramic particles, which in turn improves the extent of infiltration. The metal coatings can also increase the density of the ceramic particles, which will prevent them from floating.

Basically, the copper-or nickel-coatings onto the graphite or ceramic particles are dissolved and alloyed with the base-matrix during infiltration. This results in an increase in the hardness of these alloys.

They found that the optimum conditions for infiltration are different for different liquid metals. For example, their attempts to infiltrate liquid aluminium-13% silicon alloy, at temperatures upto  $900^{\circ}\text{C}$ , in beds of uncoated graphite, copper-coated graphite and nickel-coated graphite were unsuccessful, although Al-Si alloy wets nickel and copper. However, complete infiltration and good dispersion was obtained in case of tin-base composites.

#### **2.1.4.4 PROBLEMS OF VORTEX LIQUID METALLURGY ROUTE AND THE CONTROLLING PARAMETERS**

The major problems encountered in production of particulate composites by vortex method can be accounted as follows:

- a) Wettability : poor wettability of dispersoid ceramic particles for molten metals and alloys makes their incorporation and retention difficult. [42,63].
- b) Particle Matrix bonding : obtaining a strong bond between the ceramic particles and the matrix presents serious problems [63,67-71].
- c) Vortex formation : Mixing conditions within the melt are critical for the satisfactory retention of dispersoid particles so that they are not rejected by the melt [72-74].
- d) Segregation and flocculation of dispersoids : It is difficult to obtain a homogeneous distribution of non-metal particles in these cast composites [42,44,57].
- e) Porosity in the composites : the resulting porosity in cast-particulate composites, especially under vortex method, is a serious obstacle for achieving the desired mechanical properties [64-66].

The problems listed above are inherent with the vortex liquid metallurgy route. All these parameters, therefore, need to be optimised and controlled properly. A systematic discussion on these parameters is taken up in following pages.

(a) **WETTABILITY**

A satisfactory wetting between the non-metallic reinforced materials and the matrix in a composite is of primary importance to achieve any improvement in the mechanical properties

over that of the matrix. The interfacial bond strength is largely dependent on the surface phenomena like wetting and chemical reactions. Understanding of interface interaction of a metal-ceramic system is important also for designing an effective fabrication technique of composites.

Wettability of a solid by a liquid is measured in terms of contact angle between the two phases. Fig.2.10 shows a schematic presentation of a liquid drop resting on a solid substrate surrounded by a vapour phase. The different interfacial forces acting between solid-liquid, solid-vapour and liquid-vapour-phases are represented by vectors  $\gamma_{sl}$ ,  $\gamma_{sv}$  and  $\gamma_{lv}$  respectively. The contact angle  $\theta$  is subtended between the solid surface and the tangent at the contact point through the contour of the liquid drop. For ideal wetting, a liquid drop must spread completely over the solid surface, that is the contact angle must be zero. However, in actual practice contact angles of less than  $90^\circ$  are adequate to cause effective wetting. Similarly, complete non-wettability is defined by a contact angle of  $180^\circ$ ; however angles greater than  $90^\circ$  are practically sufficient to cause non-wettability.

At equilibrium conditions (Fig.2.10), equating the vectors in the horizontal direction gives the following relationships:

$$\gamma_{sv} = \gamma_{sl} + \gamma_{lv} \cdot \cos \theta \quad \dots\dots\dots (2.10)$$

$$\text{and therefore, } \theta = \cos^{-1} \left( \frac{\gamma_{sv} - \gamma_{sl}}{\gamma_{lv}} \right) \quad \dots\dots\dots (2.11)$$

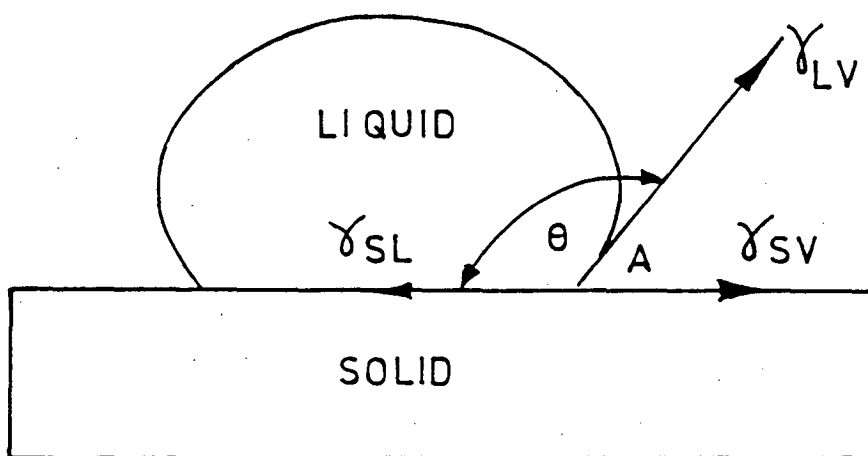


FIG.2.10 Schematic diagram of a liquid drop resting on a solid surface showing the interfacial forces and contact angle at point A. (Ref.14)

In other words, for  $\theta$  to be less than  $90^\circ$ ,  $(\gamma_{sv} - \gamma_{sl})$  must be positive. Work of adhesion of a solid to a liquid is given by the following expression [14]

$$W_{sl} = \gamma_{sv} + \gamma_{lv} - \gamma_{sl} \quad \dots\dots\dots (2.12)$$

where,  $W_{sl}$  represents the work performed in generating a unit area of the liquid and a unit area of the solid less the energy absorbed at the solid-liquid interface. Hence, very high values of  $W_{sl}$  are characteristic of stable solid-liquid interfaces. When the system has cooled to a solid-solid state, Eq.(2.12) must be modified to take into account the effect of thermal strain at the interfaces, as represented by following expression,

$$W_{ss} = \gamma_{sv} + \gamma_{lv} - \gamma_{sl} - f(\Delta\alpha) \quad \dots\dots\dots (2.13)$$

where,  $W_{ss}$  is the work of adhesion at the interface when the system has cooled, and,  $f(\Delta\alpha)$  is a function, dependent upon the difference between thermal expansion coefficients of matrix and reinforcing materials, and accounts for the interfacial strain.

Combining Eq.(2.10) and (2.12), the work of adhesion can be expressed as,

$$W_{sl} = \gamma_{lv} (1 + \cos\theta) \quad \dots\dots\dots (2.14)$$

Therefore, from this expression, the condition for a liquid to spread over a solid surface, i.e. when  $0 < 90^\circ$ , is expressed by the relationship,

$$W_{sl} > 2 \gamma_{lv} \quad \dots\dots\dots (2.15)$$



The term  $\gamma_{sv}$  represents the surface free energy of the solid phase resulting from adsorption of vapour from the liquid and may be considerably lower than the surface free energy,  $\gamma_{so}$ , of the solid in vacuum. Therefore, substituting  $\gamma_{so}$  for  $\gamma_{sv}$ , Eq.(2.10) can be expressed in the following modified form,

$$\gamma_{so} = \gamma_{sl} + \gamma_{lv} \cos \theta + \beta_{so} \quad \dots\dots\dots (2.16)$$

where,  $\beta_{so}$  is the equilibrium spreading pressure of the vapour on the solid surface and can be represented by the following equation [14]:

$$\beta_{so} = \gamma_{so} - \gamma_{sv} = R.T \int_0^{p_0} \epsilon_v \cdot d(\ln p) \quad \dots\dots\dots (2.17)$$

where,  $p$  is the vapour pressure,  $p_0$ , the equilibrium vapour pressure,  $R$ , the gas constant,  $T$ , the absolute temperature and  $\epsilon_v$ , the surface concentration of the adsorbed vapour.

The wettability of different metal-non-metal systems have been improved using a variety of techniques, such as, (i) Use of metal coatings, (ii) Addition of elements in the liquid metal, (iii) Heat-treatment of ceramic particles, (iv) Use of ultrasonics, (v) Compocasting & other methods, and, (vi) Use of ultra high vacuum in space.

#### (b) PARTICLE MATRIX BONDING

The mechanical properties and therefore the performance

in actual field application of a composite is governed by the interfacial bond strength developed as a result of wetting and chemical reaction between the matrix and the reinforcing-material. The strength of composite is achieved by transfer and distribution of load from the matrix to the reinforcing entity through a strong interface between the two. Mechanical locking and physical adherence can not provide an interface strong enough for this purpose.

Under close contact of two interacting dissimilar materials, bonding occurs by donor-acceptor interaction. V.A. Presnov [67] has suggested that the reaction leading to formation of a transition region containing new reaction products provides a strong bond between two dissimilar materials. The greatest coherency is established between the components of a composite with the formation of a chemical bond at their interface which provides the strongest interface.

Aluminium oxide ( $\text{Al}_2\text{O}_3$ ) has been found to react with many divalent transition metal oxides and forms aluminates having a crystal structure similar to mineral spinels. Several workers [68-71], therefore suggested that the reacted layers of spinels have a high potential to form strong bonds between metal and ceramics. Thus the presence of magnesium, copper, zinc, or iron in aluminium-alumina system may provide a strong bond between alumina and the matrix since they can form aluminate under appropriate conditions. Out of these elements, magnesium and copper have been favoured in composite fabrication process by

foundry technique due to their easy application in the process [63]. The presence of magnesium as an interface active element in aluminium alloy-alumina system is, however, more widely used than the addition of copper, because the reaction product, magnesium aluminate, is more stable than copper aluminate ( $\text{CuAl}_2\text{O}_4$ ). The copper aluminate decomposes into alumina and  $\text{CuO}$  at the heat-treating temperatures for Al-Cu alloy matrix [63], thus the interfacial bond containing copper aluminate is not suitable for providing strength to the composite at elevated temperature.

#### (c) VORTEX FORMATION

Optimisation of impeller diameter at a given stirring speed is very important for fluidization of the solid particles in both the central and peripheral parts of the vessel. Nagata [72] has pointed out that, when the impeller diameter is too small, the solid particles have been found to remain suspended at the periphery of the vessel even at a speed when there is no deposition in the centre. When the impeller diameter is too large, the solid particles have been found to remain undispersed in the centre of the vessel bottom. For any specific system, the value of optimum diameter of impeller has been found to vary with the impeller width, blade angle, number of blades, density of solid particles, and, finally the shape of bottom of the vessel. Incidentally the optimum diameter of the impeller has not been found to be influenced by the impeller height or liquid depth [72].

Nagata [72] further pointed out that in case, the ratio of liquid depth to vessel diameter, is larger than 1.0, usually the uniform suspension of particles does not result. Therefore, a liquid depth smaller than the vessel diameter has been recommended. Further, for uniform suspension of solid particles in an agitated vessel, Rushton [73] has suggested that an impeller height of about one sixth of the liquid depth from the vessel bottom is preferable.

In the Vortex method of fabrication of particulate composite, the particles are directly added to the Vortex formed in the vigorously stirred molten metallic bath. Success of the process, therefore, depends on the introduction and also the retention of particles inside the molten alloy. In Vortex method, incorporation of a given particle in any given molten alloy depends primarily on the stirring speed, the impeller size, and, the position of the impeller, which, in term, determines the fluidisation of solid particles in the molten alloy. Impeller blades, designed to move very close to the walls of the crucible and positioned just below the surface of the melt, have been reported by Quigley [12] to be more successful for the introduction of short fibres into the melt due to the high shear rate. P.K. Ghosh et.al. [74] demonstrated that optimum retention of  $Al_2O_3$  in Al-Mg alloy melts results when  $h/H$  ratio=0.81 and  $d/D$  ratio=0.63 at stirrer speeds of 16 revolutions per second, where  $h$  is the position of the impeller from the bottom of crucible and,  $H$ , is the depth of melt at rest in the crucible. Also,  $d$  is the dia of impeller and,  $D$ , the dia of crucible.

**(d) SEGREGATION AND FLOCCULATION OF DISPERSOIDS**

Another basic limitation of Liquid-Metallurgy-Techniques lies in the problems of segregation of dispersoids in various locations of cast particulate composites. There could be several dispersoid-rich and dispersoid-free zones inspite of all possible precautions. Uniform distribution of fine dispersoids in cast particulate composites is complicated by several factors such as, (i) different trajectories of convection currents within the liquid during stirring, (ii) density differences between the dispersoids and the liquid, (iii) wettability of dispersoid particles, (iv) settling of particles as governed by Stoke's law, during freezing, (v) rate of freezing of liquid-particle suspension, (vi) inter-dendritic spacing during freezing, and, (vii) size range of dispersoid particle. In practice, therefore, inter-particle distances may vary from 100 to as much as 1000 um or even more. Besides this, a group of ten or more number of particles may be found fused together and segregated in several locations. These distribution patterns will obviously influence the performance of cast particulate composites in actual practice.

**(e) POROSITY IN THE COMPOSITES PRODUCED BY VORTEX METHODS**

A high level of porosity or void in the composites produced by foundry technique can be considered as a characteristic feature of this process. The amount of porosity in the composite is enhanced with the increased dissolution of gases in the melt. During solidification of a slurry, the particles impose a considerable hindrance to the passage of the evolved

gases and promote porosity in the composite produced by Vortex method. This is further explained below.

Due to the presence of a negative pressure difference at the centre of the Vortex, there is suction of air bubbles inside the melt. These air bubbles may get entrapped between the particles in the slurry. The gases in the crevices of the particles also enter the slurry. Exposure of the fresh melt surface continuously to the atmosphere due to turbulence, enhances the dissolution of gases in the melt.

The pick-up of gases by the melt from the normal atmosphere can be minimised by carrying out the Vortex method making particulate composite in vacuum [75] or in an inert atmosphere [12,42,63]. The other way to minimise the amount of dissolved or entrapped gases in the slurry is to degas the stirred slurry with the help of some suitable gas-purging agent. However, the degassing of slurry by purging has not always been found successful. Mehrabian et.al. [41], for example, observed that in Al-5% Si-2%Fe alloy at temperatures above the liquidus, the ceramic particles were rejected by the melt during purging by chlorine gas. This may have happened due to the alteration of interfacial energy between the particles and the melt in presence of chlorine. However, no significant rejection of ceramic particle by the molten aluminium alloy has been observed during nitrogen purging, but it has not been found as efficient as chlorine [12,41]. The adsorbed or crevice-gasses in the particle and also the moisture can be minimised by heat treating the

particles before addition to the melt as suggested by Dixit et.al. [76]. In an attempt to prepare isotropic composite-materials in space by dispersion of short fibres and/or particles in molten metal matrix, Berghezan [77] carried out the degassing of the slurry by moving the gas bubbles along the unidirectional solidification interface.

## 2.2 SQUEEZE CASTING

### 2.2.1 INTRODUCTION

Squeeze casting process, essentially combining gravity die casting and closed die forging, is not a new process and was employed, in several forms, even during the nineteenth century. An American version, in use prior to 1875 [78], employed considerable power of a steam-hammer to produce rail car wheels. Molten steel was poured into the lower die on the hammer anvil and then the hammer head carrying the top die was allowed to descend, thus exerting considerable pressure on the rapidly solidifying steel. In another technique [78], the dies were so arranged that the top tool served as the follower of a press, actuated by screws. The top, fitting closely into the bottom die, was provided with ingates for the molten metal-either steel or cast iron. These orifices were closed with slides when the tool was full. Pressure was applied to the metal, in molten state, by the action of a screw mechanism, sufficient force being exerted to expel air and gases from the solidifying casting and to provide a sound compact component.

Traditionally casting and forging have evolved separately but the possibility of combining the two processes was initially examined in detail in the USSR during the late 30s principally by Plyatskii [79]. Welter [80] has also published results of his investigations on squeeze casting around this time. After an extensive programme of work, the process parameters governing the technique were successfully resolved, so that by the mid 60s it was claimed that in excess of 150 large batch plants were operating in the USSR, utilising more than 200 different types of squeeze cast components. After the publication of Plyatskii's authoritative work [79] on squeeze-casting, interest in this process was generated in several other countries, especially in USA, Great Britain and Japan, and active research and commercial production started using this method some two decades ago [81-83].

In the field of composites, the first report on fabrication of fibre-reinforced composite, applying high pressure, was published by C.F. Old et.al. in 1971 [84], and then later by K.F. Sahm in 1974 [85]. Using this method, Sahm [85] prepared SiC whisker/Al-alloy composites which had higher strength than that prepared by the hot press method. However, in Japan, the application of this method to ceramic fibre reinforced composites was first introduced by S. Sujuki in 1977 [86]. Fukunaga [87,88] has reported that the squeeze casting has now been satisfactorily adopted for the manufacture of a wide variety of near-net-shape castings for several industrial applications.



### 2.2.2 SQUEEZE CASTING PROCESS

Squeeze casting may be defined [89] as a forming process which combines gravity die casting with closed die-forging in a single operation. Other terms used to describe the same process include the 'extrusion-casting', 'liquid-pressing', 'liquid-metal stamping', 'pressure-crystallization' and 'squeeze-forming'.

Although considered a single operation, a number of steps are involved in squeeze casting as shown schematically in Fig.2.11, thus, (i) A measured quantity of molten metal is poured into an open preheated die cavity located on the bed of a hydraulic press. Some initial cooling of the metal occurs before the application of pressure, (ii) The upper die or the punch is then lowered, so as to come in contact with the liquid metal thus sealing it within the die, and, continues to travel until the applied pressure has reached the desired level. The time elapsed before the application of pressure needs to be precisely controlled and minimised to prevent pre-solidification of the metal in the die, (iii) The pressure is maintained until all the molten metal has solidified. During this period the metal is forced to be in intimate contact with the die surfaces, (iv) The upper punch, then, returns to its original position and the solidified casting is ejected.

Essentially two forms of the process can be differentiated depending upon whether or not, the motion of punch causes a significant displacement of the liquid-metal, although

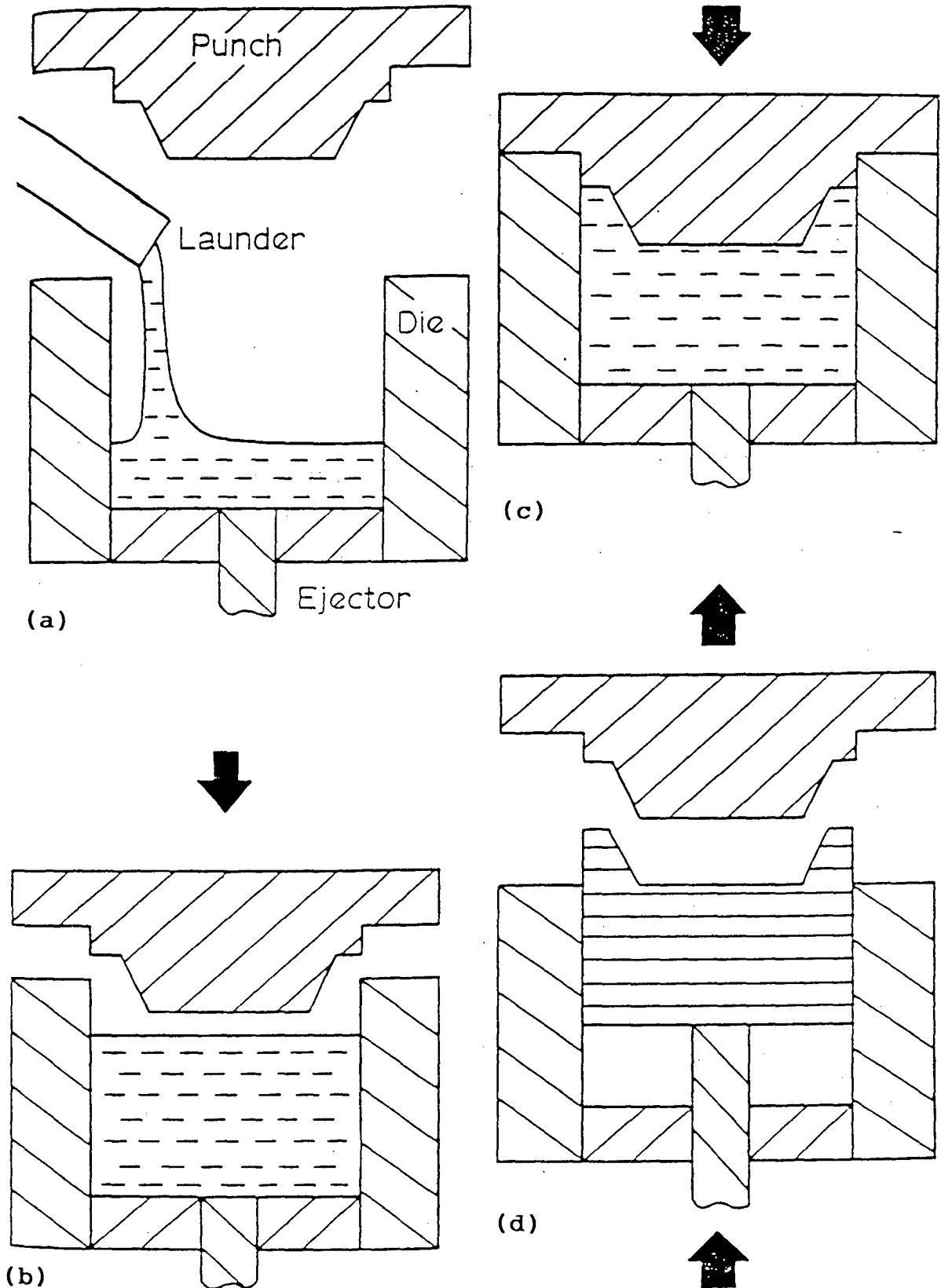


FIG.2.11 Steps in producing a squeeze casting, (a) molten metal poured into die, (b) punch activated, (c) pressure applied to molten metal, and, (d) casting ejected. (Ref.89)

Kaneko [81] has suggested that a third mode also exists. The case of squeeze casting, in which there is no significant metal displacement occurs, is illustrated in Fig.2.12(a). This form of the process is mainly suited to chunky-components having a small aspect ratio, i.e. for which the width and height of the casting are almost of similar dimensions. Automobile wheels and also the planar ingot type shapes would be a suitable configuration for squeeze casting. Franklin [89] has, however, emphasized that for such applications the use of multipart dies should be avoided.

Fig.2.12(b) shows the second form i.e. of the backward extrusion case, involving an appreciable movement of the molten metal. As the punch enters the die-cavity, the liquid metal is caused to move in a direction opposite to that of the applied force. This form of the process affords greater versatility in component shape as it can be used for castings having a larger aspect ratio. Thin-walled sections, such as cylinders can be very effectively produced by this method.

Kaneko [81] has termed the third mode as the 'indirect pressure solidification method', which is schematically shown in Fig.2.12(c). The punch does not make contact with whole of the metal surface but only with a comparatively small area, that requires higher applied forces to achieve results similar to those produced by extrusion casting [90]. It is suitable for complex shapes and closely resembles vertical die casting. This mode, in principle, should be considered as a variation of squeeze-casting rather than as its distinctive form.

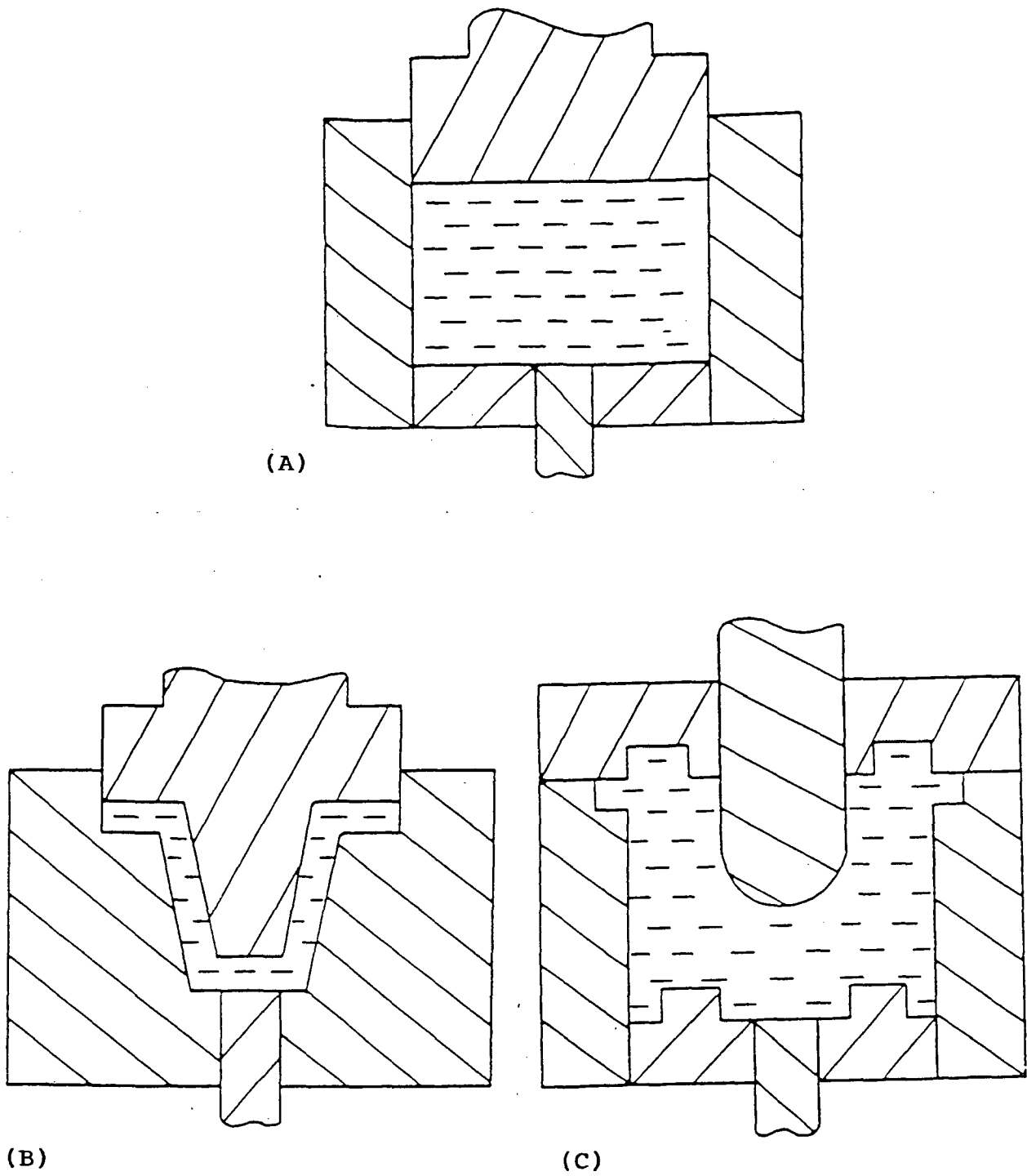


FIG.2.12 Schematic representation of squeeze casting modes. (A) squeeze casting, (B) Extrusion casting, and, (C) indirect pressure solidification. (Ref.89)

Lynch [83] has pointed out that to achieve a sound structure in squeeze casting, the aspect ratio is usually be kept below 5:1. However, substantially greater aspect ratios are possible by utilisation of extrusion casting although care must be taken with Al-base alloys as sections of the oxide skin, which readily form on the free metal surface, may be retained within the component.

#### 2.2.2.1 SPECIAL MERITS

Potentially, the combination of casting and forging, as applicable to squeeze casting technique, offers several special merits, some of which may be stated as,

- (i) In the absence of a running or feeding system, a high metal yield approaching 95%, can be achieved conveniently. Further, apart from the need for possible machining operations such as bolt holes etc., all the metal poured into the die is used to form the component.
- (ii) An excellent surface finish, closely resembling the die surface, is possible.
- (iii) Casting are heat treatable.
- (iv) Squeeze casting may result, in significantly improved mechanical properties.
- (v) Complete elimination of shrinkage and/or gas-porosity is possible.
- (vi) The possibility of manufacturing components with a wide

range of section thickness and size. Williams [91] has pointed out that (a) thicknesses in the range 0.3 mm-50 mm have been successfully tackled, although large section changes within a particular component are not recommended, (b) component sizes from 0.125 kg to 35 kg have also been successfully produced, and (c) in conjunction with use of high quality re-usable dies and thin die-coatings, good dimensional reproducibility, matching that of pressure die casting technique is possible.

- (vii) Sound castings can be produced by squeeze casting from any alloy that can be contained within a metal die.
- (viii) Recycled scrap-material can be used for components which would conventionally require a more expensive primary quality alloy.
- (ix) Sound components of forging quality can be produced by squeeze casting with an additional advantage that only a single set of dies is required instead of several, normally employed in closed die-forging.
- (x) A rapid cycle time is possible depending upon the size of the component, and this could be 2-3 times faster than that for gravity die-casting of equivalent size and shapes, and finally,
- (xi) Squeeze casting is suitable for the production of cast metal matrix composites (MMCs).

#### 2.2.2.2 COMPARISON OF SQUEEZE CASTING WITH ALTERNATE METAL-FORMING TECHNIQUES

Sand-casting provides a low fixed cost method of fabrication, also allowing complex undercuts and channels to be cast into the part but with a rough surface finish. Many small-sized parts can be cast simultaneously in the same mold, increasing output. In contrast, squeeze-casting can provide full density components without shrinkage or micro-porosity and having a smoother surface finish and closer tolerances than that obtained by sand-casting. For example, Lynch [92] observed that the shrinkage from the die for squeeze-cast bronze components was found to be only half that experienced in sand casting. Pressure applied, during and after solidification, forces the metal against the rigid die and prevents shrinkage away from the wall, which may occur in the gravity-casting methods. Even when full squeeze-cast advantages are not required in a component, the process can prove to be the most cost-effective manufacturing technique by reason of its high productivity and high metal-utilization efficiency. Savings, therefore, result from reduced energy costs for melting, reduced melt-losses, elimination of the runner and riser, removal step, and finally, the reduced machining costs.

Squeeze-casting is a useful complement to the die-casting process, being able to produce sound parts with greater section thicknesses than those normally die-cast. However, Lynch [92] has pointed out that complex-shaped, high tolerance parts upto 0.125 inch (3.175 mm) thickness, will continue to favour the high rate

die casting process. Squeeze-casting, however, offers advantages for high integrity components cast in straight draw die with a cycle time which can approach that of die casting. The direct nature of application of pressure by the punch to the solidifying component allows a smaller die to be used than that necessary in die-casting. Further life of the die, is expected to be similar to that in the die casting process-the higher specific applied pressures in squeeze casting replacing the high velocity impingement of metal spraying into the die cavity through a restricting gate characteristic of die casting.

Several interesting comparisons can be made between squeeze casting and forging. The pressure necessary to consolidate material originally in the molten state is significantly less than that which must be applied to form a like configuration in the normal hot-working temperature range. Thus, smaller capacity presses are required, and the dies themselves tend to be much smaller, the influence of the higher metal temperature relative to that employed for forging tends to affect die life adversely, but is offset by the lower forming pressure required. Part configurations tend to be less restricted for squeeze casting than for traditional forging. Cuplike configurations have successfully been made having a height twelve times greater than minimum section thickness, with the section itself varying by factors of two or three from place to place. Radii can be considerably smaller than for forging and fine surface finish is generally obtained.



Components currently manufactured as cored forgings are well suited to squeeze casting. The squeeze casting is made with the cores initially extended into the die cavity or incorporated in the punch for the molten metal to flow around, rather than by applying considerable forging force to hot pierce the required core holes. Lynch et.al. [92] have further observed that the use of molten metal and the high metal utilization level characteristic of squeeze casting combine to provide economic advantages compared to forging where preprocessed forging stock is employed and scrap must likewise be reprocessed.

### 2.2.3 THEORETICAL ASPECTS OF THE EFFECTS OF SQUEEZE-PRESSURE

#### 2.2.3.1 REDUCTION OF POROSITY

Pressure applied to the liquid metal prior to and during solidification tends to reduce or eliminate gas related porosity. It increases the solubility of the gases in the melt so that a larger concentration can be held in solution, and these gases are not evolved during solidification due to the difficulties in nucleation of bubbles against the pressure. Reddy et.al. [93] have pointed out that the liquid-forging pressure will be adequate to keep the gases in solution if the sum of the partial pressures of the gases dissolved in the metal is less than the opposing external pressure. On the other hand, if the reverse is true, the gas bubbles will form in the metal and tend to rise.

Presence of shrinkage cavities is minimised by feeding

of molten metal into these, due to the application of pressure. Shrinkage cavities form because of the inability of the molten metal to flow into narrow torturous inter-dendritic regions. These regions can be filled with liquid metal if the latter is fed under high pressure. Further, any of the shrinkage cavities not fed by molten metal under pressure have a chance to be healed by the continued application of pressure—a phenomena comparable to hot pressing. Shrinkage cavities are thus eliminated during liquid-forging, which, therefore, can produce a porosity-free and fully densified structure.

#### 2.2.3.2 EFFECT ON EQUILIBRIUM DIAGRAM AND STRUCTURE

Mechanical properties of squeeze-cast components are largely controlled by the structure and morphology obtained during solidification. Franklin and Das [89] have pointed out that 'under-cooling', below the equilibrium solidification temperature, combined with a rapid rate of heat-extraction, will generally ensure extensive nucleation and a fine equiaxed grain structure within the casting. Both these requirements can be met by squeeze-casting.

The rapid cooling and solidification, which occurs during the squeeze-casting process, is brought about by the intimate contact made between molten metal and the die-surface. The applied pressure dispenses with the air-gap which normally forms at the casting/die interface in other foundry casting techniques. Several workers [92,94,95] have, therefore, pointed out that this results in a heat flow rate which is an order of

magnitude greater than that achieved in gravity die-casting.

Nishida and Matsubara [95], measured the heat transfer rate for squeeze-casting and found it to be approximately ten times as fast as that in the gravity die-casting process. Epanchintsev [96] measured a cooling rate of  $140^{\circ}\text{C}/\text{sec}$ , when squeeze-casting an aluminium alloy in steel dies heated to approximately  $204^{\circ}\text{C}$ . Spear and Gardner [97] documented the dendritic arm spacing for several commercial aluminium alloys. Verma and Dorcic [7] observed that extrapolation of their data would indicate that a melt, cooled at the rate of  $140^{\circ}\text{C}/\text{sec}$  would have a dendritic arm spacing of  $8.94\ \mu\text{m}$ . The fine-grained structure so obtained in squeeze-cast components improves the mechanical properties considerably.

The usual equilibrium phase-diagram depicts conditions of slow cooling rates at atmospheric pressure. However these are not the conditions encountered during squeeze-casting as pointed out by Lipchin et.al. [98]. Application of pressure causes the melting point of most alloys to rise, with only metals Bi and Si being the exceptions, in a manner which obeys the Clapeyron equation -

$$\frac{\Delta T}{\Delta P} = T_m \left( \frac{V_2 - V_1}{H} \right)$$

where,  $H$  is enthalpy of fusion,  $V_2$  specific volume of liquid phase,  $V_1$  specific volume of solid phase,  $T_m$  melting temperature at atmospheric pressure, and,  $\Delta T$  is the rise in melting point resulting from increase of pressure by an amount of  $\Delta P$ .

Lipchin et.al. [99] showed that the majority of metals show a rise in melting point, ranging from 2-6°C, for every 98 MN/m<sup>2</sup> of applied external pressure. Lipchin et.al. [99] have pointed out that application of pressure also distorts the phase-diagram, when the melting point of a component in an alloy is altered by application of external pressure, the eutectic point is shifted in the direction of higher concentration of the component whose melting point is least affected. In the case of Al-Si alloys [100], it moves towards the higher silicon content as shown in Fig.2.13(a), while in Mg-Al alloys [99], the eutectic moves towards the magnesium concentration, as shown in Fig.2.13(b).

Effect of solidification under pressure on grain size can be illustrated by reference to Fig.2.13(a). Alloy x is well above the liquidus line at  $T_1$  at atmospheric pressure. The application of pressure will cause the liquidus line to move-upward, as shown by the dotted line, but it will still be below  $T_1$ , and the melt will not start to solidify until the temperature has reached the new liquidus line. Nucleation and growth processes will commence, but there will be no significant grain refinement. If, however, the initial alloy temperature is at  $T_2$  when pressure is applied, the liquidus line will move above this point and super-cooling will occur [100]. The grain-refinement effect will be proportional to the degree of under-cooling, and as pointed out by Franklin and Das [89], a true squeeze-casting will always consist of fine equiaxed grains as a result of correct pressurisation applied at the appropriate time.

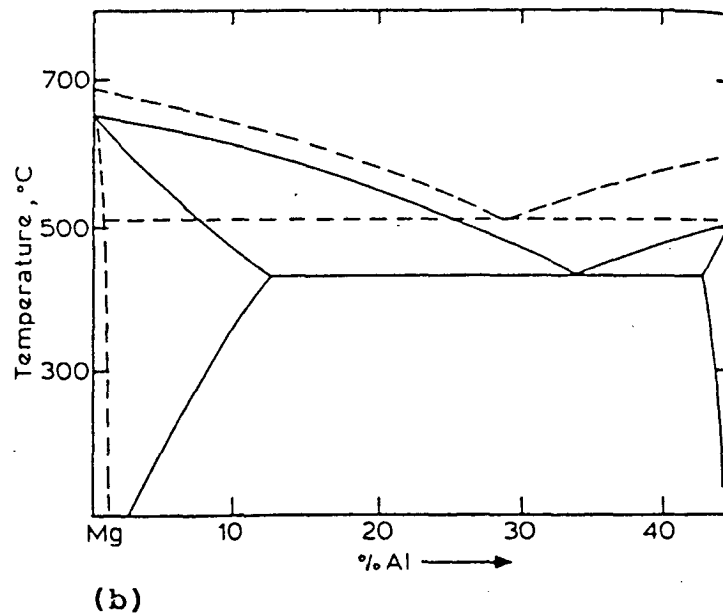
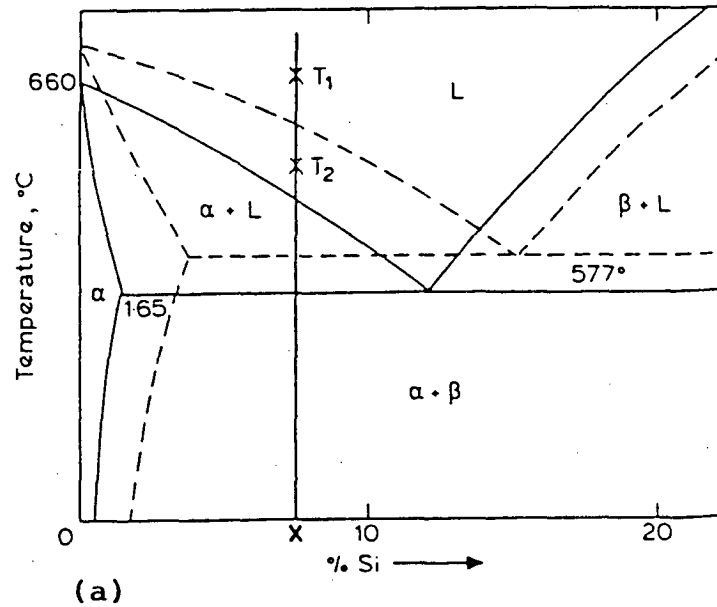


FIG.2.13 (a) A rapid cooling rate combined with pressure application causes deviation (dashed line) from equilibrium conditions (solid line) in the Al-Si equilibrium diagram (Ref.89). (b) a rapid cooling rate combined with pressure application causes deviation (dashed line) from equilibrium conditions (solid line) in the Mg-Al equilibrium diagram (Ref.89)

Further, since the dendritic arm spacing will be smaller, constituent particles will tend to remain small and therefore, a more homogeneous distribution of structural components will take place as also pointed out by Das and Chatterjee [101]. All these factors, therefore, help in production of components with improved mechanical properties by squeeze-casting process.

#### 2.2.4 PROCESS PARAMETERS

To produce successful squeeze-cast components, a number of process parameters, discussed briefly below, need to be controlled.

##### 2.2.4.1 METAL CASTING TEMPERATURE

The temperature at which the molten metal is poured into the die-cavity has an effect on the casting quality and die-life. Casting temperatures may be low compared with other casting methods. Lack of a gating-or running-system means that a lower fluid life can be tolerated, as the filling details of the mould are primarily accomplished by pressurisation of the molten metal. However, care must be taken as too low a pouring temperature could cause inadequate fluid life resulting in incomplete die-fill and/or cold laps, especially in case of castings with narrow sections. Conversely, too high a casting temperature may result in metal being forced between the die and the punch, causing flash or possible jamming of the tooling. There is also a possibility of hot-tearing in the region of mould

or core-constraint. Moreover, the life of die is also adversely affected by high pouring temperatures.

Actual casting temperatures depend upon the liquidus temperature, freezing range and die configuration. Alloys with narrow freezing range tend to form solid layers almost immediately upon making contact with the die-wall, and therefore, the degree of superheat is usually higher for these alloys.

Franklin and Das [89] have observed that for aluminium alloys, the casting temperature may range between  $19^{\circ}\text{C}$  and  $100^{\circ}\text{C}$  above liquidus temperature—the lower temperature being used for alloys such as 7075 and A390, while alloys like 3003 and A413 require temperatures in close proximity of the upper limit, and also that, copper-base alloys and steels need a superheat of the order of  $30^{\circ}\text{C}$  to  $150^{\circ}\text{C}$  as they solidify rapidly upon making contact with the metal die.

#### 2.2.4.2 TOOLING TEMPERATURE

Operating die temperature need to strike a balance between the need for sufficient heat to prevent premature solidification, thermal fatigue and cold-laps ( $150^{\circ}\text{C}$ ) while avoiding high temperatures ( $400^{\circ}\text{C}$ ) which can cause surface-and other defects. There is a tendency for welding to occur between the casting and the mould if the die temperature is too high. Franklin and Das [89] have pointed out that temperatures above  $300^{\circ}\text{C}$  are not recommended for aluminium-alloys and greater than  $400^{\circ}\text{C}$  for ferrous-alloys.

It is also important to note that commercial dies need to be sufficient size to enable the heat generated, during each casting cycle, to be dissipated. Once regular production has commenced, some means of cooling (water-or oil) the die to maintain its temperature within specified limits may be necessary, depending on the casting-configuration and die-design.

#### 2.2.4.3 MELT QUALITY AND QUANTITY

Since the metal is poured directly into the die-cavity, it is important that dross and other suspended impurities are removed before pouring. This can be accomplished by such means as fluxing, skimming, filtering or bottom-pouring. Kaneko et.al. [81] and Chatterjee and Das [102] have also pointed out that degassing is not usually necessary in this process but the possibility of any defects occurring can be minimised by keeping the melt-temperature as low as practicable.

Metering precise quantities of molten metal into the die-cavity is essential, as this determines the casting dimensions measured from the plane of contact of the punch. This has proved difficult even by using 'automatic ladling' or 'commercial metering pumps', especially for small components or multi-dies. Various methods have been suggested to alleviate this problem. Das and Chatterjee [101] have suggested that excess metal can be poured into the die and the component allowed to be oversize in a non-critical area. This however, usually requires the allowance to be in the vertical direction. Lynch



[103], has however suggested a variation to this idea, by the use of compensating hydraulic piston and cylinder to control the exact quantity of metal fed in the die. This allows any excess metal to be accommodated, to form an appendage to the component, until the predetermined size is achieved. The main advantage of this system lies in the use of multi-dies and punches. Williams and Fisher [91] have observed that it is also possible to include an overflow system into the die-set for close control of dimensions.

#### 2.2.4.4 DIE COATING/LUBRICANT

The type of die-coating or release agent used obviously depends upon the material of die and the composition of alloy being cast. However, it would appear that the release agents used in pressure die-casting can perform the same function in squeeze-casting.

A commonly used agent is water-based colloidal graphite, which is usually sprayed onto the die-surface and punch between each cycle. In gravity die-casting, the thickness of the coating can influence the solidification of the casting, but this factor is not significant in squeeze-casting. At the pressures applied during squeezing, the coating is stripped from the die-surface and this may cause surface-contamination in the component. Franklin and Das [89], however, have suggested that limiting the thickness of coating/lubricant to about 50  $\mu\text{m}$ , should prevent this problem.

#### 2.2.4.5 TEMPERATURE FOR PRESSURE APPLICATION

There is no universal agreement upon the implementation of this parameter—the point of contention being if the metal should be 'fully liquid' or 'partially solid', when the pressure is applied.

Bidulya [104] has suggested that pressure be applied when the metal is near the 'zero-fluidity temperature'. This is interpreted as being reached when continuous solid phase skeletons have formed in a two phase alloy and the metal loses its fluid-flow properties. It is usually midway between the liquidus-and solidus-of temperatures of the alloy.

However, the metal should be mainly liquid according to others [91,101], when pressure is applied, for squeeze-casting to be fully effective. Control of temperature is by 'delay-times', i.e. the interval between pouring and application of pressure. This time will vary depending upon the melt-temperature and component-geometry. As pointed out by Franklin and Das [89], these times differ greatly but generally range from a few seconds for small ferrous components to approximately one minute for large aluminium alloy components.

#### 2.2.4.6 SPECIFIC PRESSURE LEVEL AND DURATION

Differences in alloy-characteristics and component-geometry make it difficult to predict actual pressure-levels. However, as also pointed out by Williams and

Fisher [91] and Rajagopal [105], it would appear that applied pressures within the range 30 to 108 MN/m<sup>2</sup> are the minimum required to eliminate shrinkage and gas-porosity for the majority of ferrous and non-ferrous materials.

Das and Chatterjee [101] have listed some factors, that determine the pressure-level, as follows;

- (i) flow stress of the alloy near its freezing temperatures,
- (ii) the growth morphology of the alloy-crystallites, and,
- (iii) the freezing range of the alloy.

The actual pressure used is normally the minimum required to achieve a sound casting. Pressures above this level may improve mechanical properties but with a possible reduction in the life of die.

Time of application of pressure is controlled by alloy-type, casting-configuration, and, the heat transfer conditions. It is only necessary to apply pressure until solidification is complete, although slightly longer times may be used to avoid hot-tearing. Prolonged holding times provide little benefit, and may cause wall-cracking or problems with punch withdrawal due to thermal contraction of the casting on to the rigid punch. A suggested 'rule of thumb', after Rajagopal [105], suggests the maximum holding time of about 1 seconds per mm of section thickness.

#### 2.2.4.7 PRESS SPEED

Physical contact of high velocity punch with the molten metal can have adverse effects. This may result in dilation of die-parts and flash may appear at joints or parting-lines. Instantaneous peak pressures may be generated in the region of the impact zone causing premature solidification, and thereby inhibiting consolidation of the remainder of the casting. Das and Chatterjee [101] have suggested that for most practical purposes, to avoid premature solidification of the metal in the die, punch impact speeds of 0.5 meters per second may be used without detrimental effects. In the situation where there is a large distance between the punch and the die, a two-speed action may be used i.e. a rapid approach of the punch to the metal surface followed by a slower punch speed.

#### 2.2.5 DIE MATERIAL AND CONFIGURATION

The type of die-material employed depends primarily upon the type of alloy cast by this method. Ideally there should be no reaction between the molten metal and the die-surface, and the die-material should be able to withstand the service temperatures.

Franklin and Das [89] have suggested that for aluminium alloys and the majority of other non-ferrous alloys, H13 grade chromium-molybdenum hot worked die-steel is successfully employed, since it combines moderate high temperature strength with adequate wear-and thermal-fatigue-resistance. For more

severe conditions in casting of molten steel components, die-casting materials, highly alloyed with tungsten and molybdenum, are required.

Die-corrosion problem, related to turbulent-flow of metal encountered in die-casting, are not found in the slower die-filling squeeze-casting process. However, 'heat-checks' or 'crazing' can be a problem. The molten metal is solidified very quickly and the heat energy released is transferred to the bulk of the die via the metal/die interface. The temperature of the die-surface, therefore, increases rapidly. After ejection, the die-surface is usually sprayed with a mould release agent which causes surface-cooling. Successive heating and cooling cycles lead to 'heat-checking', which as pointed out by Kaneko et.al.[81], is usually attributed to over-stressing or thermal-fatigue. This can be reduced by partitioning the die to reduce thermal fatigue, which has the added benefit of eliminating trapped-air. Incomplete die-filling can be produced if air-locking occurs in any part of the die. Air-release may also be achieved along parting-lines or vent-holes in the case of deep recesses. Franklin and Das [89] have also observed that the venting dimensions must be less than 0.2 mm to avoid metal-extrusion and excessive flash.

Corner radii on punch details are usually of the order of at least 2 mm for non-ferrous materials and 3 mm for ferrous-alloys. This facilitates casting ejection. Similarly

the external die-wall draft-angles are of the order of 0.5 degree, which are increased to 1-2 degrees, on the punch-surface and die-details, around which the casting tends to contract after solidification. Franklin and Das [89] have pointed out that correct use of draft-angles can help reduce the pressure needed to eliminate porosity.

The clearance between the punch and the die is important if the correct pressure is to be applied. Kaneko et.al. [81] have also pointed out that there is a certain amount of friction-loss, which is related to the distance between the plunger and the inner diameter of the die. If the gap is large, there is a problem of excessive flash and associated die wear. Conversely, die wear occurs if the interval is small, resulting in friction and the need for a higher applied pressure to overcome it. The clearance-dimensions are determined by the heat capacities of the dies and the die assembly, and also the casting cycle and the tooling temperature. Recommended clearance, as suggested by Kaneko et.al.[81] at room temperature is around 0.15 mm. During the production of squeeze-cast components, this dimension approaches zero as a result of thermal expansion and elastic deformation of the punch.

## 2.2.6 APPLICATION OF SQUEEZE CASTING TECHNIQUE

### 2.2.6.1 GENERAL

Essentially it is the economic viability of the squeeze-casting process, which determines whether the potential

of this technique is converted into a commercial production process. Commercial products can be profitably manufactured by this process and several other workers [91,103,106] also believe that squeeze-cast components can compete both technically and economically with other methods of fabrication.

In the majority of cases, the die-costs plus the need for a hydraulic press will account for the main portion of the overall squeeze casting production expenditure. According to Stefanides [106] the economic costs result from a number of inter-related parameters, viz.,

- (i) use of metal in its least costly forms i.e. molten metal and/or scrap as source of metal,
- (ii) almost total utilisation of the metal through the elimination of gates and risers, and the minimisation of casting defects viz. flash etc.,
- (iii) smaller equipment requirements compared with forging,
- (iv) lower cost tooling with a reduction in tooling maintenance as a result of lower force levels used, and,
- (v) the adaptability of the process to highly automated handling and ancillary processing techniques.

In addition there is appreciable reduction in the amount of machining, resulting from good surface finish and good dimensional reproducibility, both leading to the production of

'near net-shape castings'. Fukunaga [88] and Shaw et.al. [107] have listed the common types of components that can be produced by this technique viz., gear-blanks, gear covers, gear housing, diesel-engine pistons, wheel-hubs, nuts, flanges, pulleys, wheels, bushings, dipper teeth, bulldozer corner-blades, composite-castings, hydraulic piston heads, compressor valve seats, drill-bit blanks, extrusion-dies, pull arm rockets, bearing caps, track wheels, wheel spindles, sprockets, pressure plate for vane pumps, gears for industrial robots, rotor and vane for inverted air-conditioner compressors, connecting rods for high speed reciprocating engines etc.

#### 2.2.6.2 SQUEEZE CASTING OF METALS AND ALLOYS

Squeeze casting is applicable to a wide range of alloys usually of both the 'casting'-and the 'forging'-types. To date, over 20 aluminium alloys have been successfully processed, ranging from the cast-alloys such as LM25 (Al-Mg-7Si) to the high strength forging-alloy such as 7075 (Al-2Mg-5Zn-1.5 Cu). The components are readily heat-treated to develop the optimum properties. In Table-2.5, compiled by Williams [108], the mechanical properties of squeeze-cast alloys have been compared with those of conventional gravity chill-cast alloys. It is noteworthy that both proof stress as well as percent elongation of failure have improved simultaneously in the squeeze-cast condition, representing thereby a substantial improvement in toughness and ductility. This is, obviously, the result of the fine, sound micro-structure, which also leads to an improved



TABLE - 2.5

TENSILE DATA FOR SQUEEZE-CAST MATERIAL COMPARED WITH PROPERTIES OF CHILL CASTINGS\*

| Alloy designation | Temper condition | Mechanical Properties of Squeeze-cast material |                          | Mechanical Properties of conventionally chill-cast material |                          |
|-------------------|------------------|--|--------------------------|---|--------------------------|
|                   |                  | 0.2%P.S. MN/m <sup>2</sup>                     | U.T.S. MN/m <sup>2</sup> | 0.2% P.S. MN/m <sup>2</sup>                                 | U.T.S. MN/m <sup>2</sup> |
| LM5               | M                | 142  | 250                      | 90  | 170                      |
| LM18              | M                | 103  | 187                      | 60  | 140                      |
| LM25              | M                | 124  | 195                      | 80  | 160                      |
| LM25              | TE               | 165  | 235                      | 130   | 190                      |
| LM25              | TF               | 250  | 300                      | 220   | 280                      |

\* abstracted from Ref. [108]

Remarks: Temper condition M = As formed; TE=Solution treated and stabilised; TF=Solution treated and aged to maximum strength.

fatigue performance, compared to the conventional chill-casting. It is interesting to note that in most of the cases, secondary-quality aluminium casting-alloys can be used without the detrimental effects of coarse iron aluminide needles. Williams [108] has suggested that this can be an economic advantage, without impairing structural performance.

Forging quality alloys are also squeeze-cast with good results, since the squeeze-cast components are isotropic in their mechanical properties. This can have significant benefits compared to the conventional forgings, particularly for the higher strength alloys which can have significant differences in properties along-and across-the grain flow. The fatigue performance of squeeze-cast wrought-alloys equivalent to the usual forgings. This is illustrated in Fig.2.14, after Williams[108], which compares the fatigue behaviour of squeeze-cast and wrought form of 6061 alloy.

It is important to note that the higher strength alloys, such as the Al-Zn-Mg type, may be heat-treated after squeeze-casting to successfully resist stress-corrosion cracking. Moreover, as also pointed out by Williams [108], the absence of grain-flow leads to particularly re-producible results with no opportunity for delamination type crack propagation.

Lynch et.al.[83] studied the squeeze-casting of aluminium-alloys in detail. The process parameters applicable to aluminium-squeeze-castings have been established and their effect

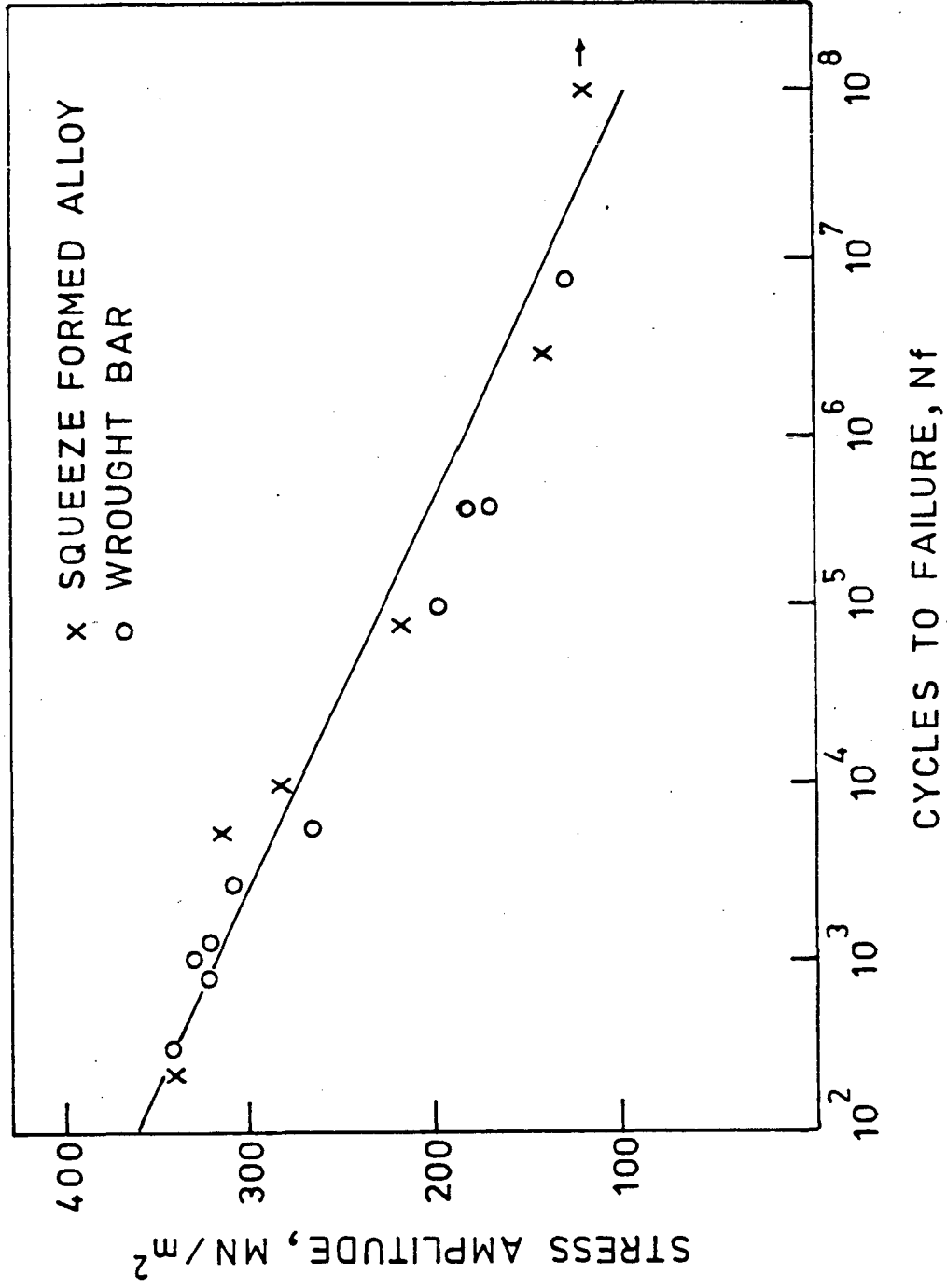


FIG. 2.14 Comparative fatigue performance for alloy 6061-T<sub>6</sub>, wrought and squeeze-formed. (Ref. 91)

on casting-soundness and micro-structure determined. Mechanical properties are reported for forging-and casting-alloys, as determined from actual squeeze-cast components. Micro-structure and properties in the as-cast and, when appropriate, heat-treated conditions, have been studied in this work [83] for A380, 356, B850 and 6061 Al-alloys. The widely used die-casting alloy, A380, does respond well to the squeeze-casting process. The common wrought alloy 6061, when squeeze-cast, exhibits mechanical properties in the T6 condition which compare favourably to those of forged 6061 alloy. Similar tensile properties were measured in the T5 condition, attained without solution heat treatment. These results, presented in Table-2.6, indicate that sufficient solute is present in solution at the completion of solidification to allow a significant precipitation hardening reaction to take place without separate solution heat-treatment. Aluminium alloy B850 containing 6%Sn is generally employed because of its excellent bearing characteristics. Lynch[83] determined compressive strength and wear properties of the squeeze-cast B850 alloy and observed that the bearing characteristics of this alloy in squeeze-cast condition were superior to those in the centrifugally-cast condition. Similar results were reported by Shaw et.al.[107] in case of squeeze-cast A356 aluminium alloy.

Reddy and Murthy[93] employed a commercial Al-alloy containing 4.26%Cu, 0.95%Si, 0.49%Mg, 0.25%Fe, 0.98%Mn, 0.34%Ni and 0.24%Cr for squeeze-casting studies. They attempted to

TABLE - 2.6

SQUEEZE CAST PROPERTIES OF 356 ALUMINIUM ALLOY\*

| Condition           | Ultimate<br>Tensile<br>Strength<br>(ksi) | Yield<br>Strength<br>(ksi) | Elongation<br>(% in 1 in.) |
|---------------------|--|----------------------------|----------------------------|
| <u>Squeeze Cast</u> |  |                            |                            |
| -T6                 | 49.4                                     | 36.0                       | 17.0                       |
| -T5                 | 48.3                                     | 36.8                       | 15.0                       |
| <u>Forged</u>       |  |                            |                            |
| -T6                 | 38.0                                     | 35.0                       | 10.0                       |

\* abstracted from Ref.[83]

optimize operating values such as specific pressure, dwell-time, pressure application time, and pouring temperature, and, observed that squeeze-casting results in considerably higher densities, finer dendritic arm spacings, isotropic microstructure and considerably improved mechanical properties compared with either sand-or metal mould-casting. Infact, the properties in the liquid-forged or squeeze-cast condition were found to be comparable with those in the wrought-condition. They [93] also reported that lower pouring temperature, higher specific pressure and minimum dwell time promotēs the production of a sound component to net-or near net-shape.

Squeeze-casting of two different copper alloys, namely the 85Cu-5Sn-5Pb-5Zn alloy and the 63Cu-1Sn-1Pb-35Zn alloy were studied by Shaw et.al. [107]. These two alloys have different melting points, freezing ranges, and solidification characteristics. In the macro-etched specimens, a columnar growth was noted in the bottom portion of the cast-component, whereas the upper rim contained equiaxed crystals. The 63-1-1-35 alloy has a liquidus range from 1675 to 1725°F or 910 to 935°C, whereas the 85-5-5-5 alloy has a liquidus range from 1570 to 1849°F or 855 to 1010°C, making it highly susceptible to micro-porosity. Alloys with wide freezing ranges are prone to inter-dendritic shrinkage because of the difficulty in feeding liquid metal through the torturous channels generated by the dendrites. In the final stages of solidification, resistance in such a path causes liquid metal to stop flowing and micro-pores

to form. The sample castings by Shaw et.al.[107] showed fine grain size, close dendritic arm spacing and absence of porosity in squeeze-cast 85-5-5-5 alloy.

Squeeze-casting of 347 stainless steel was also attempted. This necessitated use of a refractory mold coating because of high pouring temperatures, above 2700°F or 1480°C. A water-based mold wash is applied to the molds at about 350°F or 175°C. During squeeze casting, the temperature of the lower die is varied from 260 to 285°C and that of the punch from 600 to 700°F or 326 to 370°C. Grain size in the central section of the squeeze cast part is found to be extremely fine. Squeeze casting of X-40 super-alloy by Shaw [107] also showed a surface finish equivalent to that of the lower melting alloys. This super-alloy has a melting range from 2445 to 2545°F or 1340 to 1395°C. Microstructural examination of the rim and central portion of the X-40 squeeze-castings indicated a high degree of structural refinement. Because fabrication of super alloy components by 'hot-forming' process is difficult, this process offers high potential in the production of complex shaped superalloy components. In addition, the structural refinement obtainable in squeeze-casting also results in improved mechanical properties.

Brasses containing 60-65%Cu with small additions of silicon-upto 1wt% or lead upto 2wt%, are commonly fabricated for use as die-castings and forgings respectively. Standard brass compositions respond well to squeeze-casting, and Lynch[92] has reported that several prototype components have been made in

a variety of configurations. Forging brass, CDA 377, in particular, has been squeeze-cast with a high degree of success. Lynch[92] has reported that properties, comparable to typical hand book values for the wrought or extruded conditions, are obtained in squeeze-cast forging brass as presented in Table 2.7.

Distinct similarities are also noted between micrographs of material in the squeeze-cast and forged conditions, both showing fine-grained, homogeneous, porosity-free microstructures. A somewhat more isotropic distribution and sometimes finer form of the transformed Cu-rich alpha-phase is observed in the squeeze-cast material in such brasses.

Lynch[92] has further pointed out that manganese-bronze alloys, designed for forging and casting applications, have also responded well to squeeze-casting, as favourable characteristics such as 'section-soundness' and a 'uniform-fine grained structure' are observed in these. Aluminium bronzes are noted for their high strength levels, developed through a eutectoid transformation achieved by relevant heat-treatment. The corrosion resistant wrought Al-bronze, CAD 624, is well-suited to forming by squeeze-casting with properties comparable to typical forged values, as reflected by the data presented in Table-2.8.

Bearing and wear resistant bronzes have been successfully squeeze-cast. Squeeze-casting of high leaded tin bronze, CDA 932, results in 'sound castings' and a smooth machined surface-finish'. Promising results have also been



TABLE - 2.7

## COMPARATIVE PROPERTIES OF CDA 377 FORGING BRASS\*

| Condition    | Ultimate<br>Tensile<br>Strength<br>(ksi) | Yield<br>Strength<br>0.2%<br>Offset(ksi) | Elongation<br>(%) |
|--------------|--|--|-------------------|
| Squeeze Cast | 55.0                                     | 28.0                                     | 32(in 1 in.)      |
| Extruded     | 55.0                                     | 21.0                                     | 48(in 2 in.)      |

\* abstracted from Ref.[92]

TABLE - 2.8

## COMPARATIVE PROPERTIES OF CDA 624 ALUMINIUM BRONZE\*

| Condition    | Ultimate<br>Tensile<br>Strength<br>(ksi) | Yield<br>Strength<br>0.2%<br>Offset(ksi) | Elongation<br>(%) |
|--------------|--|--|-------------------|
| Squeeze Cast | 113.5                                    | 53.0                                     | 13.5              |
| Forged       | 102.0                                    | 50.0                                     | 15.0              |

\* abstracted from Ref.[92]

obtained on higher lead-alloys having greater lubricating ability but lower strength. Rapid rate of solidification, inherent to squeeze-casting, leads to the desirable feature of more uniform dispersion of lead in the cast product, which is otherwise subject to gravity-segregation resulting from the longer solidification times involved in normal casting processes.

The leaded-Sn bronze CDA 925, containing 11%Sn, is traditionally sand-cast for applications in transmission components and gears. Lynch[92] has reported that a heavy-duty transmission synchronizer ring has been successfully squeeze-cast in large quantities in CDA 925 alloy.

### 2.2.6.3 SQUEEZE CASTING OF COMPOSITE SYSTEMS

Squeeze-casting has been extensively employed in recent years for the production of 'high integrity' and 'near-net shape' castings in metal-matrix composites (MMCs). The squeeze-casting technique has been applied to a number of metal-non metal composite systems involving the dispersion of particulates, such as  $Al_2O_3$ , silicon-carbide, graphite, zircon, illite-clay, and, fibres or whiskers of many kinds. The fabrication techniques, problems involved and the characterisation of individual systems, have been dealt with, in detail, in earlier sections viz. secs.2.1.3 and 2.1.4 To summarize, the squeeze-casting route would result in the following specific effects:

(i) the production of highly densified and porosity free matrix, (ii) production of highly grain refined matrix with

considerably improved mechanical properties, occasionally exceeding even forging properties, (iii) production of the near net shape castings where machining requirements would be expected to be minimum, (iv) production of a composite with improved wear resistance and greater fatigue life, (v) production of a composite with improved elevated temperature properties, (vi) production of a cast structure with isotropic properties, and finally, (vii) very high yield (about 80%) and low total energy consumption.

Because of the many advantages mentioned above the squeeze-casting technique has been attempted in a number of composite-systems discussed briefly in the remaining part of this sub-section.

The major part of effort in this direction centred around the fabrication of squeeze-cast fibre reinforced MMCs. In some instances, the liquid metal was infiltrated into the preheated ceramic preforms and then solidified under pressure, for example, Fukunaga[8,9,88], produced 6061 alloy reinforced with  $\text{Al}_2\text{O}_3$  or  $\text{Al}_2\text{O}_3\text{-SiO}_2$  fibres or SiC whiskers using liquid metal infiltration followed by squeezed-casting route. He also showed that the above route can be successfully employed for fabrication of Al-4%Cu-SiC reinforced composites using a squeeze pressure upto 200 MPa, and further demonstrated that the above fabrication technique resulted in improved wear resistance and tensile properties upto nearly 400°C.

Das, Clegg and Zantout [16,18] attempted to disperse  $6\text{-Al}_2\text{O}_3$  fibre and NICALON SiC fibres in Al-4.5%Cu matrix alloy using 'Vortex liquid metallurgy route' followed by squeeze-casting at 140 MPa. The results of their investigations show that both of these kinds of composites display excellent ambient-as well as elevated temperature-tensile properties upto  $350^\circ\text{C}$  and display superior fatigue life and thermal stability compared with ordinary sand-cast or gravity die-cast composites. They also observed that stable bonds were developed between the fibre and the matrix that could withstand cyclic-loading between room temperature and upto  $300^\circ\text{C}$ , without deterioration. Also, at room temperatures, the tensile strength properties increased approximately linearly with increasing fibre content, but the strengthening efficiency was higher at higher temperatures. SEM of tensile fractured surfaces also did not show any loosely bonded or pulled-out fibre which therefore, indicated that fibre-damage during fabrication was minimal. They [16,18], therefore, attributed the better than expected results, obtained for the very modest amounts of fibre added, to, (i) defect-free and ductile matrix resulting from squeeze-casting and also, (ii) the uniformity of distribution and randomness of fibre-orientations. Composites of randomly oriented Alumina fibre reinforced aluminium - 12.5 wt% silicon alloy, were successfully fabricated by squeeze-casting by Ahmed [109], using 50 MPa pressure, who observed that a maximum tensile strength of 224 MPa and a maximum hardness of 74.6 VHN were achieved with

0.20 volume fraction of alumina fibre reinforcement. He[109] attributed this to the presence of alumina fibres in the squeeze-cast composites, which resulted in considerable grain-refinement as well as an improved distribution of silicon and intermetallic phases. Quigley et.al.[12] attempted to fabricate Al-Mg, Al-Cu-Mg alloy matrices- $\text{Al}_2\text{O}_3$  fibre composites, using a combination of compo-casting and squeeze-casting techniques. Through the compo-casting technique, they were able to obtain Du Pont's FP 1- $\alpha$ - $\text{Al}_2\text{O}_3$  fibres in the stirred slurry which was then allowed to solidify. In this way a three-dimensional random dispersion of  $\text{Al}_2\text{O}_3$  fibres was obtained. Thereafter the solidified composite was remelted inside a mullite crucible by means of a 7.5 KW, 3000 hz power supply and super-heated to approximately 50 K above the alloy liquidus temperature. A ceramic filter (Selee) containing about 85% voids was then inserted inside the female die-half. The super-heated composite was then poured onto the filter and the top die was pressed down on it using a 200 ton press. Using this procedure, excess liquid, amounting to approximately 50 to 70 percent, was thus squeezed out into the fine holes of the porous filter. This procedure concentrates the fibre above the filter and aligns them into a random two-dimensional mat. The measured tensile properties of the composites were superior to those of the matrix-alloys. For example, addition of 2 vol. pct FP1- $\alpha$ - $\text{Al}_2\text{O}_3$  fibres to an Al-4wt% Mg alloy matrix increased the planar random modulus of elasticity and ultimate tensile strength by

approximately 50 pct. and 40 pct. respectively.

In a similar effort, Mehrabian et.al.[62] applied the same technique for fabrication of particle-reinforced composites. Composites of wrought alloys-2012 and 2024, and one cast alloy-201 of aluminium containing 2 to 30wt% of  $Al_2O_3$  and SiC particles, in the size range of 1 to 142  $\mu m$ , were prepared. The non-metallic particles were added to a partially solid and vigorously agitated matrix alloy. Adequate retention time was provided during the stirring to facilitate formation of  $MgAl_2O_4$  spinel in the case of reinforcement by  $Al_2O_3$  particles. The cast-composite was then reheated to a superheat of 50 K and then squeezed under high pressure in a closed die forging type of apparatus. A pressure of approximately 200 MPa was applied for a duration of 90 secs to complete the process of solidification under pressure. The authors[62] comment that this applied pressure results in a structure, free of macro-porosity with a relatively homogeneous distribution of the non-metallic particles. In this case also a ceramic filter was employed to obtain high volume fraction composites. These composites were then evaluated for their elevated temperature tensile properties and wear behaviour.

Micro-structures and mechanical properties of SiC whisker (SiCw) reinforced aluminium alloys fabricated by squeeze-casting method were also investigated by Kobayashi et.al.[110]. The SiCw-reinforced aluminium alloys, fabricated

under the pressure of 90 MPa, are superior to those fabricated under lower pressure conditions, in mechanical properties. The fracture of SiCw-reinforced aluminium alloys is associated with the failure of SiCw and the interface decohesion between the whiskers and the matrix. The interface cohesion is strengthened by accelerating the interface reaction adequately. Addition of the highly reactive lithium to aluminium matrix makes the interface cohesion tight and results in lower density and greater strength composites. Composites of Al-Si alloys reinforced by SiC particles of various sizes, varying between 7 to 45  $\mu\text{m}$ , were fabricated by Bayoumi et.al.[111] using the compo-casting technique followed by squeeze-casting in the fully liquid state. During isothermal partial remelting, transformation of the initial dendritic structure occurs into a globular one and it was shown to take place more rapidly in the composites than in the un-reinforced matrix alloy. An interesting observation of Bayoumi et.al.[111] is that after this globular transformation of the matrix, the structure can be easily deformed at comparatively much lower stresses. This implies that subsequent to isothermal partial remelting, the structure can be easily squeeze-cast. In their particular cases[111], a squeeze pressure of 100 MPa and a die temperature of 300°C was employed. This work, therefore, demonstrates the usefulness of semi-solid forming technique for the fabrication of composites. However, it is to be noted that certainly the second step of isothermal partial remelting would add to the cost of fabrication of composites.

Charbonnier et.al.[112] attempted to fabricate a high performance cast-component, out of fibre reinforced MMCs, using the squeeze-casting technique. In their programme, they fabricated polycarbosilane-SiC (PCS SiC) fibre-reinforced MMCs using, (a) commercial purity 1050 Al, and, (b) Al-10%Si casting-alloy. In the fibre preform, the liquid metal was forced at a pressure of 50 MPa. Mechanical properties evaluation demonstrates that 45% PCS-SiC MMCs retained their flexural strength at the level of 450 MPa upto 350°C test temperature. Their [112] results showed that the dynamic modulus of reinforced composite exhibited a better stability upto 350°C compared with titanium TA6V alloy.

Yamada et.al. [113] made a new attempt in the direction of fabrication of hybrid fibre-reinforced MMCs. In their experiments, they dispersed whiskers and particulates in between Si-Ti-C-O fibres of 11  $\mu$ m dia in a metal matrix of Al-4%Cu, Al-3%Si and Al-5%Mg alloys, using the squeeze-casting route. A pressure of 90 MPa applied for 60 sec was used in these experiments. Based on their work, they concluded that squeeze-casting could be successfully employed for fabrication of such composites with considerably improved properties. Their results further showed that whiskers and particulates hybrid composites displayed superior longitudinal as well as transverse flexural strength compared with conventional composites.

Clegg et.al.[17], in their attempt to fabricate SiC fibre reinforced Al-4.5wt%Cu alloy and Zn-27wt% Al-3wt%Cu alloy



MMCs, demonstrated that squeeze-infiltration resulted into the fabrication of superior MMCs. They suggested that fibre damage and/or degradation should be avoided, as far as possible, during the process of fabrication. With this view in mind, they suggested that all casting processes must ensure that, (i) a controlled interaction between the molten metal and the fibre takes place, and, (ii) the structure of the matrix must remain stable. They also concluded that for the Al-alloy composite, a steady improvement was observed in the values of mechanical properties with increasing content of chopped SiC fibres, but there was a deterioration in the values, of these properties, except for the elastic modulus in case of the Zn-alloy composites with increasing concentrations of SiC. They also observed that the room temperature fatigue life of both the Al-alloy and the Zn-alloy composites showed improvement with increasing fibre content.

Diwanji and Hall[114] investigated the influence of a number of variables on performance of high modulus carbon fibre-reinforced aluminium composites, which were squeeze-cast by Honda R & D Co. Ltd., Wako-Shi, Japan. The basic composite system, against which all variations were compared in this work is aluminium alloy, A-356 containing 7wt%Si, 0.3wt%Mg and 0.3wt%Fe, reinforced with the high modulus M-40 carbon fibres, using a preform temperature of 600°C and melt temperature of 780°C, the nominal fibre volume fraction being 35%. The basic objective of this study was to investigate how manufacturing

conditions affected the fibre-matrix interface. They studied the effect of variation in fibre preform-temperature, matrix-alloying and heat-treatment on the mechanical properties and fibre-matrix interaction in carbon-aluminium composites, and, found that the mechanical properties of the continuous carbon fibre aluminium composite depended on the interface properties and also that the interface properties, in turn, depended on the manufacturing parameters. These workers, therefore, concluded that the interface shear strength in continuous carbon fibre aluminium composites was low, which resulted in an inefficient transfer of load to the fibres and hence, in weaker composites. The interface bonding in these composites is mostly a mechanical type and as such the efficiency of load transfer to the fibres is very poor.

Sample et.al.[115] fabricated unidirectional continuous graphite fibre reinforced aluminium matrix composite with the fibre volume fraction ranging from 4 to 52%. For this purpose, they employed 606 aluminium alloy as the matrix material and, pitch based type P-55 graphite fibres, as the fibre reinforcements. These fibres typically have a tensile strength of 2100 MPa and a stiffness of 379 GPa. For each casting, two identical preforms were used. For each preform, planar-random graphite fibre mats were used between the layers of the low graphite fibres. The liquid alloy was infiltrated into the preform at a temperature at 1100 K using a squeeze pressure of 250 MPa. Some of the squeeze-cast samples were heat-treated to

allow controlled metallurgical reaction between the fibre and the matrix. Interestingly, the unidirectional continuous fibre reinforced castings displayed an almost linear relationship between the tensile strength and the unidirectional fibre volume fraction in the range of 4 to 52%. They [115], therefore, concluded that the fibre to matrix bonding in the squeeze-cast composites was primarily of adhesion type and there was very little evidence of interfacial reaction between the fibre and the matrix.

Bhagat et.al.[116] also attempted to fabricate graphite fibre reinforced metal matrix composites employing, copper, aluminium, tin and babbitt matrices through high pressure squeeze-casting technique. The fibre volume fraction of these composites ranged from 5-55%. They employed both bare and nickel coated planar random graphite fibre mats. In their technique, molten metal matrix was force-infiltrated into hard made preforms of fibre mats in a metallic die without any need of preheating the die or the fibre preform. Thus, the infiltration was completed in less than 10 secs under a pressure ranging upto 500 MPa. As a result, fibre to matrix reaction at the interface was minimised. As a result, these workers [116] reported that the nickel coating remains intact on graphite fibre in the composites, and also that the bonding between the fibre and the matrices was primarily of adhesion type. This work also demonstrated the superior damping capacity of the graphite/aluminium composites-upto 7.4 times that of 6061-T6

aluminium, over a frequency range of 300 hrz to 12000 hrz. Electro-chemical corrosion studies of Gr/Al and Gr (Ni)/Al composites in 3.5% NaCl solution also revealed that presence of nickel on the coating on fibres in the fabricated composites significantly reduces the damage of the Gr (Ni)/Al composites, which was in contrast to the extensive damage suffered by Gr /Al composites because of cumulative effects of dissolution of aluminium, hydration of  $Al_4C_4$  into  $Al(OH)_3$  and, galvanic coupling between Gr and Al. The latter two mechanisms are almost non-existent in Gr(Ni)/Al composites.

The Japanese have patented [117] a method for the incorporation of stainless steel fibres in a squeeze-cast aluminium alloy connecting rod, with the principal objective of replacing a steel forging with a light weight casting.

As concluding remark one may state that, 'whilst the commercial exploitation of cast composites is in its infancy , it appears from the commitment to developmental-work throughout the world, that this will be a growth area for castings and one in which squeeze-casting will play a major role'.

## 2.3 WEAR

### 2.3.1 INTRODUCTION

There are three main ways in which mechanical components lose their usefulness viz. obsolescence, breakage, and wear. Different groups of objects feel the impact of these to different degrees. Wear is an universal phenomenon. The existence of wear has been recognised for a long time, and, several research-programmes have been undertaken in different parts of the world to correlate wear to a number of inter-related parameters such as load, the type of motion, the nature of surfaces, the presence of foreign matter, the nature and intensity of motion, etc. These research efforts can be broadly classified into different categories, viz., (i) development of wear resistant alloys, (ii) designing of components to reduce wear and improve their working life, (iii) studies in energy-conservation & energy efficiency in transport sector etc. One important area of research has been concerned with identification of the actual mechanisms involved in the material removal, resulting from wear.

Wear behaviour of a number of systems such as Al-Al<sub>2</sub>O<sub>3</sub>, Al-Si alloys, Al-graphite, LM 13-graphite, Al-Pb alloys, Al-mica etc. have been investigated in detail in recent times under dry sliding conditions. Depending upon whether a hard particle or phase or a soft particle or phase is dispersed in the base matrix, the dry sliding behaviour of the individual system has been found to be widely different.

In most of the systems mentioned above, the base matrix, which plays a vital role in the total process of wear, has been modified or strengthened through different means such as alloying and heat-treatment. It would be interesting to examine what will happen to the total process of wear, if the concerned composite is frozen under pressure i.e. squeeze-cast. This is because in squeeze-casting, a strong, tough and hard base matrix would be obtained, which would be expected to display comparatively superior wear resistance. Though work in this direction has been carried out by several workers in case of fibre reinforced composites, yet such investigations on particle reinforced MMCs are rather scarce. However, interest in this direction has been recently picking-up.

### 2.3.2 DEFINITION OF AND PARAMETERS CONTROLLING WEAR

Rabinowicz[118] defined wear as "the removal of material from solid surfaces as a result of mechanical action". A potential wear situation exists whenever there is relative motion between two solid surfaces under load. Sarkar [119] has pointed out that such motion can be unidirectional or reciprocating, either sliding or rolling, or a combination of these. Therefore, to understand wear, it is imperative to study the topography and the physico-chemical nature of surfaces. Sub-surface deformation of solids plays a fundamental role in the mechanism of friction and wear, so that the stresses at the points or surfaces of contact, and, the type of motion involved, must be studied when analysing the nature and amount of wear in the kinematic chain of

machinery.

Several parameters, play important role during the process of wear. The important ones include, (i) roughness of both surfaces in contact, (ii) temperature of the interface, (iii) sliding distance, (iv) sliding speed, (v) atmosphere (esp.oxidizing), (vi) mechanical properties of alloys (or metal), (vii) load, (viii) composition of alloys, (ix) lattice type, (x) area of contact, (xi) type of motion, (xii) lubrication, and, finally, (xiii) nature and properties of dispersoid phase.

### 2.3.3 TYPES OF WEAR

Depending on the nature of movement or the media involved in an interaction under load, Rabinowicz[118] has stated that the following types of wear may be recognized:

#### 2.3.3.1 ADHESIVE WEAR

This form of wear occurs when two smooth bodies slide over each other. The relative movement can be unidirectional or reciprocating and interaction occurs under a small amplitude-oscillatory contact under load. Due to this, fragments are pulled off from one surface and adhere to the other, later these fragments may come off the surface on which they are formed and be transferred back to the original surface, or else form loose wear particles. Generally speaking adhesive wear takes place with low velocity, small load and smooth surfaces. This is due to the adhesive forces set-up whenever atoms come into

intimate contact. This is the universal type of wear that occurs with any machine and cannot be eliminated, but only reduced.

#### **2.3.3.2 ABRASIVE WEAR**

This form of wear occurs when a rough hard surface or a soft surface containing hard particles, slides on a softer surface and ploughs a series of grooves. This takes place normally at high load more easily than adhesive wear or takes place at small loads after rotating with high revolution, or after adhesive wear has taken place and continues to rotate.

#### **2.3.3.3 CORROSIVE WEAR**

This form of wear occurs when sliding takes place in a corrosive environment. In the absence of sliding, the products of the corrosion would form a film on the surfaces, which would tend to slow down or even arrest the corrosion, but the sliding action wears the film away, so that the corrosive attack can continue.

#### **2.3.3.4 SURFACE FATIGUE WEAR**

This form of wear is observed during repeated sliding or rolling over a track. The repeated loading and unloading cycles to which the materials are exposed may induce formation of surface or sub-surface cracks, which eventually will result in the break-up of the surface with the formation of large fragments, leaving large pits in the surface.



### 2.3.3.5 OTHER FORMS OF WEAR

There are several other forms of wear which are probably as important as the above four forms, but not studied in detail. These may include fretting, cavitation and erosion. As regards fretting, it seems that it is not a primary form of wear, but a phenomenon which occurs when other wear mechanisms act together under oscillatory sliding conditions. Whether erosion or cavitation are admitted as forms of wear, depends on whether damage by impacting-particles or by the sudden boiling of a liquid are accepted as falling within the category of 'mechanical action'.

### 2.3.4 TECHNIQUES OF MEASURING WEAR

Numerous experimental devices have been developed for the study of the anti-wear and anti-friction properties of materials, additives and lubricants. Devices used for determination of anti-wear and anti-friction properties fall into two principal classes:

#### (i) Laboratory test devices

These tests use a relatively simple test specimen configuration to model frictional processes occurring in real machines or to perform frictional processes under specific conditions.

#### (ii) Real service tests

These tests use machine parts and are adequately

equipped with measuring instruments. Testing is done under real-service conditions. These tests are expensive and of long duration. Investigation costs increase substantially when passing from laboratory tests to real-service tests.

The most widely used apparatus to study anti-wear properties is pin-on-disc type testing rig. It is the simplest machine used to evaluate wear rate of materials "as occurring in application". In its common form, it generally consists of a horizontal rotating disc. The mating surface is usually a cone, a sphere or a cylindrical pin fabricated from the test materials. The test-specimen is mounted on a balanced lever arm and loaded against the rotating surface. Frictional force is commonly measured by strain gauges mounted on the vertical sides of the lever arm in such a manner as to record the horizontal bending stresses induced in the latter. The normal load may be applied as a dead-weight or by a hydraulic cylinder device. Contact temperature can be measured easily by using a thermocouple. The relative sliding velocity between the pin and the disc can be varied over a wide range either by changing the r.p.m. or by adjusting the radial distance between centre of the disc and the contact point. Wear rate can easily be calculated in terms of either weight-loss or volume-loss per unit time or per unit sliding distance.

The most common way of studying wear, consists of examination of the mass or volume of the sliding material before and after the test with any difference in these being attributed

to wear. The detection of wear generally uses one of the techniques of weighing, of mechanical gauging or of optical examination of surface and sub-surface features. Another new technique, of measuring wear incorporates use of radio-tracers. The limit of resolution of the weighing method is generally about  $10^{-7}$  kg, and, of mechanical gauging method is about  $10^{-5}$  m, which for a rider of surface area  $10^{-6}$  m<sup>2</sup>, allows one to measure down to  $10^{-1}$  mg. The horizontal limit of resolution of optical method is about  $10^{-6}$  m. Rabinowicz[118] has pointed out that the technique using radio-tracers gives accuracy of about  $10^{-6}$  to  $10^{-9}$  mg.

For measuring the friction during sliding, it is customary to use a dynamometer method in which the force required to keep one body stationary, when pressed against a moving surface, is monitored. Normally, the friction force is recorded continuously. The friction force can be readily converted to the static friction coefficient.

### 2.3.5 SOME RECENT INVESTIGATIONS INTO THE WEAR BEHAVIOUR OF ALUMINIUM ALLOYS AND COMPOSITES

#### 2.3.5.1 Al-Si SYSTEM

Al-Si alloys have been used for tribological applications under conditions of both dry and lubricated contact.

Okabayashi et.al.[120] investigated the friction and wear characteristics of selected cast aluminium-silicon alloys, and, found that the hyper-eutectic aluminium-silicon alloys had better wear-resistance. Based on their studies to determine the

influence of the primary silicon content and its distribution on the wear resistance of the alloys, they concluded that refinement of the primary silicon phase gave little improvement in wear resistance. The amount of primary silicon is a more important factor than the size of the particles. Vandelli[121] carried out wear tests on three hyper-eutectic alloys, each of which had been treated with phosphorous to refine the primary silicon phase. The 17%Si alloy showed the best wear-resistance, which was attributed to the more uniform distribution of silicon particles.

Sarkar [122] investigated the wear characteristics of two aluminium-silicon alloys-LM13, a hypo-eutectic alloy with 10.9%Si, and LM29, a hyper-eutectic alloy with 22.1%Si, and, concluded that the wear resistance of the hyper-eutectic alloy was inferior to that of the low-silicon alloy. Based on their studies, Clegg et.al. [123] also concluded that 'modification' of structure of hyper-eutectic Al-Si alloys does not influence the wear-resistance of the alloy significantly.

Mohammed Jasim and Dwarakadasa [124] studied the wear behaviour of binary aluminium-silicon alloys as a function of bearing load, sliding speed and alloy composition. Their results indicated that wear in these alloys was related to a zone of sub-surface deformation in which the silicon phase is fragmented into spheroids. They also found non-dependency of wear rate on silicon structure. The eutectic aluminium-silicon alloy exhibited the lowest wear rate. The sub-surface region did not show any signs of plastic deformation. Instead, the silicon

platelets were fragmented into spheroids under the influence of severe mechanical strain. These authors also suggest that the high temperature produced at the wear interface might have contributed to the process of fragmentation and spheroidisation of silicon platelets.

Sarkar and Clarke [125] also found that a near-eutectic alloy is the best tribological material as compared to other Al-Si alloys. They found that the wear fragments are produced by a process of delamination. Dwarakadasa et.al. [126] concluded that in Al-based alloys, as the bearing pressure is increased, the wear rate exhibits three regions viz. the oxidative wear under low loads, the metallic wear under high loads, and, a combination of the oxidative and the metallic wear in the intermediate range.

Suh [127] has suggested that for ductile materials, surface wear is influenced by the sub-surface deformation. For a system consisting of a hard second phase in a ductile matrix, the sub-surface deformation is delineated by fragmentation of the second phase as observed by Rohatgi and Pai [128] for Al-Si and Al-Si-Ni systems and by Sarkar and Clarke [129] and Jasim and Dwarakadasa [124] for Al-Si system. Pramila Bai et.al. [130] have proposed that the formation of a sub-surface zone is considered to consist of several stages. At the commencement of sliding, the force acting on the rubbing surface is transmitted to the sub-surface. The ductile matrix undergoes plastic deformation and cracks develop in hard brittle inter-dendritic silicon and

other inter-metallic compounds. Eventually these particles are fragmented. With an increase in the friction force, the immediate sub-surface area is subjected to higher plastic strain, which results in further fragmentation of particles and their dispersal in the adjacent regions. The friction force increases with sliding distance until it reaches a stable value. At this stage, the sub-surface region is subjected to plastic strain to a considerable but stable depth. Ruff [131] showed that this strain has a maximum near the surface and decreases with sub-surface depth until it is zero in the undisturbed sub-surface.

#### 2.3.5.2 Al-Pb SYSTEM

Amongst the aluminium base bearing alloys, aluminium-tin alloys are widely used in industrial bearings. Mohan et.al. [132], analysing relative economies, have emphasized that substitution of tin by lead is of interest due to the relatively lower cost of lead. It has also been observed by Avramov [133] that a considerably smaller content of lead in aluminium-lead alloys ensures better ability of the alloy to maintain an interfacial film of lubricant than tin. However, the production of aluminium-lead alloys by conventional techniques poses an acute problem due to the 'gravity-segregation' and their 'mutual immiscibility', even at elevated temperatures [134]. Sriramakrishnan et.al. [135] introduced lead in Al-Si and Al-Si-Cu-Mg alloys through vortex technique and found that these alloys possessed superior properties compared to Al-graphite

system.

Mohan et.al. [132,136] produced stir cast aluminium-lead alloys and based on their studies on these, concluded that as the lead content of stir-cast Al-Pb alloy is increased, the wear rate reduces upto 20wt%Pb beyond which the rate of wear increases drastically due to wide-spread cracking and removal of thick layers of lead, present at the wear interface.

#### 2.3.5.3 Al-GRAPHITE PARTICULATE COMPOSITES

Al-graphite composites are made by dispersing graphite powder in molten aluminium [137]. Pai and Rohatgi [53] have pointed out that the composite, which has been developed as a bearing alloy, has been found to have excellent seizure-and gall-resistance in the presence of a liquid lubricant. Pai et.al. [138] and Tokisue et.al. [139] have reported that under lubricated and highly loaded conditions, the wear resistance of Al-graphite composite increases with increase in graphite content. Recent work by Biswas et.al. [140], conducted under industrial conditions, has shown that journal bearings of this composite perform better in terms of bearing temperature rise than those of the phosphor bronze and are able to run under conditions of boundary lubrication without seizure. Recently, Surappa et.al. [141] have made similar composites by dispersing uncoated graphite in a conventional piston alloy, LM13 and Krishnan et.al. [142] have shown that pistons made from this

composite result in fuel-saving as compared with LM13 pistons. Biswas and Pramila Bai [143] have pointed out that at present, this composite is being extensively field-tested in India, Italy, Japan, USSR and other countries as a replacement for expensive conventional bearing alloys such as phosphor-bronze for piston, piston rings and cylinder liners.

The work of Suwa et.al. [144] shows that under dry conditions for a short sliding distance of less than 2 km, the wear-resistance of nickel coated Al-graphite composite increases with increasing graphite content. But Biswas et.al. [143] found that an increase in the weight percentage of graphite in the composite increases wear in the ranges of bearing pressure ( $0.006-0.08 \text{ kgf mm}^{-2}$ ), surface speeds ( $4-10 \text{ m.s}^{-1}$ ) and sliding distances (4-13 km) studied.

#### 2.3.5.4 Al-MICA PARTICULATE COMPOSITES

Mica is a lamellar solid which requires 20 times more energy than graphite to be smeared over the lamellar planes [145]. However, it is oxidation resistant and has been used as a grease-filler for wagon-axles, a bag-lubricant for moulding, and, a self-lubricant filament tube. It has been shown that additions of mica to silver [146,147], bronze [148] and nickel [149], using powder metallurgy techniques, have led to an improvement in the anti-friction properties of base materials. However, very little work has been reported on production of metal-mica composites by liquid metallurgy techniques and to establish the anti-friction



properties of such composites. Sato and Mehrabian [150] dispersed mica particles in aluminium alloys using compo-casting method. Deonath et.al. [151] reported the journal bearing characteristics and wear properties of aluminium-mica particulate composites made by a foundry technique in which the mica was dispersed above the liquids temperature of the base alloy. They found that the wear rate increases with mica content as well as with bearing pressure. This was due to the loss of mica particles which are loosely bonded to the matrix. They [151] also reported that the Al-Cu-mica-composite bearing can run under boundary lubrication, semi-dry and dry conditions where the mica free-base alloy bearing seizes. The main reason assigned for this behaviour is the presence of loose mica particles released by bearing pressure at the bearing/shaft interface. In the absence of any liquid lubricant film at this interface, the mica acts as a solid lubricant and diminishes metal-to-metal contact and thus prevents seizure.

#### 2.3.5.5 Al-FIBRE REINFORCED COMPOSITES

Fukunaga [88] studied wear behaviour of the composites with reinforcements of  $Al_2O_3$  and  $Al_2O_3-SiO_2$  fibres and SiC whiskers, which were prepared by squeeze-casting technique. The aluminium alloy 6016 containing 0.89%Mg, 0.49%Si, 0.4%Fe, 0.31%Cu, 0.24%Cr, was employed as the base matrix. He concluded that among the three composites tested, the SiC/6061 composites showed best wear-resistance. As the sliding speed increases, the

wear-rate of the composites decreases. The wear rate is very small at low normal loads, but significantly increases at the higher normal load exceeding a certain value. The author [88], therefore, suggested that the above composites in service should preferably be subjected to low normal loads and higher sliding speeds.

Verma et.al. [7] have shown that the squeeze-cast A206- $\text{Al}_2\text{O}_3$  and  $\text{SiO}_2$  discontinuous fibre reinforced composites had abrasive wear resistance comparable to induction hardened AISI 1345 steel. Comparison of the results of their performance, in this work, is presented in Table-2.9 and needs no further comments.

Peters [160] showed that there was a 70% improvement from the use of an alumina-silica ceramic fibre in the Toyota piston and an 80% improvement in the piston through the use of an alumina fibre. This improvement was achieved with only a small amount of fibre (5-7% fibre volume). A US piston manufacturer [161] reports that a Ni-resist cast iron insert can be replaced with a ceramic fibre insert resulting in equal performance and a 5-10% reduction in total piston weight. Even a small reduction in piston and connecting rod weights can have a significant impact on decreasing parasitic engine power losses. This is especially important in higher speed engines where inertial loads are critical.

TABLE - 2.9

COMPARISON OF AISI 1345 AND SQUEEZE CASTING COMPOSITE PROPERTIES\*

| Material   | Specimen No. | Initial Weight, g | Final Weight g | Weight Loss, g | Average Weight Loss, g | Average Volume Loss, mm |
|--|--------------|-------------------|----------------|----------------|------------------------|-------------------------|
| AISI 1345  | 1            | 114.4135          | 114.1204       | 0.2931         | 0.2779                 | 35.4                    |
|  | 2            | 114.3513          | 114.0807       | 0.2706         |                        |                         |
|  | 3            | 114.3439          | 114.0739       | 0.2700         |                        |                         |
| A206-T7 + Ceramic Foam                                     | 1            | 43.7071           | 43.0129        | 0.6942         | 0.6885                 | 242                     |
|  | 2            | 48.0881           | 47.4054        | 0.6827         |                        |                         |
| A206 + Al <sub>2</sub> O <sub>3</sub> and SiO <sub>2</sub> | 1            | 47.6596           | 47.4943        | 0.1653         | 0.1653                 | 55.9                    |

\* abstracted from Ref.[7]

### 2.3.5.6 Al-CERAMIC PARTICLE COMPOSITES

Several researchers have reported that incorporation of hard ceramic particles such as alumina [44,62,150], silicon carbide [41,152], silica [153] or zircon [154,155] into aluminium-alloys increased their wear-resistance. The alumina particle reinforced aluminium alloy pistons performed well. Power output increased with a remarkably low wear rate of the composite pistons [156]. Surappa et.al. [44] reported their results on the adhesive wear of Al-Al<sub>2</sub>O<sub>3</sub>, Al-11.8 wt%Si-Al<sub>2</sub>O<sub>3</sub> and Al-16 wt% Si-Al<sub>2</sub>O<sub>3</sub> composites. They found that the adhesive wear rate of aluminium and aluminium silicon alloy decreased with additions of Al<sub>2</sub>O<sub>3</sub> particles of 100  $\mu$ m size, since those particles did not pull-out during the wear process, thereby reflecting to the improved wear resistance of such materials. Hosking et.al. [62] concluded that with the increasing additions of non metals such as Al<sub>2</sub>O<sub>3</sub> and SiC, to the aluminium matrices, the wear mechanism changed from a purely adhesive to mixed mode of oxidative-abrasive wear. Increasing the applied load from 200 to 1000 gm on the 20 wt% non metal containing composites, appeared to change the wear mechanism to a purely abrasive one. They also found that, (i) the weight loss continuously increased with increasing sliding distance, (ii) introduction of the hard non-metallic particles reduced the weight loss at a given sliding distances, and, (iii) the weight loss at a given sliding distance decreased with increasing weight percent and size of Al<sub>2</sub>O<sub>3</sub> particles.

Bhansali et.al. [156] have reported that the wear resistance of a composite containing large alumina particles, 142  $\mu\text{m}$  in size, was better than that of composites containing smaller particles. However, the size of hard ceramic particles also plays an important role in the ease of machining, and, Yang et.al. [157] have reported that if the hard particles are larger than 50  $\mu\text{m}$  in size, the composites tend to be very difficult to machine. Much research [158,159] is devoted to eliminating this step by perfecting 'near net shape production techniques' such as squeeze-casting.

Yang et.al. [157] incorporated 1-20 wt% bauxite particles into Al-12 Si-1.4 Cu-1.3 Mg alloy by the rheo-casting method. The abrasive wear resistance increased with increasing amounts of particulate addition. Under low and moderate loads, the wear resistance of the composite containing 20 wt% bauxite was comparable to that of carbon steel. However, under high loads, carbon steels were superior to the composites in wear-resistance. Particle-clustering was also observed in the composites owing to the small size of the bauxite particles viz. -300 mesh size, but it had little influence on the wear-resistance of the composites.

#### 2.4 SUMMARY AND STRATEGY FOR PRESENT INVESTIGATION

It can be concluded from the preceding discussion in section 2.1.4.4 that the cast particulate MMCs suffer from mainly the following drawbacks:

- a) poor wettability of dispersoid ceramic particles for the liquid melt.
- b) poor bonding of ceramic particles with the base matrix.
- c) preferential segregation and coagulation of non-metal dispersoid particles.
- d) presence of considerable amount of porosity in the cast structure, which seriously deteriorates the performance of composites in tension.

The strategy adopted in the present set of investigation was to employ squeeze casting as a possible means of achieving a densified and grain refined matrix with near zero porosity level. It was planned to employ squeeze pressure in the range of 80 to 140 MPa in regular steps of 20 MPa with die temperature also varying as ambient, 100 and 200°C. The main objective of this study was to examine as to how and to what extent the increasing degree of squeeze pressure applied during the solidification of the stirred slurry, would influence the properties of Al-Al<sub>2</sub>O<sub>3</sub>-MgO cast particulate MMCs. Obviously for this purpose, properties of squeezed composites (at different MPa levels & the die temperatures) had to be compared with the properties of ordinary gravity chill cast composites. Another objective of present study

was to examine, as to how the standard 'MgO coating' technique developed earlier could be applied for the preparation of the stirred slurry under humid environmental conditions as existing in this region. In order to prepare the stirred slurry for present investigations (using vortex liquid metallurgy route), it was planned to keep the amount of total ( $\text{Al}_2\text{O}_3 + \text{MgO}$ ) powder mixture at a fixed level of 10wt% of melt. This parameter was fixed based on the results of an earlier study. The problem of proper bonding of dispersed  $\text{Al}_2\text{O}_3$  particles with the base matrix and the nature and chemical composition of reacted layer around  $\text{Al}_2\text{O}_3$  particles was planned to be investigated with the help of JEOL EPMA.

Another objective set for present investigation was to examine the tensile behaviour of both gravity chill cast and squeezed composites thoroughly upto  $300^\circ\text{C}$  (573K). The results of this study would be expected to show as to how and to what extent the tensile behaviour of Al- $\text{Al}_2\text{O}_3$ -MgO particulate MMCs is improved upon squeezing.

It was planned to examine also the wear behaviour of ordinary gravity chill cast and squeezed Al- $\text{Al}_2\text{O}_3$ -MgO particulate MMCs under dry sliding conditions. This was, in fact, planned to be an initial investigation into the wear behaviour of above composites. For this purpose, a standard pin-on-disc testing rig and a cylindrical wear pin of 10 mm dia and 30 mm length was planned to be employed. Only three composites namely composite Nos. 1,2 and 3 representing three extreme conditions of composite fabrication were earmarked for this study. Composite No.1

represents gravity chill cast condition while composite Nos.2 and 3 respectively represent the lowest and highest levels of squeeze pressures applied during squeeze casting operation. Three levels of bearing loads namely 500 gm, 1000 gm and 1500 gms and three levels of sliding speeds namely 9.4, 14.1 and 18.8  $\text{m}\cdot\text{sec}^{-1}\times 10^{-2}$  were planned to be employed for wear studies. The wear test for a given composite at a fixed bearing load and sliding speed was planned to be run for  $\frac{1}{2}$ , 1 and  $1\frac{1}{2}$  hrs. Thus, in all 81 wear runs were planned to be conducted for the three composites. A detailed study of the morphology of the debris particles and the sub-surface damage in different composites immediately below the worn surface was also planned to be conducted using optical and SEM techniques. The overall objective of this study was to examine as to how and to what extent the process of squeeze casting can improve the wear resistance of Al-Al<sub>2</sub>O<sub>3</sub>-MgO cast particulate MMCs as against ordinary gravity chill cast composites.



## CHAPTER 3

### EXPERIMENTAL PROCEDURE

#### 3.1 INTRODUCTION

The strategy adopted in the present work was to fabricate Al-Al<sub>2</sub>O<sub>3</sub>-MgO particulate MMCs through the 'liquid metallurgy' route. For this purpose, the standard 'MgO coating' technique developed earlier [47-49] was modified to suit the humid environmental conditions existing in this region and was termed as modified 'MgO coating' technique. The stirred slurry produced by the above technique was then squeezed (liquid forged) in the pressure range of 80 to 140 MPa. In order to ascertain the influence of submicron size MgO particles in stiffening the Al base matrix, some heats of Al-MgO composites were also prepared and then squeezed at 80 and 140 MPa (the two extreme levels of pressures employed in the present set of experiments). The squeezed Al-Al<sub>2</sub>O<sub>3</sub>-MgO particulate MMCs were then examined for their physical and mechanical properties using sophisticated techniques.

The properties of above composites were then compared with gravity chill cast composites prepared from the same stirred slurry. In particular, tensile behaviour of Al-Al<sub>2</sub>O<sub>3</sub>-MgO particulate MMCs were examined upto 300°C (573K). The reacted layer around Al<sub>2</sub>O<sub>3</sub> particles at the particle/matrix interface was also examined for its nature by the EPMA. The wear behaviour of

squeezed Al-Al<sub>2</sub>O<sub>3</sub>-MgO particulate composites was also examined in some detail under dry sliding conditions using a pin-on-disc testing equipment.

### 3.2 SPECIFICATIONS OF RAW MATERIALS

#### 3.2.1 COMMERCIALY PURE ALUMINIUM

Conformed to the following analysis:

Al - 99.7% , Mg - 0.001%

Fe - 0.224% , Mn - 0.001%

Si - 0.019 , Other elements - 0.055%

Ingots of commercially pure aluminium weighing about 25 Kgs. each were obtained from standard firms in India and it can be seen from the above analysis that this metal contained iron and silicon as the chief impurities amounting to 0.224% and 0.019% respectively.

#### 3.2.2 ALUMINA POWDER

Conformed to the following specifications :

Particle size range - 50-150  $\mu$ m

Density - 3.9 gms/cm<sup>3</sup>

Melting Point - 2050°C

Classification results of Al<sub>2</sub>O<sub>3</sub> powder employed in the present work are given below (Table-3.1).

Table - 3.1 Sieve Classification of Al<sub>2</sub>O<sub>3</sub> Powder

| S.No. | Sieve aperture<br>( $\mu\text{m}$ ) | wt% retained | Cummulative<br>wt% |
|-------|-------------------------------------|--------------|--------------------|
| 1     | + 150                               | 8.512        | 8.512              |
| 2     | + 103                               | 29.98        | 38.492             |
| 3     | + 75                                | 29.61        | 68.102             |
| 4     | + 53                                | 17.35        | 85.452             |
| 5     | - 53                                | 14.50        | 99.952             |

It is apparant from the above results that the Al<sub>2</sub>O<sub>3</sub> powder employed in the present set of experiments contained particles varying in the size range of mainly 53  $\mu\text{m}$  and 150  $\mu\text{m}$ .

The Alumina powder was obtained in sealed bottles of 500 gm each from M/S Qualigens Fine Chemicals. A division of Glindia Limited, Dr. Anne Besant Road, Bombay (India).

### 3.2.3 MAGNESIUM OXIDE POWDER

Conformed to the following specifications :

Particle size range - 0.2 to 0.3  $\mu\text{m}$

Density - 3.7 gms/cm<sup>3</sup>

Melting Point - 2800°C

The above powder was obtained in packets of 500 gm each from M/S Burgoyne Burbidges and Company (India), Lower Parel, Bombay, India.

### 3.3 BLENDING AND DEHYDROXYLATION OF CERAMIC POWDERS

( $\text{Al}_2\text{O}_3 + \text{MgO}$ ) powder mixture amounting to 10 wt% of the liquid aluminum melt (1100 gms) was weighed accurately. Thus, in each case, a powder mixture ( $\text{Al}_2\text{O}_3 + \text{MgO}$ ) of 110 gms was employed. Also, in each case, this powder mixture contained 15% MgO. Prior to blending, the weighed quantities of individual powders were given a heat treatment. The objective of this heat treatment at  $900^\circ\text{C}$  for 2 hrs was to dehydroxylate the surfaces of ceramic particles fully. After this treatment, the ceramic powders were stored in a moisture oven maintained at  $200^\circ\text{C}$  so that no further adsorption of moisture could occur on the surfaces of ceramic particles. After the powders cooled down to the oven temperature, they were blended in a eccentrically mounted steel blender ( a small ball mill ) for a period of about 30 minutes. The above blender contained about 50 small steel balls of varying diameters ranging from 3 to 6 mm. Schematic diagram of this blender is shown in Fig.3.1. The blended mixture was stored carefully in a dessicator for further use in the preparation of the stirred slurry.

In few cases, above powder mixture ( $\text{Al}_2\text{O}_3 + \text{MgO}$  containing 15%MgO) amounting to only 5% of the aluminium melts was also employed to obtain comparative property performance data on the resulting composites.

### 3.4 EXPERIMENTAL SET UP EMPLOYED FOR THE PREPARATION OF THE STIRRED SLURRY

The set-up fabricated for the preparation of the stirred

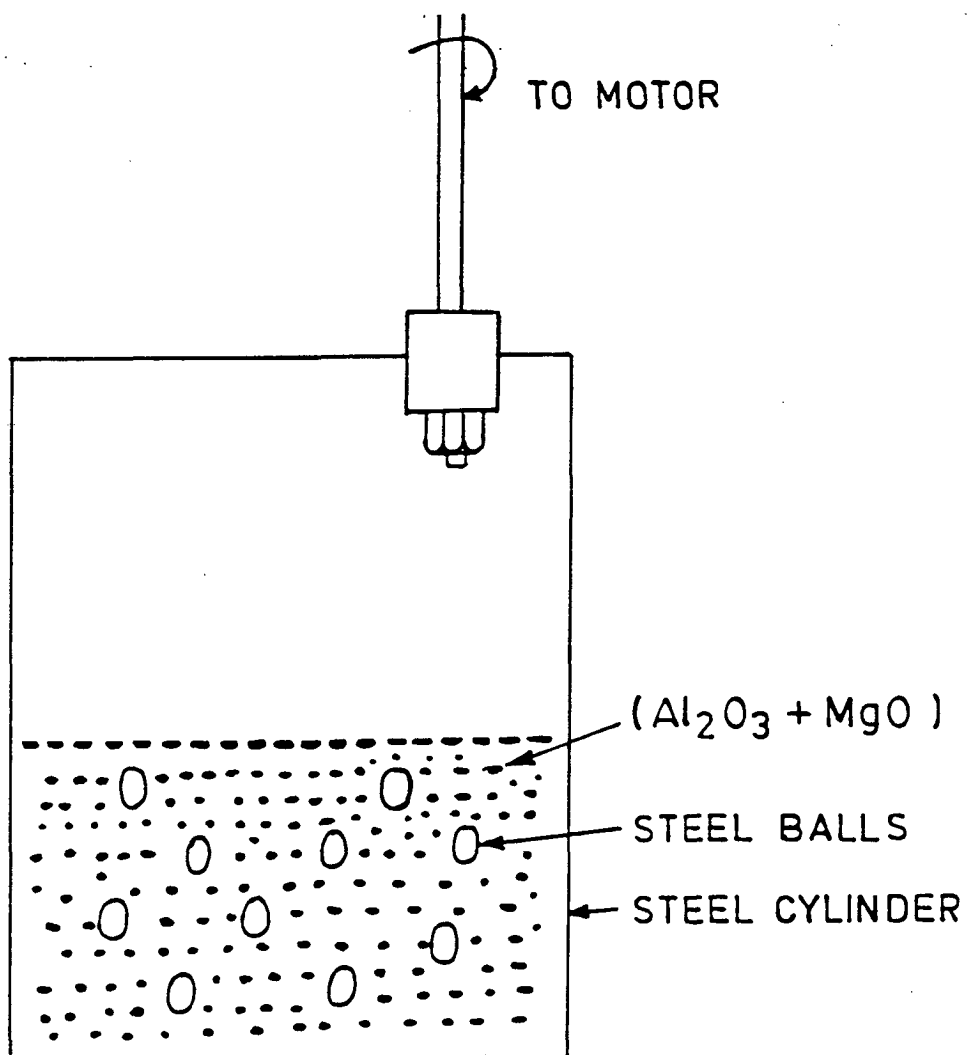


FIG.3.1 Schematic diagram showing eccentrically mounted blender for the preparation of MgO coated  $Al_2O_3$  powder.

slurry is shown in Fig.3.2. It consists of :

a) A Kanthal Wound resistance heating furnace of 2.5 KW capacity employed for melting and superheating of aluminium melt. Kanthal wire of 18 SWG was wound in parallel on the walls of a vertical type rectangular muffle (20x20x33 cm), one end closed, to result in an operating current of about 10 amps. After proper insulation, the muffle was enclosed in a suitable steel frame. Power input to the furnace was controlled through the dimmerstate (Max.Capacity - 28 Amps.) and Aplab automatic temperature controller, to within an accuracy of  $\pm 5^{\circ}\text{C}$  of the preset temperature. A chromel-alumal thermocouple dipped within the liquid melt to a depth of about 30 mm from the surface and connected to a potentiometer was employed to monitor the temperature of the liquid melt. Another thermocouple was placed close to the muffle wall whose objective was to indicate and control the temperature of the furnace. The resistance Wound muffle furnace designed and fabricated in the present work was a sturdy one and could be used for long durations. Approximately 80 melts were prepared using this set-up. The graphite crucible employed in the present work could contain about 2 Kgs of liquid aluminium easily.

b) A marine blade impeller of the three blade type driven by 1/20 FHP motor having a max. speed of 4000 rpm was used to create a clear vortex in the molten aluminium. The effective diameter of this steel stirrer (d) was about 6 cm and the ratio between the impeller diameter (d) and the crucible diameter (D)

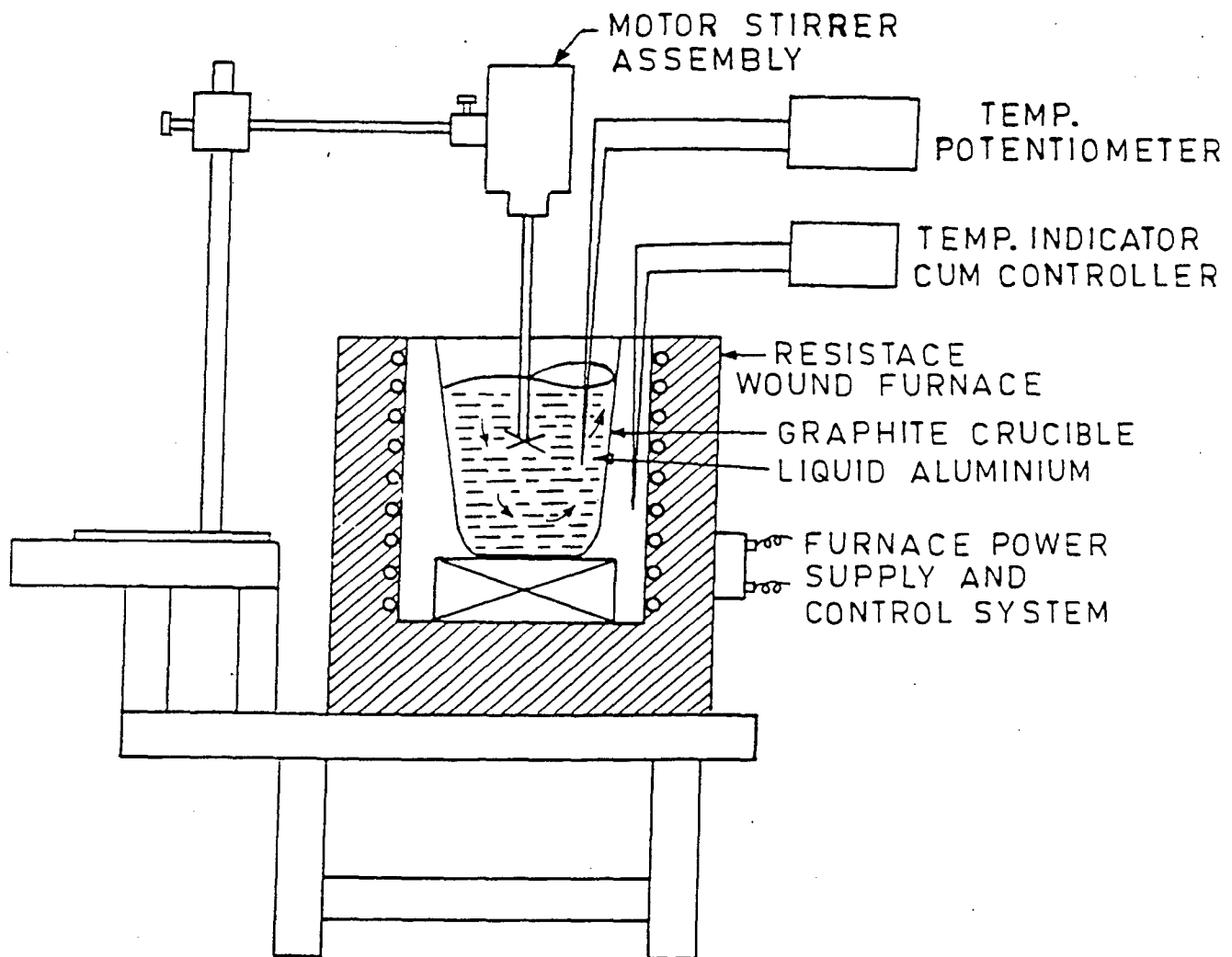


FIG.3.2 Schematic diagram showing the experimental set-up for preparing the stirred slurry.

was selected to be 0.60. This ratio was selected based on the findings of Ghosh, Ray and Rohatgi [74]. These workers have shown that best retention of  $\text{Al}_2\text{O}_3$  is obtained in the composite at this particular ratio. At this particular ratio, proper convective currents are set-up within the liquid which result in effective suspension and distribution of dispersoid particles throughout the entire liquid. This may be the reason why the above workers obtained optimum retention of  $\text{Al}_2\text{O}_3$  in the composite at this particular ratio.

### 3.5 PREPARATION OF THE STIRRED SLURRY : PROCESS DETAILS

#### 3.5.1 DEVELOPMENT OF THE MODIFIED 'MgO COATING' TECHNIQUE

Standard 'MgO coating' technique developed earlier [47-49] was required to be modified for application under humid environmental conditions existing in this region. It is because the trial runs indicated that the standard 'MgO coating' technique did not yield satisfactory results with respect to the retention of  $\text{Al}_2\text{O}_3$  in the composite. This problem was thought to be related with high hydrogen potential of superheated liquid aluminium melt due to humid environmental conditions existing in this region. It was observed during trial runs that even dehydroxylating the alumina surfaces at  $900^\circ\text{C}$  for two hours did not yield any appreciable retention of  $\text{Al}_2\text{O}_3$  in the melt. As such, it was decided to modify the standard 'MgO coating' technique as under.

In this modification, basically, the molten aluminium bath



was planned to be degassed as completely as possible so that the hydrogen potential of the bath could be drastically reduced. After this treatment, the despersoid particles could be expected to be brought in suspension with the melt. Following this strategy, the well superheated aluminium melt ( $860^{\circ}\text{C}$ ) was degassed with the help of fully dried hexachloroethane tablets. For a 1100 gm commercially pure Aluminium melt, 10 gm hexachloroethane tablet was found to be adequate. After this, the scum was completely removed and Mg plunging was commenced. Tiny Mg lumps wrapped in Aluminium foil were quickly plunged deep into the melt and held there close to the bottom with the help of steel perforated holders for a period of about 10 secs till the reaction seemed to subside. A systematic study with respect to the exact amount of Mg needed to give the desired results was carried out. For this purpose, Mg employed for plunging was varied from 0.4 to 0.7 wt% in regular increments of 0.1%. Importantly, liquid metal degassing followed by Mg plunging was carried out in quick succession one after the other just prior to the creation of vortex. In each such trials, fully dehydroxylated ( $\text{Al}_2\text{O}_3 + \text{MgO}$ ) powder mixture containing 15% MgO and amounting to 10% of the melt was then added gradually along the walls of this vortex and the stirred slurry so obtained was then frozen in permanent moulds. Upper and bottom sections of the gravity chill cast castings so obtained were then examined for a)  $\%V_f$  retention of  $\text{Al}_2\text{O}_3$ , b) microhardness of base matrix, c) density, and, d) tensile properties. An examination of this data revealed that 0.5%Mg plunging gives nearly 13% $V_f$  retention of  $\text{Al}_2\text{O}_3$  in the composite

and that further additions of magnesium made no very significant improvement in this regard. Mg additions beyond 0.5% however slightly improved the tensile properties of the composite, which may be attributed directly to the solid solution strengthening effect of magnesium on the aluminium base matrix. It was therefore, concluded from this study that plunging of magnesium to the tune of 0.5% is just adequate and yields satisfactory results with respect to the retention of  $Al_2O_3$  in the base matrix. Detailed results of this study are presented in the next chapter under 'Results and Discussion'. This strategy of the preparation of the stirred slurry was followed in all other subsequent squeeze casting experiments and was termed as 'Modified MgO coating', technique.

### 3.5.2 PROCESS CONTROL DURING VORTEX FORMATION

As shown by earlier workers [74] a proper positioning of the stirrer from the bottom of the crucible is vital to the creation of the vortex and to the maximum retention of the dispersoid particles in the melt. Using their results, a  $(\frac{h}{H})$  ratio of 0.81 was selected so as to obtain in optimum retention of  $Al_2O_3$  particles in the melt. In this relationship, h denotes position of the stirrer from the bottom of the crucible and H is the depth of the melt at rest in the crucible. Also using the results of Ghosh, Ray and Rohatgi [74], a speed of  $16 \text{ rev. sec}^{-1}$  was maintained during stirring. It was shown by these workers that an optimum retention of  $Al_2O_3$  is obtained in the composite at

this particular speed. The stirrer was preheated to a temperature of approximately  $200^{\circ}\text{C}$  prior to introducing it into the melt and positioned always along the central longitudinal axis of the crucible. The stirring of the melt was required to be continued for about 90 secs to fully incorporate the dispersoid particles in the melt. The total operation of degassing, Mg plunging and incorporation of the powder in the melt consumed nearly 5 minutes.

The temperature of the melt at the start of the formation of the vortex was maintained at around  $860^{\circ}\text{C}$  and after the completion of the stirring, the temperature of the melt dropped down to  $800^{\circ}\text{C}$ . At this point, the stirred slurry was either poured in permanent moulds or was squeeze-cast using die and plunger. A speed of 960 rpm was found adequate to create a clear vortex in liquid aluminium melt. Every precaution was taken to ensure that no scum moved into the die.

### 3.5.3 PREPARATION OF Al-MgO COMPOSITES

Following the same procedure as discussed in sections 3.5.1 and 3.5.2 above, Al-MgO composites were prepared. In this case, the percent MgO stirred in aluminium melt was varied as 0.5, 1.0 and 1.5% of the melt. As discussed earlier, the total ( $\text{Al}_2\text{O}_3 + \text{MgO}$ ) powder mixture, added to the melt for the preparation of the stirred slurry amounted to 10 wt% of the melt. This total powder mixture contained 15% MgO meaning thereby that the actual MgO present in the total powder mixture amounting to 1.5% of the aluminium melt. As mentioned in section 3.5.1, part of this

submicron powder was utilised in physically coating the larger  $\text{Al}_2\text{O}_3$  particles. It is for this reason that in the present set of experiments, the quantity of MgO powder added to the melt was varied as 0.5, 1.0 and 1.5% of the aluminium melt in order to prepare Al-MgO composites. The MgO powder was fully dehydroxylated and maintained at  $200^\circ\text{C}$  prior to its addition to the vortex to prevent any moisture pick-up. The stirred slurry so obtained was partly gravity chill cast and partly squeezed at 80 and 140 MPa. The objective of this study was to ascertain the influence of submicron MgO particles on the hardness and strength of aluminium base matrix. This work was undertaken to experimentally verify the hypothesis put forward in the earlier work [47-49], where it was suggested that sub-micron MgO particles cause stiffening of the base matrix through the dispersion strengthening effect. Results pertaining to this study are reported in the next chapter 'Results and Discussion' (Section 4.3.1).

### **3.6 SQUEEZE CASTING (LIQUID FORGING) AND GRAVITY CHILL CASTING OF THE STIRRED SLURRY**

The major part of the stirred slurry was squeeze cast using a 60t semi-automatic hydraulic press and alloy cast iron die and plunger. The dimensions of the die and plunger are shown in Fig.3.3. This resulted in the preparation of cylindrical castings of 70 mm dia and 60 mm length. A metered quantity of stirred slurry free from any dross or scum was poured in alloy cast iron die and the plunger was placed in position over the die. The two

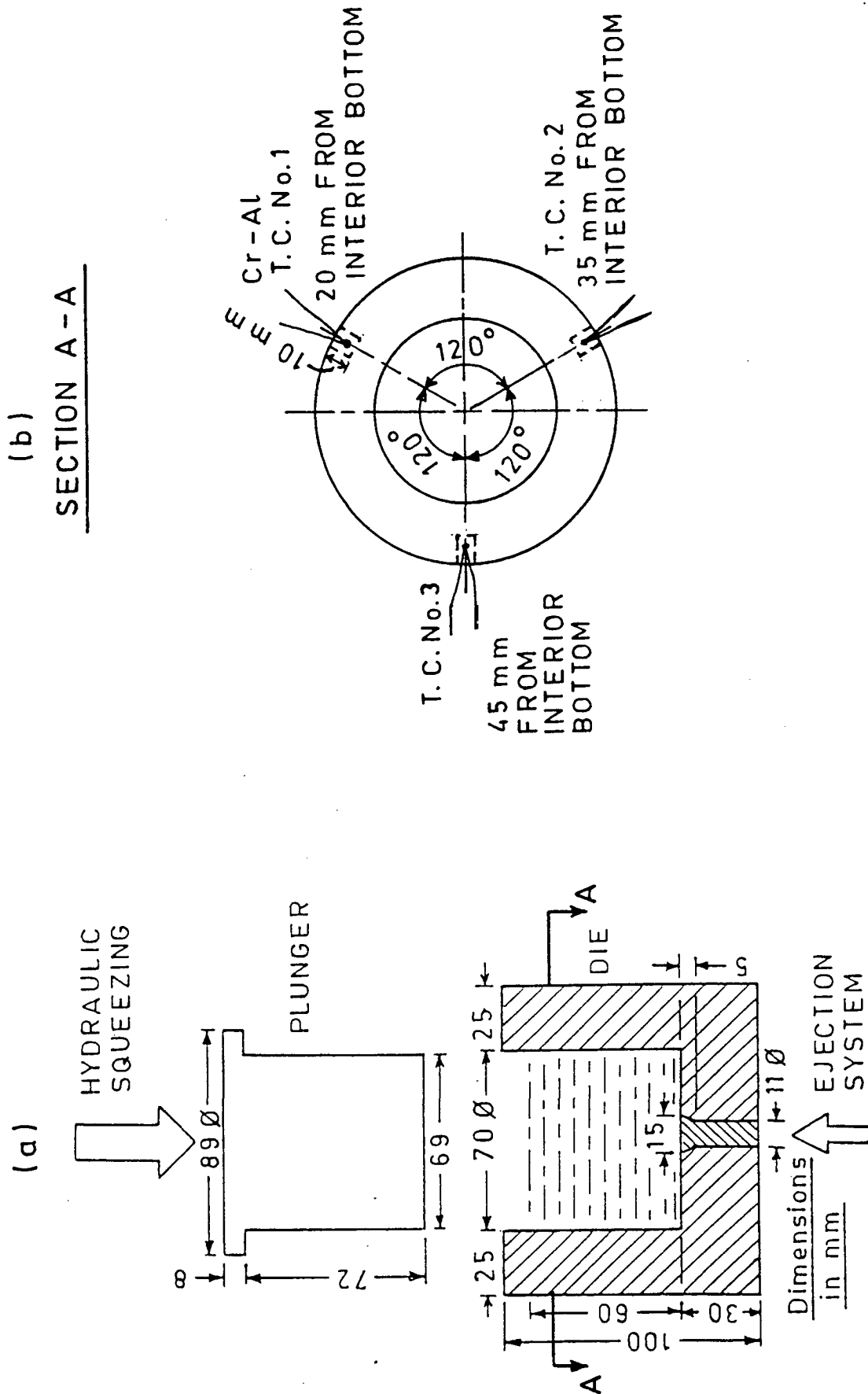


FIG. 3.3 Schematic diagram showing (a) the squeeze casting arrangement and (b) the plan of placement of thermocouples (No.1,2 and 3) in the side walls of die to precisely monitor the temperature of die just prior to pouring the stirred slurry in the cavity.

were then transferred quickly to the press and squeezed in the pressure range of 80 to 140 MPa. The entire process of transferring the stirred slurry to the die and then placing the die and plunger together under the press consumed nearly 10 secs. The slurry was squeezed for 40 secs in each case. The die temperature was varied as ambient, 100 and 200 °C. The temperature of the die was measured with the help of chromel-alumel thermocouples placed at three different locations 120° apart and nearly 1 cm deep into the wall of the die as shown in Fig.3.3. Interior of the die and plunger surfaces were thoroughly dried and dressed with colloidal graphite powder suspended in acetone prior to their actual use. The die and plunger were heated over a period of nearly 45 minutes and their temperature controlled so as to ensure that a steady state condition had reached. Soon after, within a matter of 5-6 secs, this set of die and plunger was employed for squeeze casting the stirred slurry. After every experiment, the die and plunger surfaces were thoroughly cleaned, slightly polished and then dressed again before commencing the next experiment. Alloy cast iron employed for the fabrication of the die and plunger is a well known material which can withstand repeated thermal shocks without much problem. It is for this reason that this material is employed for the preparation of glass moulds, stoker chain links, grate bars etc. [162]. A rough estimate of the heat capacity of this die shows that it can be a good sink for the heat content of the stirred slurry. It was shown by some investigators that fairly rapid heat transfer can occur between the molten slurry and the die surface under

pressurised freezing conditions [96,97].

Rest of the stirred slurry was frozen into split cylindrical permanent moulds to result in the preparation of gravity chill cast castings. Cylindrical castings of 40 mm dia and 125 mm length were obtained this way.

### 3.7 OPTICAL AND SEM EXAMINATIONS

#### 3.7.1 TOPOGRAPHIC STUDY OF COATED AND UNCOATED $\text{Al}_2\text{O}_3$ PARTICLES AND SUBMICRON MgO POWDERS

The morphology of ceramic powders employed in the present set of experiments ( $\text{Al}_2\text{O}_3$  and submicron MgO particles) was examined with the help of the SEM. The  $\text{Al}_2\text{O}_3$  particles prior to and after MgO coating were examined in detail using this technique. The submicron MgO particles being very fine were sprinkled onto an aluminium adhesive tape and then examined by the SEM. The powder specimens were gold plated in each case to result in good contrast of SEIs.

#### 3.7.2 EXAMINATION OF POLISHED SURFACES OF COMPOSITE SPECIMENS

##### 3.7.2.1 PREPARATION OF METALLOGRAPHIC SPECIMENS

Cylindrical specimens sliced from the top and bottom sections of gravity chill cast composites were ground and polished following the standard procedures and then etched with Keller's reagent (1%HF conc., 1.5%HCl conc., 2.5% $\text{HNO}_3$  conc. and balance distilled water). The final polishing of these specimens was carried out on polishing cloth using polishing grade-III  $\text{Al}_2\text{O}_3$

suspension. In each case, the specimens were thoroughly cleaned with the help of water and acetone prior to etching. The etching was required to be carried out for about 20 to 30 secs using the Keller's reagent mentioned above and then the specimen was washed and dried. The squeeze cast composite casting was sliced through the centre along the longitudinal axis. After repeated slicing through the centre nearly 12 to 15 thin slices were obtained for subsequent tests such as optical and SEM examination, micro-hardness measurements, tensile tests etc. From one of these slices, two metallographic specimens of nearly 10 mm thickness were obtained from the top and bottom portion. These metallographic specimens were ground, polished and etched in the same manner using standard metallographic procedures as mentioned above.

The objectives of examining these specimens were as under:

- (1) To study the location and distribution of  $\text{Al}_2\text{O}_3$  particles in the base matrix.
- (2) To estimate the sizes of the dispersoid  $\text{Al}_2\text{O}_3$  particles.
- (3) To determine the  $\%V_f$  retention of  $\text{Al}_2\text{O}_3$  particles in base matrix using quantitative metallographic techniques.
- (4) To determine dendritic arm spacings in the cast structure
- (5) To examine particle matrix interface closely for the presence of any voids etc at higher magnifications.



- (6) To examine the character and composition of the reacted layer around  $\text{Al}_2\text{O}_3$  particles at particle/matrix interface using EPMA technique . A full discussion on this particular aspect is presented in subsequent sections.

### 3.7.2.2 QUANTITATIVE METALLOGRAPHY

Reichert Jung optical microscope, model MeF3 was employed to carry out quantitative metallographic studies. In order to measure the dimensions of retained  $\text{Al}_2\text{O}_3$  particles in the matrix, a graduated scale was introduced in the eye piece. This graduated scale was then calibrated with the help of standard scale (1mm divided into 100 parts, the least count of this scale being 0.01 mm ) at 100X. It was found that the least count of the graduated scale fixed into the eye piece was 11  $\mu\text{m}$  at 100X. Also in this eye piece, a grid could be introduced. The length of the side of this square grid was determined in the same manner at 100X using the same standard scale (1mm divided into 100 parts). It was found that the length of the side of this square grid was 0.28 mm at 100X and therefore this grid would cover an area of 0.08  $\text{mm}^2$  on the specimen surface observed. The objective of employing this grid was to count the number of  $\text{Al}_2\text{O}_3$  particles retained in a section of known dimensions. The above technique of estimating the number of  $\text{Al}_2\text{O}_3$  particles retained in a section of known dimensions is termed as 'point counting technique' [163].

Certain basic precautions were regularly observed in connection with the above studies. The first and foremost

precaution observed was that measurements were carried out at numerous locations throughout the length and breadth of the specimen totalling to over 150 to 200 locations. This results in thorough scanning of the specimen and also more reliable and dependable average values are obtained this way. Another important precaution observed was that only single  $\text{Al}_2\text{O}_3$  particles were considered during counting and size measurements and other morphologies such as clusters, agglomerates of irregular shapes, chainlike formations and voids etc were neglected. It should be mentioned that the occurrence of such defect morphologies as mentioned above was found to be maximum in case of gravity chill cast composites, while the squeeze cast composites were found to be relatively free from such defects. While measuring the dimensions of  $\text{Al}_2\text{O}_3$  particles, precaution was taken to measure the dimensions of each particle at  $90^\circ$  across and then averaged.

From the above observations, an average size and number of  $\text{Al}_2\text{O}_3$  particles retained in a given specimen was obtained. The data pertaining to the average number of  $\text{Al}_2\text{O}_3$  particles retained in a given composites are thus obtained in terms of number of particles/ $0.08 \text{ mm}^2$  area of the specimen. This data was later converted to the average number of particles retained/ $\text{mm}^2$  and then finally to the number of  $\text{Al}_2\text{O}_3$  particles retained/ $\text{mm}^3$  using the Schwartz - Saltikov formula [164] given below:

$$N_V = 2.38 \cdot N_A^{1.6} \quad \dots\dots\dots (3.1)$$

where,  $N_A$  = Number of particles/mm<sup>2</sup>

$N_V$  = Number of particles/mm<sup>3</sup>

The %V<sub>f</sub> retention of Al<sub>2</sub>O<sub>3</sub> particles in a given specimen was determined using the following equation :

$$\%V_f = \frac{4}{3} \pi \cdot \left(\frac{d}{2}\right)^3 \cdot N_V \cdot 100 \quad \dots\dots\dots (3.2)$$

where, d indicates the average diameter of Al<sub>2</sub>O<sub>3</sub> particles retained in the matrix.

The dendritic arm spacing of the cast structure was also determined using the same graduated eye piece. For this purpose the metallographic specimens were etched with Keller's reagent. As a matter of routine practice, each specimen was examined at least at 80 to 100 locations so as to scan the entire cross-section fully. These values were then averaged to obtain mean dendritic arm spacing for a given specimen.

### 3.8 EPMA EXAMINATION OF THE REACTED LAYER AROUND Al<sub>2</sub>O<sub>3</sub> PARTICLES

A polished and etched metallographic specimen was employed for this study using JEOL superprobe microanalyser model JXA 8600 M. The objective of this study was to ascertain the nature of the reacted layer around Al<sub>2</sub>O<sub>3</sub> particles retained in the base matrix. The main thrust of the investigation was to ascertain whether some MgO existed in the reacted layer or not.

The strategy adopted for the MgO analysis at different locations of the base matrix and  $\text{Al}_2\text{O}_3$  particles is shown schematically in Fig.3.4. This analysis was carried out at three different locations on the polished surface separated from each other by about 4 to 5 mm (see Fig.3.4). For MgO analysis, standard of Olivine mineral of known analysis (MgO-51.57,  $\text{SiO}_2$ -41.84, MnO-0.12, FeO-6.51 and NiO-0.20%) was employed. Also, the line analysis of this specimen was carried out with respect to Al and Mg along the marker shown in Fig.3.4. The objective of this study was to ascertain whether some Mg would get concentrated at the particle/matrix interface, which would be expected to occur according to Gibbs adsorption isotherm [14]. An acceleration voltage of 20 KV was employed for these studies and intensities for pure Al and Mg stored in the computer were used as the reference point. Analysis of MgO at different points shown in Fig.3.4 was undertaken in the hope that the reacted layer would be a spinel ( $\text{Mg Al}_2\text{O}_4$ ) as reported by Mehrabian and Coworkers [13] and, therefore, the MgO content in the reacted layer would be expected to be much higher than the body of the  $\text{Al}_2\text{O}_3$  particle.

### 3.9 MEASUREMENTS OF DENSITY

Density of the composite specimen was measured using Archimedes' principle. Kerosene oil in place of distilled water was employed for these measurements as the former wets the sample more uniformly. Keroy single pan balance capable of weighing accurately upto .00001 gm was employed for these estimations. In

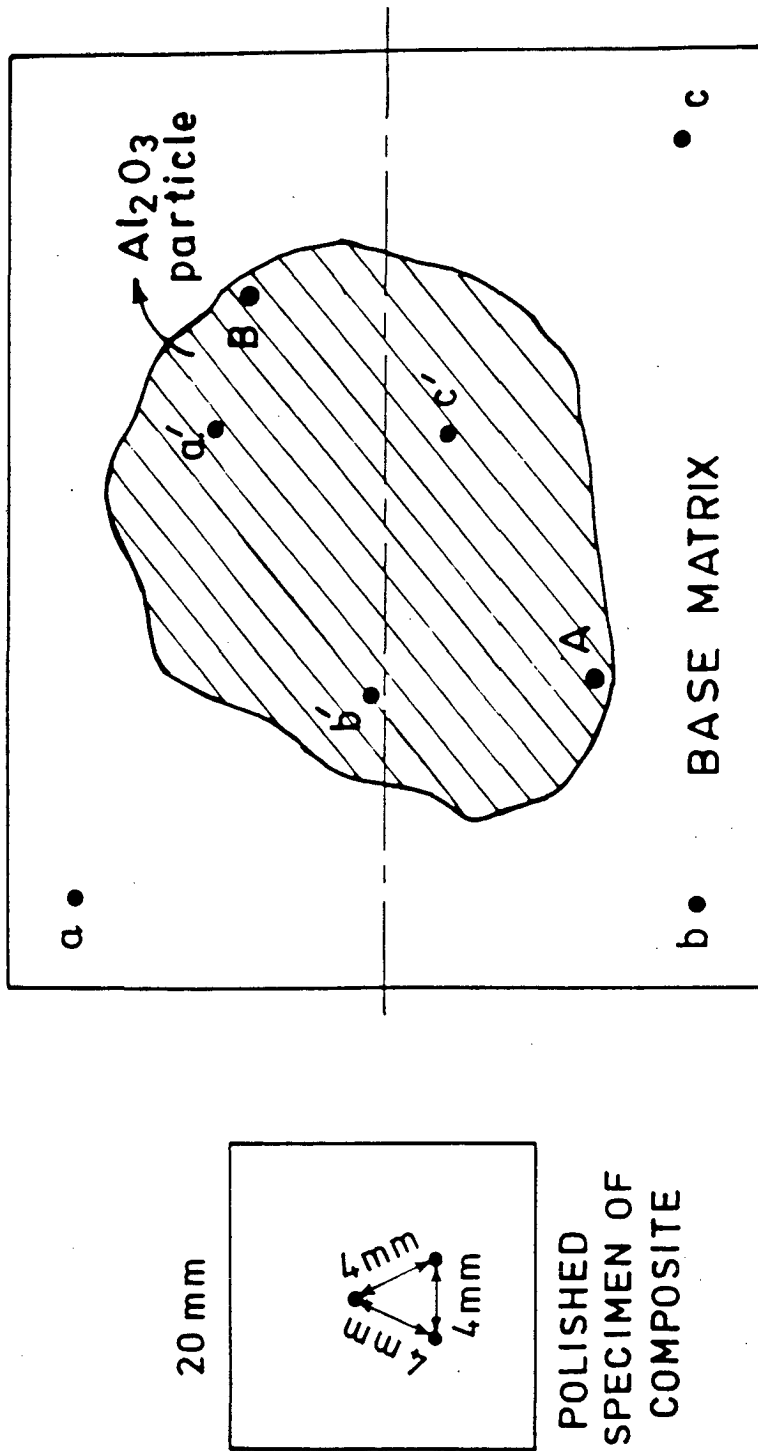


FIG.3.4 Schematic representation of the strategy adopted for MgO analysis at different locations of the matrix and  $Al_2O_3$  particle.

each case, at least 4 readings were taken and 2 readings closest to each other were taken to be the correct value. Specimens for these measurements were drawn from the edges or surfaces of the composite castings as they would be expected to be relatively free from any porosity.

### 3.10 MECHANICAL PROPERTY EVALUATION

#### 3.10.1 VICKER'S HARDNESS AND MICROHARDNESS MEASUREMENTS

Vicker's hardness [ $HV_5$ ] of all the composites was determined using Brinnel cum Vicker's hardness tester model HPO 250 at 5 kg load. As a matter of routine practice, indentations at least at 50 different locations were taken and the resulting hardness values averaged to obtain the mean hardness values.

Microhardness measurements were taken in several instances. In the beginning, this study was directed at estimating the microhardness of the base matrix of squeezed composites to determine a) the influence of squeeze pressure on the microhardness of the base matrix and b) to determine the dispersion strengthening effect of submicron MgO particles on aluminium base matrix. In latter studies on the wear behaviour of squeeze cast composites under dry sliding conditions, the oblique section was subjected to microhardness measurements. The objective of this study was to ascertain the extent of work hardening caused in the subsurface layer due to bearing load and other shear stresses acting at the wear surface. The attempt was to correlate this extent of work hardening with the degree of

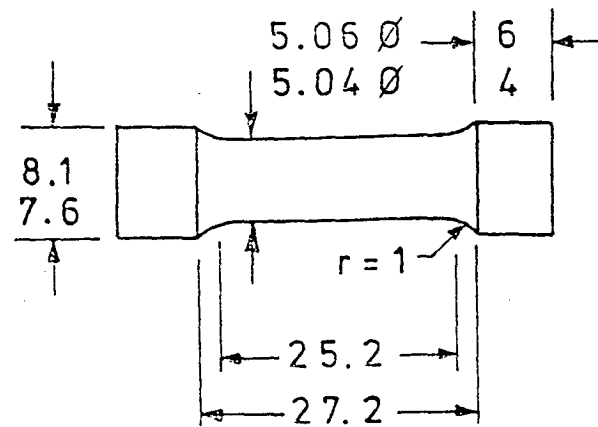
squeeze pressure applied during the fabrication of composites.

Table type TUKON microhardness tester model BM 300 was employed for the above studies. Generally a load of 5 gm was found adequate in most cases and as a matter of routine practice, indentations were taken at least at 50 different locations in each case and then averaged to obtain the mean hardness value. Prior to making these measurements, the instrument was properly calibrated with the help of standard samples provided with the instrument.

### 3.10.2 TENSILE PROPERTY EVALUATION UPTO 300°C (573K)

Tensile properties of gravity chill cast and squeezed composites were determined using 5t universal Instron Testing Machine, model TTC, MC at a constant cross head speed of  $5 \times 10^{-4} \text{ m.min}^{-1}$  yielding a conventional strain rate [165] of  $3 \times 10^{-4} \text{ sec}^{-1}$  on a specimen gauge length of  $25 \times 10^{-3} \text{ m}$ . Dimensions of a standard tensile specimen employed in the present work are shown in Fig.3.5. The tests were performed at ambient, 100°C (373K), 200°C (473K) and 300°C (573K). For commercial pure aluminium sample, the test was required to be performed at 225°C only instead of 300°C as the strength of the material deteriorated sharply beyond 200°C. Tensile samples were prepared from the longitudinal slices cut from the cylindrical squeezed and gravity chill cast composites. For each test, three specimens were pulled in tension and then the resulting values were averaged.

For tensile property evaluation at elevated temperature, A 2 KW Kanthal resistance wound furnace of adequate inner volume



Dimensions in mm

FIG.3.5 Schematic diagram of tensile specimen (dimensions in mm).



was used in test position to cover the tensile grips and the specimen fully. Furnace openings were then sealed properly from both the ends. A thermocouple set close to the muffle wall and attached with temperature control system helped to regulate the temperature of furnace to within  $\pm 2^{\circ}\text{C}$  of the preset temperature. Another thermocouple was positioned close to the centre of the gauge length of tensile specimen. This arrangement is shown schematically in Fig.3.6. Each sample was then homogenised for a period of 30 to 40 minutes at a preset test temperature prior to applying the load. Load-extension plots were obtained on the strip chart recorder attached to the Instron Machine. The X-axis on which extension is obtained was magnified 20 times to obtain the extension value more accurately. This load-extension plot was then converted to a stress-strain curve from which 0.2% offset Y.S. values were determined. Percent elongation and percent reduction in C.S. area were determined by measuring the initial and final gauge length and cross sectional area before and after tensile testing respectively.

### 3.11 SEM EXAMINATION OF TENSILE FRACTURE SURFACES

Philips Scanning Electron Microscope Model 501 was used to examine the fracture surfaces of tensile specimens pulled at different test temperatures to ascertain the mechanism of fracture operative in gravity chill cast and squeezed composites. This study would be expected to reveal clearly the advantages to be gained from the squeeze casting operation. Another objective of this study was to pointedly examine the occurrence of microporosity

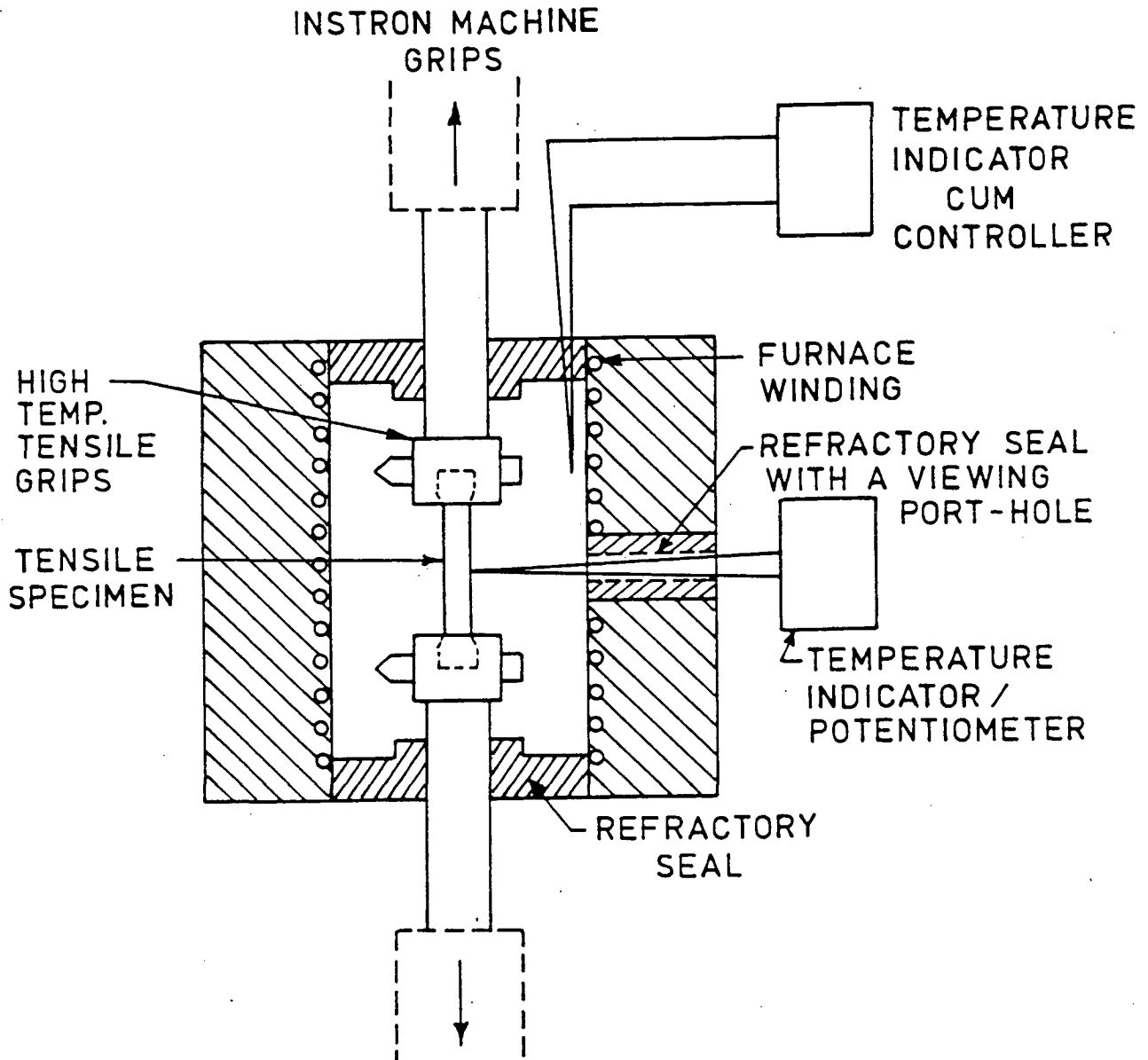


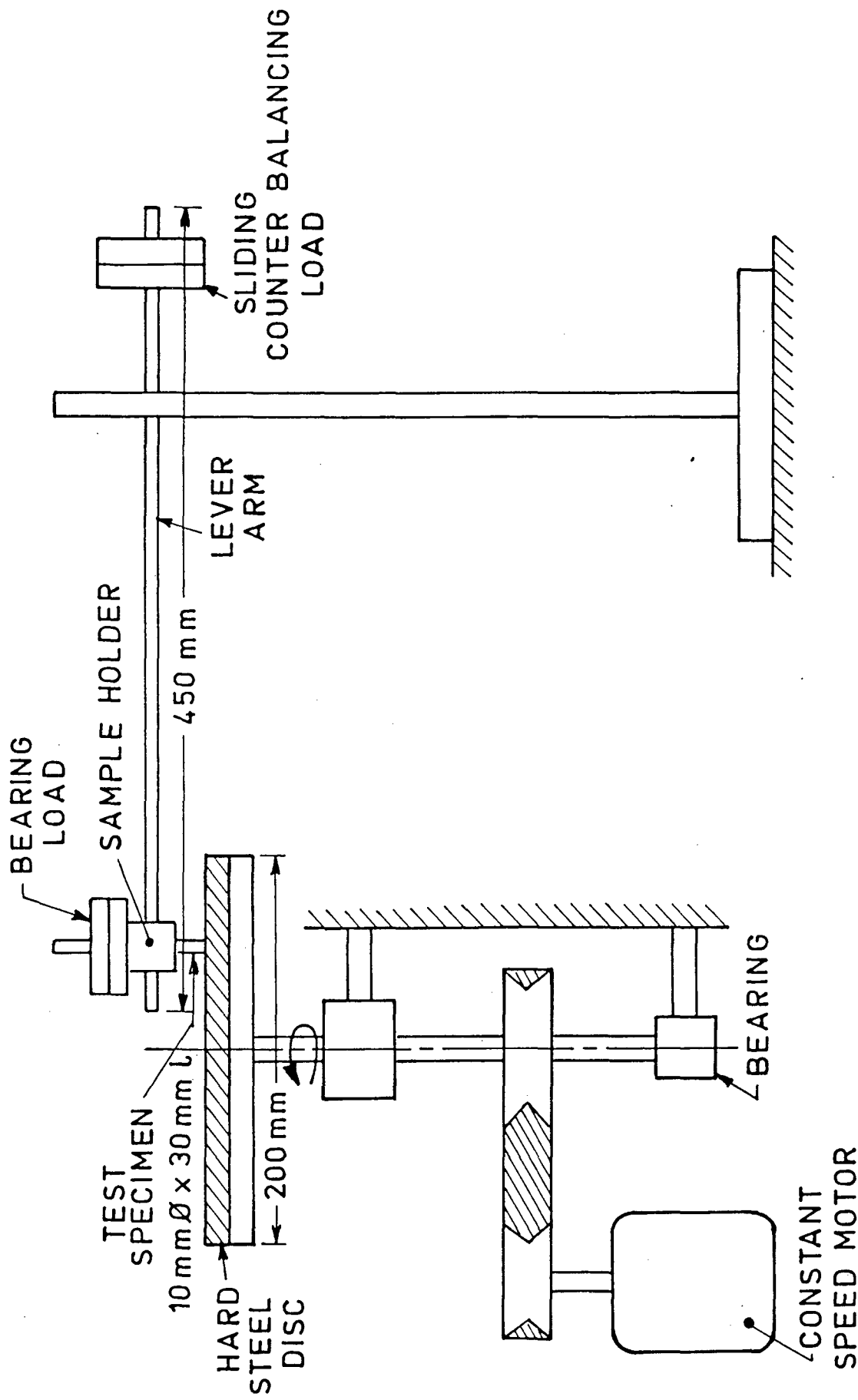
FIG.3.6 2 KW. Kanthal resistance wound furnace shown with the tensile specimen gripped within the chamber of the furnace. Above arrangement employed for the determination of tensile properties of composites at elevated temperatures upto  $300^{\circ}\text{C}$  ( $573\text{K}$ ).

in the cast structure. An extensive study of most of the tensile fracture surfaces obtained at different test temperature was undertaken to monitor the change, if any, in the mechanism of fracture due to the exposure of tensile specimens to elevated temperatures.

### 3.12 EVALUATION OF WEAR BEHAVIOUR UNDER DRY SLIDING CONDITIONS

#### 3.12.1 FABRICATION OF THE WEAR TESTING RIG

A standard pin-on-disc type of testing rig was designed and fabricated for use in the present work. A schematic diagram of the set-up is shown in Fig.3.7 indicating the details of the counterface steel disc, cylindrical specimen and the loading arm. For counterface material, a steel disc of about 200 mm dia and hardened to 177 HV<sub>30</sub> average hardness was mounted onto a disc support and continuously driven by a 0.25 FHP motor through a reduction gear system. The counterface steel disc was so mounted as to be perfectly horizontal. An average speed of 45 rpm was obtained on the rotating steel disc. This speed was cross checked several times during the long durations of wear runs with the help of hand Tachometer having a resolution of  $\pm 1$  rpm. Wear specimens of 10 mm dia and 30 mm length, sliced and machined out from the composite cylindrical castings were inserted in the specimen holder and held firm with the help of side-screws. The other end of the specimen holder was attached to the lever arm, which was balanced as perfectly as possible with the help of balancing dead weights. Under this situation, the pin specimen was held



### PIN - ON - DISC ASSEMBLY

FIG.3.7 Schematic diagram of the pin-on-disc wear testing rig.

perfectly vertical such that its entire lower surface was in contact with the counterface steel disc. A predetermined and variable quantity of load could be applied directly onto the cylindrical pin. This load applied to the specimen is usually termed as bearing load. The counterface surface of the hardened steel disc was polished upto 4/0 emery paper before commencing any test run. Also, before starting any subsequent wear run, the surface of counterface steel disc was reconditioned and ground similarly. The test pin was also ground upto 4/0 emery paper so that the starting surface conditions of both the counterface steel disc as well as the test pin were identical. A medium carbon steel was employed for the counterface steel disc. Instead of changing the rpm of the steel disc, the position of the vertical wear pin was varied from the centre of the steel disc so as to achieve three different sliding speeds at the wear interface.

### 3.12.2 SELECTION OF COMPOSITES FOR WEAR STUDIES

Only three composites namely composite Nos.1 (gravity chill cast), 2 (squeeze cast at 80 MPa and ambient die temperature) and 3 (squeeze cast at 140 MPa and ambient die temperature) were selected for wear studies. It is basically because these three composites represented three different extreme conditions of fabrication of Al-Al<sub>2</sub>O<sub>3</sub>-MgO particulate MMCs. As a result, their corresponding properties will also represent three different extreme levels. For example, gravity chill cast composites (Composite No.1) would be expected to display poorest

properties owing to coarse grained structure, porosity and unfed interdendritic regions in the matrix. Contrary to these composites, the squeezed composites would be expected to display much superior properties. Among the range of squeeze pressures applied during the fabrication of these composites, 80 MPa represents the lowest limit and 140 MPa represents the highest. The properties of other composites prepared at intermediate pressures such as 100 and 120 MPa, would be expected to lie in between the two extreme levels mentioned above. It is for this reason that the composites fabricated at the two extreme levels mentioned above namely 80 and 140 MPa were selected for wear studies. As mentioned above, these two composites are respectively designated as composite Nos.2 and 3. The basic objective behind this selection was to ascertain as to how the wear behaviour of Al-Al<sub>2</sub>O<sub>3</sub>-MgO particulate composites would be influenced by the degree of squeeze pressure applied during the fabrication of these composites. Apparently, therefore, the behaviour of composite No.1 (gravity chill cast) would serve to function as the datum level for the comparison of the behaviour of composite No.2 and 3 under identical conditions of wear. This strategy was adopted also in view of the fact that %V<sub>f</sub> retention of Al<sub>2</sub>O<sub>3</sub> particles in the matrix of most composites (gravity chill cast or squeezed) was nearly identical and therefore, this was not the parameter of any significance influencing the properties of the composites. As such, it was only the degree of squeeze pressure applied that would be expected to materially influence

the properties of the composites. It was, therefore, thought logical that the wear behaviour of Al-Al<sub>2</sub>O<sub>3</sub>-MgO particulate MMCs should be studied as a function of the degree of squeeze pressure applied during the fabrication of above composites. This strategy ultimately led to the selection of composite Nos.1,2 and 3 for detailed wear studies under different sets of experimental conditions.

### 3.12.3 WEAR TEST PROCEDURE AND PARAMETERS

The wear test was run for a predetermined bearing load and sliding speed for a fixed length of time. Under these conditions the wear pin would traverse a fixed distance of track length. The variable parameters and their ranges are shown in Table-3.2. It can be seen from the table that for a given composite, 27 experiments were conducted and in all 81 experiments were carried out for all the three composites.

In case of individual composite specimen, the position of vertical wear pin was varied from the centre of the steel counterface disc so as to achieve three different sliding speeds at the wear interface. At 2,3 and 4 cms away from the centre of the steel disc, sliding speeds of 9.4, 14.1 and  $18.8 \times 10^{-1} \text{ m. sec}^{-1}$  respectively could be realised. At each such position of the wear pin, a bearing load of 500, 1000 and 1500 gms was applied to the specimen. Also, for each such position of the wear pin and bearing load, the wear test was run for 30, 60 and 90 minutes resulting in the wear pin traversing different track lengths.

TABLE - 3.2

VARIABLE PARAMETERS AND THEIR RANGES EMPLOYED DURING WEAR EXPERIMENTS.

| <u>S.No.</u> | <u>Variable Parameter</u> | <u>Range of Variable Parameter</u>                     |
|--------------|---------------------------|--|
| 1            | Composite                 | Three, (Composite Nos.1,2 and 3)                       |
| 2            | Bearing Load              | 500, 1000 and 1500 gms.                                |
| 3            | Sliding Speed             | 9.4,14.1 and $18.8 \times 10^{-2} \text{ m. sec}^{-1}$ |
| 4            | Test Duration             | 30, 60 and 90 minutes                                  |

---

Remarks: (1) Total number of experiments =  $3 \times 3 \times 3 \times 3$   
= 81

(2) Composite No.1 - gravity chill cast

Composite No.2 - squeeze cast at 80 MPa and ambient die temperature

Composite No.3 - squeeze cast at 140 MPa and ambient die temperature

(3) Fixed Parameters -

Counterface steel disc diameter = 200 mm

Speed of disc = 45 r.p.m.

Average Steel disc hardness = 177 HV<sub>30</sub>

Counterface surface ground to 4/0 emery paper

Wear pin dimensions = 10 mm dia, 30 mm length



Thus for a fixed sliding speed and composite, 9 experiments were conducted and a given composite was subjected to in all 27 experiments. Exactly the same procedure was adopted for all the three composites under investigation namely composite Nos.1,2 and 3.

All the tests mentioned above were carried out under dry sliding conditions. As mentioned earlier the surface of both the steel disc and wear pin were properly degreased and then ground with 4/0 grade emery paper. Thus the starting conditions for every wear run were exactly identical.

Within about a few minutes of the start of a new run, it was observed that the track is smeared with dark debris material. No effort was made to remove these particles and the run was continued till the end. Actual wear conditions in the present set of experiments, therefore, represent a three-body interaction and the nature of wear would be expected to be adhesive cum abrasive type. In the present set of experiments, steady state conditions were attained within about 5 minutes of start and, therefore, test runs extending upto minimum half an hour duration would be expected to yield steady state wear rate data for a fixed set of experimental conditions and parameters.

For a given set of wear run (under fixed parameters), weight loss in terms of gms was determined from the initial and final weight of the wear pin after the completion of wear run. From this weight loss data, wear rate was computed in terms of  $\text{Kg.Km}^{-1} \times 10^{-6}$  in individual cases.

Some of the expressions used during calculations are given as under :

$$\text{Sliding distance (L)} = 2\pi d N t \dots\dots\dots (3.3)$$

where, d = distance of the pin specimen axis from the centre of the rotating steel disc.

N = Speed of steel disc, rpm

t = Period of wear testing, minutes.

Sliding speed(S) at the interface of wear pin and the steel disc was given by:

$$S = 2 \pi d N \dots\dots\dots (3.4)$$

Wear rate ( $K_L$ ) was calculated as weight loss per unit sliding distance

$$K_L = \frac{W}{2 \pi d N t} \dots\dots\dots (3.5)$$

where W is the weight loss measured in gms.

#### 3.12.4 SEM EXAMINATION OF THE WORN SURFACE

Freshly formed wear tracks on the wear pin were examined in detail by the SEM. This technique is eminently suitable for such examinations because the specimen can be examined directly under the SEM without any further preparation except that the worn surface is gold plated to result in better contrast. Thus the worn surface obtained at the end of a given wear run remains perfectly undisturbed. This helps in the examination of all

relevant features in detail which reveal essentially various mechanisms operating during the actual process of wear. Additionally, the SEM has the advantage of an excellent depth of field. Simultaneously, the specimen could be tilted also through an angle of about  $10^\circ$  which helps in providing a better view of the wear tracks. The wear tracks were examined upto considerably high magnification to reveal the real nature of the worn material still sticking to the crest and trough portions of the grooved track marks. The SEM technique was employed extensively to examine the wear tracks and other features in fullest possible details.

### 3.12.5 EXAMINATION OF SUBSURFACE DAMAGE

After the completion of a run, the wear pin was taper sectioned and polished at  $5^\circ$  as per the details shown in Fig.3.8 schematically. In all cases, the polishing was done such that the wear tracks were perpendicular to the line of intersection of the plane of polishing with the worn surface. The oblique polished section was then examined optically and also by the SEM. The objective of this study was to ascertain the nature and extent of subsurface damage in the material just underneath the wear tracks.

This technique of oblique sectioning was developed and described by Dwarakadasa et al [124]. Subsequent to polishing, the surface was etched also by Keller's reagent for optical examinations. By this method, the extent of subsurface damages could be measured quantitatively and also the nature of damage upto the undisturbed

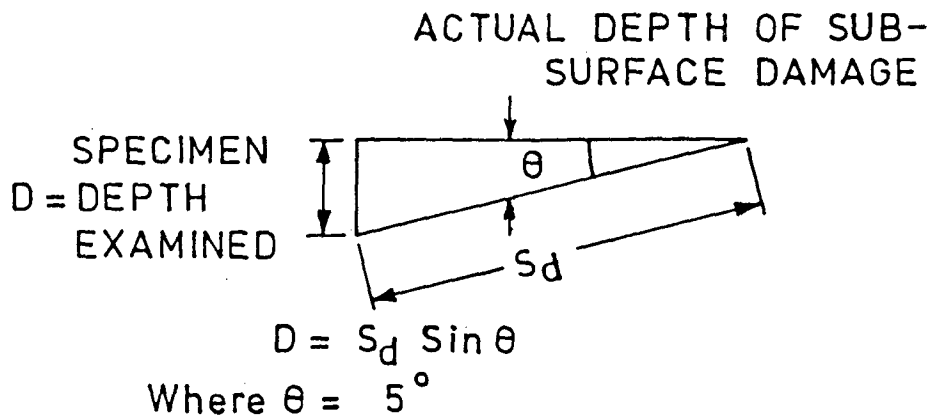
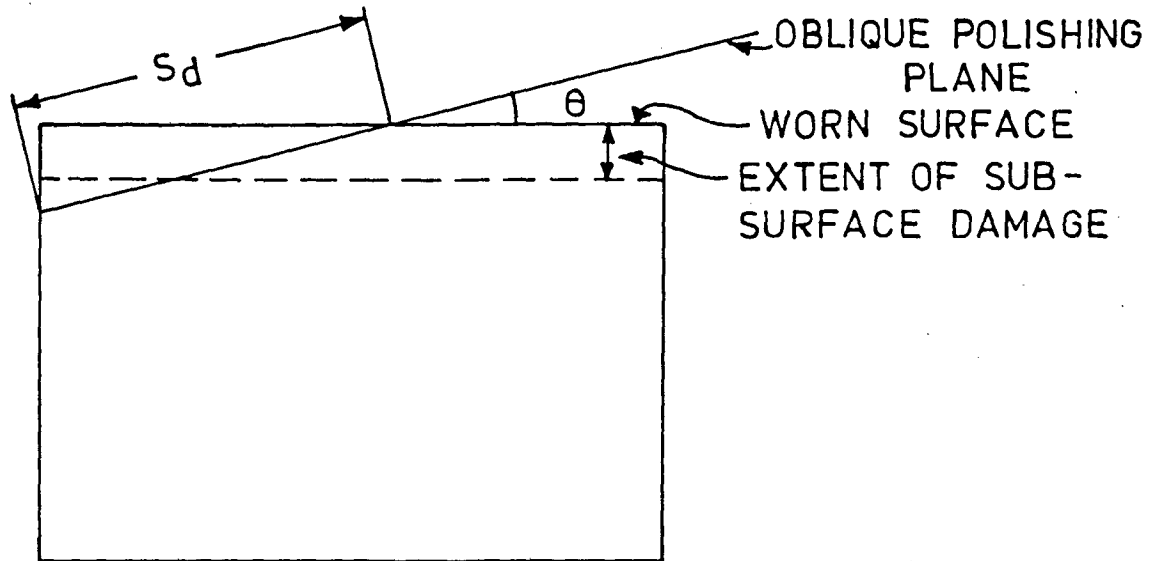


FIG.3.8 Schematic representation of oblique polishing of worn wear pin specimen for subsurface damage study.

region could be precisely ascertained. In a single phase material like the one employed in the present case (commercially pure aluminium matrix), it is difficult to ascertain the extent of damage of work hardening through simple optical and SEM observations. In other cases such as aluminium-silicon eutectic or hypo or hyper-eutectic alloys, it is possible to ascertain the nature of damage in the subsurface region immediately below the wear tracks through optical and SEM observations [124,126,128-130]. It is because the hard and brittle primary silicon phase undergoes fragmentation and produces tiny spheroidal particles close to the wear interface. This signifies the extent of work hardening undergone by this subsurface region immediately below the worn surface. Thus, in such cases, it is easily possible to clearly discern the depth of work hardening region. But such a approach is difficult to be adopted in case of single phase materials such as commercially pure aluminium. For this reason, a different strategy was adopted to ascertain the depth of work hardening region in case of present composites.

A detailed micro-hardness examination of this subsurface region was carried out to ascertain the depth of work hardening region in case of present composites. Microhardness measurement ( $HM_{10gm}$ ) were taken at close intervals along this oblique surface starting from the edges of visible wear tracks. A thorough investigation was carried out throughout the length and breadth of this oblique section. Table type TUKON microhardness tester model BM 300 was employed for these studies. Results of these

measurements were plotted as a function of the distance from the edge of the visible track marks in case of different composites. Obviously, the hardness close to the edge of visible track marks would be expected to be the highest and these values would tend to taper off as the undisturbed region of base matrix is approached gradually. Using this method the depth of work hardening region was precisely determined in each case. A similar approach has been adopted by other workers also to estimate the depth of work hardened region [143].

The optical and SEM examination of tapered section was employed basically to study the nucleation and growth pattern of micro subsurface cracks emanating from layers deep into the subsurface region and finally opening up into the worn surface. This was indicative of the mechanism of subsurface damage and fragmentation of matrix material.

### 3.12.6 EXAMINATION OF WEAR DEBRIS

The debris material generated during wear experiments was carefully collected periodically into a vial for examination and stored in a dessicator. Some fine debris material was observed sticking to the counterface steel disc but no effort was made to scratch this material out. Instead, these debris patches sticking to the counterface steel disc were examined separately by the optical microscope. An effort was made to examine the freshly collected debris material under the SEM as soon as possible to prevent any undue oxidation of these particles. Some debris

particles exhibited a tendency to agglomerate, therefore, they were made to disperse in an organic solvent like Acetone before examination. The debris particles were glued onto a conducting aluminium tape and then gold plated before examination under the SEM. The objective of this study was to examine the morphology of debris particles and the propagation of cracks in these particles, if any. This study was expected to reveal valuable information pertaining to the mechanism of material removal in case of different composites under investigation.

## CHAPTER 4

### RESULTS AND DISCUSSION

#### 4.1 INTRODUCTION

The results of present study are divided into three major sections. The first major section deals with preparation and initial characterisation of gravity chill cast and squeezed Al-Al<sub>2</sub>O<sub>3</sub>-MgO and Al-MgO particulate MMCs. The second main section deals with mechanical property evaluation of above composites upto 300°C (573K). The third major section is devoted to a study of the wear behaviour of mainly three representative composites namely Composite No. 1 (gravity chill cast), No.2 (squeezed composite at 80 MPa and ambient die temperature) and No. 3 (Squeezed composite at 140 MPa and ambient die temperature) under dry sliding conditions. The strategy adopted is that the relevent results are presented first and then these results are discussed simultaneously in the same sub-section.

#### 4.2 PREPARATION AND INITIAL CHARACTERISATION OF GRAVITY CHILL CAST AND SQUEEZED Al-Al<sub>2</sub>O<sub>3</sub>-MgO AND Al-MgO PARTICULATE COMPOSITES

##### 4.2.1 ROLE OF MODIFIED 'MgO COATING' TECHNIQUE IN THE PREPARATION OF COMPOSITES. [166,168-170]

As discussed in section 3.5.1 previously, the standard 'MgO coating' technique developed earlier [47-49] was modified to suit the humid environmental conditions existing in this region.



Results pertaining to a study of this aspect are summarised in Table-4.1 [166]. It can be seen from these results that magnesium plunging to the tune of 0.5 to 0.6 percent is adequate to result in nearly 13%  $V_f$  retention of  $Al_2O_3$  in the composite. Further addition of magnesium to the melt does not bring about any major improvement in the amount of  $Al_2O_3$  particles retained in the composite, although the ultimate tensile strength of the composite registers some noticeable improvement at 0.7% magnesium addition which may be attributed to the strengthening caused by dissolved magnesium. There is virtually no material change in the microhardness of the base matrix although the density of the composite improves marginally due to progressive addition of magnesium to the melt. Keeping the above results in mind, the magnesium plunging was fixed at the level of 0.5% only for subsequent preparation of the stirred slurry. This stirred slurry was later planned to be squeezed in the pressure range of 80 to 140 MPa. It is noteworthy that the amount of magnesium needed for modified 'MgO coating' technique is just only 12 to 16% of the quantity needed for usual 'Mg plunging method' developed by other workers [14,44].

In an excellent review, Banerji, Rohatgi and Rief [14] have discussed the influence of magnesium addition on the question of incorporation of ceramic particles into the aluminium melt. They have shown that addition of small pieces of magnesium to the surface of the melt alongwith dispersoids is more effective in dispersing these particles than the case when magnesium was

TABLE - 4.1

CHARACTERISTICS OF COMPOSITES PREPARED BY 'MODIFIED MgO COATING' TECHNIQUE USING VARYING AMOUNTS OF METALLIC Mg FOR PLUNGING.

| Expt. No. | Casting Condition | Total Al <sub>2</sub> O <sub>3</sub> + MgO Powder in li-Mixture quid added, Al wt% of melt | %Mg Plunging in li-Mixture quid added, Al | %Vf of Al <sub>2</sub> O <sub>3</sub> retained in composite | Microhardness HM5 gm | Density, gms/cc. in Kerosene Oil | Mechanical Properties   |                                     |              |                    |  |
|-----------|-------------------|--|---|---|----------------------|----------------------------------|-------------------------|-------------------------------------|--------------|--------------------|--|
|           |                   |  |   |   |                      |                                  | UTS MN, m <sup>-2</sup> | 0.2% offset Y.S. MN.m <sup>-2</sup> | Elongation % | Red in C.S. area % |  |
| 1         | 2                 | 3  | 4   | 5   | 6                    | 7                                | 8                       | 9                                   | 10           | 11                 |  |
| 1.        | Gravity Cast      | 10   | 0.4                                       | 11.61(U)<br>11.12(B)  | 62.96(U)<br>63.59(B) | 2.7882(U)<br>2.7791(B)           | 137.7                   | 84.5                                | 5.7          | 4.0                |  |
| 2.        | Gravity Cast      | 10   | 0.5                                       | 12.59(U)<br>11.98(B)  | 62.89(U)<br>63.11(B) | 2.801(U)<br>2.795(B)             | 137.8                   | 85.6                                | 5.7          | 5.5                |  |
| 3.        | Gravity Cast      | 10   | 0.6                                       | 13.40(U)<br>13.13(B)  | 61.27(U)<br>63.10(B) | 2.8194(U)<br>2.8129(B)           | 137.2                   | 87.1                                | 5.9          | 5.7                |  |
| 4.        | Gravity Cast      | 10   | 0.7                                       | 14.25(U)<br>13.82(B)  | 61.51(U)<br>60.54(B) | 2.8400(U)<br>2.8301(B)           | 144.1                   | 88.4                                | 6.3          | 6.2                |  |
| 5.        | Squeeze Cast      | 5  | 0.5                                       | 9.78  | 66.60                | 2.8512                           | 160.3                   | 83.3                                | 7.8          | 7.4                |  |

Remarks: (a) Total powder mixture (Al<sub>2</sub>O<sub>3</sub>+MgO) contains 15% MgO.

(b) Composite shown at Sr.No.5 squeeze-cast at 115 MPa for 20 sec. Alloy cast iron die temperature-200°C.

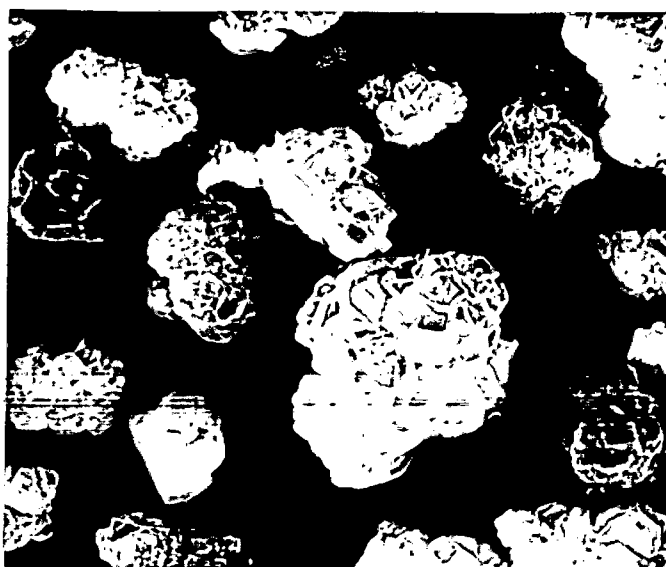
(c) Sample taken from the top portion of casting(U)  
Sample taken from the bottom portion of casting (B).

already present in the melt. They suggest that this may be probably because magnesium added to liquid aluminium initially melts and spreads on the melt surface, thereby wetting the dispersoid particles. Magnesium is known to wet the above particles because of its much lower surface tension ( $559 \text{ MN.m}^{-2}$ ) than that of pure aluminium ( $760 \text{ MN.m}^{-2}$ ) at the usual melt temperature (993K). Although the alloy addition of magnesium decreases the surface tension of aluminium considerably, from  $760 \text{ MN.m}^{-2}$  for pure aluminium to  $620 \text{ MN.m}^{-2}$  for Al-3% Mg alloy at 993K, the surface tension of latter is still greater than that of pure magnesium. Whatever the mode of addition, the magnesium present in the melt can further enrich at the surface of dispersoids according to the Gibb's Adsorption isotherm. It can be seen from the above facts that the freshly added magnesium just prior to the addition of dispersoids is more effective in causing the retention of dispersoid particles in the melt. Under favourable conditions, this magnesium may react also with the dispersoid particles forming reaction products at the particle matrix interface. This aspect will be taken up later during the discussion on EPMA examination of the reacted layer.

As discussed in the section 3.5.1, the ceramic particles were dehydroxylated at  $900^{\circ}\text{C}$  for two hours to fully remove adsorbed moisture layers from the surface of these particles so as to create favourable energy conditions between these particles and the melt to result in their proper incorporation in the stirred slurry. As suggested by Surappa and Rohatgi [44], the

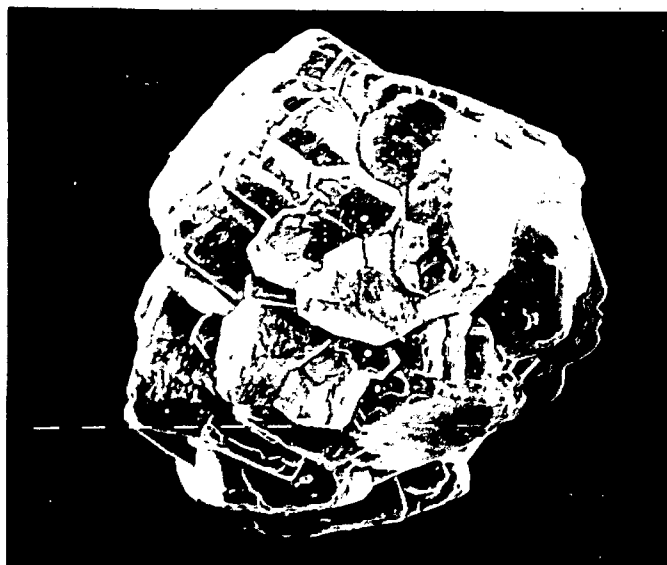
dehydroxylation treatment at  $900^{\circ}\text{C}$  for two hours results in an increase in the surface energy of  $\text{Al}_2\text{O}_3$  particles by about  $0.49 \text{ Joules m}^{-2}$ . This increase in the surface energy tends to improve the wetting behaviour of  $\text{Al}_2\text{O}_3$  particles and therefore, facilitates their incorporation and retention in aluminium melt. In the present work, both the  $\text{Al}_2\text{O}_3$  and submicron MgO particles were heat treated at  $900^{\circ}\text{C}$  for two hours prior to their mixing in a blender.

The objective of mixing the larger  $\text{Al}_2\text{O}_3$  particles ( $50\text{-}150 \mu\text{m}$ ) and the submicron MgO particles ( $0.2$  to  $0.3 \mu\text{m}$ ) in a blender for a period of about 30 minutes was to obtain a physical coating of submicron MgO particles onto the larger  $\text{Al}_2\text{O}_3$  particles. The SEM pictures of both uncoated and coated  $\text{Al}_2\text{O}_3$  particles are shown in Figs.4.1 and 4.2. It can be seen from these pictures that submicron MgO particles are filled into the spaces between different crystallites of  $\text{Al}_2\text{O}_3$  particles jetting out into different directions and are adhering nicely to their surfaces. The submicron MgO particles were employed in the technique of 'MgO coating' basically because MgO is known to display excellent wettability for liquid aluminium [61]. Using the above physical coating technique, it was shown in earlier investigations [47-49] that an excellent and uniform retention of  $\text{Al}_2\text{O}_3$  particles can be obtained in aluminium base matrix. It should be mentioned that in this particular work [47-49], no melt pre-treatment such as magnesium plunging etc. as mentioned above, was carried out and found necessary because the conditions



a

x320



b

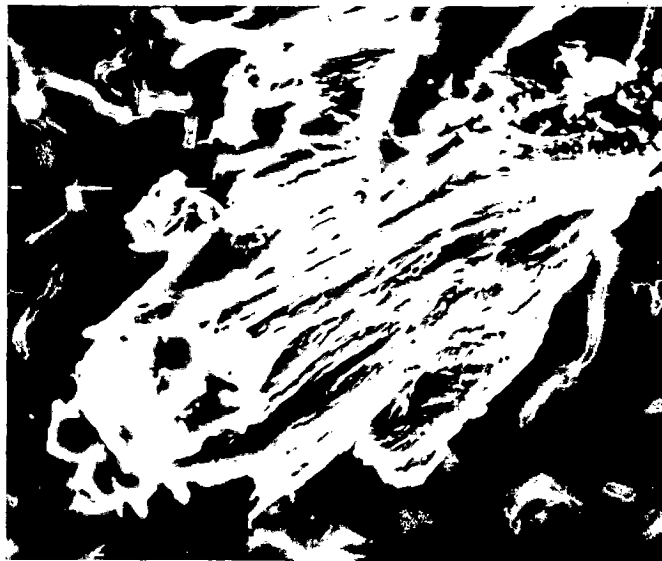
x640

FIG.4.1 (a) SEM picture of some Al<sub>2</sub>O<sub>3</sub> particles showing their morphology, (b) details of a single Al<sub>2</sub>O<sub>3</sub> particle showing an assemblage of crystallites.



a

x1250



b

x5000

FIG.4.2 SEM pictures showing MgO coated  $\text{Al}_2\text{O}_3$  particles.  
(a) a single MgO coated  $\text{Al}_2\text{O}_3$  particle,  
(b) a single crystallite of  $\text{Al}_2\text{O}_3$  particle coated with sub-micron MgO particles.

existing at Baghdad were extremely dry. This implies that the hydrogen potential of the bath was extremely low and therefore energy conditions were favourable for the incorporation and retention of  $\text{Al}_2\text{O}_3$  particles in aluminium base matrix. But under humid environmental conditions as existing in this region, extensive and thorough melt treatment was found necessary to satisfactorily-incorporate  $\text{Al}_2\text{O}_3$  particles in the melt.

The total melt pre-treatment consisted of proper degassing followed by magnesium plunging. The objective of degassing is to flush out the dissolved hydrogen from the melt as fully as possible. It was found to be an important step without which no incorporation of  $\text{Al}_2\text{O}_3$  could be possible in the melt. Additionally, the next step of magnesium plunging followed immediately after, helps to lower the surface tension of the melt.

The two steps together then establish suitable energy conditions for a successful incorporation and retention of  $\text{Al}_2\text{O}_3$  particles in the melt. This modification involving the pre-treatment of the melt plus the standard 'MgO coating' technique together is termed as "modified MgO coating technique".

The hydrogen content of the composites, before and after above pre-treatment, was analysed carefully using Leco instrument based on Vacuum Hot Extraction (VHE) technique [167]. The results pertaining to this study are shown below:

H<sub>2</sub> CONTENT OF COMPOSITES BEFORE AND AFTER PRE-TREATMENT

| Sr.No. | Casting Condition                            | Melt Pre-treatment                    | H <sub>2</sub> Content (ppm) |
|--------|--|---------------------------------------|------------------------------|
| 1.     | Gravity chill cast                           | No pre-treatment                      | 72                           |
| 2.     | Gravity chill cast                           | Degassing + Mg plunging(0.5% of melt) | 35                           |
| 3.     | Squeeze Cast, 140 MPa, 200°C die temperature | -do-                                  | 13                           |

It can be seen from the above results that the hydrogen content of the stirred slurry decreases from a level of 72 ppm to just 35 ppm due to extensive pre-treatment given to the melt. Upon squeezing, the hydrogen content of the composite decreases further to a low level of 13 ppm. It can be seen that the hydrogen content of squeezed composite is only 18% of the amount of hydrogen present in ordinary gravity chill cast composite, prepared without any pre-treatment. Also, the hydrogen content of squeezed composite is only 37% of what is present in gravity chill cast composite, which was given the same pre-treatment as the squeezed composites.

This implies that the hydrogen content of composite further decreases upon squeezing the stirred slurry at 140 MPa. The possible explanation for this can be that dissolved hydrogen precipitates out from the melt as a result of the application of high pressure during the process of solidification of the stirred slurry. It is basically because there is a large difference in the solubility of hydrogen in solid and molten aluminium [186]. As a high pressure is applied



to the stirred slurry during the squeeze casting operation, the melt is suddenly undercooled [89]. The extent of undercooling is rather severe along the walls of die and plunger as high rate of heat transfer is reported to occur across these locations [96,97]. This severe undercooling will result in a quick change of state of the stirred slurry from liquid to the solid state particularly along the walls of the die initially. This solidification then progresses rapidly towards the centre of the composite casting. As a result, the excess hydrogen in solution with the stirred slurry would precipitate out and escape the system. And as the melt is fully enclosed by the die and plunger from all sides and as the solidification itself is a very rapid process, there will be practically no opportunity for the melt to gain additional hydrogen from any outside source. As such, the squeezed composites would be expected to contain much lower levels of dissolved hydrogen as against ordinary gravity chill cast composites. The results of above investigation clearly signify the importance of pre-treatment given to the melt and the role of squeeze casting operation in achieving low levels of dissolved hydrogen in the cast composites.

Based on the results of an earlier study [47-49], composites were prepared with the addition of 10wt.% ( $\text{Al}_2\text{O}_3 + \text{MgO}$ )

powder mixture containing 15%MgO as this was found to be the optimum quantity resulting in optimum %V<sub>f</sub> retention of Al<sub>2</sub>O<sub>3</sub> and the best tensile properties. In one particular case, however, this quantity was halved to examine the properties of the resulting composite such as %V<sub>f</sub> retention of Al<sub>2</sub>O<sub>3</sub>, density, hardness, tensile properties etc.

Using the above stirred slurry, gravity chill cast and squeezed composites were prepared in the pressure range of 80 to 140 MPa following the procedure laid down in section 3.6. The pre-treated aluminium melt was also employed for the preparation of gravity chill cast and squeezed Al-MgO composites. Some Al-MgO composites were also prepared without the use of 0.5%Mg plunging in order to ascertain the effect of this step of pre-treatment on the properties of this composite (as per the procedure outlined in Section 3.5.3). Since the dispersion of submicron MgO particles is expected to cause dispersion strengthening of aluminium matrix [47-49], these aspects pertaining to the characterisation of Al-MgO composites are discussed in fuller details in Section 4.3.1.

#### 4.2.2 OPTICAL AND SEM EXAMINATION OF THE CAST STRUCTURE [166,168-170]

##### 4.2.2.1 GRAVITY CHILL CAST COMPOSITES

A separate discussion on gravity chill cast composites is considered necessary at this place because such composites were found to display special features. Optical pictures selected for this discussion are shown in two plates, termed as Figs.4.3 and 4.4.

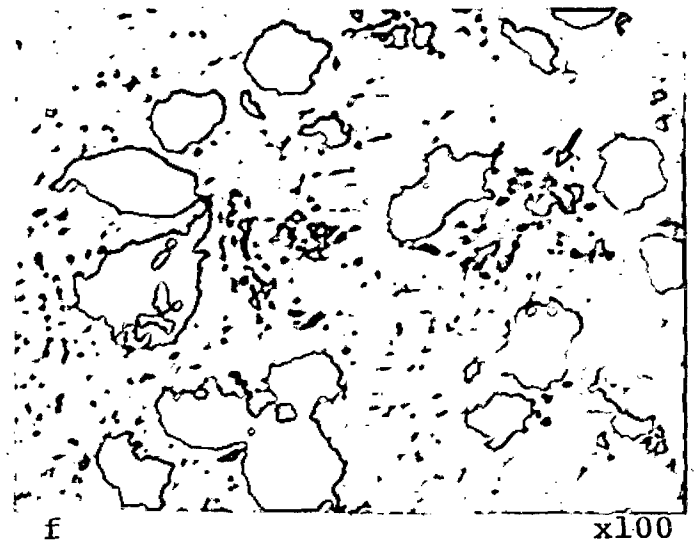
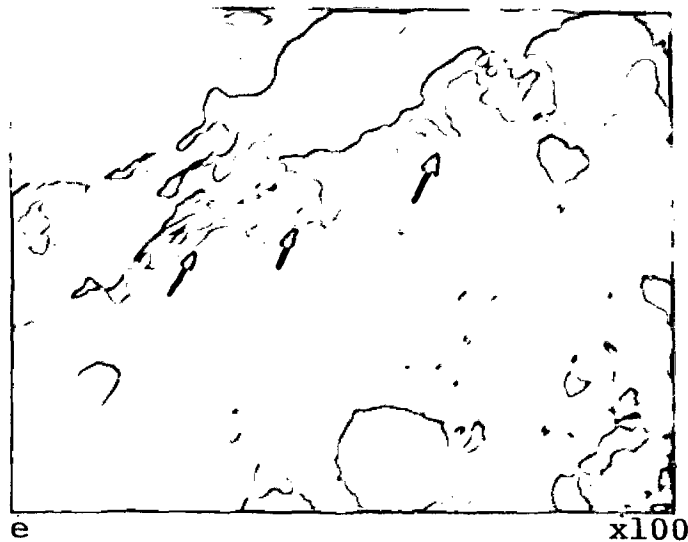
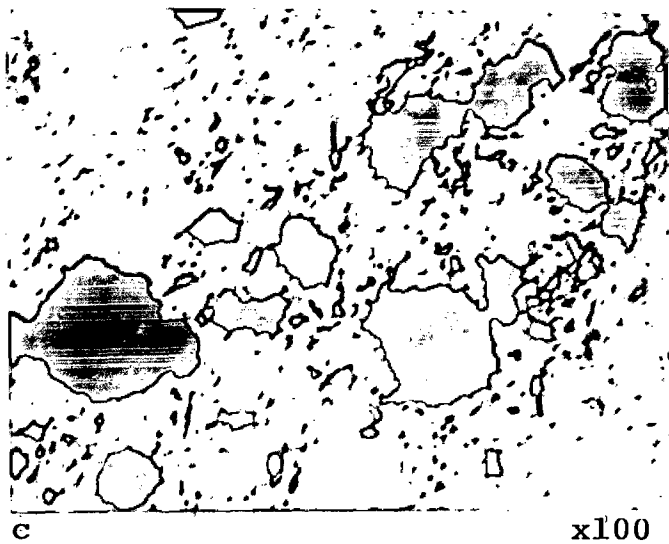
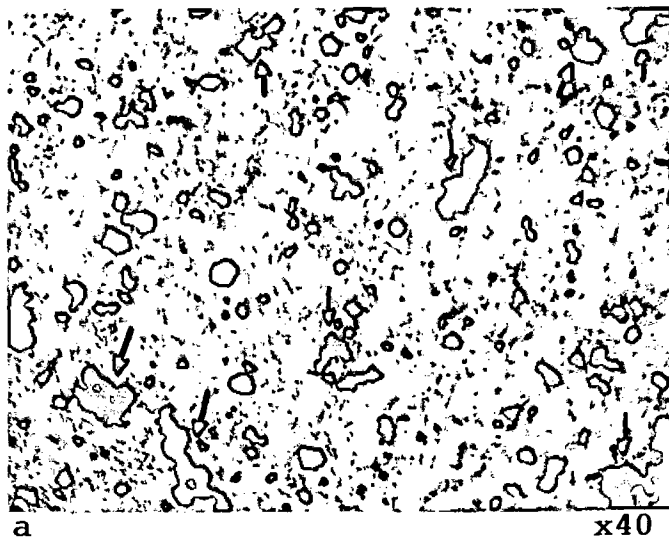
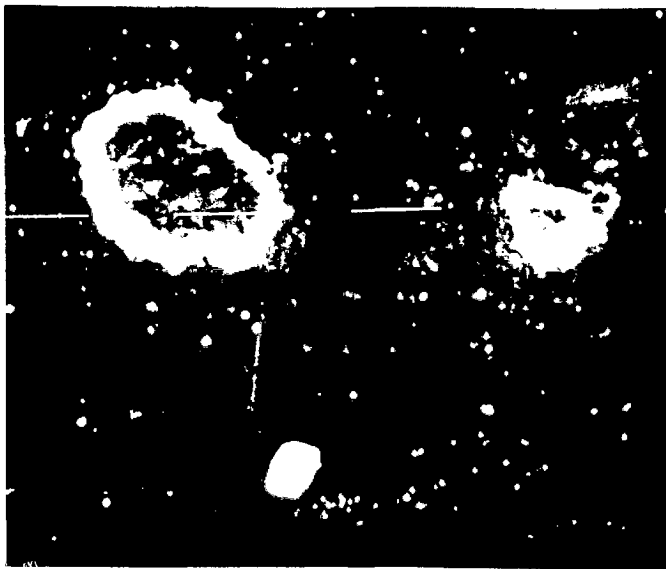
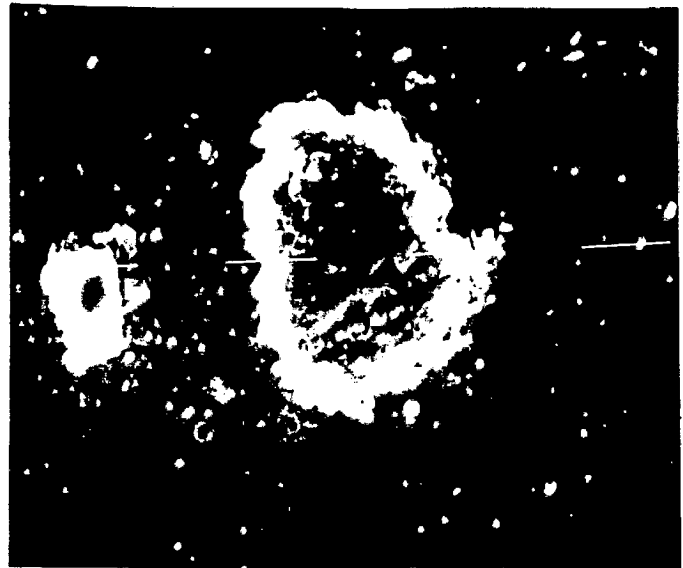


FIG.4.3 Optical pictures showing typical characteristics observed in gravity chill cast composite. Locations showing typical problems are marked by arrows. (a) Coagulation of Al<sub>2</sub>O<sub>3</sub> particles occurring in many locations, (b) Occurrence of porosity in the matrix in general and close to particle matrix interface in many locations, (c) and (d) same as in case of (b), (e) Unfed interdendritic regions, and, (f) same as (b) above.



a

x1250



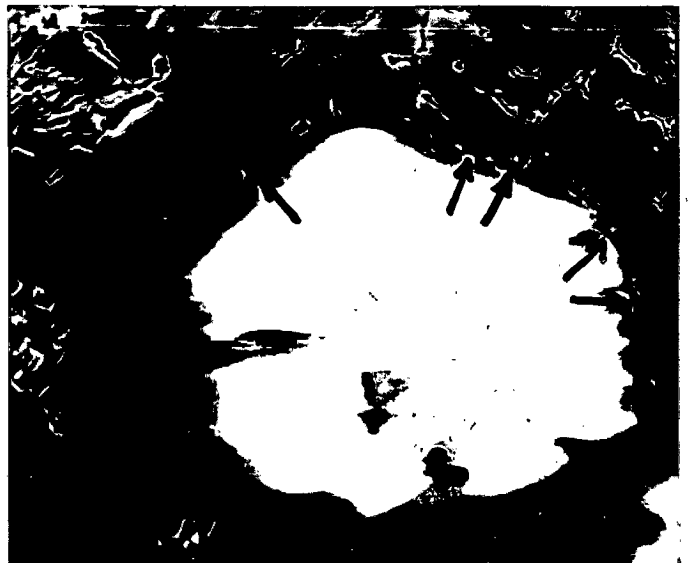
b

x1250



c

x320



d

x320

**FIG.4.4** SEM pictures of polished specimen, showing typical characteristics of gravity chill cast composites.  
 (a) and (b) SEM pictures of polished specimens showing MgO coating around  $Al_2O_3$  particle. Note that part of the coating has been erased during polishing. Also, the coating can be seen to be intact on comparatively smaller  $Al_2O_3$  particle,  
 (c) picture shows coagulation of  $Al_2O_3$  particles forming a chain-like structure,  
 (d) SEM picture showing the presence of micro voids at particle/matrix interface.

Optical micrographs shown in Fig.4.3(a to f) show the special features pertaining to gravity chill cast composites. It can be seen from Fig.4.3(a) that a good retention of  $\text{Al}_2\text{O}_3$  is obtained in the composite although the dispersed  $\text{Al}_2\text{O}_3$  particles show a tendency for coagulation at numerous places. Some of these locations are pin pointed by an arrow in the micrographs. Coagulation of some  $\text{Al}_2\text{O}_3$  particles is a basic limitation of 'Liquid Metallurgy Route' and is commonly observed in cast structure [47-49]. Such a coagulation of some  $\text{Al}_2\text{O}_3$  particles is shown in Figs.4.3(b)(marked by an arrow) and 4.4(d). Numerous such and other morphologies like the segregation of  $\text{Al}_2\text{O}_3$  particles along the grain boundaries in a single chain like fashion and other worm like caterpillar formations within the grain were observed extensively in an earlier study also [47-49]. Nevertheless,  $\text{Al}_2\text{O}_3$  particles can be seen to be nicely bonded with the base matrix. An evidence of this can also be seen in SEM pictures of polished specimen shown in Fig.4.4(a to d). It is noteworthy that part of the reacted layer on some of the  $\text{Al}_2\text{O}_3$  particles has been erased during polishing(Figs.4.4-a and b). But the particle can be seen to be nicely bonded with the base-matrix.

Occurrence of considerable amount of porosity or sponginess of the cast structure is another characteristic feature/limitation of gravity chill cast composites. This porosity could be micro or macro in size or could be interconnected or clustered giving a spongy appearance to the cast structure. This problem is commonly found in gravity chill cast

composites and is shown by arrows in Fig.4.3(b to f). Unfed areas between the arms of dendrites are also usually associated with the spongy structure, which is shown with the help of arrows in Fig.4.3(e). A detailed study of this aspect was carried out with the help of SEM examination of tensile fracture surfaces of gravity chill cast composites. These unfed dendritic regions are pulled out during tension revealing the arms of dendrites jetting out into the void space. A fuller discussion on this aspect is presented later during a study of the tensile fracture surfaces of gravity chill cast composites under the SEM (Section 4.3.3.1). In some instances, porosity can be seen occurring close to particle/matrix interface also. This is pointed by an arrow in Figs.4.3(b,c,d) and 4.4(d). This defect will result in premature particle/matrix decohesion during tension and will therefore, result in poor tensile properties of the cast composites. In such a case, less energy is required to be spent for the creation of voids at particle/matrix interface during tension, because such voids are already present at these locations in the cast structure. Therefore, particle/matrix decohesion leading to final fracture, would occur at much lower stress than expected. The gravity chill cast composite, therefore, displays much lower tensile strength than normally attainable. It is thus apparent that occurrence of these different kinds of porosities or sponginess in the cast structure will not permit full potential of the composite to be realised in actual practice in terms of the mechanical properties achievable.

In a recent work, Ghosh and Ray [64-66] estimated the influence of porosity on the mechanical properties of rheocast Al alloy-Al<sub>2</sub>O<sub>3</sub> cast particulate composites. They demonstrated in this work that the porosity can drastically decrease the tensile properties of cast particulate composites. With the help of the model proposed in this work, true or an ideal behaviour of any composite in terms of the mechanical properties achievable at zero porosity level can be determined [64-66].

Wide variety of reasons can contribute to the occurrence of these defects mentioned above. An abrupt increase in the solubility of H<sub>2</sub> at the melting point of aluminium and its subsequent precipitation upon solidification is the prime cause of formation of micro-porosity in the composites prepared by 'Vortex Liquid Metallurgy' route. Particular melting practice, use of protective atmospheres during melting, stirring of melt and its duration, ambient humidity levels, temperature of melt, level of dehydroxylation of particles added, the kind of mould employed for freezing the composites, degassing of melt etc. all influence the level of porosity present in the composite. In actual practice, the level of porosity can be minimised by taking adequate precautions during melting, stirring and casting. Also, porosity can be brought down to a bare minimum level by simply 'squeeze casting' (or liquid forging) the stirred slurry instead of casting the same in ordinary permanent moulds under gravity. It is one of the reasons why 'squeeze casting' has found such a wide spread acceptance throughout the world for the fabrication of near net shape, sound and high integrity castings.

#### 4.2.2.2 SQUEEZE CAST COMPOSITES

Results pertaining to this study are shown in two plates termed as Figs.4.5 and 4.6.

It can be seen from the optical micrograph shown in Fig.4.5(a) that almost uniform distribution of  $Al_2O_3$  particles is obtained in the matrix with minimum incidence of particle coagulation. The SEM picture shown in Fig.4.5(b) also shows similar features. Optical pictures of squeezed composites taken at comparatively higher magnification(Figs.4.5-c,d,e,f) show that the  $Al_2O_3$  particles are nicely bonded with the base matrix. Another feature noteworthy is that the particle/matrix interface is continuous and free from any defects like voids and spongy matrix close to the interface. These particular features make the squeezed composites distinctly superior than ordinary gravity chill cast composites. Under these circumstances, the applied load (for example during tension) will be effectively shared by both the hard  $Al_2O_3$  particles as well as the softer base matrix and the particle/matrix decohesion would be relatively more difficult. This kind of sound interface would therefore be expected to result in higher UTS values for squeeze cast composites. A thorough examination of the sliced specimen obtained from the cylindrical castings revealed that this particular feature of sound interface could be found even at the core section of the casting. This implies that the influence of squeeze pressure is transmitted right upto the core section of the casting. Apparently, therefore, the usual problem of section



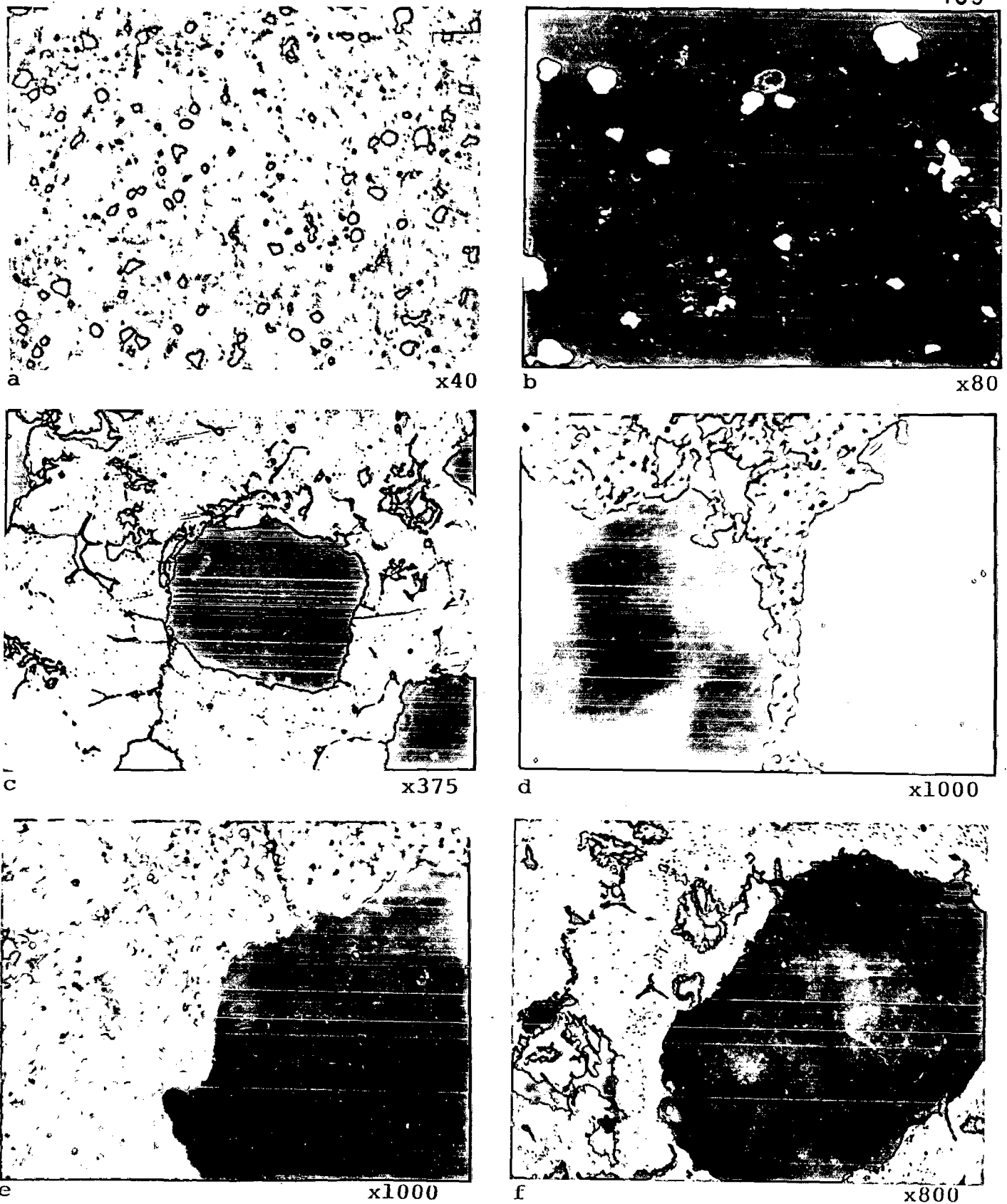


FIG.4.5 Optical and SEM pictures depicting the characteristics of squeeze cast composites. (a) Optical picture showing a uniform distribution of  $\text{Al}_2\text{O}_3$  particles in the matrix, (b) SEM picture showing the retention of  $\text{Al}_2\text{O}_3$  particles in the matrix, (c) optical picture showing that  $\text{Al}_2\text{O}_3$  particle is nicely bonded with the base matrix, (d), and (e) optical pictures showing that particle matrix interface is continuous and free from the presence of voids, and, (f) Optical picture showing the presence of some second phase constituents in the matrix. Also, this picture shows good bonding of  $\text{Al}_2\text{O}_3$  particle with the matrix.

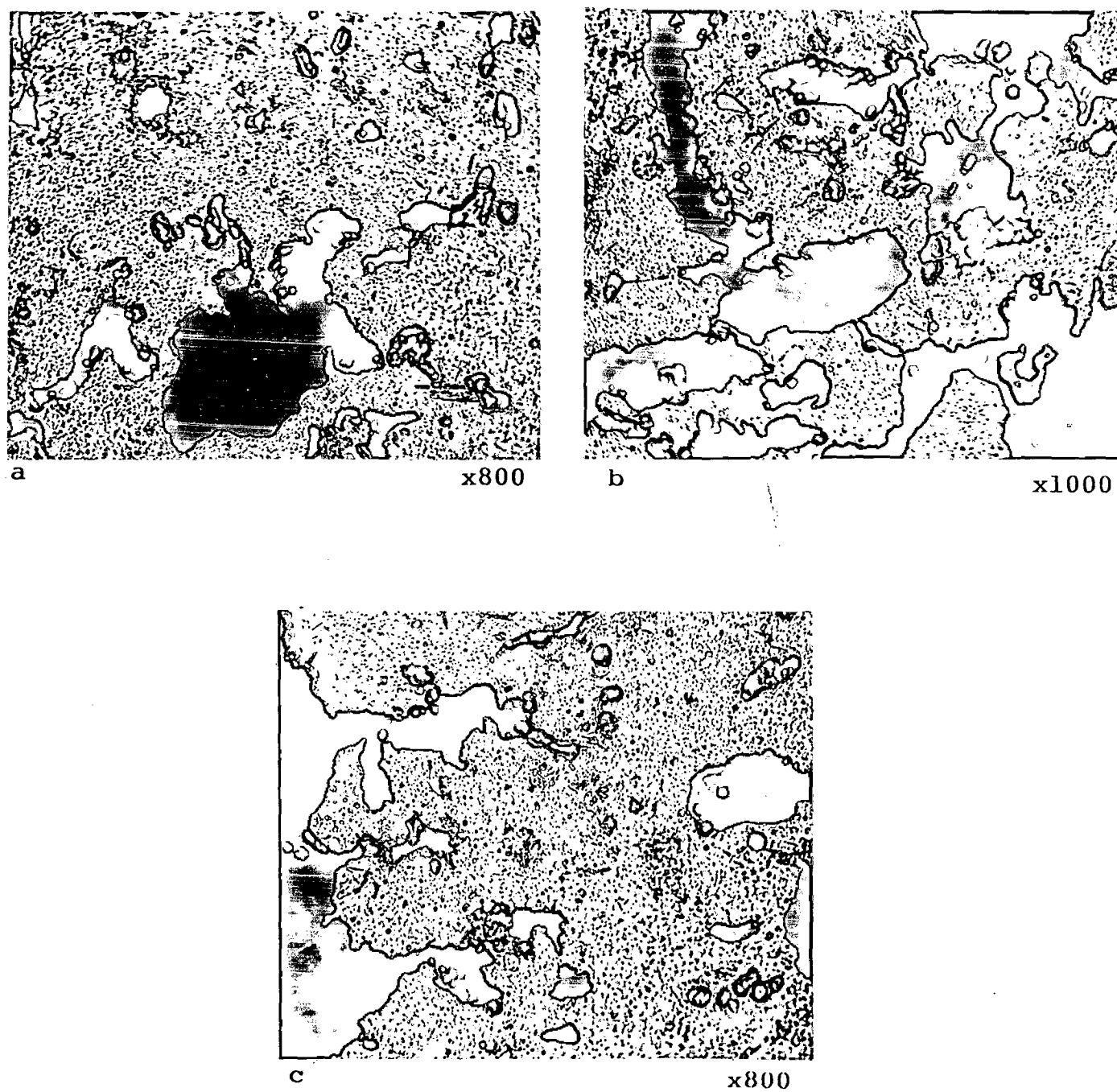


FIG.4.6 Optical pictures showing the presence of considerable quantity of second phase constituents in the matrix owing to the presence of iron and silicon as chief impurities in commercial purity aluminium.

sensitivity commonly observed with gravity chill cast composites is overcome to a great extent in case of squeeze cast composites. These composites, however, were found to contain some second phase constituents in the base matrix, which can be attributed to the presence of impurities of iron and silicon in commercially pure aluminium employed for the preparation of the stirred slurry [134]. Some of these second phase constituents present in the matrix are shown in Figs.4.5(f) and 4.6(a,b and c).

#### 4.2.3 INFLUENCE OF SQUEEZE PRESSURE ON % $V_f$ RETENTION OF $Al_2O_3$ , DENSITY AND MEAN DENDRITIC ARM SPACING OF COMPOSITES [169,172]

Results pertaining to this study are summarised in Table-4.2 and plotted in Figs.4.7 and 4.8.

Table-4.2 shows % $V_f$  retention of  $Al_2O_3$ , mean dendritic arm spacing and density of composites under different experimental conditions. For the sake of comparison, results pertaining to gravity chill cast and squeezed pure aluminium at 110 MPa and gravity chill cast composites are also included in Table-4.2. A typical case of composite squeezed at 115 MPa where only 5wt.% of total ( $Al_2O_3$ +MgO) powder mixture instead of usual 10% was stirred in the melt is presented at Sl.No.16 of Table-4.2. The results pertaining to percent increment in density vs the squeeze pressure applied are plotted in Fig.4.7. The relationship of mean dendritic arm spacing of different composites with the degree of squeeze pressure applied for the three die temperatures is plotted in Fig.4.8.

TABLE - 4.2

SOME CHARACTERISTICS OF GRAVITY CHILL CAST AND SQUEEZED COMMERCIALY PURE ALUMINIUM AND Al-Al<sub>2</sub>O<sub>3</sub>-MgO PARTICULATE COMPOSITES.

| Melt Sr.No. | Material  | Casting Condition | Pressure MPa | Die temp. °C | Total (Al <sub>2</sub> O <sub>3</sub> + MgO Powder | % retention of Al <sub>2</sub> O <sub>3</sub> | Density in Ker- osene Oil gms/cc | % Increment in density | Mean Dendritic Arm spacing, μm |
|-------------|-----------|-------------------|--------------|--------------|--|---|----------------------------------|------------------------|--------------------------------|
| 1           | Pure Al   | Gravity Cast      |              |              |  |   | 2.6107                           |                        | 48                             |
| 2           | Pure Al   | Squeeze Cast      | 110          | RT           | -  | -   | 2.7160                           | 4.03                   |                                |
| 3           | Composite | Gravity Cast      | 0            |              | 10   | 12.3  | 2.789                            | -                      | 46                             |
| 4           | -do-      | Squeeze Cast      | 80           | RT           | 10   | 12.4  | 2.8519                           | 1.926*                 | 30                             |
| 5           | -do-      | -do-              | 80           | 100          | 10   | 11.61   | 2.8521                           | 1.933                  | 34                             |
| 6           | -do-      | -do-              | 80           | 200          | 10   | 13.83   | 2.8520                           | 1.929                  | 36                             |
| 7           | -do-      | -do-              | 100          | RT           | 10   | 12.90   | 2.8672                           | 2.473                  | 24                             |
| 8           | -do-      | -do-              | 100          | 100          | 10   | 12.02   | 2.8674                           | 2.480                  | 29                             |
| 9           | -do-      | -do-              | 100          | 200          | 10   | 13.40   | 2.8670                           | 2.466                  | 32                             |
| 10          | -do-      | -do-              | 120          | RT           | 10   | 12.20   | 2.8843                           | 3.084                  | 19                             |
| 11          | -do-      | -do-              | 120          | 100          | 10   | 12.30   | 2.8841                           | 3.077                  | 22                             |
| 12          | -do-      | -do-              | 120          | 200          | 10   | 11.88   | 2.8840                           | 3.074                  | 24                             |
| 13          | -do-      | -do-              | 140          | RT           | 10   | 12.70   | 2.9010                           | 3.681                  | 12                             |
| 14          | -do-      | -do-              | 140          | 100          | 10   | 11.78   | 2.9008                           | 3.674                  | 16                             |
| 15          | -do-      | -do-              | 140          | 200          | 10   | 11.99   | 2.9012                           | 3.688                  | 18                             |
| 16          | Composite | Squeeze Cast      | 115          | 200          | 5  | 9.78  | 2.8512                           | 1.901                  | 27                             |

\* Density of chill cast composite taken as the basis for calculations of % increment in the density of squeezed composites.  
 Squeezing time - 40 secs (each case)  
 Stirring started from 860°C  
 Pouring temp. of slurry in the die-800°C  
 Time spent in transferring the melt in the die and placing the same under the hydraulic press for squeezing = 4 to 6 secs.  
 RT - Room Temperature

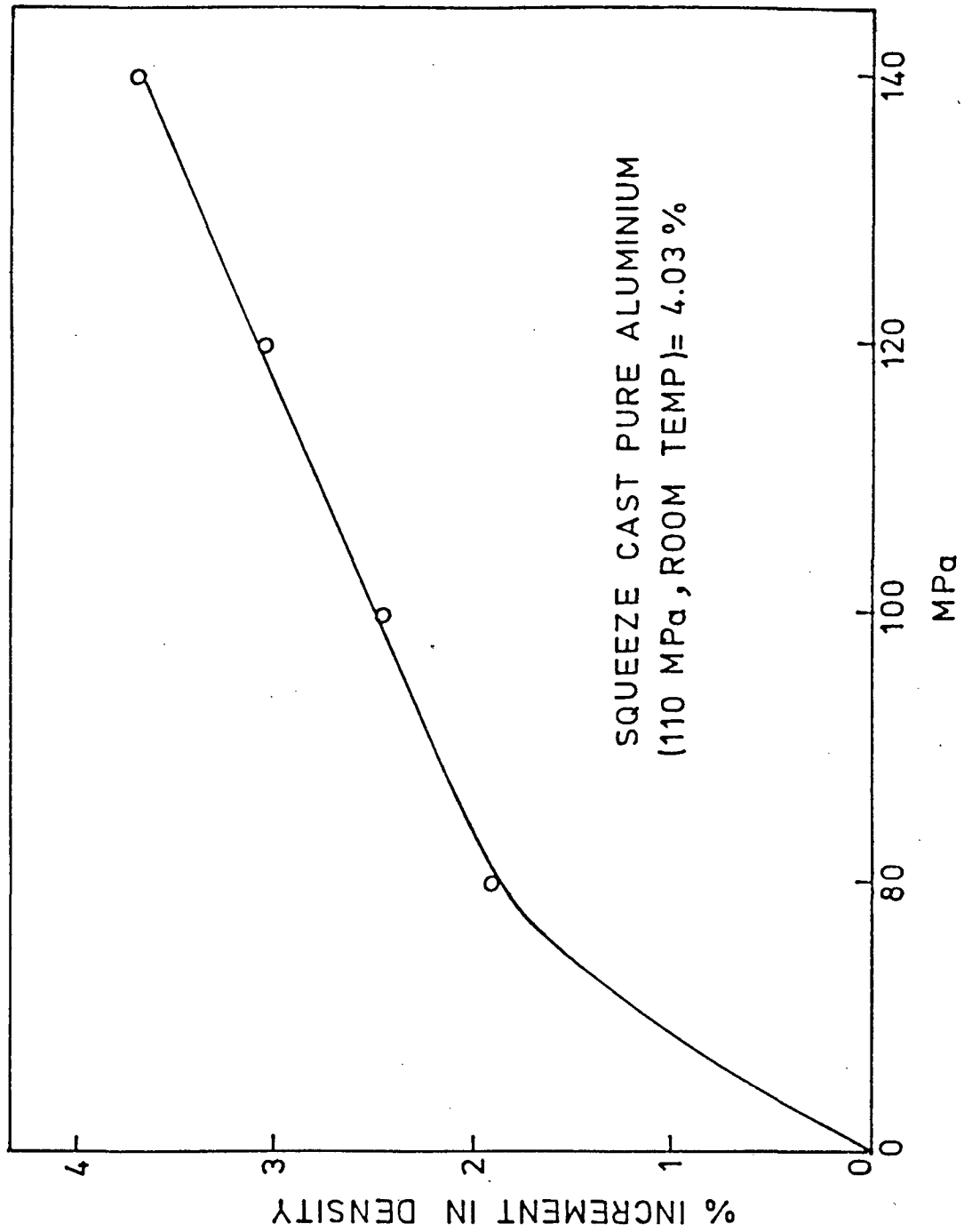


FIG.4.7 Percent increment in density of composites shown as a function of the squeeze pressure applied.

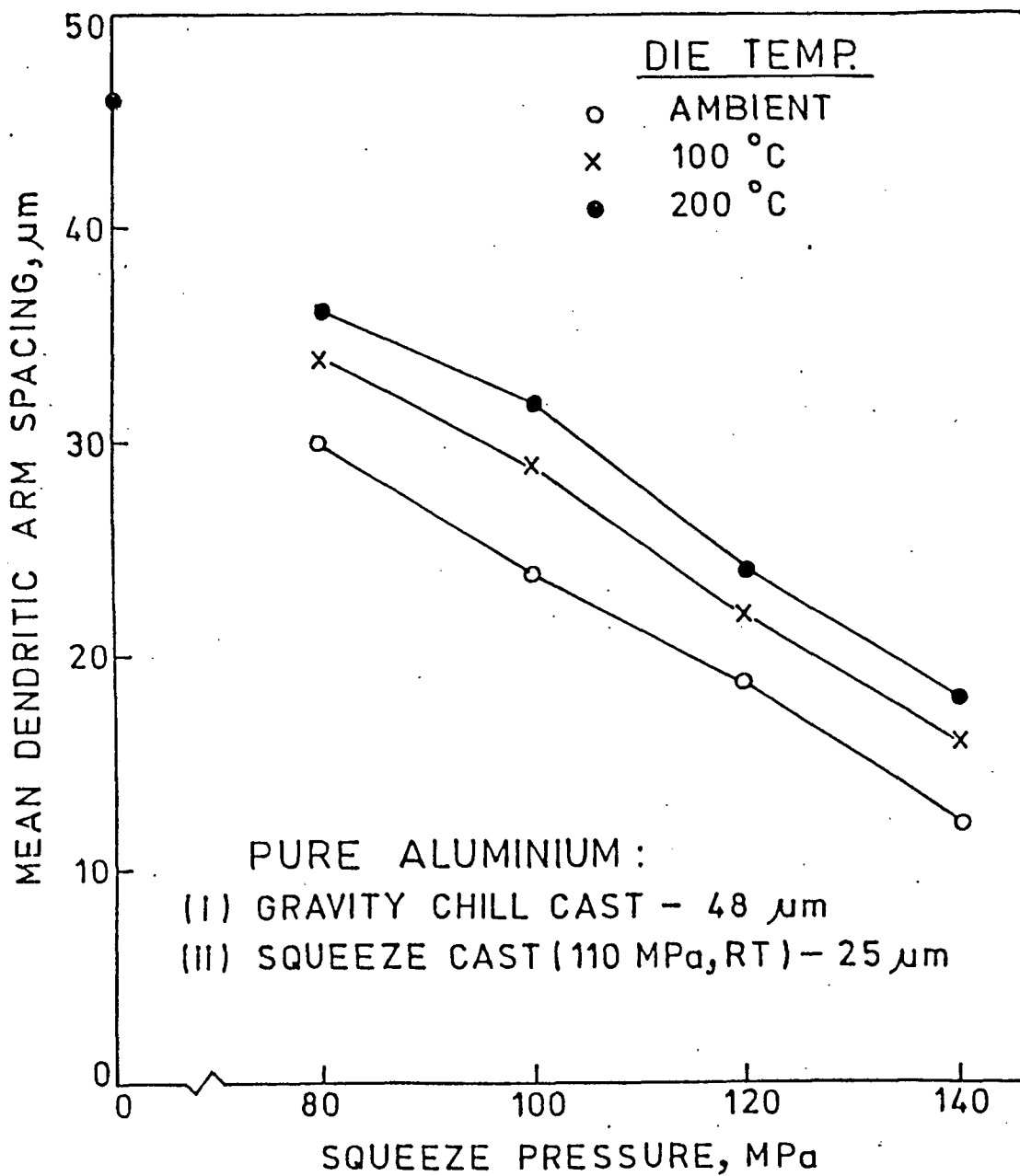


FIG.4.8 Variation in mean dendritic arm spacing of composite obtained at three different die temperatures shown as a function of the squeeze pressure applied.

It can be seen from the results recorded in Table-4.2 that  $\%V_f$  retention of  $Al_2O_3$  in the composite is not materially influenced by either the die temperature or the degree of squeeze pressure applied. It is because this factor is influenced mainly by the MgO content of total powder mixture and the net amount of this  $(Al_2O_3+MgO)$  powder mixture stirred in the melt. This is apparent from the results of heat No.16, where only 5% of total powder mixture containing 15%MgO was stirred in the melt. Based on the results of an earlier investigation [47-49], only 10% total powder mixture containing 15%MgO was added uniformly to all the melts employed for subsequent squeeze casting operations.

The process of squeeze casting would naturally result in densifying the composites. This is extremely beneficial in the sense that it signifies a proportionate decrease in the level of porosity present in the composites. It can be seen from Table-4.2 and Fig.4.7 that the density of composites progressively increases as the degree of squeeze pressure applied is systematically raised in steps. There is a jump of 1.926% in the density of composite when the slurry is squeezed at 80 MPa. For these calculations, the density of gravity chill cast composite is taken as the reference point. This increment in density becomes significant only when the level of squeeze pressure is taken to the next higher step. The influence of die temperature on this factor appears to be rather negligible. The increment in density finally rises to 3.688% at 140 MPa squeeze pressure. It would naturally be expected that the composite can be densified even further by

taking the squeeze pressure to still higher levels such as 160 to 240 MPa. There must, however, be a limit to densifying the composites, and this level must be close to the theoretical density of this composite system. The relationship between % increment in density and the squeeze pressure can be seen to be linear in the region of 80 to 140 MPa (Fig.4.7), but beyond this region upto 240 MPa, this tendency would be expected to taper off giving rise to an overall parabolic behaviour pattern.

As a consequence of the densification of composites, the porosity existing in the composite would be expected to decrease proportionately. Squeezing the stirred slurry would result in distinctly the following effects :

- 1) A drastic decrease in the formation of gas porosity precipitated during solidification under high pressure.
- 2) Plugging of unfed interdendritic regions due to pressurized feeding.
- 3) Press forging of the composite at just below the solidus temperature for a limited period of time during the later stages of squeezing operation leading to some degree of grain refinement. Major grain refinement of the cast structure is obtained because of considerable degree of under cooling experienced by the melt under pressurized feeding conditions. In this respect, the influence of squeeze pressure on the phase diagram and the Clausius-Clapeyron equation has been discussed in detail in chapter-2, section - 2.2.3.2.



The influence of squeeze pressure on the extent of grain refinement attained in the cast structure is shown in Fig.4.8. It can be seen from these results that progressive increase in grain refinement is attained as the squeeze pressure is systematically raised. The effect of die temperature on this parameter is also entirely on the expected lines. It would, thus, appear that the composites squeezed at ambient die temperature would display the best mechanical properties. It can be seen from the results shown in Fig.4.8 that the pattern of grain refinement obtained between 80 to 140 MPa is practically linear at all the three die temperatures employed. It would, therefore, be expected that increasing the squeeze pressure beyond 140 MPa would refine the structure still further. This improved grain refinement obtained beyond 140 MPa together with proportionate decrease in the porosity of composites would lead to further improvement in the tensile behaviour of the resulting composites. This aspect is worth further investigations. Pre-heating the die to about 200 °C may become necessary in actual practice to avoid premature solidification of the melt in case of smaller components. In such a case, the squeeze pressure may be raised to a suitably higher level to realise the same degree of refinement in the cast structure leading to almost similar properties as achieved at ambient die temperature. In larger components, however, this kind of manipulation may not be necessary.

In a fundamental study relating to this aspect, Nishida and Matsubara [95] demonstrated that the heat transfer rate during

the squeeze casting are nearly 10 times as fast as obtained in gravity chill casting. Epanchintsev [96] measured a cooling rate of  $140^{\circ}\text{C}/\text{sec}$  when squeeze casting an aluminium alloy in steel dies heated to approximately  $204^{\circ}\text{C}$  ( $477\text{K}$ ). Using the results of Spear and Gardner [97], Verma and Darcic [7] demonstrated that a mean dendritic arm spacing of  $8.94\ \mu\text{m}$  would be obtained when the melt is cooled at the rate of  $140^{\circ}\text{C}/\text{sec}$ . They practically obtained a mean dendritic arm spacings of nearly  $5\ \mu\text{m}$  near the head surface of the squeeze cast piston. This implies that the 'case' immediately below the punch is quenched to the punch temperature of  $204^{\circ}\text{C}$  within a matter of about 0.6 secs. However, this effect of ultra fine equiaxed non dendritic structure will be limited only to this 'casing' where very high cooling rates of the order of  $750^{\circ}\text{C}/\text{sec}$  are experienced. The structure below this 'casing', however, would be expected to display dendritic structure with comparatively larger dendritic arm spacing (in the range of 10-12  $\mu\text{m}$ ). The minimum mean dendritic arm spacing of 12  $\mu\text{m}$  obtained in the present work corresponding to 140 MPa squeeze pressure and ambient die temperature agree very well with the practical findings of Verma and Darcic [7]. A mean dendritic arm spacing of 20  $\mu\text{m}$  is reported by Reddy and Murthy [93] for an aluminium alloy at 110 MPa and  $200^{\circ}\text{C}$  die temperature. These workers studied the effect of specific pressure, dwell time, pressure application time and pouring temperature of the melt on the density and mechanical properties of the squeezed alloy. In a similar study, Franklin and Das [89] have also quoted a dendritic arm spacing of 20  $\mu\text{m}$  for a squeeze cast aluminium alloy. As

mentioned earlier, a given value of dendritic arm spacing can be obtained under different experimental conditions just by manipulating the squeeze pressure applied and the corresponding die temperature.

It can be seen from the results of present investigation summarised in Table-4.2 and plotted in Fig.4.8 that the mean dendritic arm spacing obtained for gravity chill cast composite is nearly 4 order of magnitude higher than the value obtained for the composite squeezed at 140 MPa and ambient die temperature. This is a single vital factor which will influence directly the performance of composites under tension. It is interesting to see that the value of 20  $\mu\text{m}$  quoted by Franklin and Das [89] and Reddy and Murthy [93] for squeezed aluminium alloys roughly corresponds to two different but independent conditions of composite fabrication in the present work. These two fabrication conditions are: one composite fabricated at 120 MPa and ambient die temperature and another fabricated at 140 MPa and 200°C die temperature. This is what is meant by saying that the same mean dendritic arm spacing can be obtained under different conditions of squeeze casting. In case the squeeze pressure is taken to about 210 MPa, probably a mean dendritic arm spacing of 5  $\mu\text{m}$  can be realised in present composites also as quoted by Verma and Dorcic [7] in their work.

#### 4.2.4 PARTICLE MATRIX BONDING : EXAMINATION OF THE REACTED LAYER AROUND $\text{Al}_2\text{O}_3$ PARTICLES BY THE EPMA [168,171]

Results of this study are recorded in Table-4.3 and the

SEM picture of the particle examined is shown in Fig.4.9. Results of the line analysis for Al and Mg carried out along the marker shown on the picture (Fig.4.9) are recorded in Fig.4.10. The strategy adopted for MgO analysis at different locations of base matrix and  $\text{Al}_2\text{O}_3$  particles is shown schematically in Fig.3.4 (Section 3.8).

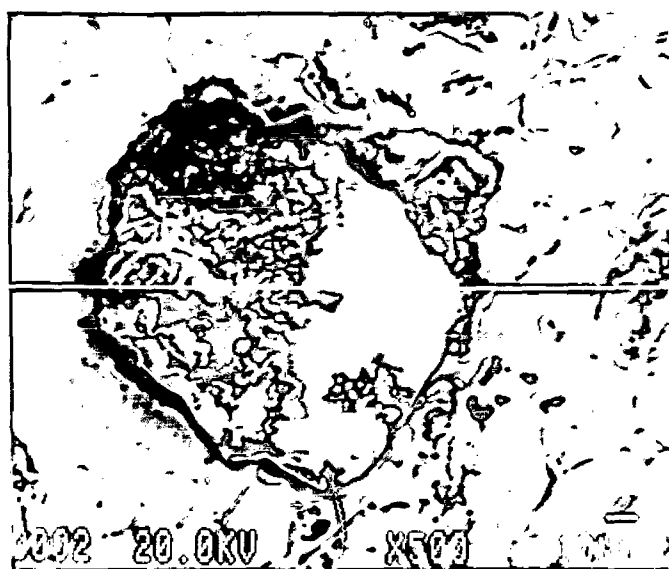
From the results shown in Fig.4.10, it can be seen that Mg tends to concentrate at the interface of  $\text{Al}_2\text{O}_3$  particle and the base matrix and its concentration tapers off as the centre of particle is approached. This behaviour of Mg would be expected also according to Gibbs adsorption isotherm.[14]. A similar concentration of Mg at fibre/matrix interface was noted by Mehrabian and co-workers also while fabricating Al/ $\text{Al}_2\text{O}_3$  fibre reinforced composites [12,62]. Under these circumstances, if a reaction product is formed, the concentration of MgO in the reacted layer at the interface would be expected to be the highest. Results of present study recorded in Table-4.3 confirm this contention. It was found that the concentration of MgO at two points very close to the interface (marked as points A and B in Fig.18) was as high as 3.448% and 3.102% respectively, while the interior locations of  $\text{Al}_2\text{O}_3$  particle (marked by a', b' and c' on Fig.18) registered MgO concentrations ranging between 0.714% and 2.627%. It is thus apparent that the concentration of MgO at the particle/matrix interface was much higher than the interior portions of the particle. The results of line analysis (Fig.4.10) and the point analysis (Table-4.3) therefore, support each other

TABLE - 4.3

POINT ANALYSIS FOR %MgO CONTENT AT DIFFERENT LOCATIONS OF THE COMPOSITE

| S.N. | Details of Location | Base Matrix |       |       | Al <sub>2</sub> O <sub>3</sub> Particle |       |       |
|------|---------------------|-------------|-------|-------|---|-------|-------|
|      |                     | a           | b     | c     | a                                       | b     | c     |
| 1.   | Location 1.         | 4.252       | 5.100 | 4.543 | 2.627                                   | 2.530 | 2.236 |
| 2.   | Location 2.         | 4.376       | 4.038 | 3.671 | 1.172                                   | 0.714 | 2.079 |
| 3.   | Location 3.         | 4.451       | 4.531 | 5.633 | 1.982                                   | 1.845 | 2.148 |

- Note:-** (1) Refer Fig.18 for details of the points selected on the base matrix and the Al<sub>2</sub>O<sub>3</sub> particle for MgO analysis.
- (2) Locations 1,2 and 3 on the polished surface of the composites were separated from each other by about 4mm (Fig.18)
- (3) Olivine mineral standard of known analysis employed for %MgO analysis.
- (4) MgO content at Al<sub>2</sub>O<sub>3</sub> particle/matrix interface.  
Points A and B (Fig.18) = 3.448 and 3.108% respectively.



x500

FIG.4.9 SEM picture of the Al<sub>2</sub>O<sub>3</sub> particle examined by Jéol JXA 8600 M EPMA.

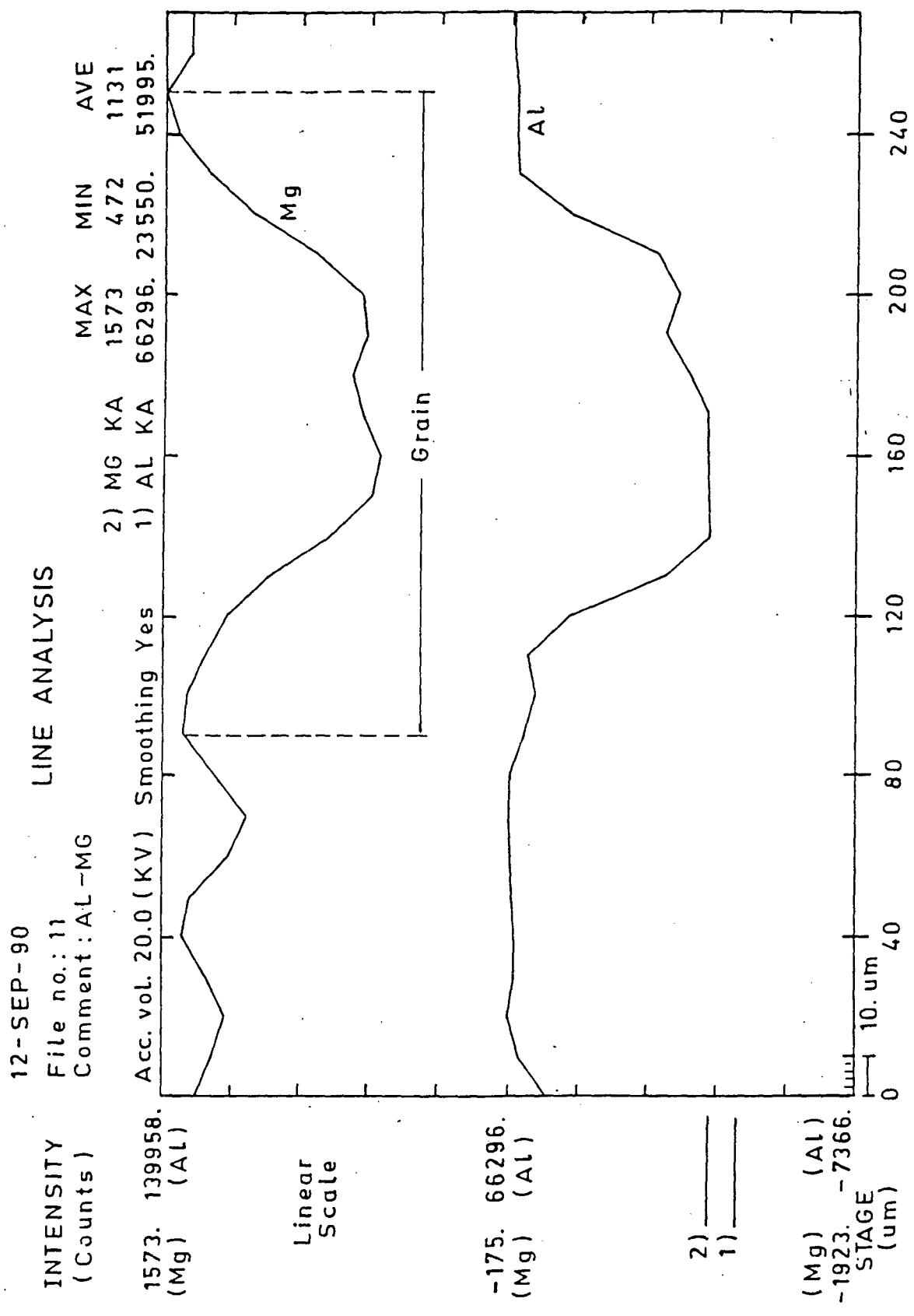


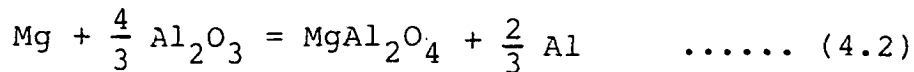
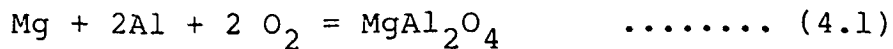
FIG.4.10 Line analysis for Al and Mg obtained by Jeol EPMA across the Al<sub>2</sub>O<sub>3</sub> particle shown in Fig.4.9.

fully. It can thus safely be concluded from these studies that the reacted layer around  $\text{Al}_2\text{O}_3$  particles does contain a noticeable amount of MgO.

Data pertaining to the MgO content of the base matrix (Table-4.3) reveals another aspect. Considerable quantity of MgO detected at several locations of the base matrix is due to the special 'MgO coating' technique employed for the fabrication of composites in the present work. This technique results in the retention of considerable quantity of submicron MgO particles in the base matrix of composites. It was shown in an earlier study [47-49,170] that these retained MgO particles also cause dispersion strengthening of the base matrix. In fact, the retention of submicron MgO particles in the matrix is readily attained basically because these particles display excellent wettability for liquid aluminium [61]. It is for these reasons that a noticeable quantity of MgO is detected in the base matrix also (Table-4.3).

The exact chemical nature of this reacted layer around  $\text{Al}_2\text{O}_3$  particle is likely to be a spinel  $\text{MgAl}_2\text{O}_4$  as reported by Mehrabian and co-workers [12,13,14,62]. While examining the fibre/matrix interface using Auger and electron diffraction technique, they found that Mg formed discrete crystals of  $\text{MgAl}_2\text{O}_4$  spinel on the fibre surface [12,13]. The fibres are thought to provide a suitable substrate for the growth of a spinel. The formation of a spinel is proposed to occur according to the following reactions [12,13]:





In the present case also, the possibility of formation of spinel around dispersed  $\text{Al}_2\text{O}_3$  particle is fairly high. A high concentration of MgO observed at the particle/matrix interface is a pointer to this possibility. As shown in SEM pictures (Figs.4.4a and b), this reacted layer adheres very tenaciously with the particle surface. It is interesting that Mehrabian [12] observed the formation of similar kind of reacted layers around the dispersed particles/fibres in other systems also. For example, he mentions that in Al-Cu alloy, interactions produced discrete particles of a copper rich phase around the fibre. This phase, however, disappeared after heat treatment. He found that interaction zone consisted of  $\text{CuAl}_2\text{O}_4$ , fine  $\alpha\text{-Al}_2\text{O}_3$  and possibly  $\text{CuAl}_2$ . As in the case of Mg spinel, the cupric aluminate could form directly in the melt and grow onto the fibre surface. In a Al-Cu-Mg alloy, Mehrabian found the enrichment of both Mg and Cu at the fibre matrix interface. He suggests that interaction zone most likely consisted of  $\text{MgAl}_2\text{O}_4$ ,  $\alpha\text{-Al}_2\text{O}_3$  and  $\text{CuAl}_2\text{O}_4$  [12].

### 4.3 MECHANICAL PROPERTY EVALUATION

#### 4.3.1 VICKER'S HARDNESS AND MICROHARDNESS OF COMPOSITES [166,169,170]

Results pertaining to a study of the Vicker's hardness and microhardness of gravity chill cast and squeezed composites

TABLE - 4.4

MEAN VICKER'S HARDNESS (HV<sub>5</sub>) AND MEAN MICROHARDNESS (HM<sub>5gm</sub>) OF GRAVITY CHILL CAST AND SQUEEZED COMMERCIALY PURE ALUMINIUM AND Al-Al<sub>2</sub>O<sub>3</sub>-MgO PARTICULATE COMPOSITES.

| Melt Sl.No. | Material                             | Squeeze Pressure (MPa)  | Die Temperature (°C) | Total Al <sub>2</sub> O <sub>3</sub> + MgO) Powder, wt.% | %V <sub>f</sub> retention of Al <sub>2</sub> O <sub>3</sub> | Mean Vicker's Hardness, HV <sub>5</sub> | Mean Microhardness of the base matrix, HM <sub>5gm</sub> |
|-------------|--------------------------------------|-------------------------|----------------------|--|---|---|--|
| 1           | Commercially Pure Aluminium          | Nil(Gravity Chill Cast) | -                    | -  | -   | 31.60                                   | 33.8   |
| 2           | Squeezed Commercially Pure Aluminium | 110                     | Ambient              | -  | -   | 43.38                                   | 47.6   |
| 3           | Composite                            | Nil(Gravity Chill Cast) | -                    | 10   | 12.30   | 41.83                                   | 59.6   |
| 4           | Squeezed Composite                   | 80                      | Ambient              | 10   | 12.40   | 60.90                                   | 79.9   |
| 5           | Squeezed Composite                   | 80                      | 100                  | 10   | 11.61   | 58.50                                   | 79.1   |
| 6           | Squeezed Composite                   | 80                      | 200                  | 10   | 13.83   | 56.30                                   | 78.9   |
| 7           | Squeezed Composite                   | 100                     | Ambient              | 10   | 12.90   | 63.64                                   | 81.6   |
| 8           | Squeezed Composite                   | 100                     | 100                  | 10   | 12.02   | 62.20                                   | 81.0   |
| 9           | Squeezed Composite                   | 100                     | 200                  | 10   | 13.40   | 61.00                                   | 80.8   |
| 10          | Squeezed Composite                   | 120                     | Ambient              | 10   | 12.20   | 67.76                                   | 85.1   |
| 11          | Squeezed Composite                   | 120                     | 100                  | 10   | 12.30   | 66.10                                   | 84.8   |
| 12          | Squeezed Composite                   | 120                     | 200                  | 10   | 11.88   | 64.00                                   | 84.5   |
| 13          | Squeezed Composite                   | 140                     | Ambient              | 10   | 12.70   | 73.18                                   | 87.2   |
| 14          | Squeezed Composite                   | 140                     | 100                  | 10   | 11.78   | 71.00                                   | 87.0   |
| 15          | Squeezed Composite                   | 140                     | 200                  | 10   | 11.99   | 68.30                                   | 86.9   |
| 16          | Squeezed Composite                   | 115                     | 200                  | 5  | 9.78  | 48.50                                   | 63.5   |

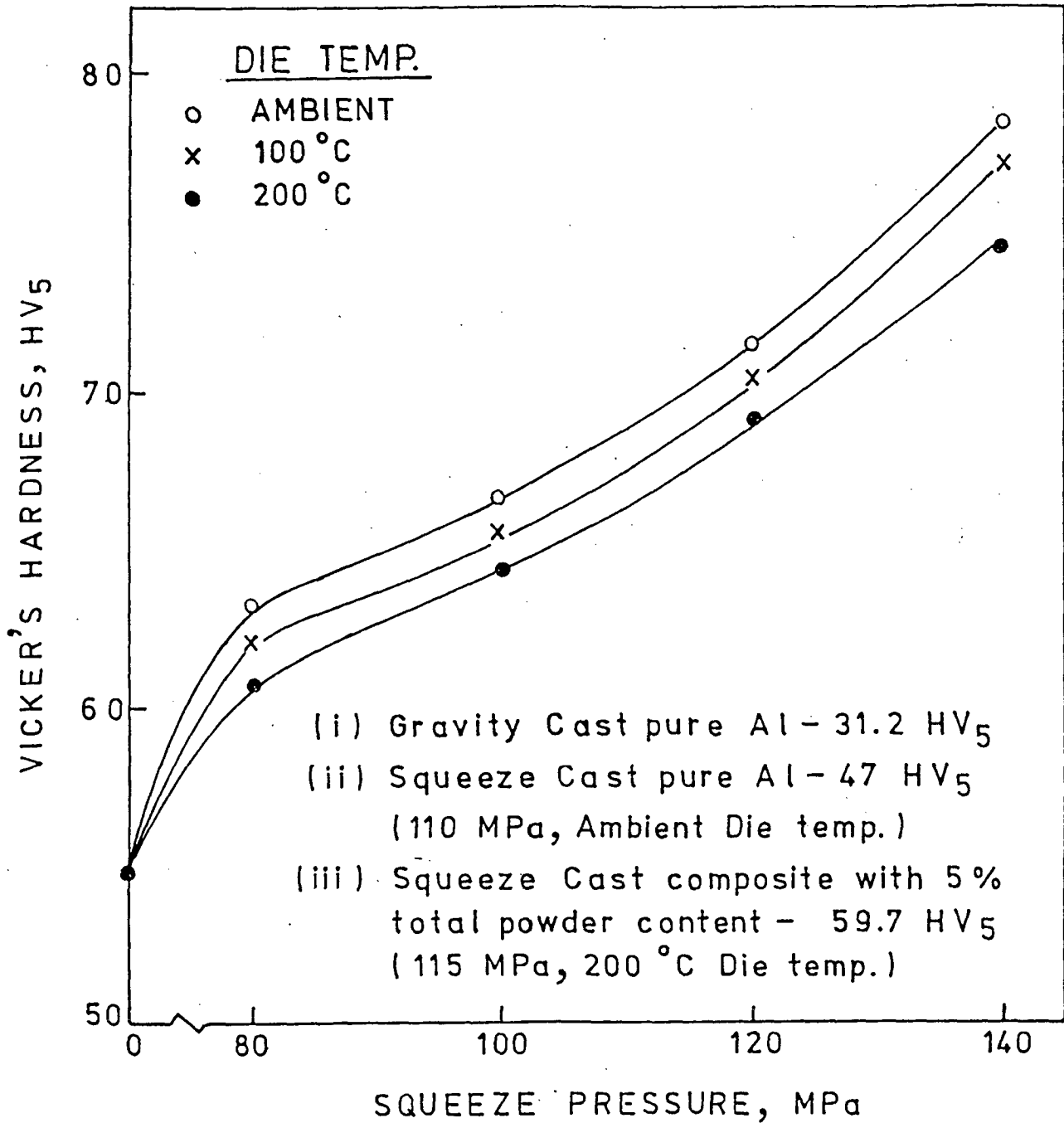
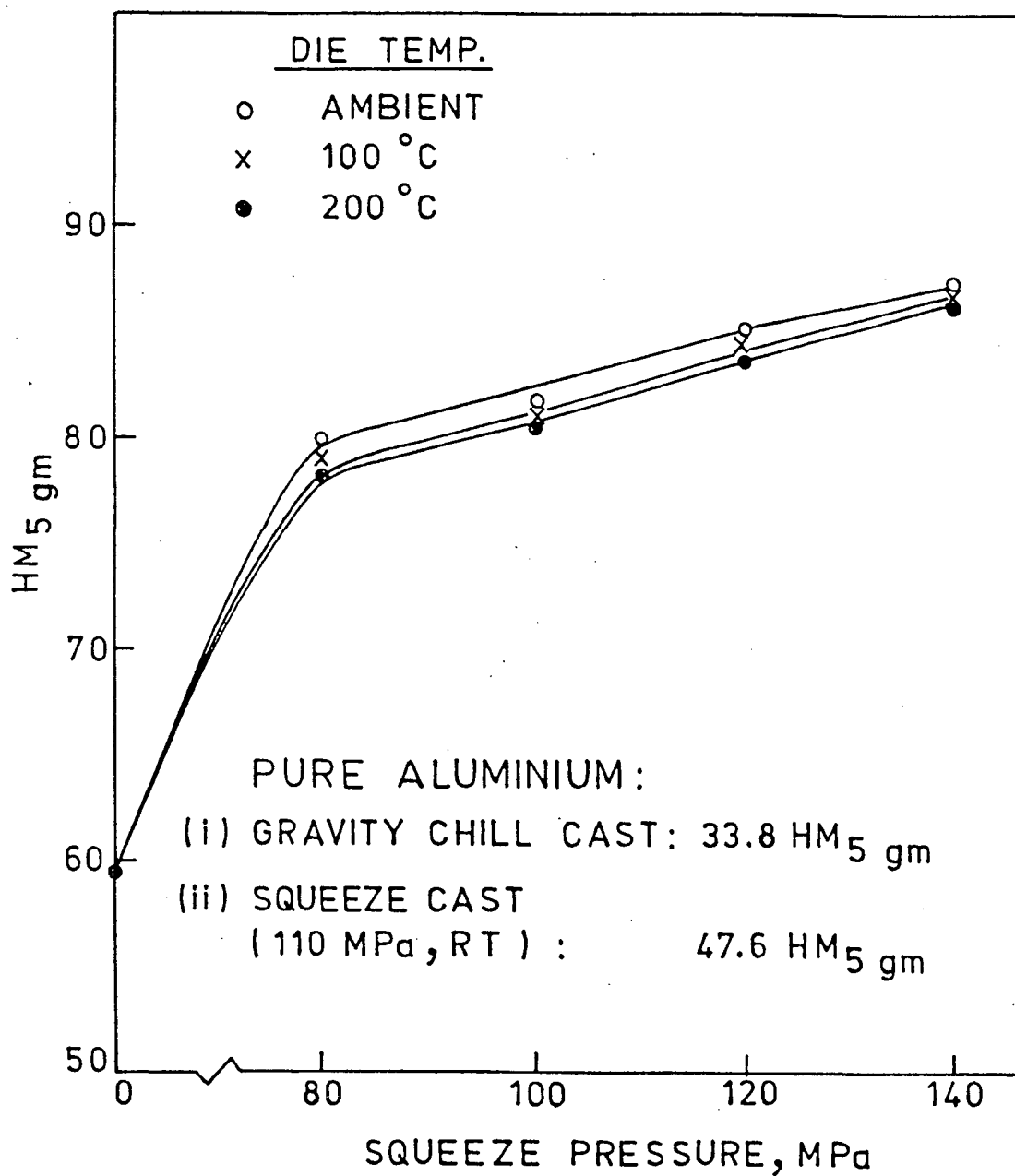


FIG.4.11 Vicker's hardness of composites obtained at three die temperatures shown as a function of the squeeze pressure applied.



**FIG. 4.12** Microhardness of the base matrix obtained at three different die temperatures shown as a function of the squeeze pressure applied.

are recorded in Table-4.4 and plotted in Figs.4.11 and 4.12 respectively. It can be seen from these results that the Vicker's hardness ( $HV_5$ ) of the composite progressively improves as the squeeze pressure is systematically raised from 80 MPa to 140 MPa (Fig.4.11). The effect of higher die temperature, such as 100 and 200°C, is to proportionately decrease the hardness attained, which is entirely expected because the mean dendritic arm spacing would progressively increase with increasing die temperature at a fixed squeeze pressure applied (Table-4.2, Fig.4.8). This progressive decrease in hardness of the matrix with increasing die temperatures will directly reflect in the tensile behaviour of the resulting composites. Also, this hardness pattern will have a direct bearing on the wear behaviour of these composites under dry sliding conditions. These two aspects are discussed in subsequent sections.

Also the microhardness data ( $HM_{5gm}$ ), plotted in Fig.4.12, displays the same pattern. It can be noted from the results that the microhardness of the base matrix of gravity chill cast composites improves by about 76% compared to the microhardness of gravity chill cast pure aluminium. This is attributed to the dispersion strengthening effect of submicron MgO particles on the base matrix as proposed in an earlier study [47-49]. These particles may also show a tendency for segregation towards the grain boundaries or also in interdendritic regions [47-49, 173].

#### 4.3.2 STUDIES ON Al-MgO COMPOSITES: DISPERSION STRENGTHENING EFFECT OF SUBMICRON MgO PARTICLES [168,170]

Results pertaining to a detailed examination of the

dispersion strengthening effect of submicron MgO particles on the matrix are summarised in Table-4.5 and plotted in Figs.4.13, 4.14 and 4.15. These results provide an experimental verification of the hypothesis proposed earlier [47-49] that submicron MgO particles do cause dispersion strengthening of Al base matrix. It can be seen from the results that whenever Mg plunging to the tune of 0.5% of Al-melt is employed in addition to normal MgO dispersion, the matrix is stiffened a little further. This would be naturally expected because the small amount of Mg going in solution with the melt would cause solid solution strengthening of the matrix. This aspect was intentionally investigated particularly because Mg plunging to the tune of 0.5% of melt is an integral part of "Modified MgO coating technique", and is commonly employed for the preparation of Al-Al<sub>2</sub>O<sub>3</sub>-MgO gravity chill cast/squeezed composites.

It is apparent from the results shown in Table-4.5 and Figs.4.13-4.15 that optimum strengthening of the matrix is obtained at 1.0% addition of MgO powder to the melt. Below this level, optimum strengthening effect is not realised due to inadequate quantity of particles dispersed in the melt and beyond this level, the optimum strengthening effect is lost due to over crowding of particles, a situation similar to overageing. In case of normal Al-Al<sub>2</sub>O<sub>3</sub>-MgO composites, the quantity of submicron MgO particles required to cause this effect of dispersion strengthening works out to be 1.5% of aluminium melt. In the present set of experiments, however, this optima is observed at

TABLE - 4.5

## CHARACTERISATION OF Al-MgO COMPOSITES PREPARED WITH AND WITHOUT Mg PLUNGING

| Sl. No.                            | Casting Condition    | % MgO Stirred in Al melt | HV5  | HM <sub>5</sub> gm | TENSILE PROPERTIES     |                                    |          |                     |
|------------------------------------|----------------------|--------------------------|------|--------------------|------------------------|------------------------------------|----------|---------------------|
|                                    |                      |                          |      |                    | UTS MN.m <sup>-2</sup> | 0.2% offset Y.S. MN. <sup>-2</sup> | % Elong. | % Redn in C.S. area |
| WITHOUT Mg PLUNGING                |                      |                          |      |                    |                        |                                    |          |                     |
| 1.                                 | Gravity Chill Cast   | 0.5                      | 33.0 | 48.4               | 92.5                   | 52.3                               | 9.4      | 8.5                 |
|                                    |                      | 1.0                      | 34.3 | 53.2               | 102.7                  | 57.0                               | 6.9      | 5.9                 |
|                                    |                      | 1.5                      | 32.5 | 47.7               | 71.9                   | 40.9                               | 10.1     | 9.3                 |
| 2.                                 | Squeeze Cast 80 MPa  | 0.5                      | 50.7 | 68.4               | 104.4                  | 59.5                               | 11.2     | 10.3                |
|                                    |                      | 1.0                      | 52.4 | 73.0               | 117.1                  | 66.7                               | 8.3      | 7.4                 |
|                                    |                      | 1.5                      | 50.0 | 67.6               | 86.6                   | 48.5                               | 12.1     | 11.2                |
| 3.                                 | Squeeze Cast 140 MPa | 0.5                      | 63.3 | 73.7               | 142.6                  | 81.3                               | 17.1     | 16.2                |
|                                    |                      | 1.0                      | 64.7 | 78.3               | 157.9                  | 91.6                               | 14.7     | 13.9                |
|                                    |                      | 1.5                      | 62.9 | 72.1               | 124.8                  | 69.8                               | 18.2     | 17.3                |
| WITH Mg PLUNGING (0.5% of Al Melt) |                      |                          |      |                    |                        |                                    |          |                     |
| 4.                                 | Gravity Chill Cast   | 0.5                      | 34.0 | 50.2               | 94.3                   | 53.7                               | 8.9      | 8.0                 |
|                                    |                      | 1.0                      | 35.4 | 55.4               | 104.0                  | 59.5                               | 6.1      | 5.4                 |
|                                    |                      | 1.5                      | 33.4 | 49.1               | 74.8                   | 41.9                               | 9.6      | 8.8                 |
| 5.                                 | Squeeze Cast 80 MPa  | 0.5                      | 51.8 | 70.5               | 106.9                  | 60.9                               | 10.6     | 9.8                 |
|                                    |                      | 1.0                      | 53.4 | 74.8               | 119.8                  | 68.3                               | 7.7      | 6.9                 |
|                                    |                      | 1.5                      | 51.0 | 69.3               | 89.5                   | 51.9                               | 11.5     | 10.7                |
| 6.                                 | Squeeze Cast 140 MPa | 0.5                      | 64.3 | 75.6               | 145.2                  | 84.2                               | 16.5     | 15.7                |
|                                    |                      | 1.0                      | 65.8 | 80.1               | 160.4                  | 93.0                               | 14.1     | 13.4                |
|                                    |                      | 1.5                      | 63.8 | 74.2               | 127.3                  | 73.8                               | 17.7     | 16.8                |

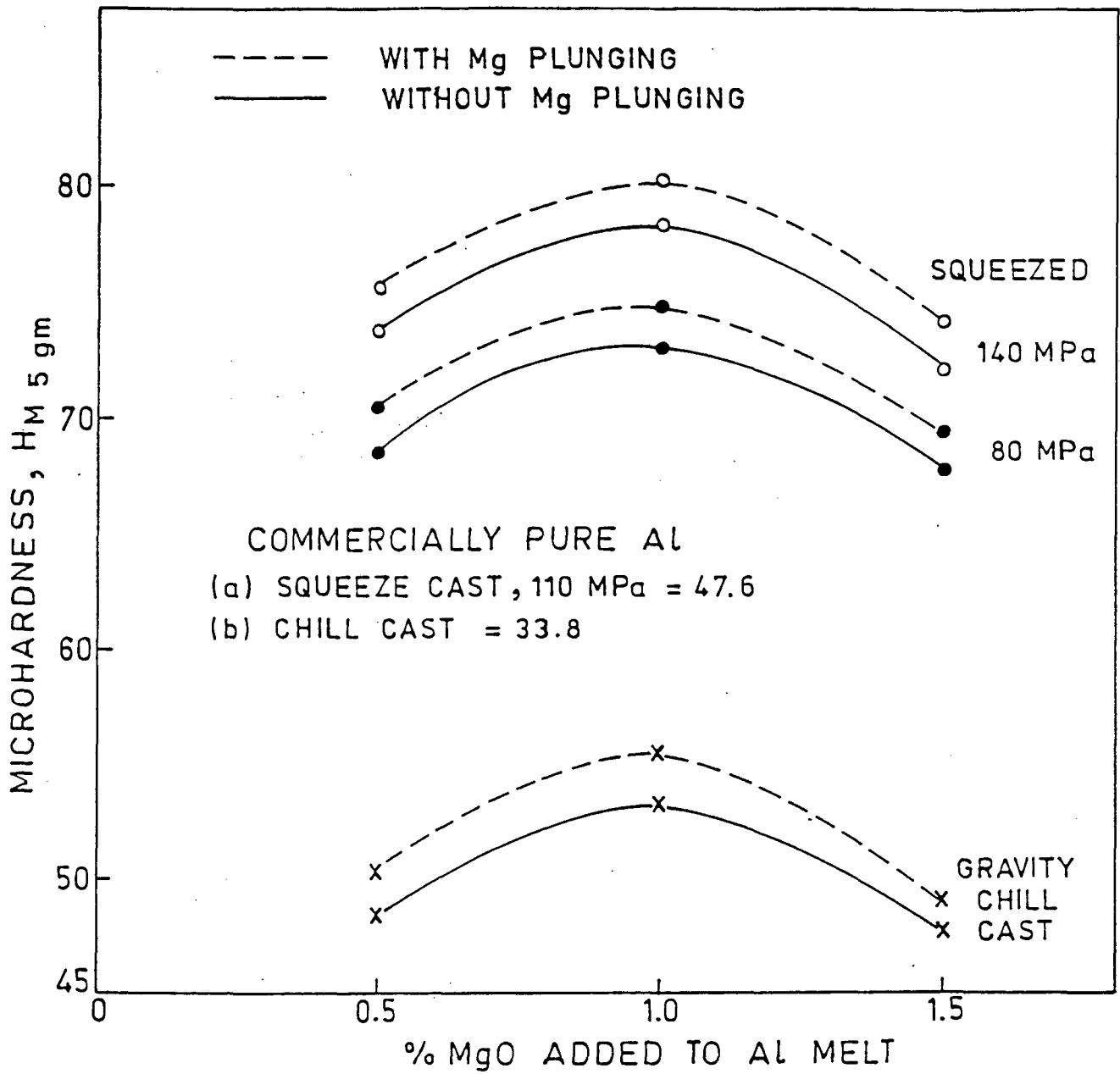


FIG.4.13 Influence of the extent of dispersion of sub-micron MgO particles and the degree of squeeze pressure applied on the microhardness ( $HM_{5\text{ gm}}$ ) of Al-MgO composites.



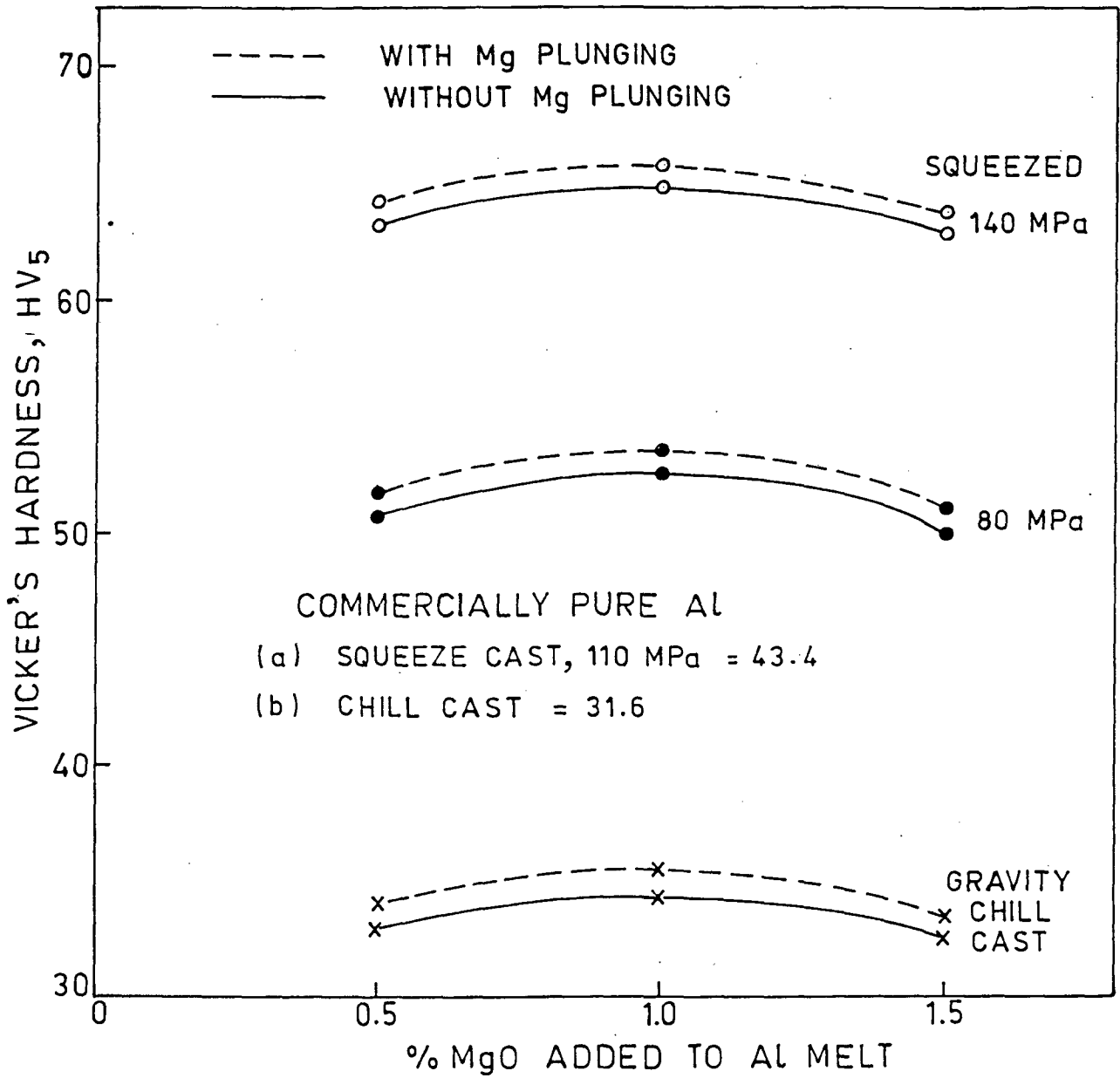


FIG.4.14 Vicker's hardness of Al-MgO composites shown as a function of the amount of sub-micron MgO particles dispersed and the degree of squeeze pressure applied.

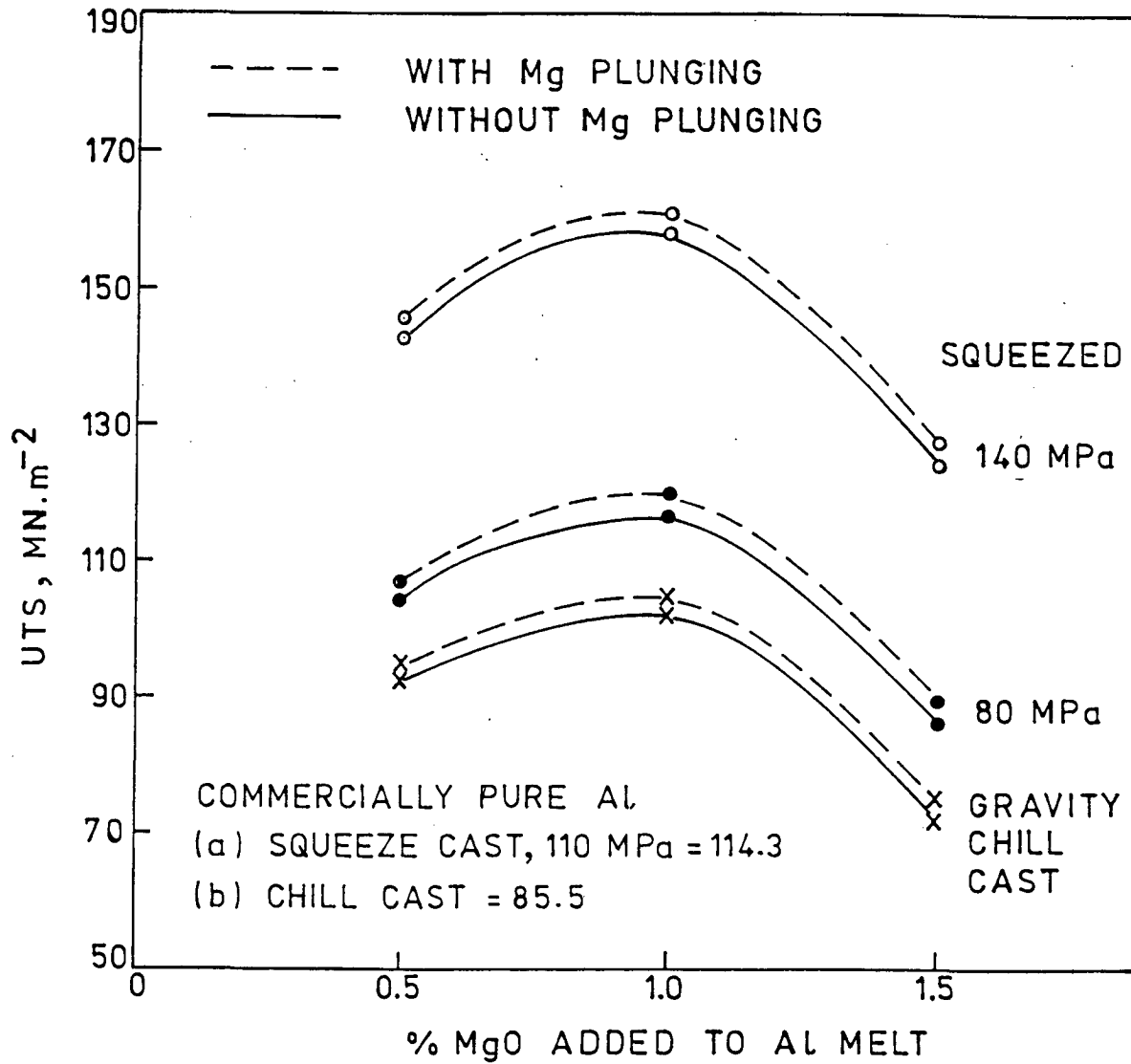


FIG.4.15 UTS of Al-MgO composites as influenced by the amount of sub-micron MgO particles dispersed and the extent of squeeze pressure applied.

1% of aluminium melt (Figs.4.13, 4.14 and 4.15). This discrepancy occurs mainly because during 'MgO Coating' technique, part of MgO powder is consumed in the process of coating the larger  $\text{Al}_2\text{O}_3$  particles and it is only the remaining quantity (of MgO) which gives dispersion strengthening effect. The present set of experiments on Al-MgO composites thus conclusively show that sub-micron MgO particles do cause dispersion strengthening of the base matrix of Al- $\text{Al}_2\text{O}_3$ -MgO cast particulate MMCs. Also, it is apparent from the results shown in Figs. 4.13, 4.14 and 4.15 that the application of a higher degree of squeeze pressure during the fabrication of Al-MgO composites serves only to shift the relative position of concerned property curves upwards, but the overall behaviour pattern remains the same. This will be entirely expected. These results imply that the dispersion strengthening effect of submicron MgO particles will be obtained at all levels of squeeze pressure applied.

The dispersion strengthening caused by sub-micron MgO particles will have far reaching consequences. Primarily, this dispersion will result in comparatively improved tensile properties of Al- $\text{Al}_2\text{O}_3$ -MgO particulate MMCs at ambient temperature. But the real advantage of this dispersion would be expected to be obtained at elevated test temperatures. It is because, these particles unlike precipitates obtained during ageing would not tend to agglomerate and coarsen. As such, these particles would continue to impart stiffness to the matrix even at elevated temperatures. This dispersion would, therefore, be

expected to be a positive contributing factor in the attainment of superior tensile properties of Al-Al<sub>2</sub>O<sub>3</sub>-MgO particulate MMCs at elevated test temperatures.

#### 4.3.3 TENSILE PROPERTIES UPTO 300°C (573K) [169,171,172,175]

##### 4.3.3.1 GENERAL

The results pertaining to the tensile behaviour of gravity chill cast and squeezed composites are summarised in Tables-4.6-4.9 and these results are plotted systematically in Figs.4.16-4.27. In principle, the entire data on the tensile behaviour of composites is spread in four tables for the sake of clarity. Each table includes tensile data obtained at fixed test temperature. The entire discussion on tensile properties is divided in two sections; the first pertaining to the ambient temperature properties and the second devoted to the elevated temperature properties upto 300°C (573K).

##### 4.3.3.2 AMBIENT TEMPERATURE TENSILE PROPERTIES

Results pertaining to this aspect are summarised in Table-4.6 and plotted in Figs.4.16-4.18.

It can be seen from these results that the tensile behaviour of the composites progressively improves as the degree of squeeze pressure applied is systematically raised in steps from 80 to 140 MPa. Before proceeding to a further discussion of these results, it would be interesting to discuss the Engineering stress vs. Engineering strain plot shown in Fig.4.16. In this

TABLE - 4.6

TENSILE PROPERTIES OF GRAVITY CHILL CAST AND SQUEEZED COMMERCIALY PURE ALUMINIUM AND Al-Al<sub>2</sub>O<sub>3</sub>-MgO PARTICULATE COMPOSITES AT AMBIENT TEST TEMPERATURE.

| Melt Sl.No. | Material                             | Squeeze Pressure (MPa)  | Die temperature (°C) | Total (Al <sub>2</sub> O <sub>3</sub> + MgO) Powder wt. % | %V <sub>f</sub> retention of Al <sub>2</sub> O <sub>3</sub> | Tensile Properties at ambient test temperature |                                      |              |                          |
|-------------|--------------------------------------|-------------------------|----------------------|---|---|--|--------------------------------------|--------------|--------------------------|
|             |                                      |                         |                      |   |   | U <sub>TS</sub> , MN.m <sup>-2</sup>           | 0.2% offset Y.S., MN.m <sup>-2</sup> | Elongation % | Reduction in C.S. area % |
| 1           | Commercially Pure Aluminium          | Nil(Gravity Chill Cast) | -                    | -   | -   | 84.0   | 56.0                                 | 19.30        | 19.00                    |
| 2           | Squeezed Commercially Pure Aluminium | 110                     | Ambient              | -   | -   | 114.3  | 59.8                                 | 24.49        | 21.70                    |
| 3           | Composite                            | Nil(Gravity Chill Cast) | -                    | 10  | 12.30   | 136.3  | 85.6                                 | 5.70         | 5.50                     |
| 4           | Squeezed Composite                   | 80                      | Ambient              | 10  | 12.40   | 168.1  | 87.2                                 | 7.20         | 6.60                     |
| 5           | Squeezed Composite                   | 80                      | 100                  | 10  | 11.61   | 165.0  | 86.1                                 | 8.00         | 7.50                     |
| 6           | Squeezed Composite                   | 80                      | 200                  | 10  | 13.83   | 163.0  | 84.5                                 | 10.30        | 10.00                    |
| 7           | Squeezed Composite                   | 100                     | Ambient              | 10  | 12.90   | 180.3  | 94.6                                 | 8.60         | 8.00                     |
| 8           | Squeezed Composite                   | 100                     | 100                  | 10  | 12.02   | 173.2  | 91.7                                 | 9.40         | 8.80                     |
| 9           | Squeezed Composite                   | 100                     | 200                  | 10  | 13.40   | 172.1  | 89.9                                 | 11.40        | 10.90                    |
| 10          | Squeezed Composite                   | 120                     | Ambient              | 10  | 12.20   | 185.9  | 100.3                                | 10.40        | 9.90                     |
| 11          | Squeezed Composite                   | 120                     | 100                  | 10  | 12.30   | 183.3  | 97.8                                 | 11.20        | 10.60                    |
| 12          | Squeezed Composite                   | 120                     | 200                  | 10  | 11.88   | 181.8  | 95.6                                 | 13.50        | 13.10                    |
| 13          | Squeezed Composite                   | 140                     | Ambient              | 10  | 12.70   | 207.9  | 119.5                                | 13.30        | 12.80                    |
| 14          | Squeezed Composite                   | 140                     | 100                  | 10  | 11.78   | 198.6  | 108.5                                | 13.90        | 13.76                    |
| 15          | Squeezed Composite                   | 140                     | 200                  | 10  | 11.99   | 193.3  | 102.9                                | 16.50        | 16.10                    |
| 16          | Squeezed Composite                   | 115                     | 200                  | 5   | 9.78  | 160.3  | 83.3                                 | 7.75         | 7.36                     |

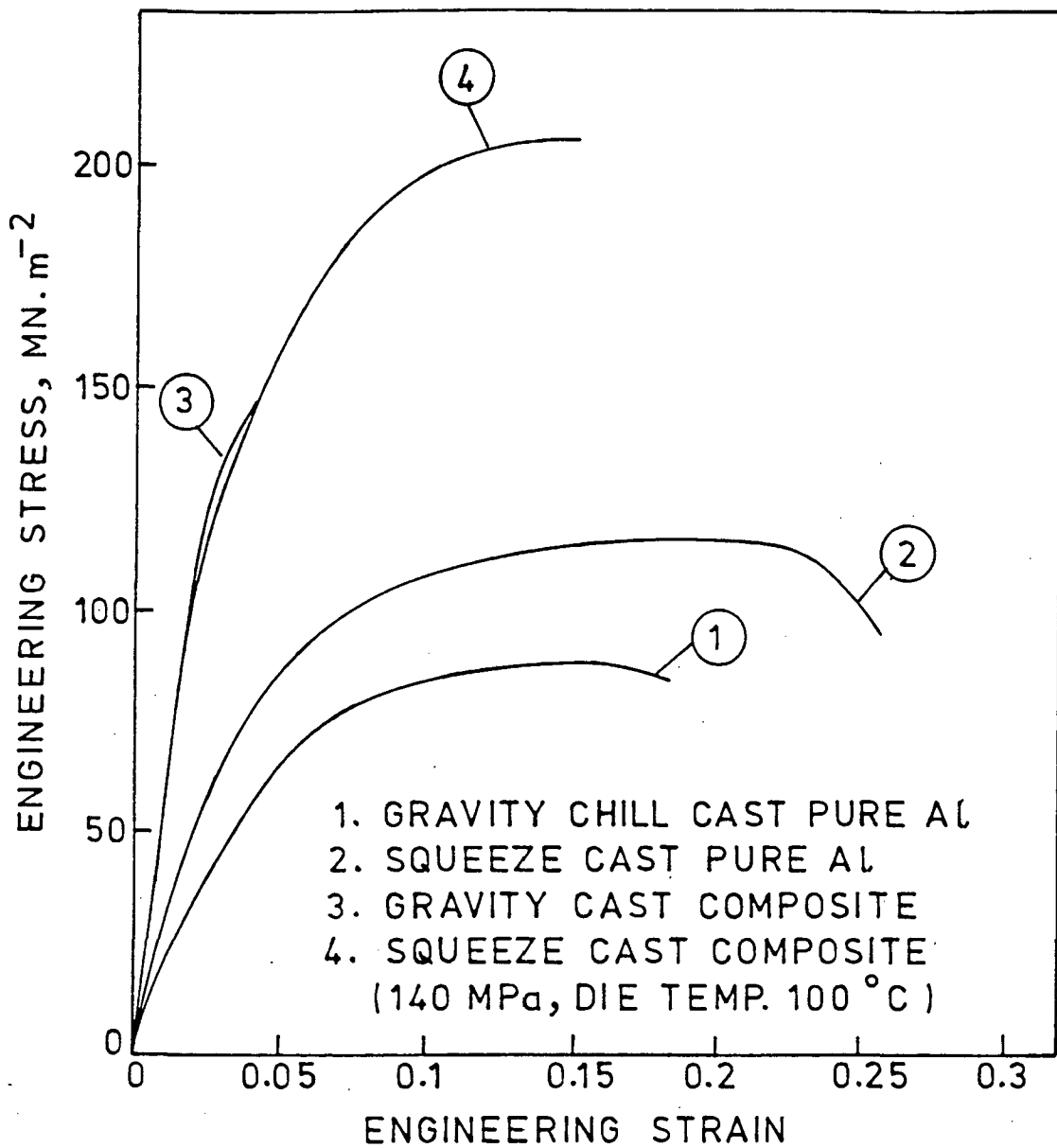


FIG.4.16 A typical engineering stress vs. strain curve obtained in different cases of gravity chill cast and squeezed composites and commercially pure aluminium.

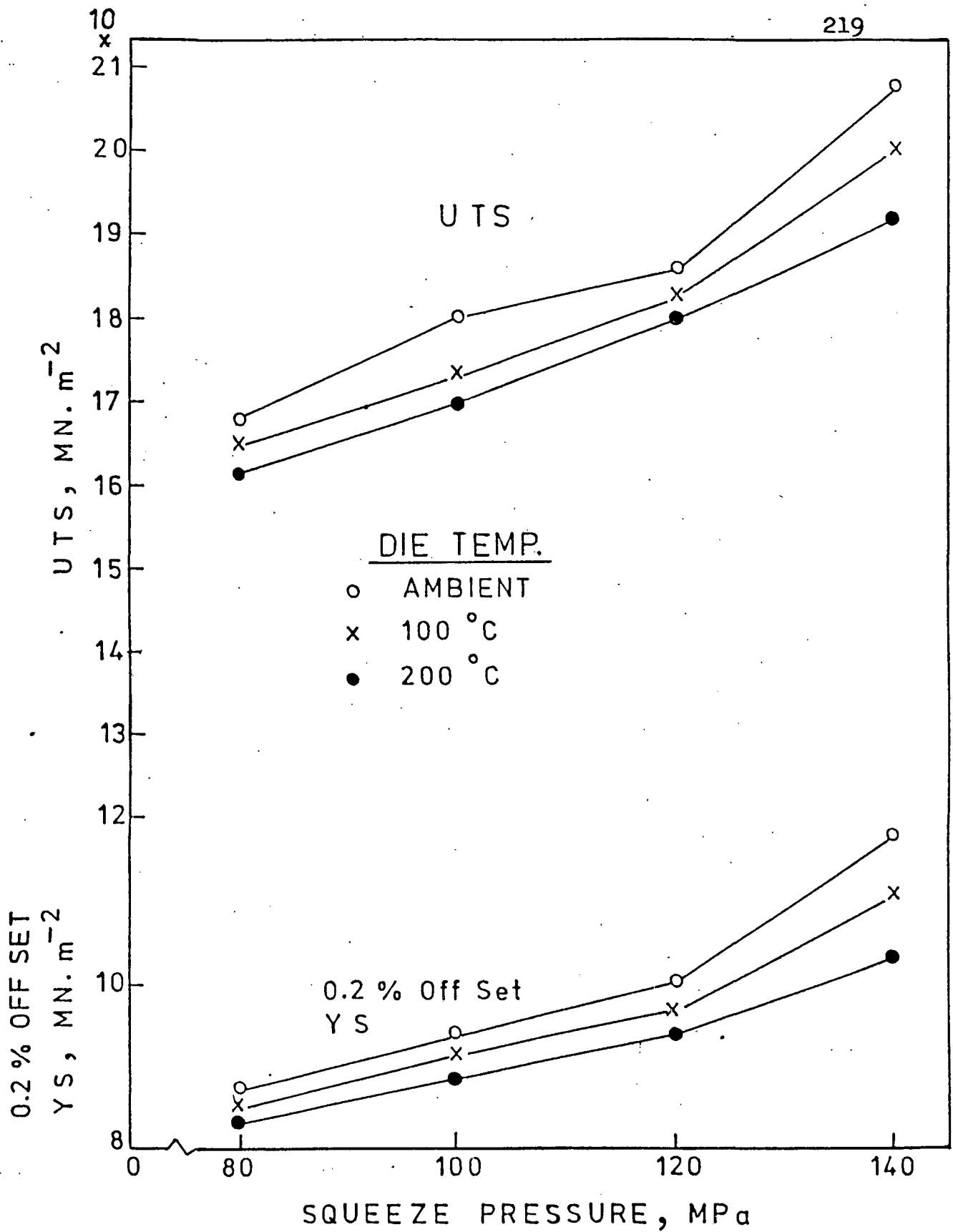


FIG.4.17 UTS and 0.2% offset Y.S. data of composites at different die temperatures shown as a function of the squeeze pressure applied (Ambient test temperature).

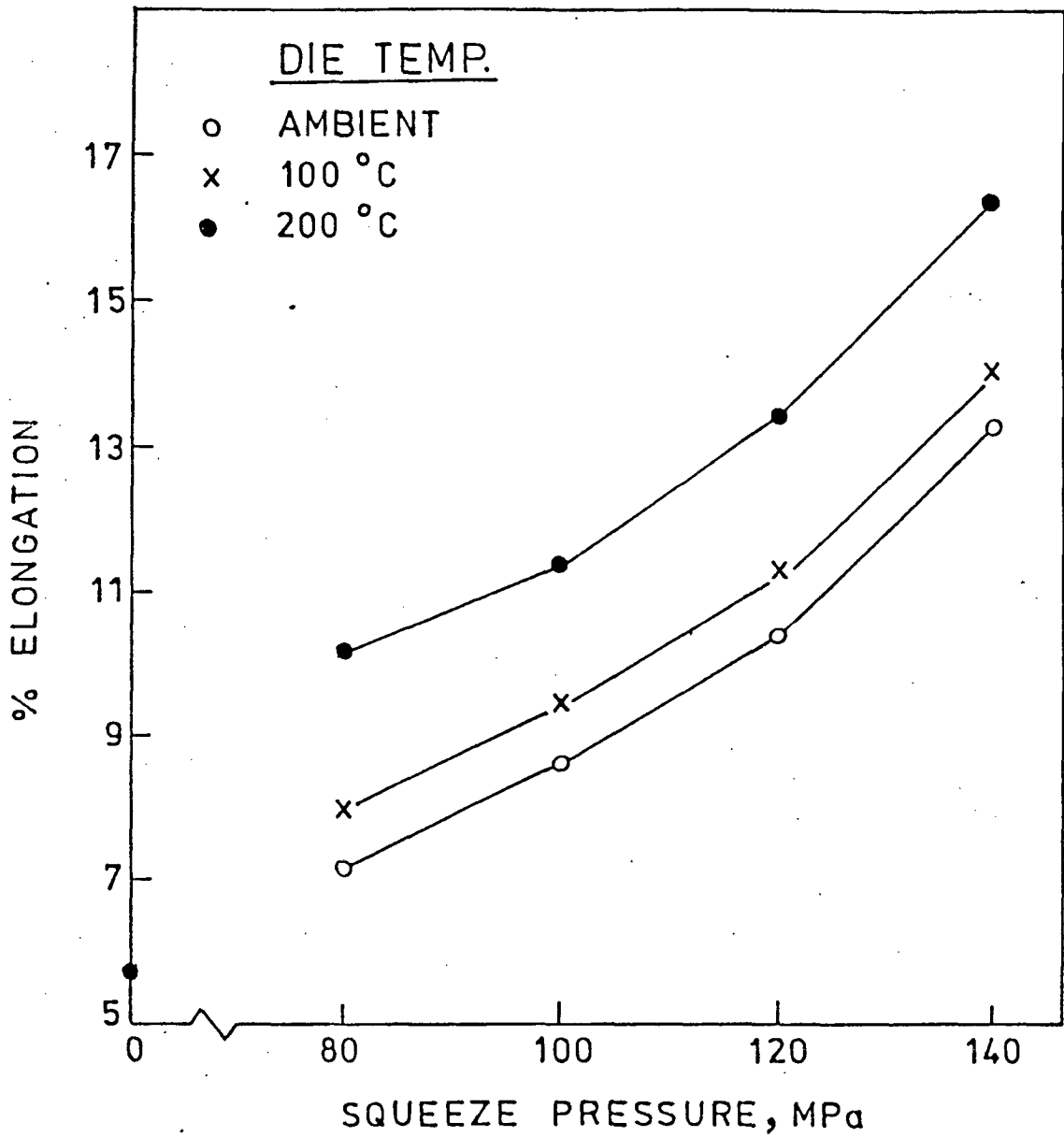


FIG.4.18 Percent elongation of composites shown as a function of the squeeze pressure and the die temperature (Ambient test temperature).



particular curve, different cases of gravity chill cast and squeezed pure aluminium and composite are depicted. It can be seen from this curve that gravity chill cast composites undergo premature failure although the nature of plot in this case upto the point of failure is similar to the one of squeezed composite.

This behaviour of gravity chill cast composite may be attributed to the presence of large amount of porosity in the cast structure which basically constitutes gas porosity plus unfed interdendritic regions. The experience of other investigators in this regard is similar, though the composite systems involved and the preparation techniques employed are different [64-66,174]. The objective of discussing the plot shown in Fig.4.16 is to pin point the fact that gravity chill cast composites would show not only inferior tensile properties but also poor ductility as against squeezed composites.

It is thus apparent that squeeze pressure is the single vital parameter which controls the tensile behaviour of composites. It is because, a certain level of squeeze pressure applied results in a specific level of densification of composite. This level of densification in turn controls other vital parameters such as the amount of porosity, hardness and mean dendritic arm spacing of the cast structure. All these parameters mentioned above would directly control the tensile behaviour of the composites. It is apparant from the results that increasing degree of squeeze pressure applied improves not only the UTS but also the ductility of the composite indicated by

percent elongation simultaneously (Table-4.6, Figs.4.17 and 4.18).

It can be seen from the data recorded in Table-4.6 that the UTS of the composite improves from  $168 \text{ MN.m}^{-2}$  at 80 MPa and ambient die temperature to  $207.9 \text{ MN.m}^{-2}$  at 140 MPa and ambient die temperature, signifying an improvement of 24%. Compared to the properties of the gravity chill cast composite, this improvement can be seen to be 53%. But what is even more significant is the observation that % elongation of the squeezed composite at 140 MPa and ambient die temperature is higher by 85% compared to the composite squeezed at 80 MPa and ambient die temperature. This improvement can be seen to 133% when a similar comparison is made with the ductility of gravity chill cast composite. This combination of high strength and high ductility obtained in the composite squeezed at 140 MPa and ambient die temperature can be directly attributed to a near absence of porosity and a refined grain structure realised in the base matrix. It is apparent from the results shown in Table-4.6 that the best composite produced in the present work corresponds to 140 MPa and ambient die temperature. Also, it is apparent from the results that a wide variety of combination of strength and ductility can be achieved in the composite by simply manipulating the operating parameters. If the results of present study are extrapolated, it can be seen that much superior quality composites can be produced by taking the squeeze pressure to still higher levels such as 180 to 240 MPa. Results of present

study can also be utilised for the production of thin/thick walled castings and for this purpose, suitable parameters can be selected to result in specific mechanical properties in the end product.

It can be seen from the results (Table-4.6, Fig.4.17) that comparatively lower UTS values are obtained in the composite as the die temperature is systematically raised to 200°C. This is found to be true at all levels of squeeze pressure applied. This behaviour is entirely expected because comparatively lower hardness and higher dendritic arm spacing would be expected to be obtained in the cast structure (Tables-4.2 and 4.4) as the die temperature is progressively raised. And these factors will have a direct bearing on the tensile behaviour of the composites.

An examination of the fractured surfaces of tensile specimens can clearly reveal how the nature of fracture changes from a semi-ductile to brittle kind (obtained in case of gravity chill cast composite) to a fully ductile one (obtained in case of squeezed composites), as the degree of squeeze pressure applied is systematically raised. The examination of tensile fracture surfaces through the powerful tool of SEM can thus supplement percent elongation data. A detailed account of the SEM examination of tensile fracture surfaces is presented in subsequent section No.4.3.4.

#### **4.3.3.3 ELEVATED TEMPERATURE TENSILE PROPERTIES**

The results pertaining to this study are summarised in

Tables-4.7-4.9 and the vital data is plotted in Figs.4.19-4.27.

It can be seen from the results that the performance of the composites gradually improves as the squeeze pressure is systematically raised from 80-140 MPa. Figs.4.19 and 4.20 show this comparison of performance. Percent elongation data are plotted in Figs.4.21 and 4.22 for different test temperatures separately in order to avoid overcrowding of points. The data derived from Figs.4.19 and 4.20 are plotted in Figs.4.23-4.27 showing percent drop in UTS and 0.2% offset yield strength in Figs.4.23 and 4.24 respectively, and the ratio of YS/UTS in 4.27.

Figs.4.25 and 4.26 show percent UTS and percent 0.2% offset YS retained at different test temperatures in the form of histograms.

The gravity chill cast composite loses strength faster at the elevated test temperatures compared to squeezed composites. Increasing the squeeze pressure in steps gradually improves the performance of the composite upto 300°C (573K) test temperature. Also, it can be seen that increasing the die temperature uniformly deteriorates the properties of the composite at any level of squeeze pressure applied. The best performance is exhibited by a composite squeezed at 140 MPa and ambient die temperature (Figs.4.19 and 4.20). The UTS of this composite is higher by 52.33% compared to gravity chill cast composite at 100°C (373K) test temperature. This figure rises to 161% and 162.5% at 200°C (473K) and 300°C (573K) test

TABLE - 4.7

TENSILE PROPERTIES OF GRAVITY CHILL CAST AND SQUEEZED COMMERCIALY PURE ALUMINIUM AND Al-Al<sub>2</sub>O<sub>3</sub>-MgO PARTICULATE COMPOSITES AT 100°C TEST TEMPERATURE.

| Melt Sl.No. | Material                    | Squeeze                 | Die temperature (°C) | Total (Al <sub>2</sub> O <sub>3</sub> + MgO) Powder wt.% | %V <sub>f</sub> retention of Al <sub>2</sub> O <sub>3</sub> | Tensile properties at 100°C test temperature |                                     |              |                          |
|-------------|-----------------------------|-------------------------|----------------------|--|---|--|-------------------------------------|--------------|--------------------------|
|             |                             |                         |                      |  |   | U <sub>T</sub> S, MN.m <sup>-2</sup>         | 0.2% offset Y.S. MN.m <sup>-2</sup> | Elongation % | Reduction in C.S. area % |
|             |                             |                         |                      |  |   |  |                                     |              |                          |
| 1           | Commercially Pure Aluminium | Nil(Gravity Chill Cast) | -                    | -  | -   | 58.6   | 43.3                                | 41           | 37                       |
| 2           | Composite                   | Nil(Gravity Chill Cast) | -                    | 10   | 12.30   | 119.7  | 76.4                                | 10           | 10                       |
| 3           | Squeezed Composite          | 80                      | Ambient              | 10   | 12.40   | 130.4  | 85.6                                | 13           | 12                       |
| 4           | Squeezed Composite          | 80                      | 100                  | 10   | 11.61   | 127.8  | 81.5                                | 16           | 16                       |
| 5           | Squeezed Composite          | 80                      | 200                  | 10   | 13.83   | 121.7  | 78.9                                | 20           | 20                       |
| 6           | Squeezed Composite          | 100                     | Ambient              | 10   | 12.90   | 144.6  | 93.8                                | 18           | 16                       |
| 7           | Squeezed Composite          | 100                     | 100                  | 10   | 12.02   | 141.6  | 90.0                                | 21           | 20                       |
| 8           | Squeezed Composite          | 100                     | 200                  | 10   | 13.40   | 140.0  | 84.0                                | 26           | 24                       |
| 9           | Squeezed Composite          | 120                     | Ambient              | 10   | 12.20   | 163.0  | 97.0                                | 22           | 20                       |
| 10          | Squeezed Composite          | 120                     | 100                  | 10   | 12.30   | 159.1  | 94.4                                | 25           | 25                       |
| 11          | Squeezed Composite          | 120                     | 200                  | 10   | 11.88   | 147.7  | 90.7                                | 30           | 28                       |
| 12          | Squeezed Composite          | 140                     | Ambient              | 10   | 12.70   | 197.8  | 117.3                               | 25           | 22                       |
| 13          | Squeezed Composite          | 140                     | 100                  | 10   | 11.78   | 168.1  | 103.6                               | 28           | 26                       |
| 14          | Squeezed Composite          | 140                     | 200                  | 10   | 11.99   | 166.2  | 101.0                               | 33           | 32                       |

TABLE - 4.8

TENSILE PROPERTIES OF GRAVITY CHILL CAST AND SQUEEZED COMMERCIAALLY PURE ALUMINIUM AND Al-Al<sub>2</sub>O<sub>3</sub>-MgO PARTICULATE COMPOSITES AT 200°C TEST TEMPERATURE.

| Melt Sl.No. | Material                    | Squeeze Pressure (MPa)  | Die temperature (°C) | Total (Al <sub>2</sub> O <sub>3</sub> + MgO) Powder wt. % | %Vf retention of Al <sub>2</sub> O <sub>3</sub> | Tensile Properties at 200°C test temperature |                                     |                                       |    |
|-------------|-----------------------------|-------------------------|----------------------|---|---|--|-------------------------------------|---------------------------------------|----|
|             |                             |                         |                      |   |   | UTS, MN.m <sup>-2</sup>                      | 0.2% offset Y.S. MN.m <sup>-2</sup> | Elongation % Reduction in C.S. area % |    |
| 1           | Commercially Pure Aluminium | Nil(Gravity Chill Cast) | -                    | -   | -   | 51.1   | 34.6                                | 50                                    | 44 |
| 2           | Composite                   | Nil(Gravity Chill Cast) | -                    | 10  | 12.30   | 68.5   | 61.1                                | 15                                    | 14 |
| 3           | Squeezed Composite          | 80                      | Ambient              | 10  | 12.40   | 116.6  | 84.0                                | 18                                    | 19 |
| 4           | Squeezed Composite          | 80                      | 100                  | 10  | 12.40   | 111.6  | 78.9                                | 22                                    | 23 |
| 5           | Squeezed Composite          | 80                      | 200                  | 10  | 13.83   | 109.1  | 71.3                                | 27                                    | 26 |
| 6           | Squeezed Composite          | 100                     | Ambient              | 10  | 12.90   | 135.0  | 88.7                                | 27                                    | 26 |
| 7           | Squeezed Composite          | 100                     | 100                  | 10  | 12.02   | 132.4  | 85.6                                | 30                                    | 30 |
| 8           | Squeezed Composite          | 100                     | 200                  | 10  | 13.40   | 127.8  | 82.8                                | 35                                    | 33 |
| 9           | Squeezed Composite          | 120                     | Ambient              | 10  | 12.20   | 147.7  | 94.3                                | 31                                    | 30 |
| 10          | Squeezed Composite          | 120                     | 100                  | 10  | 12.30   | 145.1  | 91.7                                | 34                                    | 35 |
| 11          | Squeezed Composite          | 120                     | 200                  | 10  | 11.88   | 132.4  | 82.1                                | 39                                    | 38 |
| 12          | Squeezed Composite          | 140                     | Ambient              | 10  | 12.70   | 179.0  | 115.0                               | 35                                    | 34 |
| 13          | Squeezed Composite          | 140                     | 100                  | 10  | 11.78   | 152.8  | 95.7                                | 38                                    | 36 |
| 14          | Squeezed Composite          | 140                     | 200                  | 10  | 11.99   | 150.8  | 94.2                                | 42                                    | 40 |

TABLE - 4.9

TENSILE PROPERTIES OF GRAVITY CHILL CAST AND SQUEEZED COMMERCIALY PURE ALUMINIUM AND Al-Al<sub>2</sub>O<sub>3</sub>-MgO PARTICULATE COMPOSITES AT 300°C TEST TEMPERATURE.

| Melt Sl.No. | Material                    | Squeeze Pressure (MPa)  | Die temperature (°C) | Total (Al <sub>2</sub> O <sub>3</sub> +MgO) Powder wt. % | %Vf retention of Al <sub>2</sub> O <sub>3</sub> | Tensile Properties at 300°C test temperature |                                     |              |                      |
|-------------|-----------------------------|-------------------------|----------------------|--|---|--|-------------------------------------|--------------|----------------------|
|             |                             |                         |                      |  |   | UTS, MN.m <sup>-2</sup>                      | 0.2% offset Y.S. MN.m <sup>-2</sup> | Elongation % | Reduction C.S.area % |
| 1.          | Commercially Pure Aluminium | Nil(Gravity Chill Cast) | -                    | -  | -   | 26.6 (225°C)                                 | 13.3 (225°C)                        | 65 (225°C)   | 60 (225°C)           |
| 2           | Composite                   | Nil(Gravity Chill Cast) | -                    | 10   | 12.30   | 61.1   | 55                                  | 26           | 12                   |
| 3           | Squeezed Composite          | 80                      | Ambient              | 10   | 12.40   | 99.3   | 75.2                                | 28           | 25                   |
| 4           | Squeezed Composite          | 80                      | 100                  | 10   | 11.61   | 96.8   | 73.5                                | 30           | 29                   |
| 5           | Squeezed Composite          | 80                      | 200                  | 10   | 13.83   | 94.2   | 67.6                                | 35           | 32                   |
| 6           | Squeezed Composite          | 100                     | Ambient              | 10   | 12.90   | 114.6  | 85.1                                | 34           | 32                   |
| 7           | Squeezed Composite          | 100                     | 100                  | 10   | 12.02   | 112.5  | 84.0                                | 37           | 36                   |
| 8           | Squeezed Composite          | 100                     | 200                  | 10   | 13.40   | 109.1  | 72.3                                | 41           | 39                   |
| 9           | Squeezed Composite          | 120                     | Ambient              | 10   | 12.20   | 132.9  | 90.8                                | 39           | 37                   |
| 10          | Squeezed Composite          | 120                     | 100                  | 10   | 12.30   | 126.3  | 90.1                                | 42           | 41                   |
| 11          | Squeezed Composite          | 120                     | 200                  | 10   | 11.88   | 122.2  | 77.4                                | 46           | 44                   |
| 12          | Squeezed Composite          | 140                     | Ambient              | 10   | 12.70   | 160.4  | 112.8                               | 45           | 43                   |
| 13          | Squeezed Composite          | 140                     | 100                  | 10   | 11.78   | 142.6  | 94.2                                | 47           | 44                   |
| 14          | Squeezed Composite          | 140                     | 200                  | 10   | 11.99   | 138.1  | 91.7                                | 51           | 48                   |

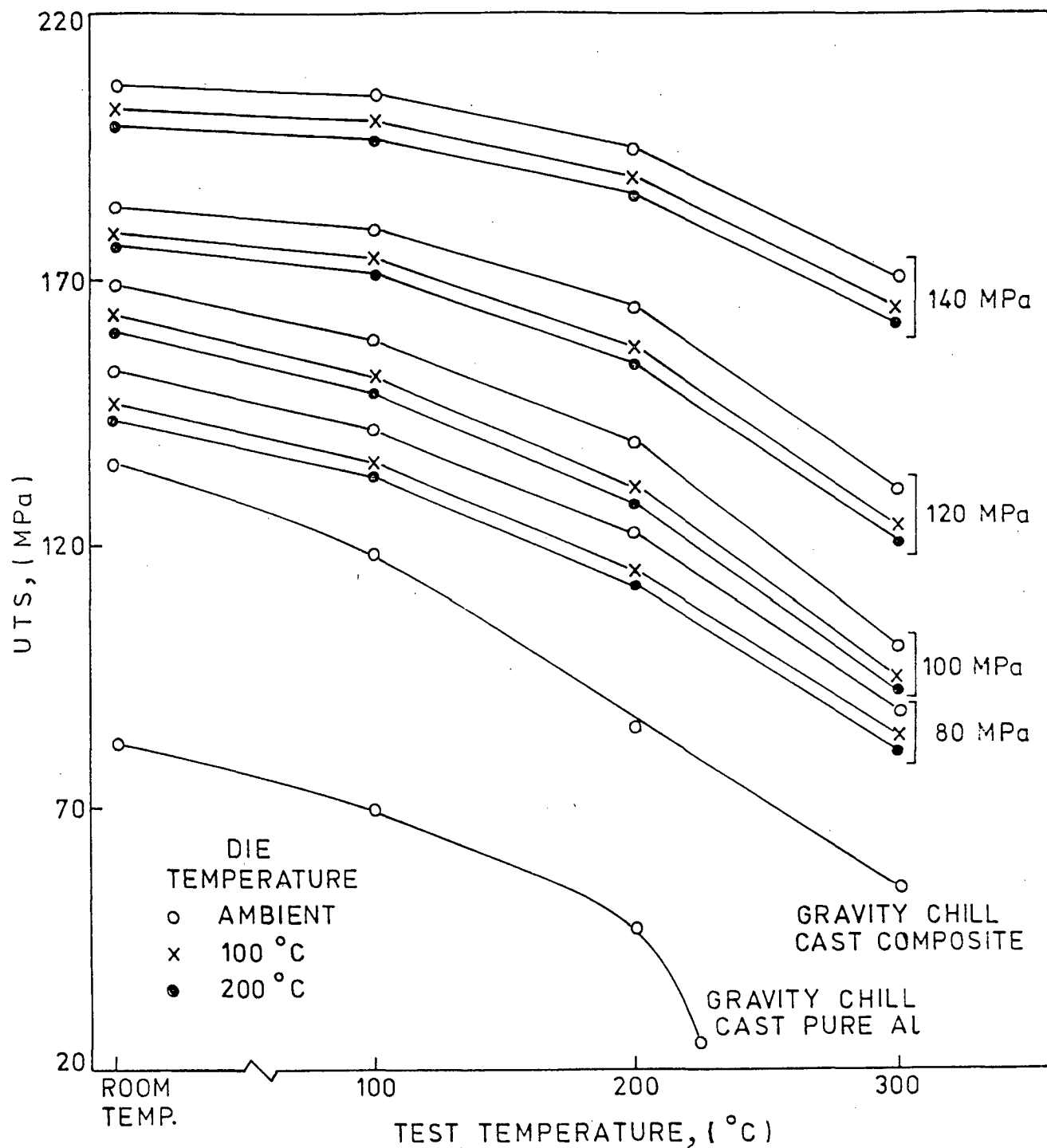


FIG.4.19 UTS of gravity chill-cast and squeezed composites shown as a function of the test temperatures. Squeezed composites prepared at three die temperatures: (o) ambient, (x) 100°C, (●) 200°C.



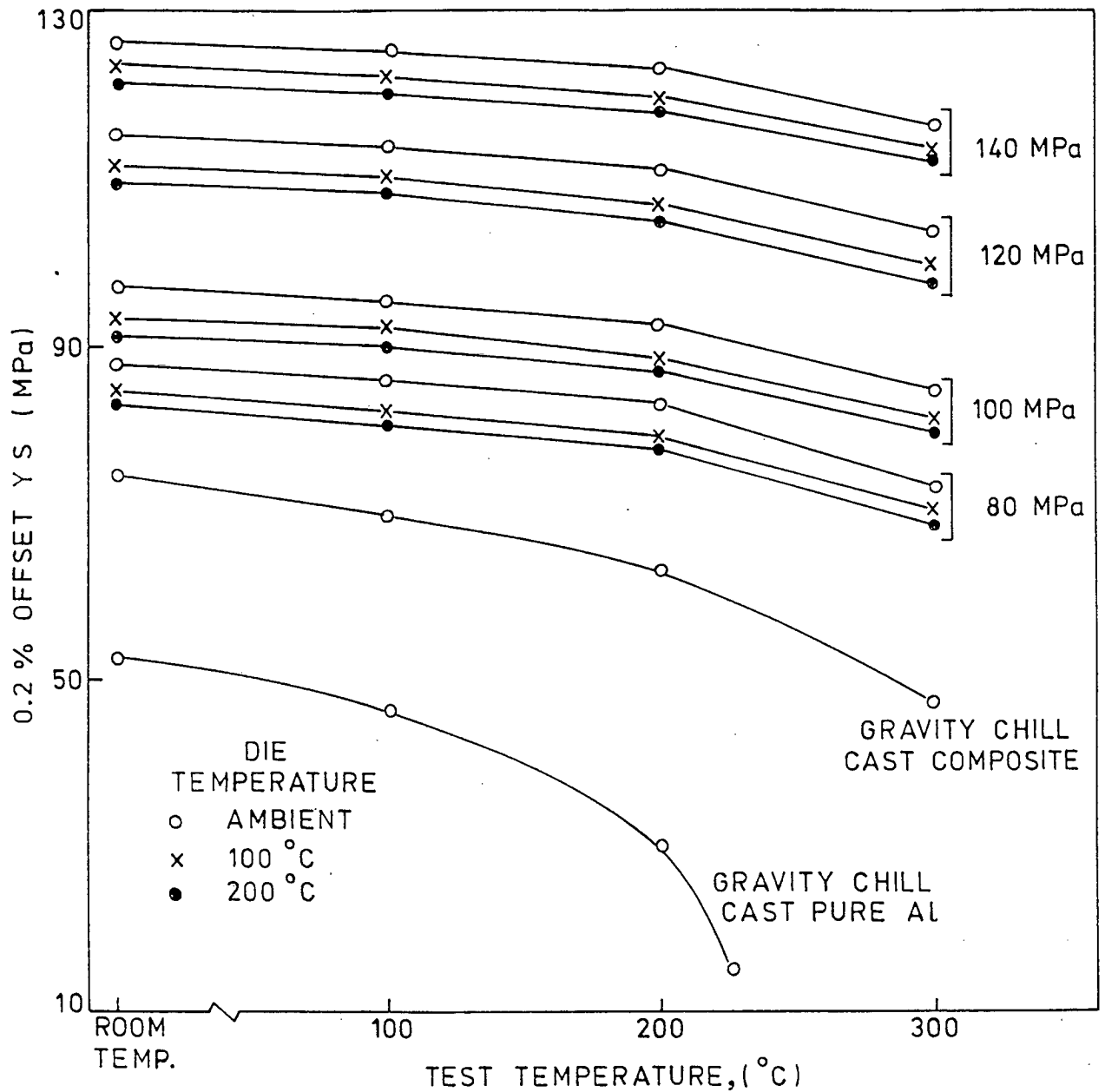


FIG.4.20 0.2% offset Y.S. of gravity chill-cast and squeezed composites shown as a function of the test temperatures. Squeezed composites prepared at three die temperatures: (o) ambient, (x) 100°C, (●) 200°C.

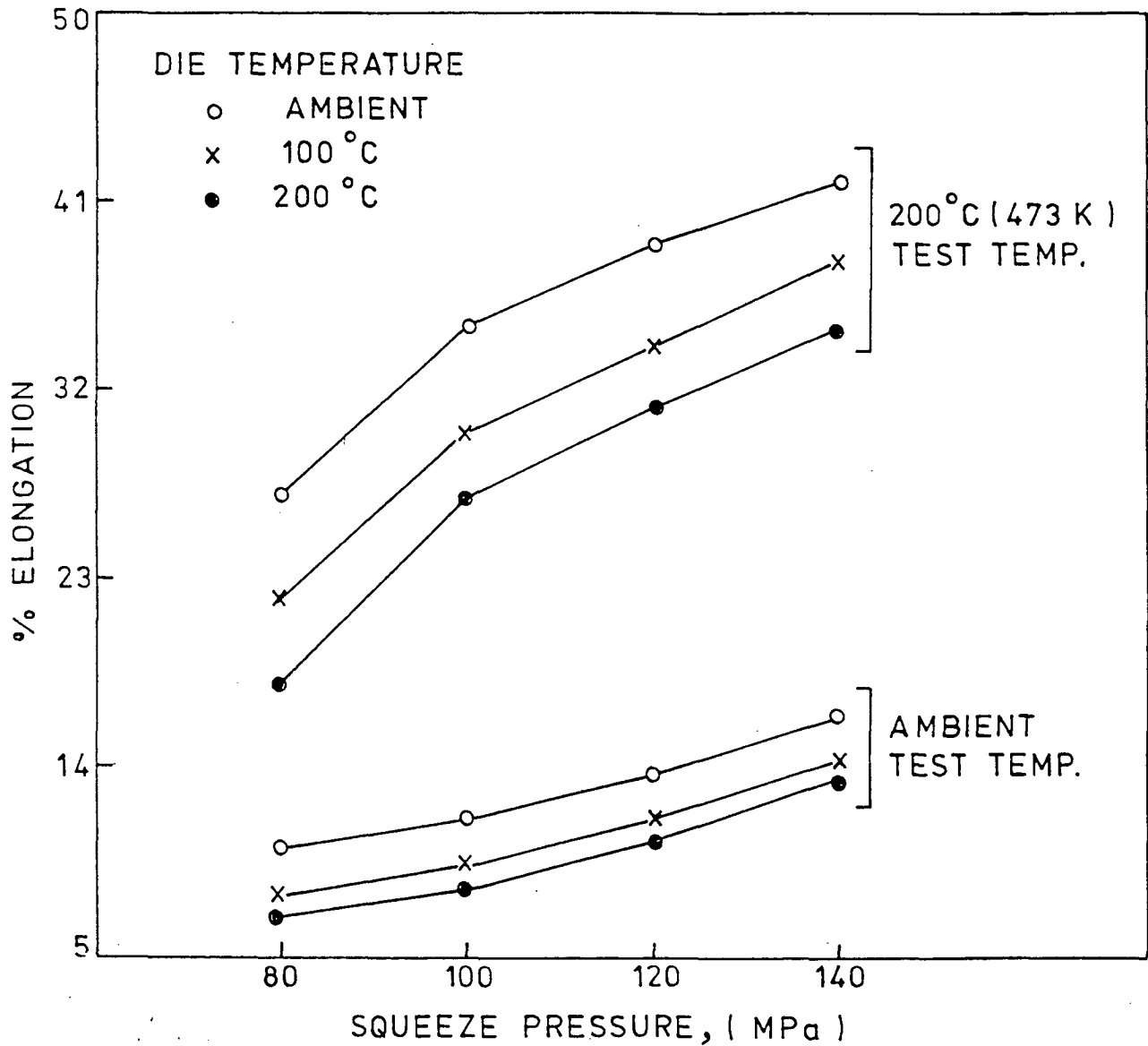


FIG.4.21 Percent elongation of squeezed composites obtained at ambient and 200°C test temperatures shown as a function of the degree of squeeze pressure applied at three die temperatures:(○) ambient,(x) 100°C, (●) 200°C.

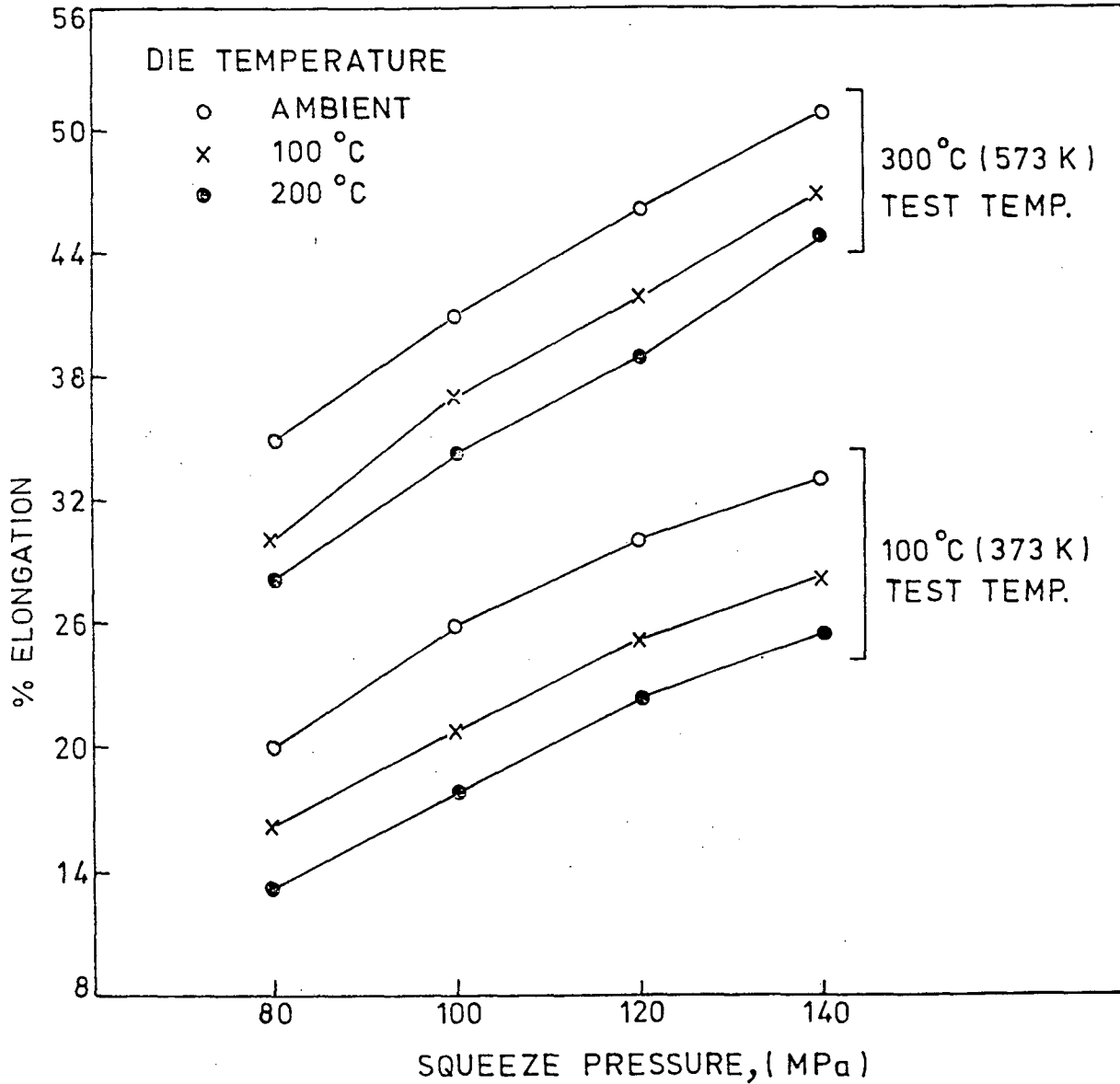


FIG.4.22 Percent elongation of squeezed composites obtained at 100 and 300°C test temperatures shown as a function of the degree of squeeze pressure applied at three die temperatures: (○) ambient, (x) 100°C, (●) 200°C.

temperatures respectively. This analysis reveals the real benefit to be gained from the squeeze-casting process; that the composite squeezed at 140 MPa and ambient die temperature retains its strength better upto 300°C (573K) compared to ordinary gravity chill cast composite. This composite retains about 77% of its ambient UTS value at 300°C (573K) test temperature, while the gravity chill cast composite retains only 44% of its ambient UTS value. It would be expected that the performance of these composites would improve further if the degree of squeeze pressure is taken to still higher levels, such as 160 to 240 MPa.

This improvement in the tensile behaviour of squeezed composites can be directly attributed to (a) the virtual absence of porosity in the cast structure due to a high level of densification achieved, and (b) an increasing degree of grain refinement obtained upon squeezing.

The role of coarser  $\text{Al}_2\text{O}_3$  particles and submicron MgO particles in stiffening the aluminium base matrix has been discussed in detail in earlier publications [47-49]. The role of sub-micron MgO particles in stiffening the base matrix has further been investigated in detail in the present work to experimentally verify the hypothesis proposed in the previous work [47-49]. As shown in section 4.3.1 and 4.3.2, the sub-micron MgO particles do cause the strengthening of the base matrix through the dispersion strengthening effect. It should further be emphasised that the dispersion strengthening effect caused by sub-micron MgO particles is superior to the usual age

hardening effect so far as the elevated temperature properties of the composites are concerned. It is because, the submicron MgO particles do not suffer from the drawback of overageing as is the case with standard ageing process. Therefore, the total strengthening obtained through the coarser  $Al_2O_3$  particles as well as submicron MgO particles results in improved tensile properties of the composites at elevated temperatures. Also, it can be seen from the data recorded in Tables-4.2, 4.6-4.9 that increasing degree of grain refinement obtained upon squeezing has a profound effect on the tensile behaviour of the composites.

The performance of composites with regard to 0.2% offset YS values is of prime interest as this is the basic design criterion employed in actual practice. It can be seen from the data recorded in Tables-4.6-4.9 that the 0.2% offset YS value of the best composite prepared in this work (140 MPa and ambient die temperature) is higher by 53% compared to the value of gravity chill cast composite at 100°C (373K) test temperature. These values progressively magnify to 88.5% and 105% at 200°C (473K) and 300°C (573K) test temperatures respectively. This is basically because the squeezed composite retains its yield strength better than simple gravity chill cast composite at elevated test temperatures. For example, the squeezed composite referred to above, retains 94.4% of its ambient YS value at 300°C (573K) test temperature, while ordinary gravity chill cast composite retains only 64.2% of its ambient YS value at the same test temperature. It is, therefore, apparent that the

performance of squeezed composites is far superior than ordinary gravity chill cast composites at all the test temperatures employed.

The basic aspect of loss of strength of different materials at elevated temperatures is compared in Figs.4.23 and 4.24. It should be noted that the rate of loss of strength for commercially pure aluminium and gravity chill cast composite becomes fairly steep between 200 and 300°C test temperatures. Particularly for pure aluminium, the tensile tests could not be conducted beyond 225°C (498K) because this material lost strength very rapidly beyond 200°C. This rate of loss of strength beyond 200°C tapers off gradually as the squeeze pressure is progressively raised. It can be seen that the overall behaviour pattern of loss of strength between 100 and 300°C test temperatures is practically linear for composites squeezed at 120 and 140 MPa. Moreover, the overall loss of strength (UTS) progressively decreases as the squeeze pressure is systematically raised in steps. It should, therefore, be logically possible to improve the performance of these composites even further if the squeeze pressure is taken to still higher levels such as 160-240 MPa.

While referring to Fig.4.24, it can be seen that the performance of squeezed composites is distinctly different and superior to ordinary gravity chill cast composite. Also, among the group of squeezed composites, the best performance is

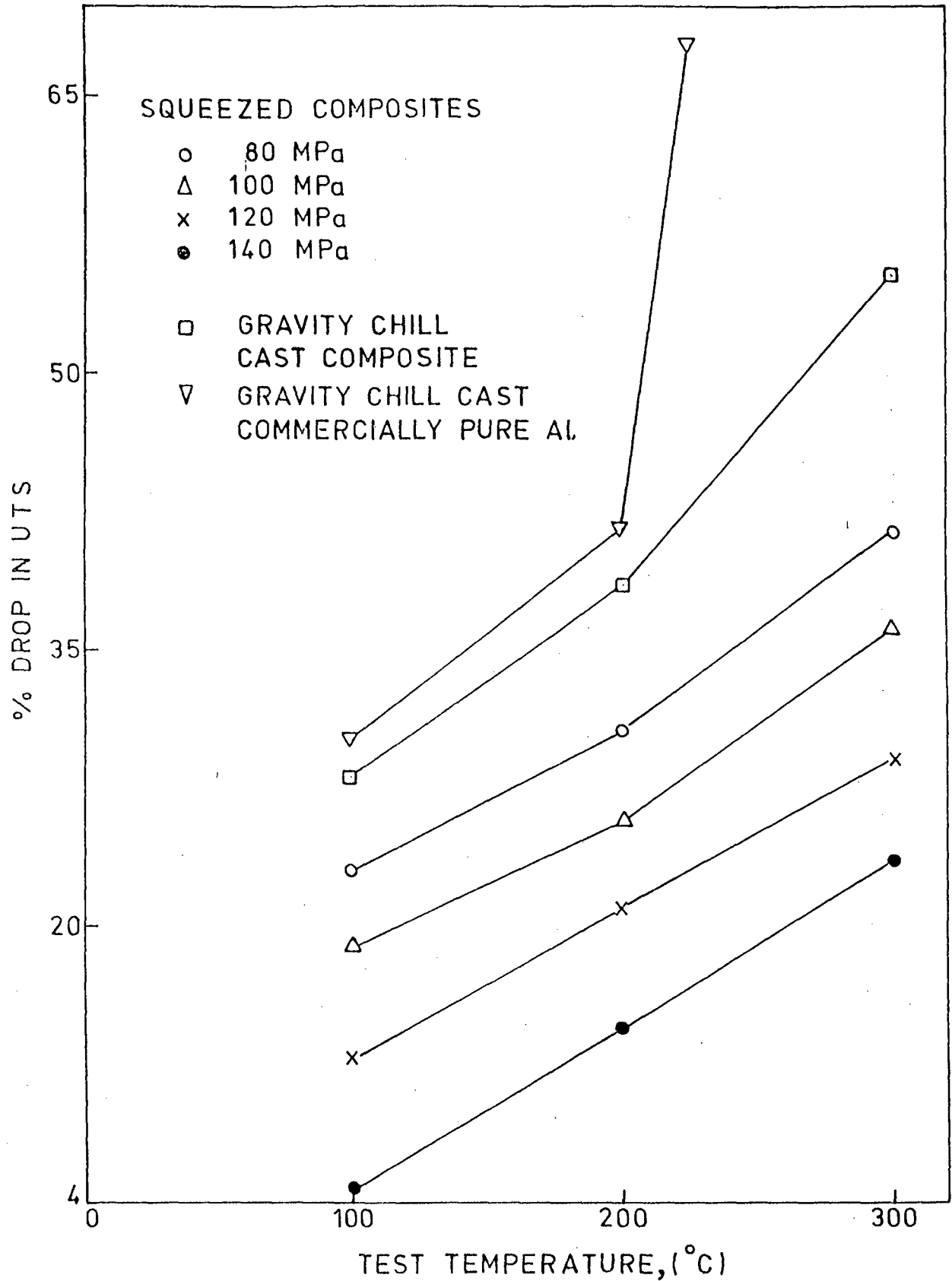


FIG.4.23 Percent drop in UTS obtained in (▽) commercially pure aluminium, (□) gravity chill-cast and (○,△,x,●) squeezed composites (ambient die temperature) shown as a function of the three test temperatures, and at (○) 80 MPa, (△) 100 MPa, (x) 120 MPa, (●) 140 MPa.

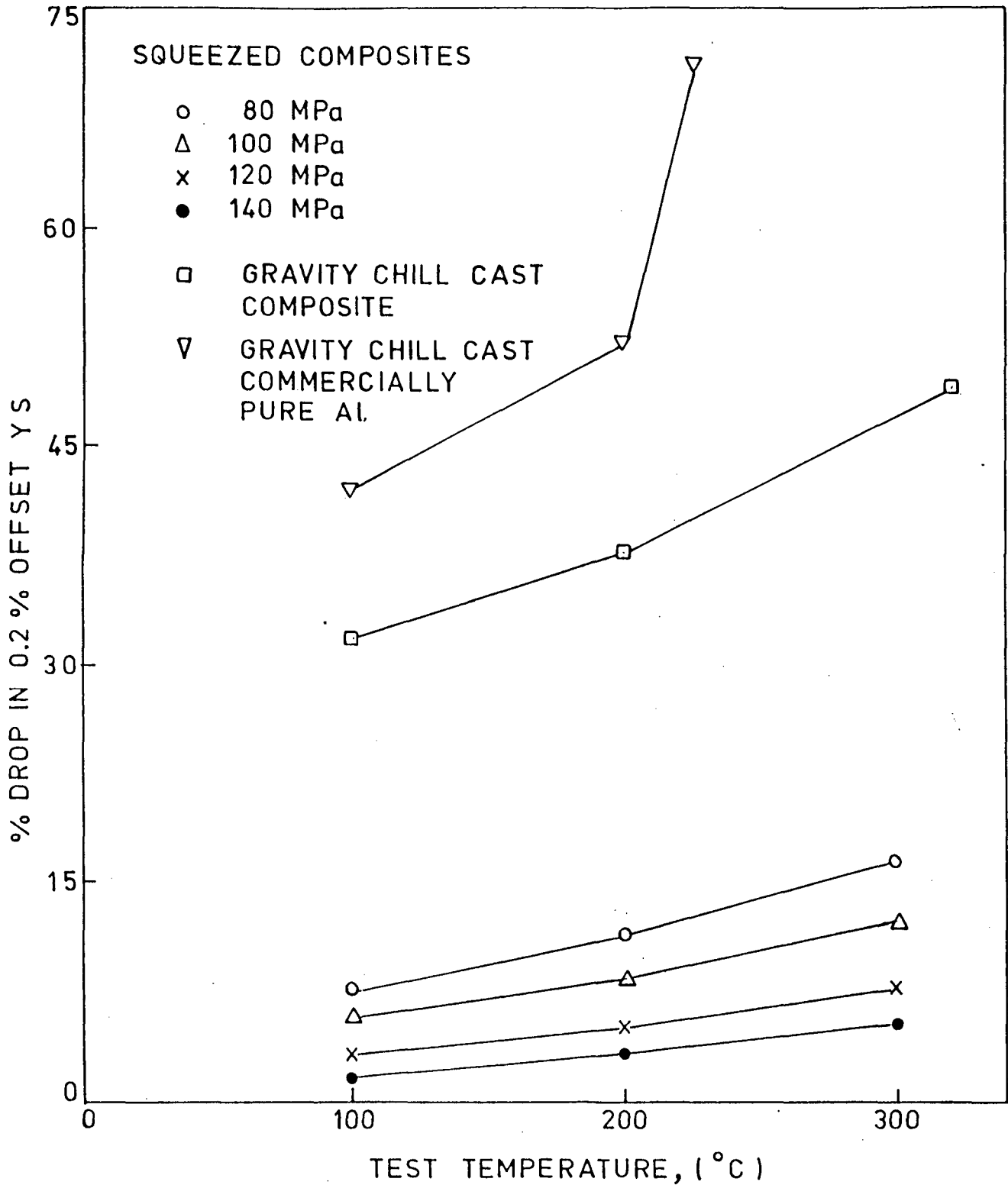


FIG.4.24 Percent drop in 0.2% offset Y.S. obtained in (▽) commercially pure aluminium, (□) gravity chill cast and (○, △, x, ●) squeezed composites (ambient die temperature) shown as a function of the three test temperature, and, at (○) 80 MPa, (△) 100 MPa, (x) 120 MPa, (●) 140 MPa.



displayed by the composites squeezed at 120 and 140 MPa. Apparently, the composite squeezed at 140 MPa can be put to practical application upto 300°C (573K) with fairly good assurance of performance reliability. The elongation data plotted in Figs.4.21 and 4.22 show entirely expected results.

The histograms displayed in Figs.4.25 and 4.26 show the percent UTS retained and percent 0.2% offset YS retained by composites Nos.1,2 and 3 at the three different elevated test temperatures. Composites Nos.1,2 and 3 respectively represent gravity chill cast and squeezed composites fabricated at 80 and 140 MPa and ambient die temperature. These composites are selected for this comparison because they represent three different extremes of property performance levels. Fig.4.25 shows the comparative performance of the three composites with respect to the % UTS retained at three test temperatures. Similarly Fig.4.26 shows the relative performance of composites with respect to the % yield strength retained at the three test temperatures. For the calculation of percent UTS and YS retained at different test temperatures, obviously the ambient test temperature properties were considered to be the datum level. It can be seen from the results shown in Fig.4.25 that composite No.3 retains its UTS better than other two composites used for comparison. At the highest test temperature (300°C), for instance, the UTS of composite No.3 is higher by 61.5% compared to composite No.2 (Table-4.9). Also it can be seen that the percent UTS retained by composite No.3 is higher by a value of 18

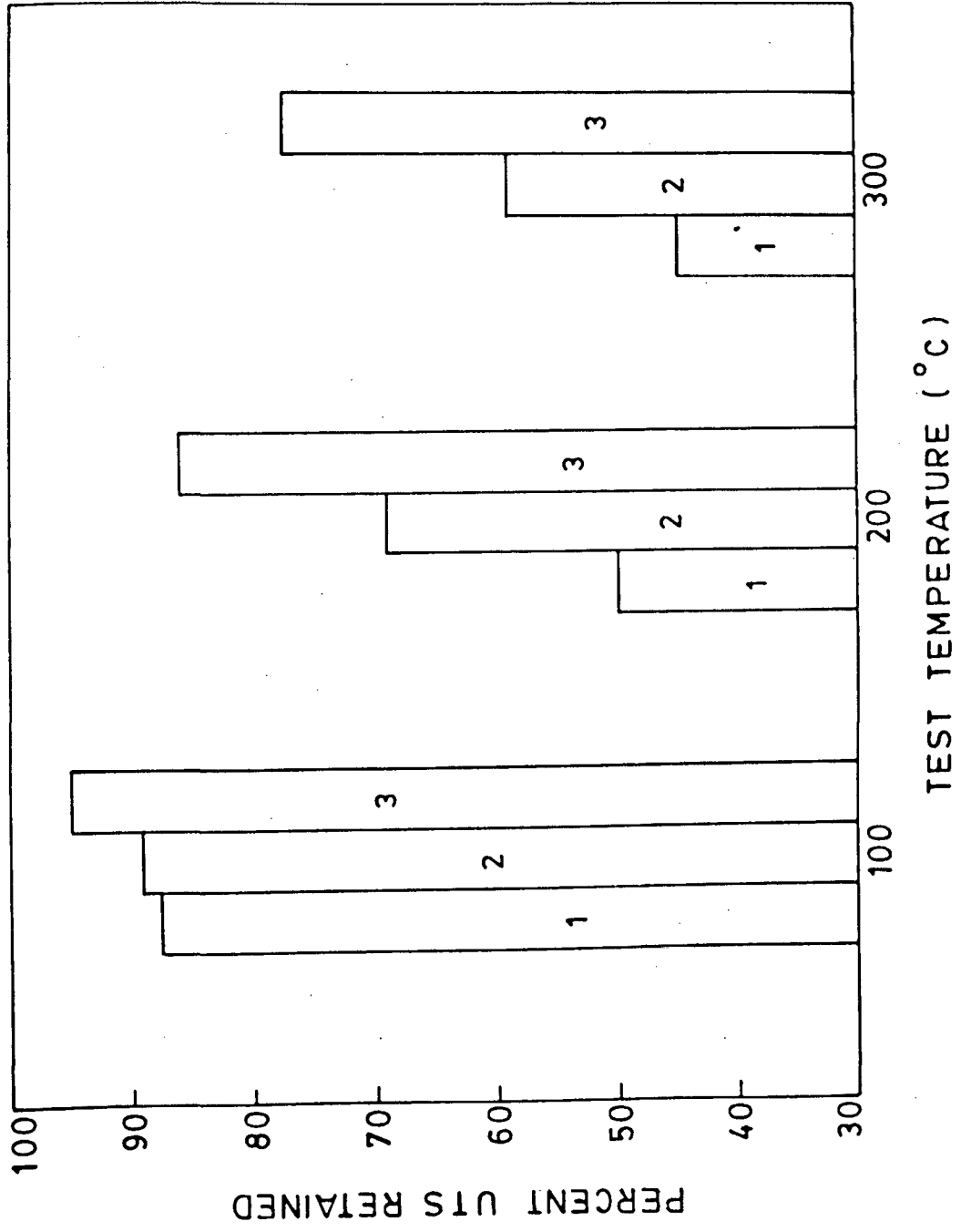


FIG.4.25 Histogram showing percent UTS retained by composite Nos.1, 2 and 3 upto 300°C test temperature.

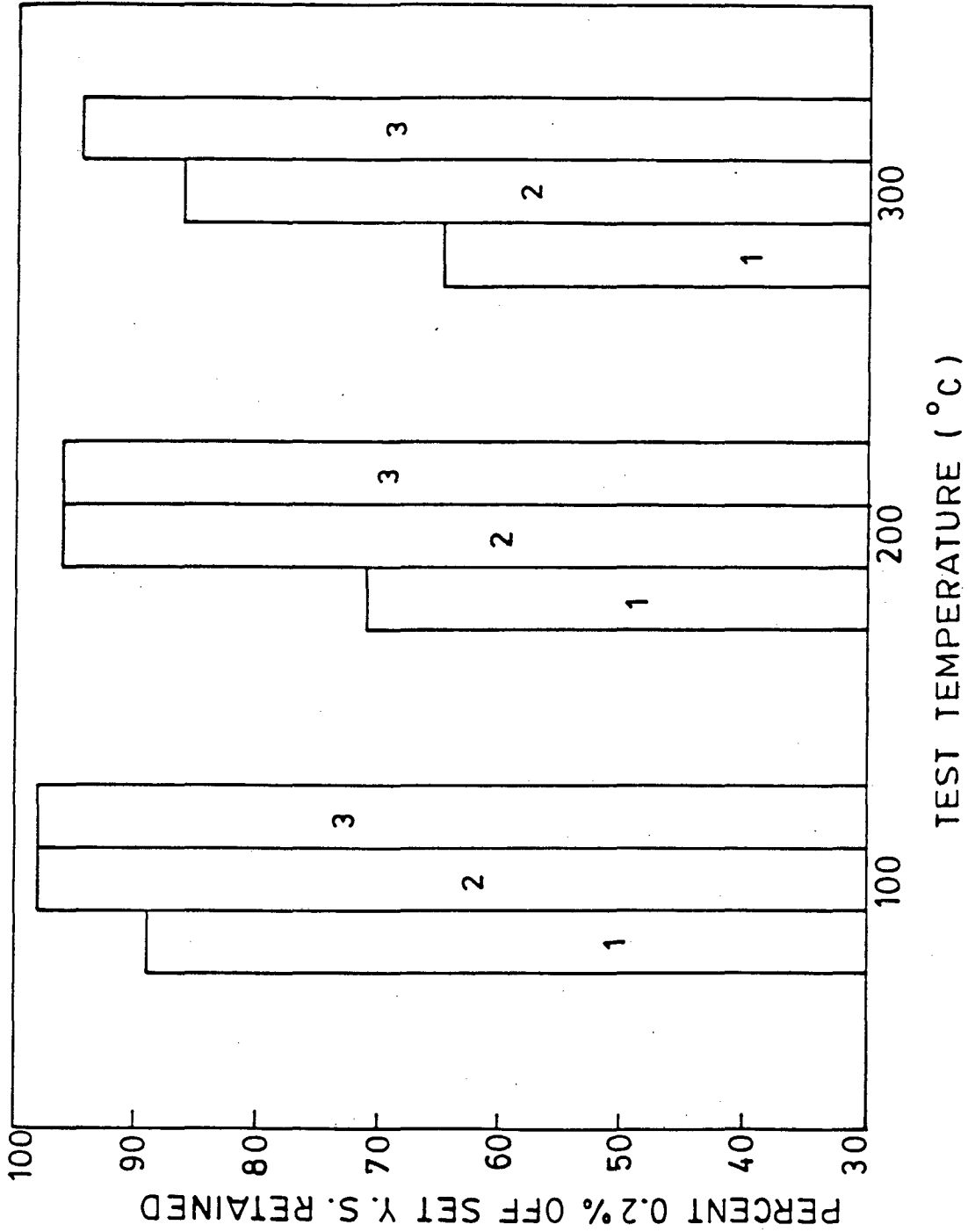


FIG. 4.26 Histogram showing 0.2% offset yield strength retained by composite Nos. 1, 2 and 3 upto 300°C test temperature.

compared to composite No.2. Thus it can be seen that the relative performance of composite No.3 is superior by a factor of 1.3 compared to composite No.2 at 300°C test temperature (the factor,  $1.3 = \text{percent UTS retained by composite No.3} / \text{percent UTS retained by composite No.2}$ ). Similarly it can be seen that the relative performance of composite No.3 as against composite No.1 is superior by a factor of 1.72. It is thus apparent that the performance of composite No.3 with respect to percent UTS retained at elevated test temperature is distinctly superior than both composite Nos.2 and 1. Also, it can be said that the comparative performance of composite No.3 progressively improves as the test temperature is systematically raised to 300°C.

Referring to the results plotted in Fig. 4.26, it can be seen that the performance of composite Nos.2 and 3 at 100 and 200°C test temperatures is nearly identical. The real superiority of composite No.3 with respect to its capability to retain yield strength at elevated test temperatures is demonstrated clearly at 300°C. At this test temperature, composite No.3 retains 94% of its ambient yield strength as against only 86% yield strength retained by composite No.2. The performance of composite No.1 falls behind considerably as it retains only 64% of its ambient yield strength at the above test temperature (300°C). It is thus apparent that the performance of composite No.3 is distinctly superior than the performance of either composite Nos.2 or 1. The basic reason why the performance of composite No.3 is far superior than others is

primarily because of its most densified and grain refined structure. It can, therefore, be surmised from these results that the performance of these composites can be improved still further. Perhaps, one of the approaches can be to change the matrix to an alloy (instead of pure aluminium) and raise the squeeze pressure to higher levels (in the range of 160 to 240 MPa for instance).

The YS/UTS ratio plotted in Fig. 4.27 as a function of test temperatures is indicative of much superior performance of squeezed composites compared to ordinary gravity chill cast composites. The objective of this plot is to show that squeezed composites retain their 0.2% offset YS better than ordinary gravity chill cast composites at elevated test temperatures. The YS/UTS ratio is higher for gravity chill-cast composites primarily because they undergo premature failure in tension due to the presence of voids in the cast structure. This implies that such composites do not develop the expected UTS values in actual practice and, therefore, their YS/UTS ratio is on the higher side. On the other hand, this ratio drops sharply in case of commercially pure aluminium with increasing test temperature, which would be entirely expected.

#### 4.3.4 SEM EXAMINATION OF TENSILE FRACTURE SURFACES [166,168, 169,170,172,175]

Results pertaining to this study are shown in five different plates termed as Figs.4.28 - 4.31.

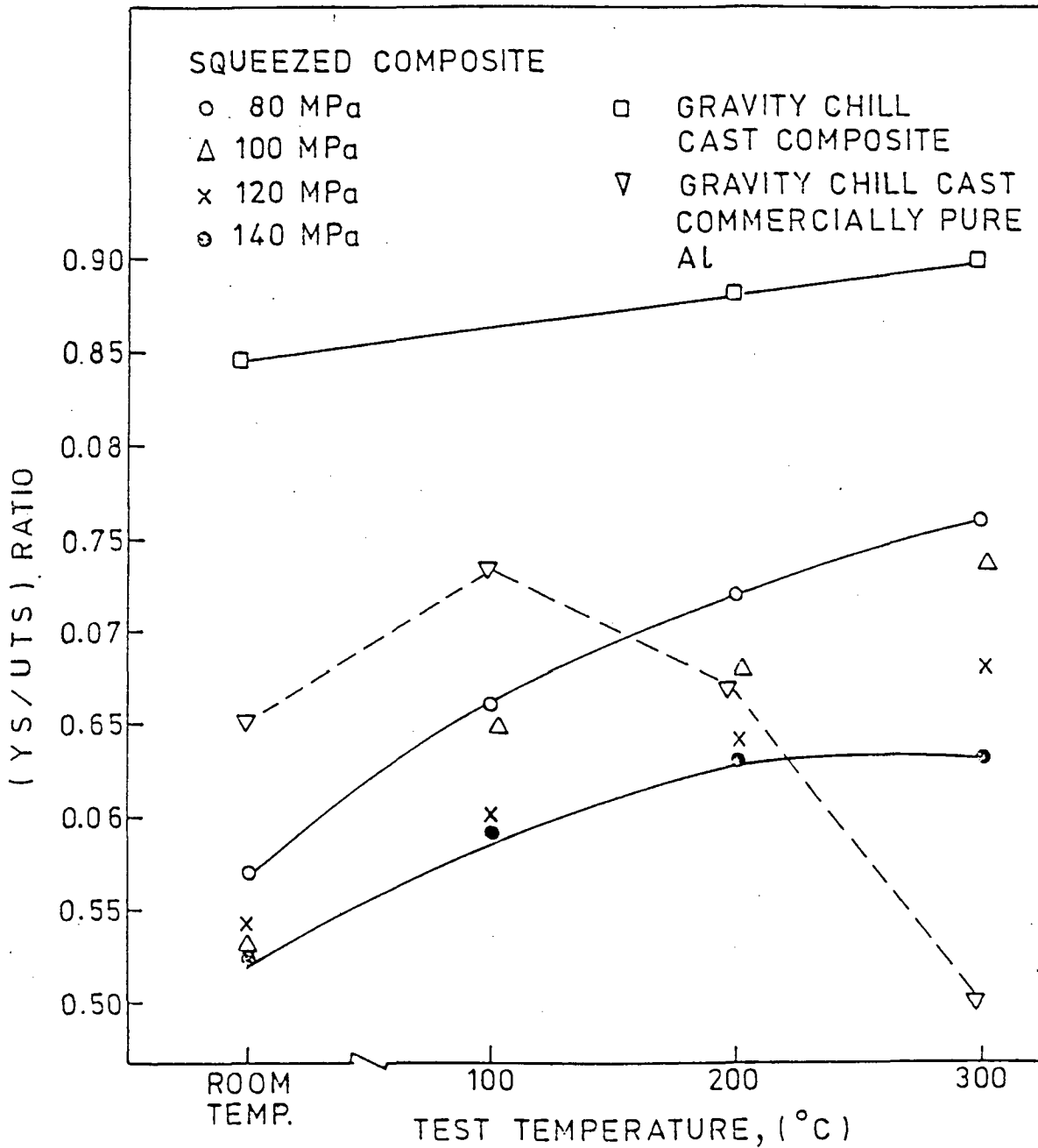
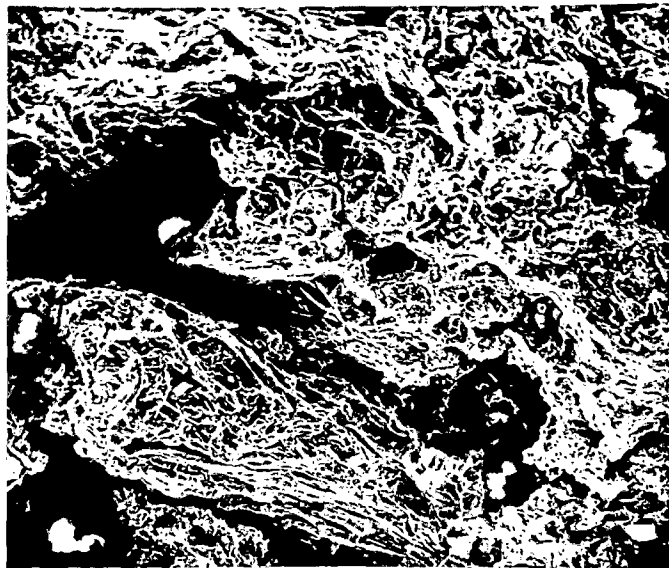


FIG.4.27 Relationship between YS/UTS ratio and the three different test temperatures obtained for (▽) commercially pure aluminium, (□) gravity chill-cast and (○, △, ×, ●) squeezed composites (ambient die temperature), at (○) 80 MPa, (△) 100 MPa, (×) 120 MPa, (●) 140 MPa.

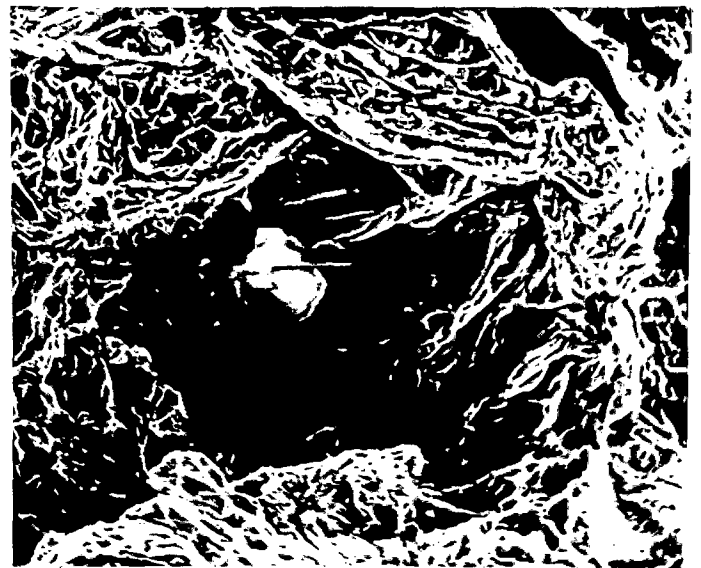
#### 4.3.4.1 FEATURES OF GRAVITY CHILL CAST COMPOSITES

SEM pictures shown in Fig.4.28(a-d) pertain to gravity chill cast composite. A detailed examination of the fractured surfaces of tensile specimens by the SEM reveals that gravity chill cast composites exhibit semi-ductile to brittle fracture features. The fractured surface was seen punctuated with a large number of locations where void spaces pulled to a long distance under tensile stress could be seen. Such a typical picture is shown in Fig.4.28(a). Another location shown in Fig.4.28(b) exhibits big void space where a tiny  $\text{Al}_2\text{O}_3$  particle can be seen sticking to an edge of this void space. Also, it is apparent from the SEM pictures shown in Fig.4.28(a & b) that matrix has under gone failure through a semiductile to brittle mode of failure. It is because the matrix does not show any evidence of ductile mode of fracture. It is apparent that the  $\text{Al}_2\text{O}_3$  particle sticking to the interior walls of the void surface as shown in Fig.4.28(b) will not be in a position to participate in the total process of fracture. It is because this  $\text{Al}_2\text{O}_3$  particle loosely bonded to the matrix will not be in a position to share any load applied to the matrix. Thus, the purpose of dispersing hard ceramic particles into the softer aluminium base matrix is totally lost in case of such gravity chill cast composites. It should be mentioned that such innumerable locations exhibiting voids were observed in gravity chill cast composites. From these observations it can be concluded that a fairly good number of  $\text{Al}_2\text{O}_3$  particles existing in such locations will not be able to participate in the total strengthening process of the base matrix.



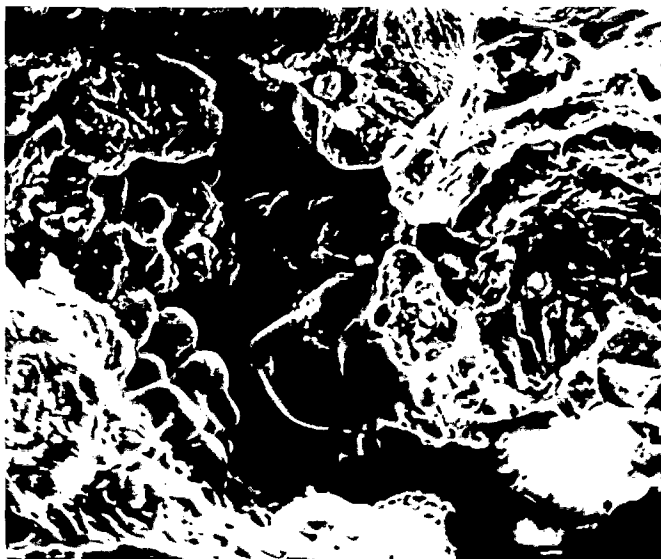
a

x320



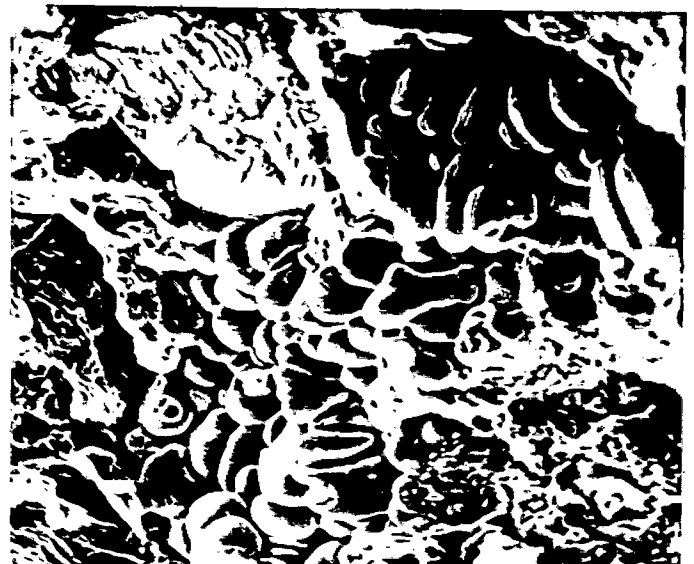
b

x640



c

x640



d

x640

FIG.4.28 SEM pictures of the tensile fractured surfaces of gravity chill cast composite.

(a) showing the presence of large sized voids pulled and enlarged under tension,

(b) showing typical brittle fracture features. Note one MgO coated  $Al_2O_3$  particle sitting at the base of the void. This particle is apparently loosely bonded to the matrix,

(c) and (d) showing the presence of interdendritic solidification contraction areas. Note the dendritic arms jetting out into the void space from the opposite solidification fronts.



Because of the kind of voids depicted in Fig.4.28(a & b), the gravity chill cast composite will be expected to exhibit lower ultimate tensile strength and also poor ductility. Actual observations (Table-4.6 and Fig.4.16) provide support to this contention. It is because such a cast structure with many void spaces will not be able to take up the same level of stress during tension as a relatively densified structure would take and would therefore exhibit comparatively lower UTS values. Because of the presence of these voids, such a cast structure will also exhibit lower ductility and will ultimately undergo premature failure during tension as shown in Fig.4.16. The occurrence of such voids can be directly attributed to the phenomenon of precipitation of dissolved gases, particularly hydrogen, during the process of freezing of the stirred slurry.

Another interesting feature of these fractured surface was the presence of unfed interdendritic regions. These locations are characterised by the presence of protruding dendritic arms in the unfed void space pulled apart and enlarged under the tensile stress. These typical features are shown in Fig .4.28(c&d). Such characteristic features were also observed during an early study of the fracture surfaces of gravity chill cast Al-Al<sub>2</sub>O<sub>3</sub>-MgO particulate composites [166,168]. Apparently, this defect occurs mainly because of lack of supply of liquid feed metal to these regions and this kind of problem is commonly observed in gravity chill cast composites. Although these precise fracture features were not observed by earlier workers [64-66,174], but they certainly appreciated the role of total

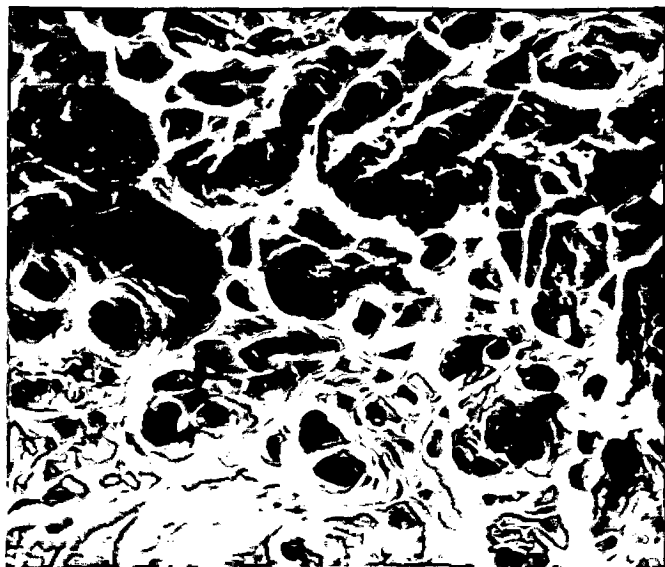
porosity in influencing the strength and ductility of gravity chill cast composites. When such features as shown in Fig.4.28(c&d) are present in large locations, they give rise to a considerable amount of discontinuity in the cast structure. It can be seen from Fig.4.28(c) that the two advancing solidification interfaces moving in opposite direction are not able to meet and the protruding dendritic arms jetting out from the opposite solidification fronts can be seen projecting out into the void space between the two fronts. Such a situation presents serious discontinuity in the cast matrix.

The two kinds of porosities put together (gas porosity plus unfed interdendritic regions) cause a considerable damage to the cast structure. The continuity of the matrix is lost and the dispersed ceramic particles are not able to participate in the strengthening process. These factors ultimately lead to a display of poor strength and inferior ductility by such gravity chill cast composites. One possible means of overcoming these problems is to solidify the stirred slurry under high pressure.

#### 4.3.4.2 FEATURES OF SQUEEZED COMPOSITES

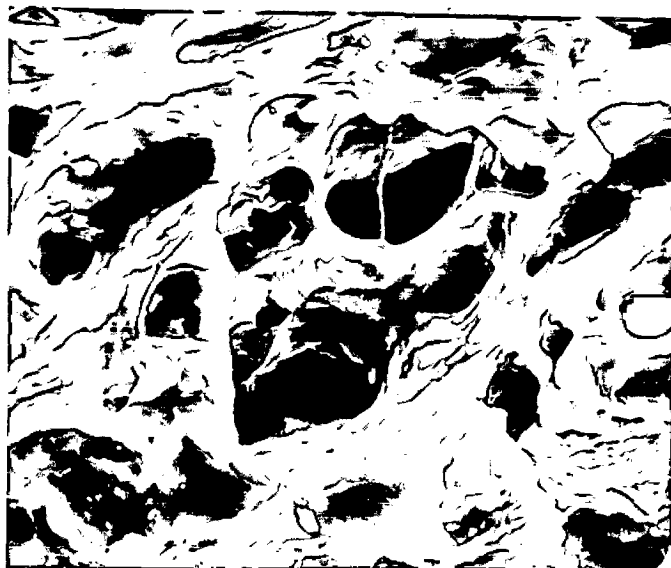
##### (a) FRACTURE FEATURES AT AMBIENT TEST TEMPERATURE

SEM pictures showing the fracture features obtained at ambient test temperature are displayed in Figs.4.29 and 4.30. In the case of the fractographs shown in Fig.4.30, only 5% total ( $\text{Al}_2\text{O}_3 + \text{MgO}$ ) powder mixture was stirred in aluminium melt so as to obtain comparative performance data of these composites as against



a

x320



b

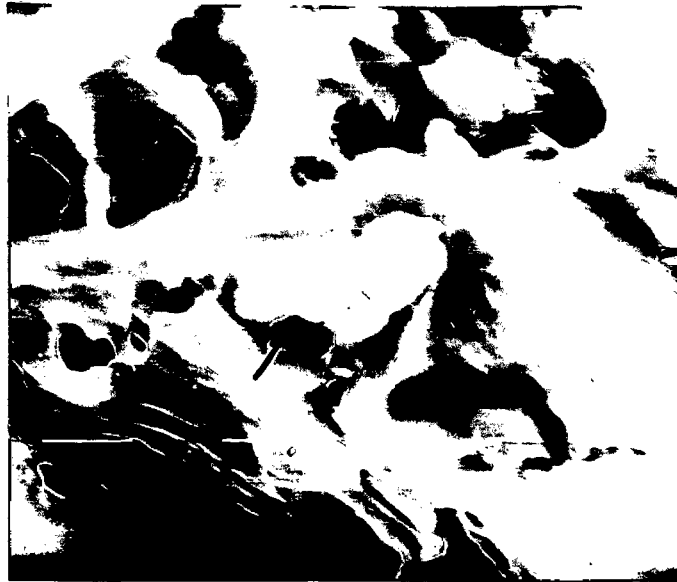
x640



c

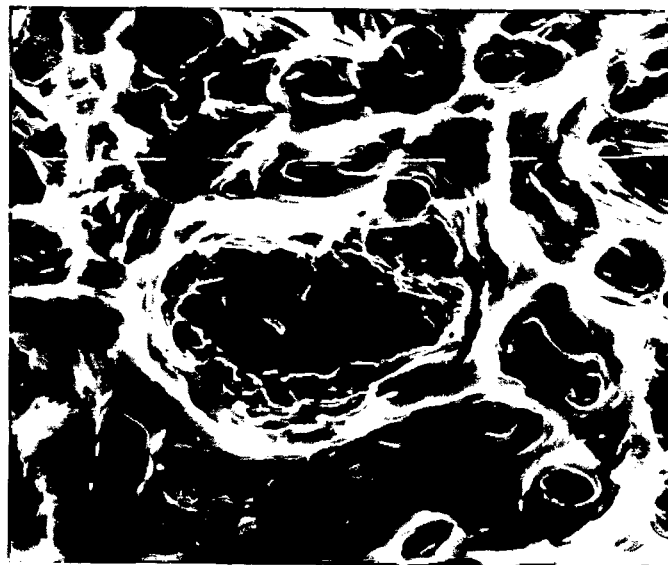
x1250

FIG.4.29 SEM pictures of the tensile fractured surfaces of the composite squeezed at 140 MPa and ambient die temperature. (a) and (b) showing the presence of deep dimples characteristics of a ductile fracture, (c) showing the chisel-point separation of intervening matrix between two adjoining dimples typical of a ductile fracture.



a

x1250



b

x640

**FIG.4.30** Fractographs of the composite with 5 wt.% total ( $\text{Al}_2\text{O}_3 + \text{MgO}$ ) powder mixture stirred in the melt and squeezed at 115 MPa and ambient die temperature.  
 (a) SEM picture showing fairly good ductile fracture feature. Note one large  $\text{Al}_2\text{O}_3$  particle sitting at the base of the crater where partial particle/matrix decohesion has occurred at the location marked by an arrow.  
 (b) SEM picture showing typical ductile fracture features depicting the presence of a large number of deep dimples. In addition to many smaller dimples, a relatively larger dimple is seen in the centre of the fractograph.

the usual ones where 10% total ( $\text{Al}_2\text{O}_3+\text{MgO}$ ) powder mixture was stirred in the melt. Properties of these composites at ambient test temperature are listed at Sl. No.16 of Table-4.6. SEM fractographs shown in Fig.4.29 pertain to the best composite prepared in this work (140 MPa and ambient die temperature).

It can be seen from the SEM pictures presented in Fig.4.29(a-c) that the composite squeezed at 140 MPa and ambient die temperature displays fully ductile fracture features. These observations indirectly support the ductility data recorded in Table-4.6. It can be seen that the entire fracture surface of squeezed composite is characterized by the presence of deep dimples with extensive deformation markings along the walls of individual craters (Fig.4.29). These SEM pictures shown in Fig.4.29 exhibit fracture features quite typical of a ductile material. It can be noted that the individual dimples are very deep signifying that the matrix was pulled to a long distance before final fracture. The presence of extensive deformation markings along the walls of individual craters also signify that the matrix is capable of taking considerable amount of plastic deformation before final fracture. This kind of fracture is produced by the coalescence of voids under the tensile stress. A considerable amount of energy is spent in this process of particle/matrix interface decohesion, formation of micro voids and void-sheets at the interface, ultimately leading to the formation of voids, which are enlarged under the tensile stress as the matrix is undergoing deformation [165,169]. The

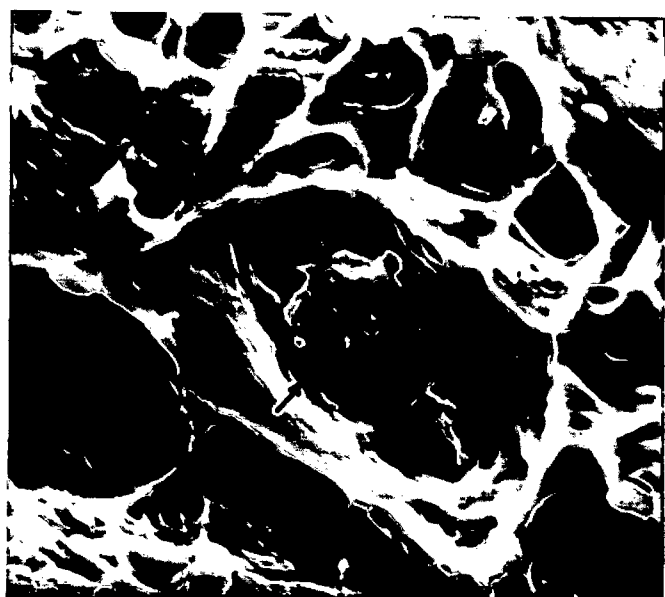
intervening matrix between the voids so created separates out in the present case through a mode of chisel-point or knife-edge separation at the point of fracture (Fig.4.29 b&c). This is indicative of an excellent ductility displayed by the squeezed composite. Because of the reasons mentioned above, the matrix takes considerable amount of stress before final fracture. This is the basic reason why squeezed composites display much superior UTS as well as percent elongation compared to gravity chill cast composites (Fig.4.16, Table-4.6). As discussed in previous section 4.3.4.1, gravity chill cast composites are not able to show the expected level of ductility because of the presence of voids in the cast structure. But in case of squeezed composites, as the degree of squeeze pressure is progressively raised, the void space progressively decreases in the cast structure, and therefore, the resulting composite displays increasingly superior ductile behaviour.

It can be seen from the SEM fractographs shown in Fig.4.29(a-c) that the dimples are not of uniform size. It is because the present composite contains dispersion of  $Al_2O_3$  particles with a wide spectrum of size range varying from 50-150  $\mu m$  (Table-3.1). This particular fact results in a non-uniform size of dimples being obtained on the tensile fracture surfaces of the composites. The presence of several smaller dimples in the vicinity of a larger dimple as shown in Fig.4.29(c) can be attributed to this particular reason.

Referring to the fractographs shown in Fig.4.30(a&b), which pertain to the composite with 5% total ( $\text{Al}_2\text{O}_3+\text{MgO}$ ) powder addition, it can be seen that the fracture features are almost similar to the ones discussed above. These features are similar primarily because this composite was also squeezed at 115 MPa. It is interesting to note from Fig.4.30(a) as to how particle/matrix decohesion occurs along the surface of dispersed  $\text{Al}_2\text{O}_3$  particle. It can be seen from this SEM picture that the  $\text{Al}_2\text{O}_3$  particle is still sitting at the base of the crater but the partial particle/matrix decohesion has occurred at a particular location (marked by an arrow). A closer examination of this picture shows that the  $\text{Al}_2\text{O}_3$  particle is firmly bonded with the base matrix. In this situation, considerable amount of energy will have to be spent to create particle/matrix decohesion leading to final fracture. This is a single vital factor which results in the display of higher UTS values by the squeezed composites. Also, it is apparent from all the fractographs presented in this section that the base matrix is virtually free from the presence of voids and unfed interdendritic regions as commonly observed in case of gravity chill cast composites. As discussed in section 4.3.4.1, the mode of fracture would be entirely different when voids of any kind are present in the cast structure.

**(b) FRACTURE FEATURES AT ELEVATED TEST TEMPERATURE**

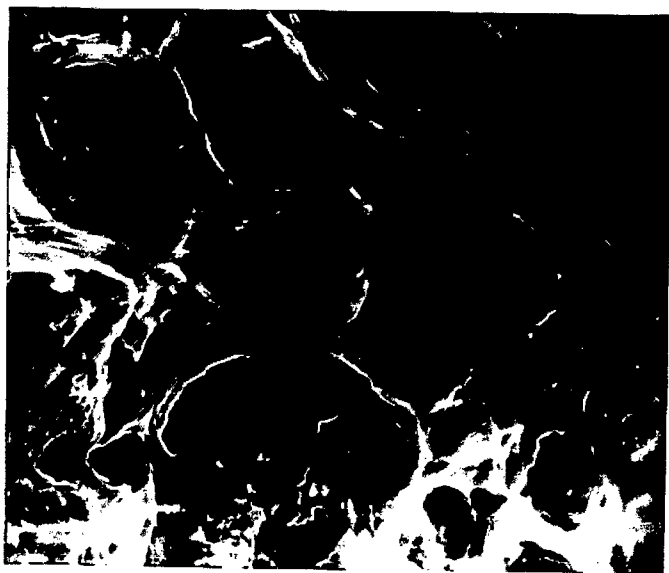
Results pertaining to a study of the fractures of the tensile specimens pulled at elevated test temperatures are shown in Fig.4.31(a-d). The typical features discussed above are the



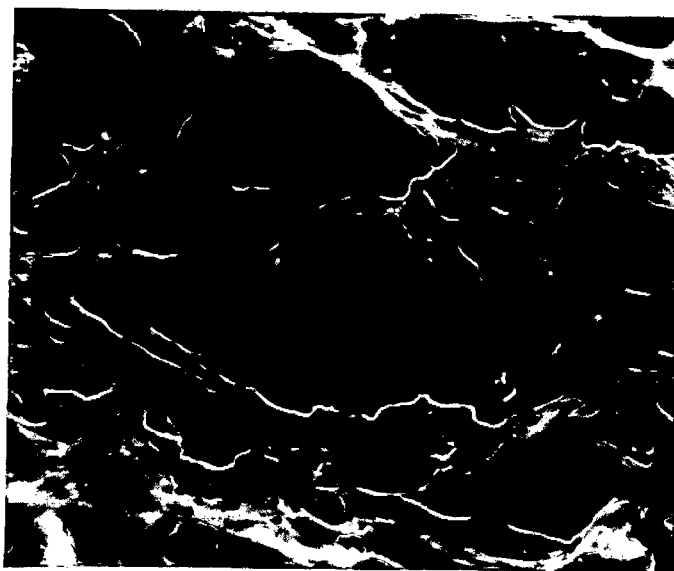
a x640



b x320



c x320



d x320

FIG.4.31 Scanning Electron Micrographs of the tensile fracture surfaces of the composite squeezed at 140 MPa and ambient die temperature and (a) pulled in tension at 100°C (373K) and (b,c, and d) pulled in tension at 300°C (573K). (a) Note particle/matrix decohesion almost along 3/4th surface area of the  $Al_2O_3$  particle marked by an arrow, (b),(c) & (d) typical ductile fracture features showing relatively larger average size of dimples than what is obtained at ambient temperature.



same except that the average size of dimples progressively increases as the test temperature is systematically raised. Fractographs shown in Fig.4.31(a) pertains to 100°C test temperature while the rest of the three fractographs pertain to 300°C test temperature. The composite examined in all the four cases is the same (140 MPa and ambient die temperature). The fractograph shown in Fig.4.31(a) is interesting in the sense that it shows the process of void formation through particle/matrix decohesion at the surface of  $Al_2O_3$  particle. The  $Al_2O_3$  particle sticking to the base of the crater is shown by an arrow in this picture. It can be seen that particle/matrix decohesion has occurred in this case almost along 80% surface area of the  $Al_2O_3$  particle. Also, deformation markings along the walls of the craters can be clearly seen. A number of smaller dimples can be seen surrounding the larger crater as was depicted in an earlier fractograph (Fig.4.29-c). If the size of the dimples shown in Fig.4.31(b-d) are compared with the dimples shown in Fig.4.29(b), it can be clearly seen that the size of the dimples obtained at 300°C test temperature are much larger than the ones obtained at ambient test temperature. Although the fractograph shown in Fig.4.29(b) was taken at 640X but the dimples visible therein are much smaller compared to the dimples visible in the fractographs shown in Fig.4.32(b-d), which were photographed at just half the magnification i.e. 320X. A rough estimate of the average size of dimples shows that the size of dimples obtained at ambient test temperature range between 5 to 10  $\mu m$  (Fig.4.29-b), while the

size of dimples obtained at 300°C test temperature range between 20 to 30  $\mu\text{m}$  (Fig.4.31,b-d ). This will be entirely expected. Thus, increasing the test temperature does not bring about any basic change in the mode of fracture, except that the average size of the dimples progressively increases [175]. This particular feature was noted by other investigators also, involving a slightly different composite system [66]. It is apparent from a study of the SEM fractographs that the ductile fracture features of squeezed composites observed at all the test temperatures are indirectly supported by the percent elongation data recorded in individual cases (Table Nos.4.6-4.9).

#### **4.4 WEAR BEHAVIOUR OF COMPOSITE NOS.1,2 AND 3 UNDER DRY SLIDING CONDITIONS [171,172,180]**

##### **4.4.1 GENERAL**

The results of present study are summarised in Table-4.10 and plotted in Figs.(4.32-4.34, 4.38, 4.44-4.46, 4.50-4.58). A systematic study of the stages of wear and the mechanism of material removal during dry sliding wear was carried out with the help of the SEM examination of the worn surfaces of wear pins. The debris material produced during the wear process was also examined by the SEM. Some of these features and also the worn patches sticking to the counterface steel disc were examined optically. SEM and optical pictures pertaining to these aspects are shown in Figs.(4.51-4.56). The worn surface of the test pin was then taper sectioned at 5° inclination, polished and

TABLE - 4.10

WEAR DATA OF COMPOSITE NO. 1, 2 AND 3

| Material    | Duration of Wear Test HRS. | Track length m | Sliding Speed m.sec <sup>-1</sup> . 10 <sup>-2</sup> | Wear loss, mg. at different bearing loads |          |          | Wear Rate, Kg.Km <sup>-1</sup> .10 <sup>-6</sup> . at differnt bearing loads in gms. |          |          |
|-------------|----------------------------|----------------|--|---|----------|----------|--|----------|----------|
|             |                            |                |  | 500 gm.                                   | 1000 gm. | 1500 gm. | 500 gm.  | 1000 gm. | 1500 gm. |
|             | 2                          | 3              | 4  | 5   | 6        | 7        | 8  | 9        | 10       |
| Gravity     | ½                          | 169.5          |  | 3.72                                      | 4.58     | 6.08     | 21.9   | 27.0     | 35.0     |
| Chill cast  | 1                          | 339.0          | 9.4  | 8.90                                      | 11.86    | 17.08    | 26.2   | 34.9     | 50.3     |
| Composite   | 1½                         | 508.5          |  | 12.82                                     | 20.96    | 31.10    | 25.2   | 41.2     | 61.1     |
| No.(1)      | ½                          | 254.4          |  | 6.00                                      | 7.20     | 9.80     | 23.5   | 28.3     | 38.5     |
|             | 1                          | 508.8          | 14.1   | 11.10                                     | 15.38    | 21.96    | 21.8   | 30.2     | 43.1     |
|             | 1½                         | 763.2          |  | 14.90                                     | 25.40    | 37.60    | 19.5   | 33.2     | 49.2     |
|             | ½                          | 339.0          |  | 8.30                                      | 10.58    | 15.04    | 24.4   | 31.2     | 44.3     |
|             | 1                          | 678.0          | 18.8   | 13.26                                     | 19.54    | 28.50    | 19.5   | 28.8     | 42.0     |
|             | 1½                         | 1017.0         |  | 17.00                                     | 30.12    | 44.90    | 16.7   | 29.6     | 44.1     |
| Squeezed    | ½                          | 169.5          |  | 1.90                                      | 2.40     | 4.30     | 11.2   | 14.1     | 25.3     |
| Composite   | 1                          | 339.0          | 9.4  | 4.36                                      | 6.80     | 11.48    | 12.8   | 20.0     | 33.8     |
| (80 MPa     | 1½                         | 508.5          |  | 5.90                                      | 12.22    | 20.30    | 11.6   | 24.0     | 39.9     |
| and ambi-   | ½                          | 254.4          |  | 3.20                                      | 4.16     | 6.74     | 12.5   | 16.3     | 26.4     |
| ent die     | 1                          | 508.8          | 14.1   | 5.62                                      | 8.62     | 14.54    | 11.0   | 16.9     | 28.5     |
| temperatu-  | 1½                         | 763.2          |  | 6.98                                      | 14.80    | 24.02    | 9.1  | 19.3     | 31.4     |
| re)Composi- | ½                          | 339.0          |  | 4.50                                      | 6.08     | 9.90     | 13.2   | 17.9     | 29.2     |
| te No.(2)   | 1                          | 678.0          | 18.8   | 6.64                                      | 11.26    | 18.26    | 9.7  | 16.6     | 26.9     |
|             | 1½                         | 1017.0         |  | 8.24                                      | 17.66    | 28.00    | 8.1  | 17.3     | 27.5     |
| Squeezed    | ½                          | 169.5          |  | 1.32                                      | 1.78     | 3.02     | 7.7  | 10.5     | 17.8     |
| Composite   | 1                          | 339.0          | 9.4  | 2.50                                      | 4.60     | 8.00     | 7.3  | 13.5     | 23.5     |
| (140 MPa    | 1½                         | 508.5          |  | 3.42                                      | 8.10     | 14.82    | 6.7  | 15.9     | 29.1     |
| and ambi-   | ½                          | 254.4          |  | 2.02                                      | 3.02     | 4.80     | 7.9  | 11.8     | 18.8     |
| ent die     | 1                          | 508.8          | 14.1   | 3.42                                      | 6.02     | 10.22    | 6.7  | 11.8     | 20.0     |
| temperat-   | 1½                         | 763.2          |  | 4.02                                      | 9.98     | 17.96    | 5.2  | 13.0     | 23.5     |
| ure)Compo-  | ½                          | 339.0          |  | 2.90                                      | 4.40     | 7.08     | 8.5  | 12.9     | 20.8     |
| site        | 1                          | 678.0          | 18.8   | 4.26                                      | 7.94     | 13.46    | 6.2  | 11.7     | 19.8     |
| No.(3)      | 1½                         | 1017.0         |  | 5.00                                      | 12.18    | 21.48    | 4.9  | 11.9     | 21.1     |

then examined optically and also by the SEM. The objective of oblique sectioning was to estimate the extent of sub-surface damage beneath the worn surface. Optical and SEM pictures pertaining to this examination are shown in Fig. 4.57. Fig. 4.58 shows data pertaining to microhardness measurements taken along this tapered section commencing from the edge of visible grooved track marks. The objective of this study was to ascertain the extent of work hardening undergone by the subsurface layers immediately below the grooved track marks. A discussion on the influence of various operating parameters on the wear rate of composite Nos. 1,2 and 3 is first taken up followed by a discussion of the texture of worn surface and the subsurface damage. The latter part of this discussion includes a scrutiny of the morphology of debris material produced during the process of wear.

#### 4.4.2 BEARING LOAD-WEAR RATE RELATIONSHIPS

Results of this study are summarised in Figs. 4.32, 4.33 and 4.34 for progressively increasing sliding speeds of 9.4, 14.1 and 18.8  $\text{m}\cdot\text{sec}^{-1} \times 10^{-2}$  respectively. It can be seen from these results that these relationships are basically linear in each case except that a change of slope beyond 1000 gm bearing load can be noted at each sliding speed employed. This change of slope beyond 1000 gm bearing load is not very sharp either, though it is easily noticeable. This implies a slow or a rather mixed transition from one mode of wear (upto 1000 gm) to another (beyond 1000 gm). A similar but sharp transition was noted in

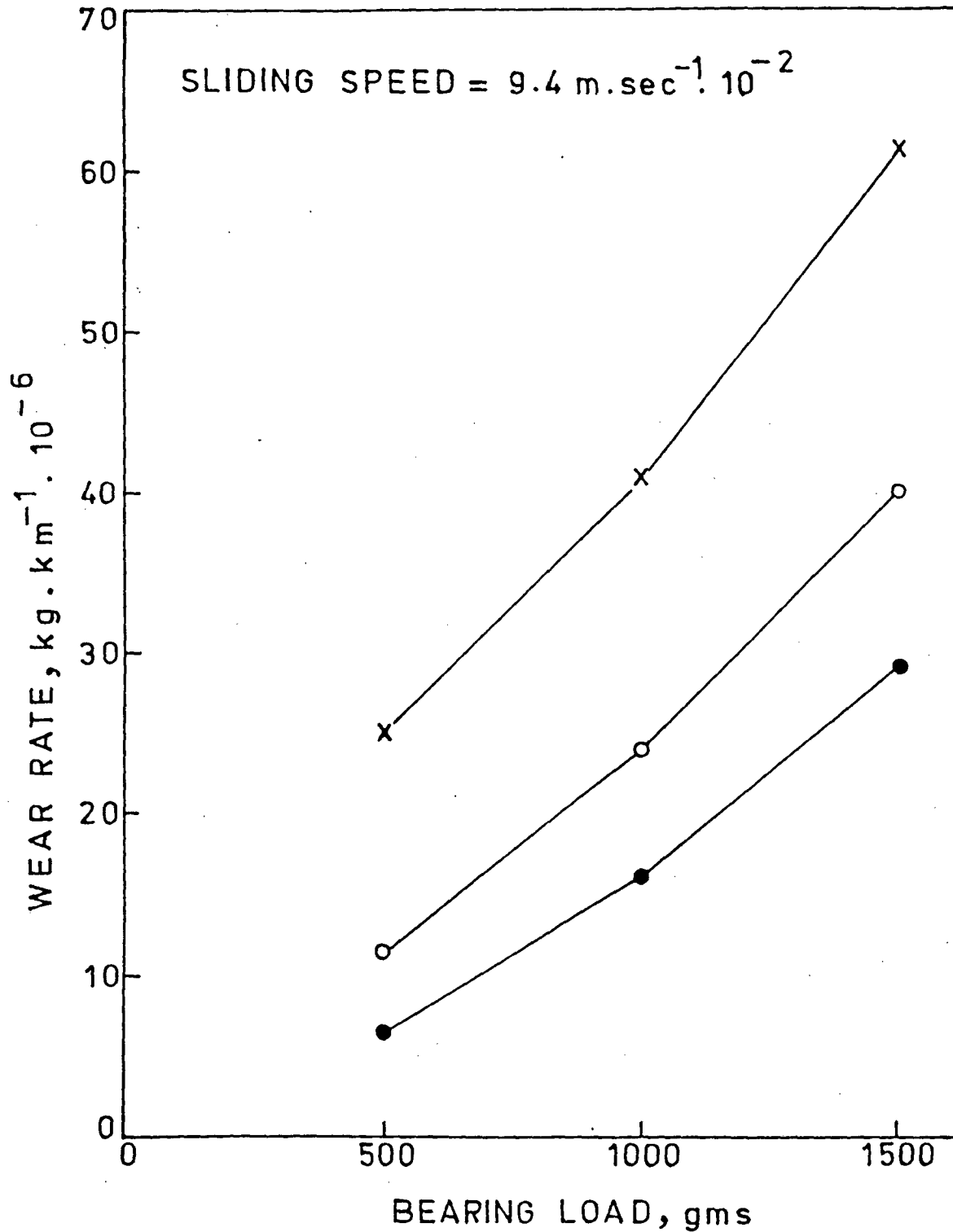


FIG.4.32 Wear rate plotted as a function of bearing load (gms) for composite No.1 (gravity chill cast) (x), Composite No.2 (squeezed at 80 MPa, and ambient die temperature) (o), and Composite No.3 (●), at a sliding speed of  $9.4 \text{ m} \cdot \text{sec}^{-1} \cdot 10^{-2}$ , sliding distance 508.5 m.

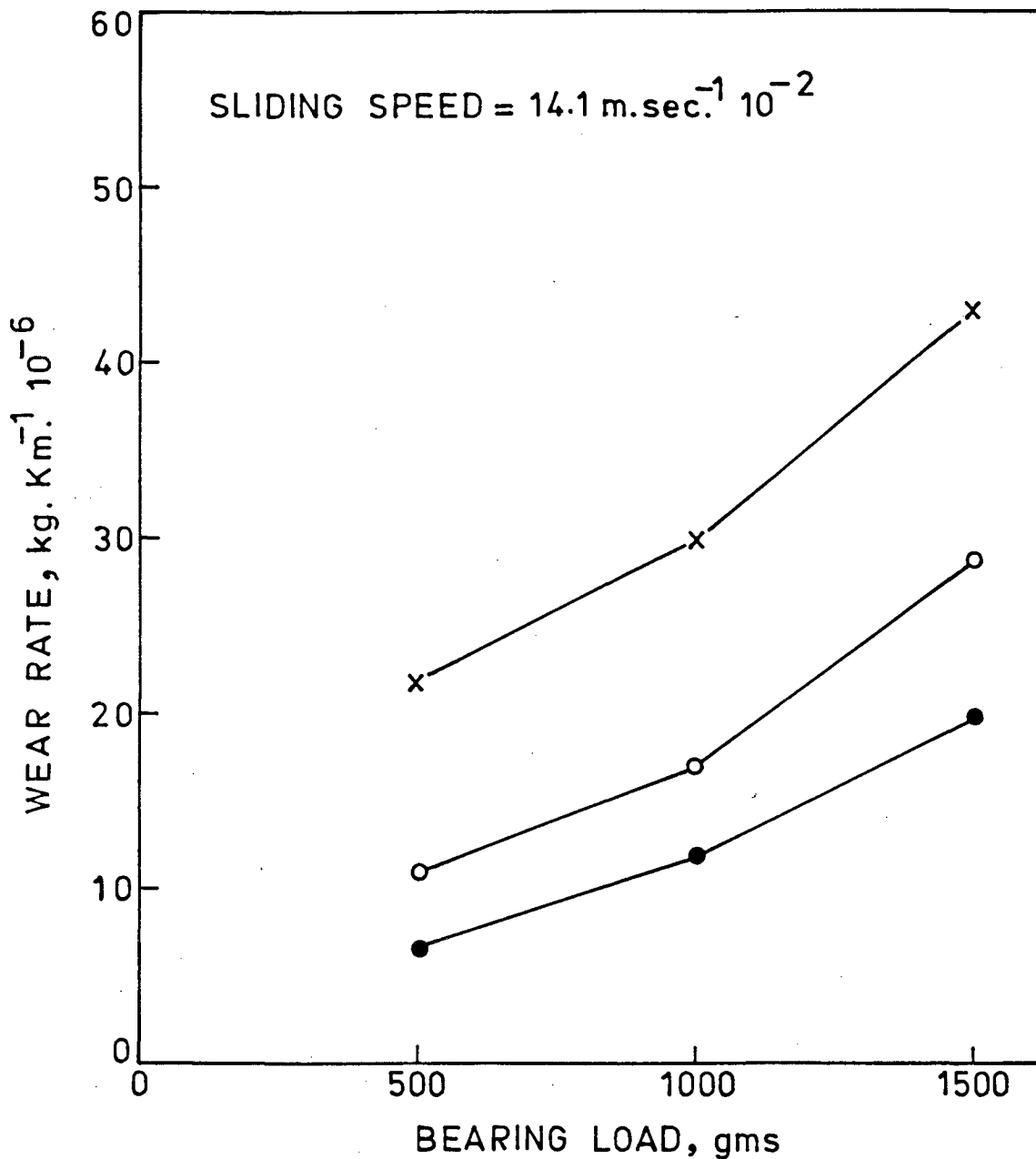


FIG. 4.33 Wear rate plotted as a function of bearing load (gms) for Composite No.1 (gravity chill cast) (x), Composite No.2 (squeezed at 80 MPa, and ambient die temperature) (o), and Composite No.3 (●) at a sliding speed of  $14.1 \text{ m. sec}^{-1} \cdot 10^{-2}$ , sliding distance 508.5 m.

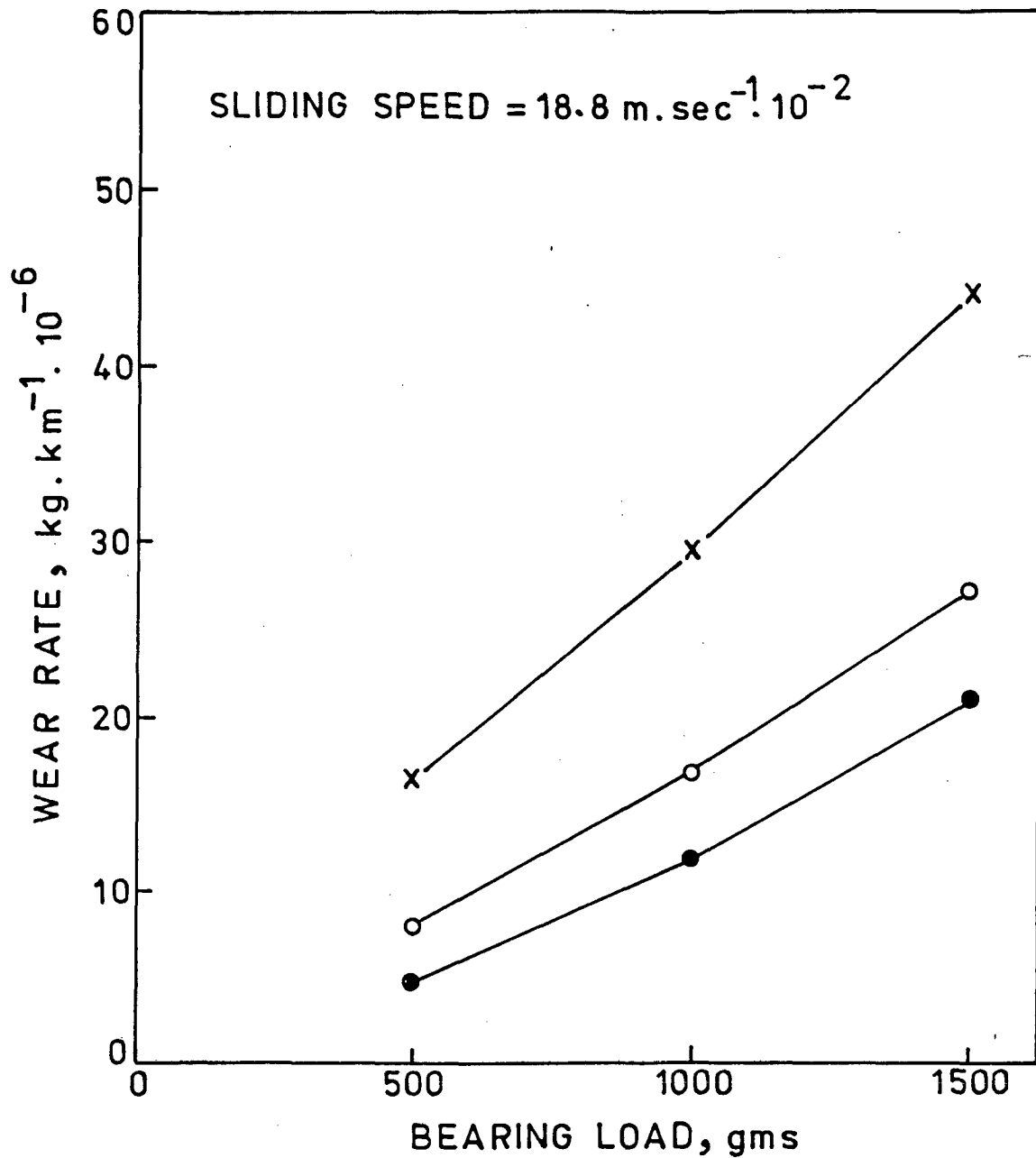


FIG.4.34 Wear rate plotted as a function of bearing load (gms) for composite No.1,(gravity chill cast) (x), composite No.2 (squeezed at 80 MPa, ambient die temperature) (o), Composite No.3 (squeezed at 140 MPa, ambient die temperature) (●), at a sliding speed of  $18.8 \text{ m} \cdot \text{sec}^{-1} \times 10^{-2}$ , sliding distance 508.5 m.

the wear behaviour of pure aluminium [176], Al-Al<sub>3</sub>Ni eutectic alloy [177], Al-22%Si alloy [124,126], Bauxite particles reinforced Al-alloy [157], 2024-Al<sub>2</sub>O<sub>3</sub> particle composites [62,150] and discontinuous ceramic SiC and Al<sub>2</sub>O<sub>3</sub> fibre reinforced aluminium alloy composites [88]. Typical results pertaining to binary Al-Si alloys [124], Al-Bauxite composites [157] and discontinuous ceramic SiC and Al<sub>2</sub>O<sub>3</sub> fibre reinforced Al-alloy composites [88] are shown in Figs. 4.35, 4.36 and 4.37 respectively. It can be seen that the results of present investigations are in agreement with the findings of above workers. Actually this kind of sudden transition in the wear behaviour of most composites has been noted at about 500 gm bearing load. It is basically because, at loads less than 4.9N (500 gm), it is the oxidative or mild wear which is predominant and at loads exceeding 500 gms, the abrasive wear becomes predominant. The results of present study, therefore, show that what is predominantly happening in the present class of composites is basically abrasive wear. If data on oxidative wear regime is to be generated then one has to move to bearing loads smaller than 500 gm. Moving to bearing loads smaller than 500 gm can thus generate valuable data on the oxidative wear behaviour of different composites. This aspect is interesting from practical applications point of view. Under the conditions of low bearing loads and higher sliding speeds, a number of composite systems have been investigated. As mentioned above, this situation corresponds with a number of practical applications. For example, based on the wear behaviour of the



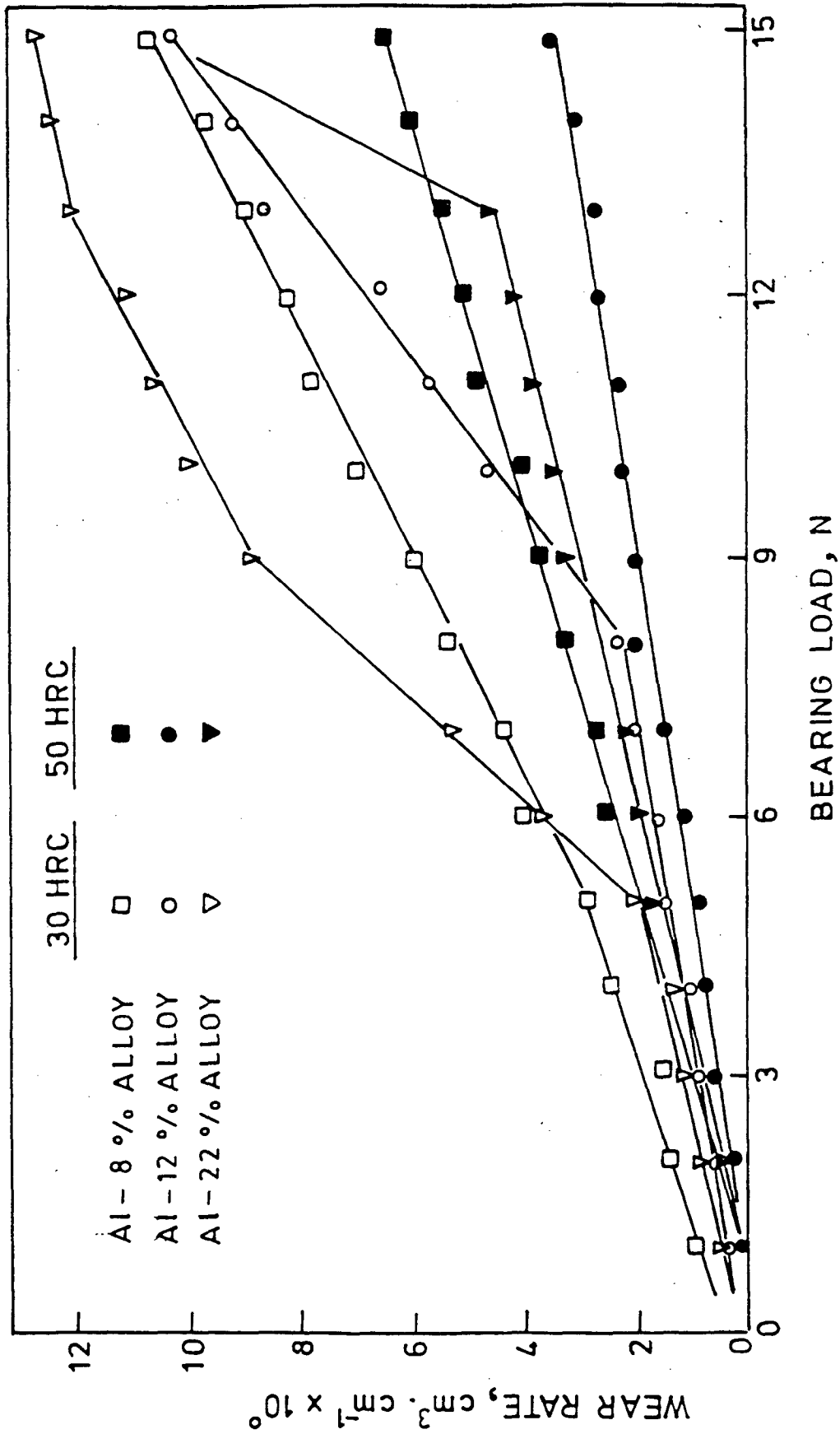


FIG.4.35 Variation in the adhesive wear rates of binary aluminium-silicon alloys as a function of bearing load.(Ref.124)

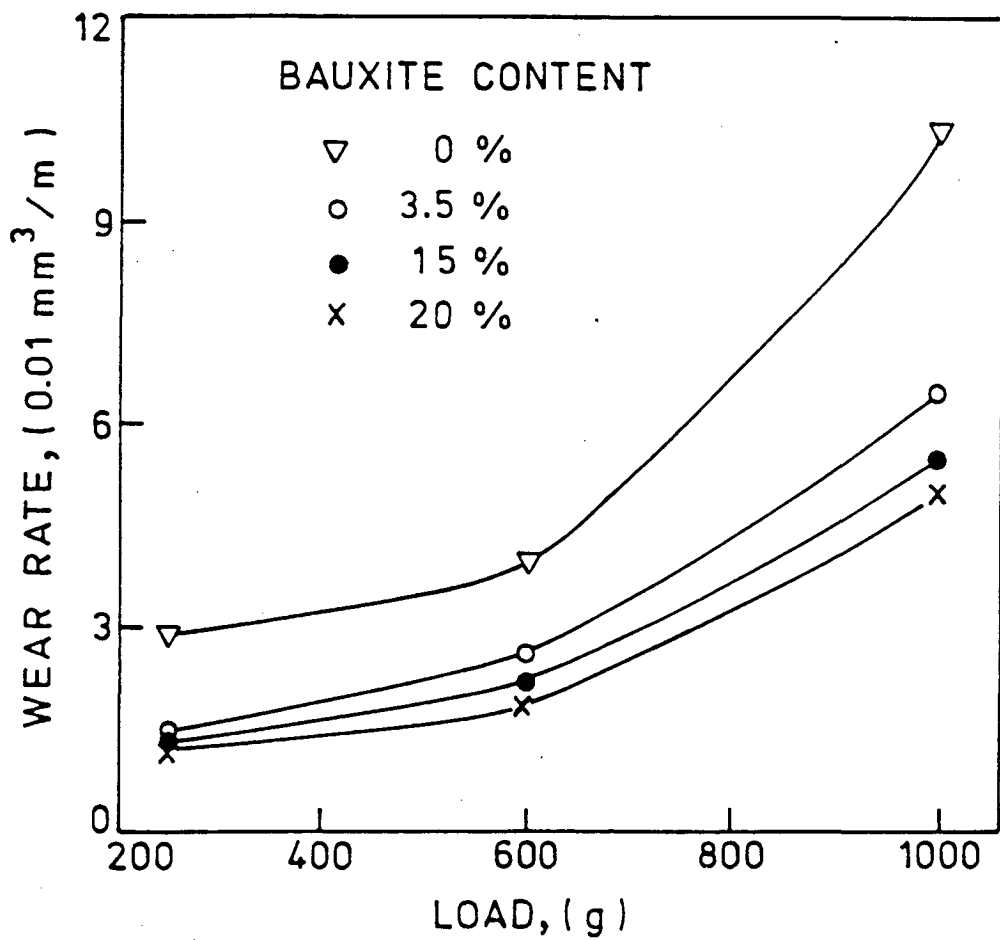


FIG.4.36 Wear rate vs. load in the matrix alloy and composites containing 3.5, 15 and 20wt% bauxite particles.(Ref.157)

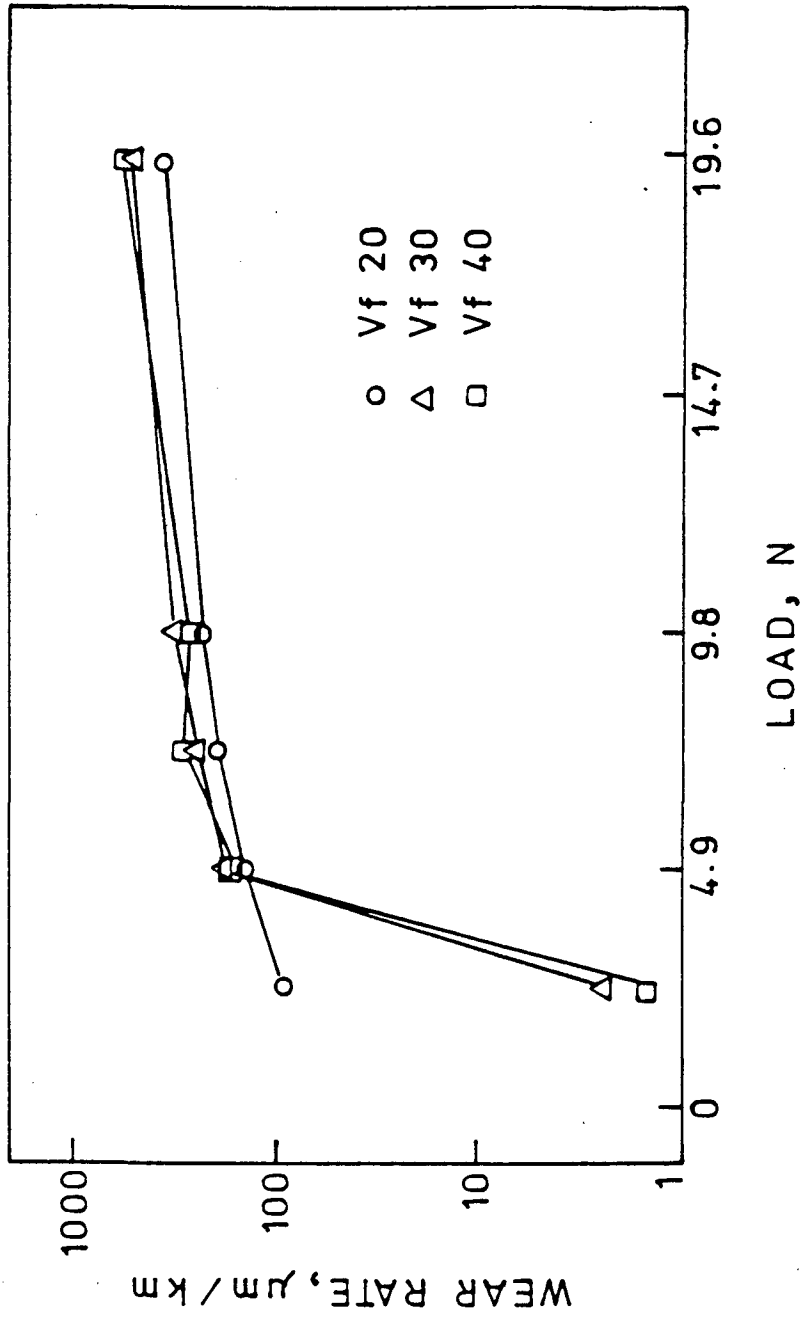


FIG.4.37 Effect of normal load and volume fraction of fibre on the wear rate of  $\text{Al}_2\text{O}_3/6061$  composite (velocity =  $1\text{m}\cdot\text{sec}^{-1}$ ). (Ref.88)

composites at low loads and higher sliding speeds, Fukunaga [88] suggested that SiC and  $\text{Al}_2\text{O}_3$  discontinuous fibre reinforced Al-alloy composites should preferably be subjected to above service conditions only. In the present case of composites, possibly the transition point was shifted to higher loads (1000 gm at all the three sliding speeds investigated) owing to higher counterface hardness of composite No. 1,2 and 3 wear pins. Similar features were noted by Dwarakadasa [124] and Shivanath et.al. [178,179] in case of Al-Si alloys. But this, however, can not be said with any certainty unless wear behaviour of composite Nos. 1,2 and 3 is investigated at bearing loads smaller than 500 gms. This aspect calls for a systematic study.

It can also be noted from the results shown in Figs. 4.32, 4.33 and 4.34 that under a fixed set of experimental conditions, the wear loss of Al- $\text{Al}_2\text{O}_3$ -MgO composites progressively decreases as the squeeze pressure is systematically raised in steps. It is apparent from the results shown in Figs.4.32, 4.33 and 4.34 that the net loss of material for composite No.3 in terms of wear rate is minimum for any set of experimental conditions. The effect of increasing the bearing load is to proportionately increase the wear rate in case of each composite. The slope of lines can be seen to be nearly identical between different bearing loads. The simple pattern is that the quantity of wear rate is shifted to higher values as the bearing load is progressively raised in steps of 500 gms. This behaviour will be entirely expected.

#### 4.4.3 EFFECT OF SLIDING SPEEDS ON WEAR BEHAVIOUR

Results pertaining to this study are summarised in Fig. 4.38. It can be seen from the results that the wear rate of different composites progressively decreases as the sliding speed is systematically raised in steps from 9.4 to 18.8  $\text{m}\cdot\text{sec}^{-1}\times 10^{-2}$ . It should be mentioned that compared to other workers, the sliding speeds employed in the present set of experiments are rather on the lower side. Sliding speeds of the order of 1 to 4  $\text{m}\cdot\text{sec}^{-1}$  are quite common, while Hosking et.al. [62] employed comparatively a slower sliding speed of 0.1  $\text{m}\cdot\text{sec}^{-1}$  in their experiments. It would be worthwhile examining the wear behaviour of present composites also in the sliding speed range of 1 to 4  $\text{m}\cdot\text{sec}^{-1}$  as this parameter has a strong bearing on the wear rate of composites. It would be interesting basically because the wear behaviour of composites under low bearing loads and high sliding speeds can be of significance from practical applications point of view.

It can be seen from the results depicted in Fig.4.38 that the influence of sliding speed on the wear rate is more predominant at comparatively higher loads (1500 gms in the present work). Also, the drop in wear rate is maximum under the conditions of higher load mentioned above, when the sliding speed is raised from 9.4 to 14.1  $\text{m}\cdot\text{sec}^{-1}\times 10^{-2}$ . Thereafter, also, the wear rate decreases slightly for all the composites under all levels of bearing loads (500, 1000 and 1500 gms) if the sliding speed is further raised to 18.8  $\text{m}\cdot\text{sec}^{-1}\times 10^{-2}$ . The results of present investigation are in agreement with the findings of other

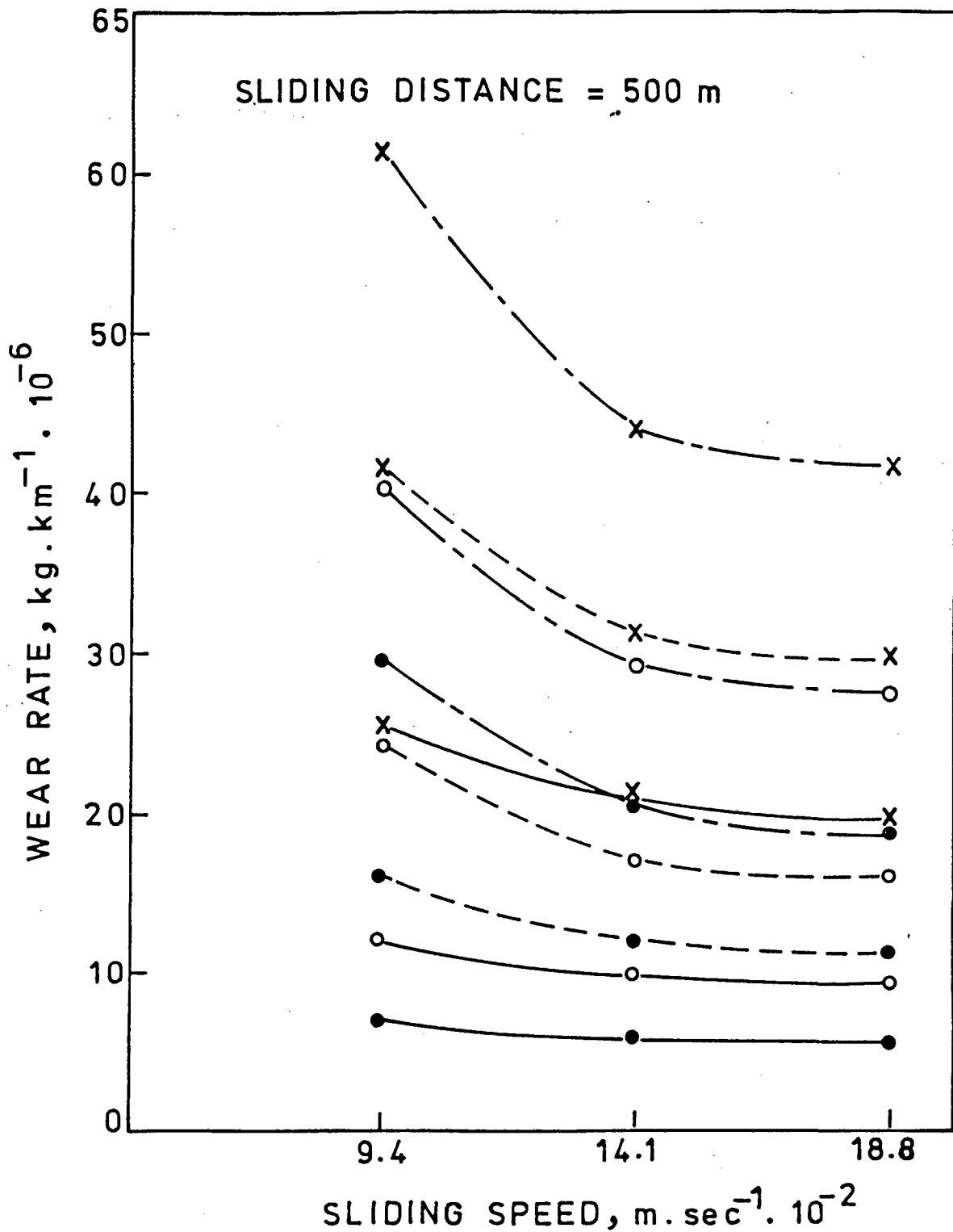


FIG.4.38 Wear rate of composite Nos.1 (x), 2(o) and 3(●) shown as a function of sliding speed at three different bearing loads of 500 gms. (———), 1000gms. (-----) and 1500gms. (- · - · -). Track length=500 m in each case.

workers such as Jasim and Dwarakadasa [124,126], Biswas and Pramila Bai [143] and Fukunaga [88]. Typical results of above workers are reproduced in Fig.Nos.4.39 [126], 4.40 [143] and 4.41 [88] respectively.

Varying explanations have been offered by different workers for this kind of behaviour of different metals, alloys and composites. Hirst and Lankaster [181] for example, suggest that with decreasing speed the subsurface undergoes repeated loading at increasing stress levels as the stress levels of welded joints increase. This gives rise to a fatigue type of failure in the substrate resulting in wear which increases with decreasing speed. N.P. Suh [127] on the other hand suggests that as the sliding speed increases, the interface temperature at the wear surface also increases. "The consequences of this temperature rise are : the decrease in the flow stress of metals, the formation of different oxide layers on the surface, which change the surface traction, phase transformations, and/or increased diffusion across the contact interface" [127]. It was shown by Razavizadeh and Eyre [182], Fig. 4.42, that the temperature of wear surface of different alloys progressively increases as the bearing load is systematically raised. Also, it was shown by Biswas and Pramila Bai [143] that there is a rapid initial increase in temperature at the wear interface and that this temperature rise assumes a steady state value after a certain sliding distance. They measured this rise of temperature in wear specimen at two different sliding speeds of  $4.17 \text{ m.sec}^{-1}$  and  $8.50 \text{ m.sec}^{-1}$ . Their typical results are shown in Fig.4.43.

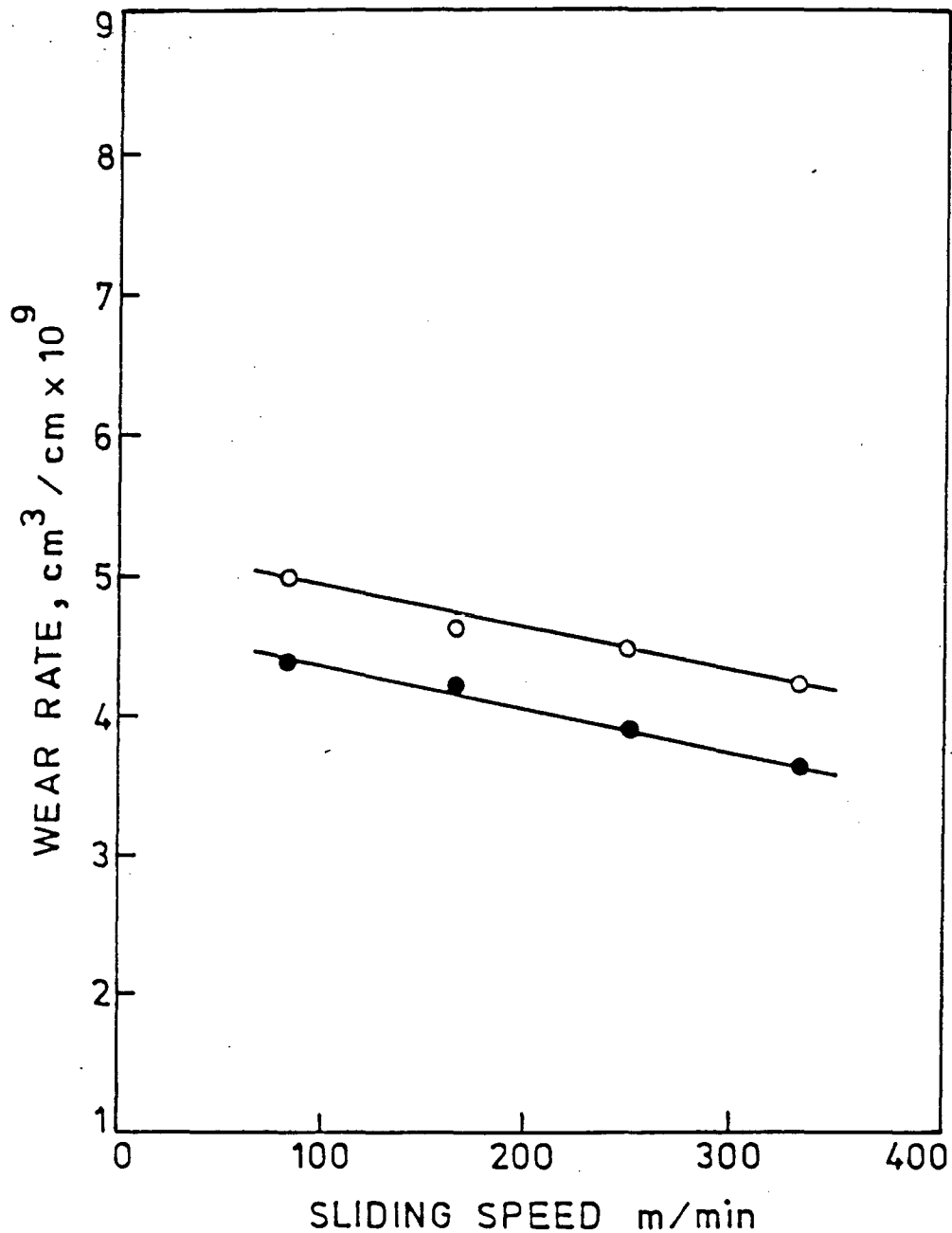


FIG.4.39 Effect of sliding speed on the wear rate in Al-22wt%Si (○) and pure aluminium (●) (bearing pressure, 13 KPa, sliding circle diameter, 180 mm; dry sliding on a steel surface of hardness 30HRC). (Ref.126)



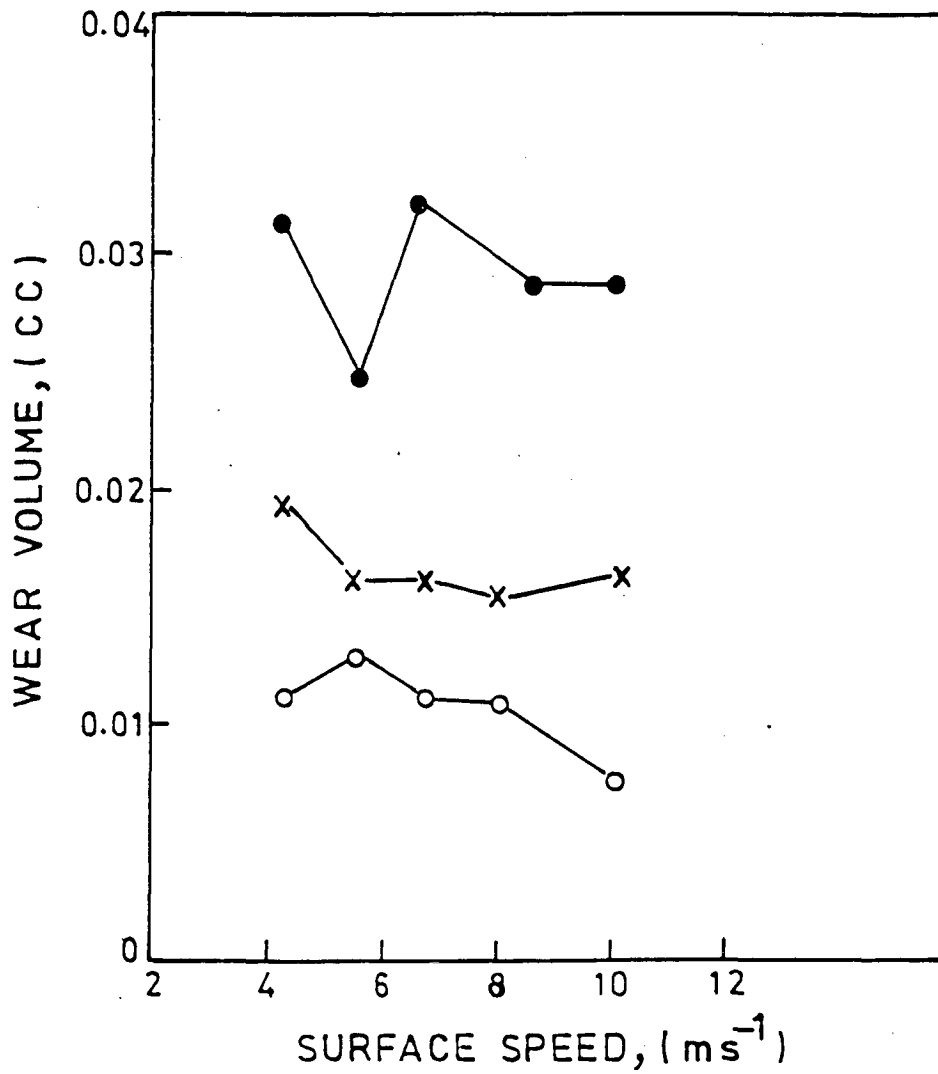


FIG.4.40 Wear loss vs. surface speed characteristics for base alloy (O), low graphite composite (x) and high graphite composites (●); (sliding distance,  $8 \times 10^3$  m; bearing pressure,  $0.08 \text{ kgf.mm}^{-2}$ ). (Ref.143)

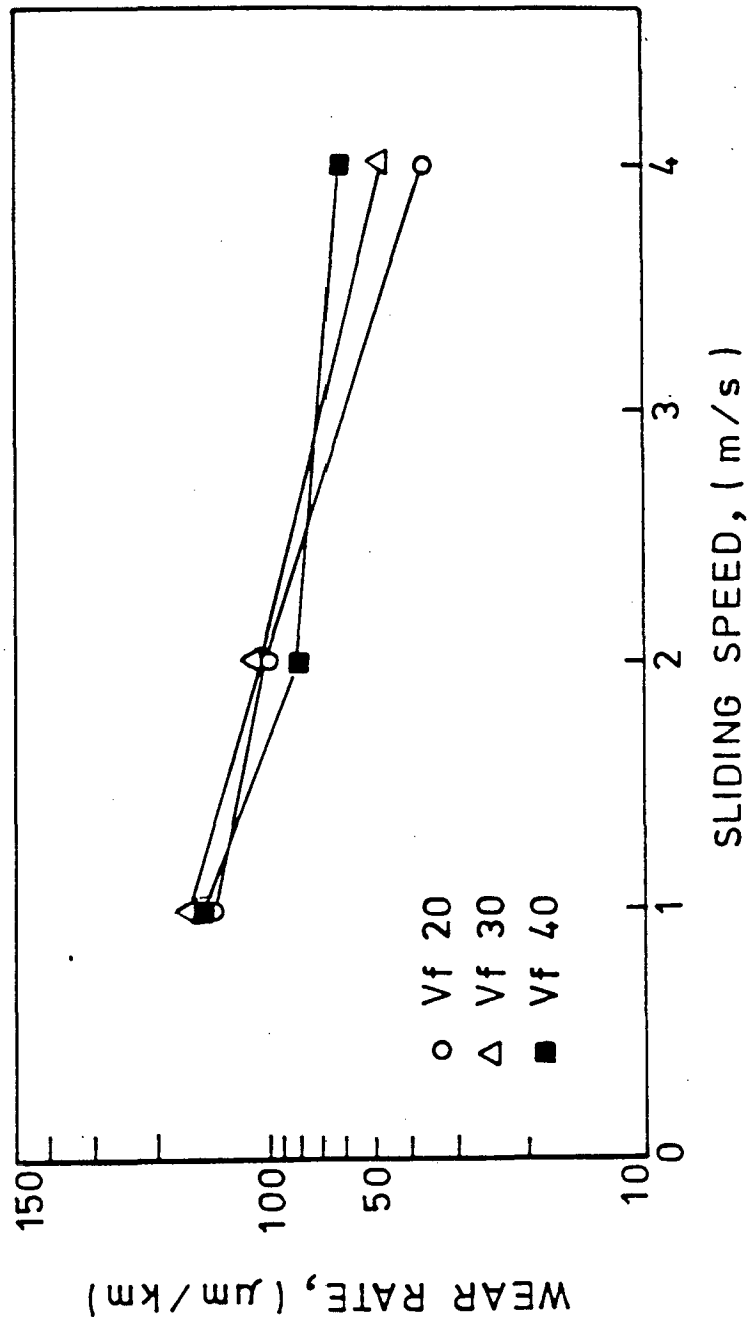


FIG.4.41 Effect of sliding speed and volume fraction of fibre on the wear rate of  $Al_2O_3/6061$  composite (load=4.9 N). (Ref.88)

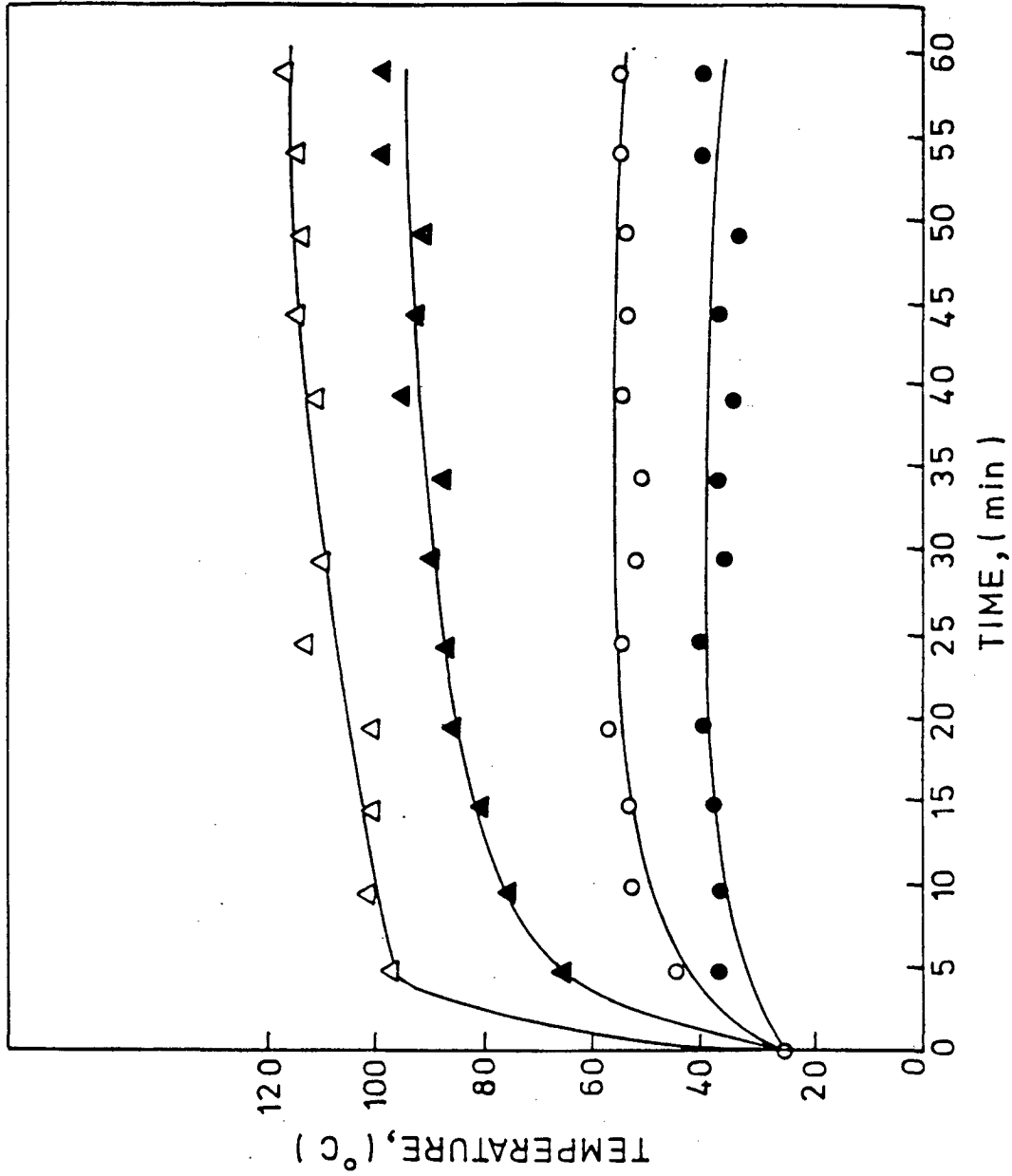


FIG.4.42 Temperature at a distance of 3mm from the rubbing surface on Al-16%Si-1%Cu alloy: ●-2 kgf; ○-8 kgf; ▲-12 kgf; Δ- 18 kgf.(Ref.182)

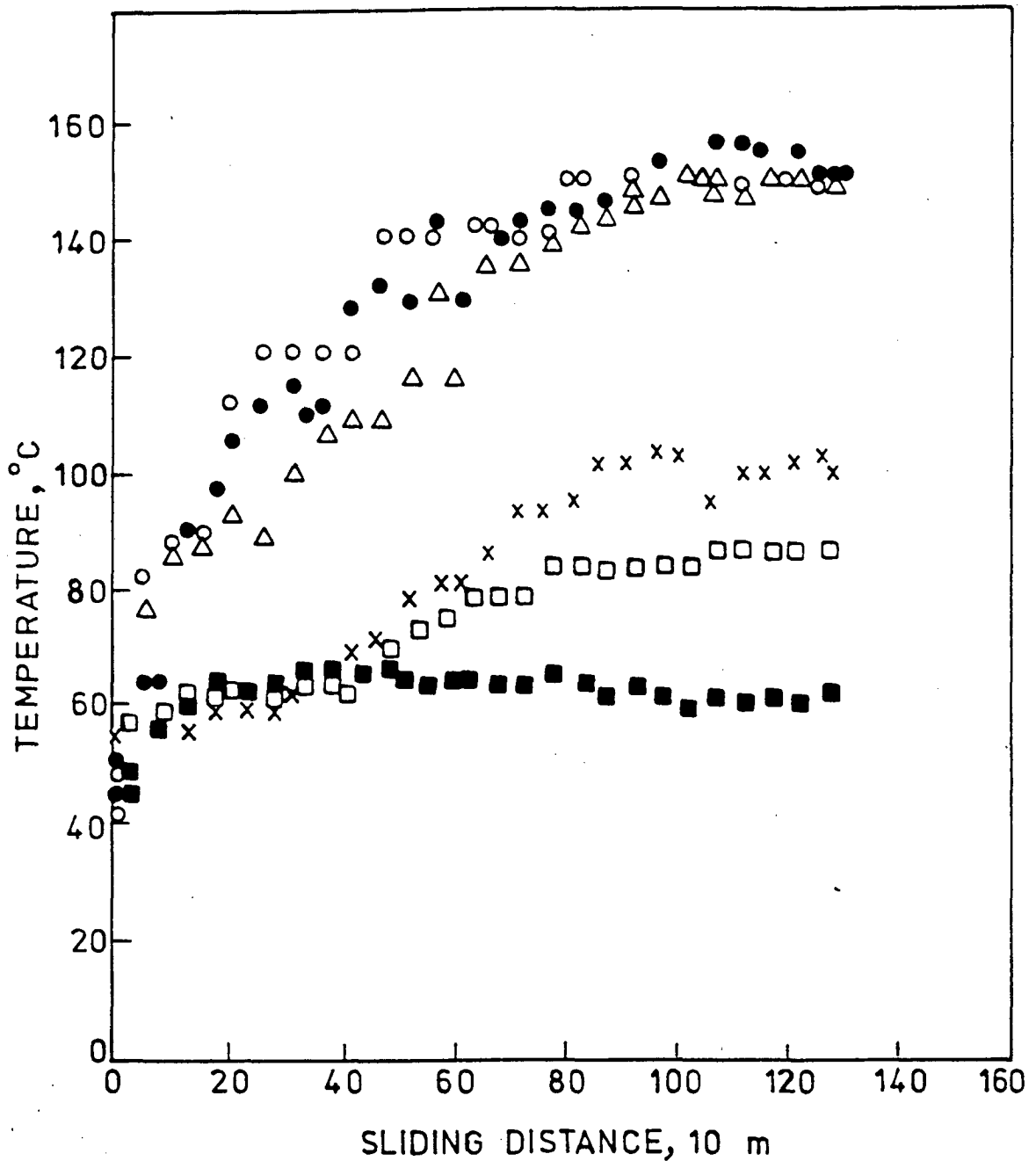


FIG.4.43 Temperature vs. sliding distance characteristics at two speeds  $4.17 \text{ m}\cdot\text{sec}^{-1}$  ( $\square, \blacksquare, x$ ) and  $8.5 \text{ m}\cdot\text{sec}^{-1}$  ( $\circ, \bullet, \triangle$ ):  $\square, \circ$ , base alloy;  $x, \triangle$ , low graphite composite;  $\blacksquare, \bullet$ , high graphite composite. (Ref.143)

It can be seen from their results that a relatively higher temperature is developed at a comparatively higher sliding speed.

It is thus apparent that the frictional heating plays an important role in influencing the wear rate of materials. Increasing temperature at the interface implies a decrease in plastic deformation because 85% of the energy input for plastic deformation is generally dissipated as heat [143]. The temperature characteristics in turn can be expected also to influence the strength of the welded junction and subsurface shear strength adversely. It is thus apparent from the above reasoning that increasing temperatures developed at the wear interface at comparatively higher sliding speeds are responsible for a decrease in the wear rate. This perhaps can be a probable explanation for the kind of behaviour obtained in Fig. 4.38 in case of present composites also. The argument advanced by Fukunaga [88] is also nearly on the same lines as he suggests that perhaps the formation of ferrous oxide film on the sliding surface due to the rise of temperature at the interface is responsible for the lower wear rates obtained at higher sliding speeds.

#### **4.4.4 EFFECT OF SLIDING DISTANCE ON THE WEIGHT LOSS DURING WEAR**

Results pertaining to this study are summarised in Fig. Nos. 4.44, 4.45 and 4.46. These results are plotted at three different sliding speeds namely 9.4, 14.1 and  $18.8 \times 10^{-2}$  m.sec<sup>-1</sup>. At a particular sliding speed, the wear pin traverses a fixed length of distance because the duration of wear test was limited to a

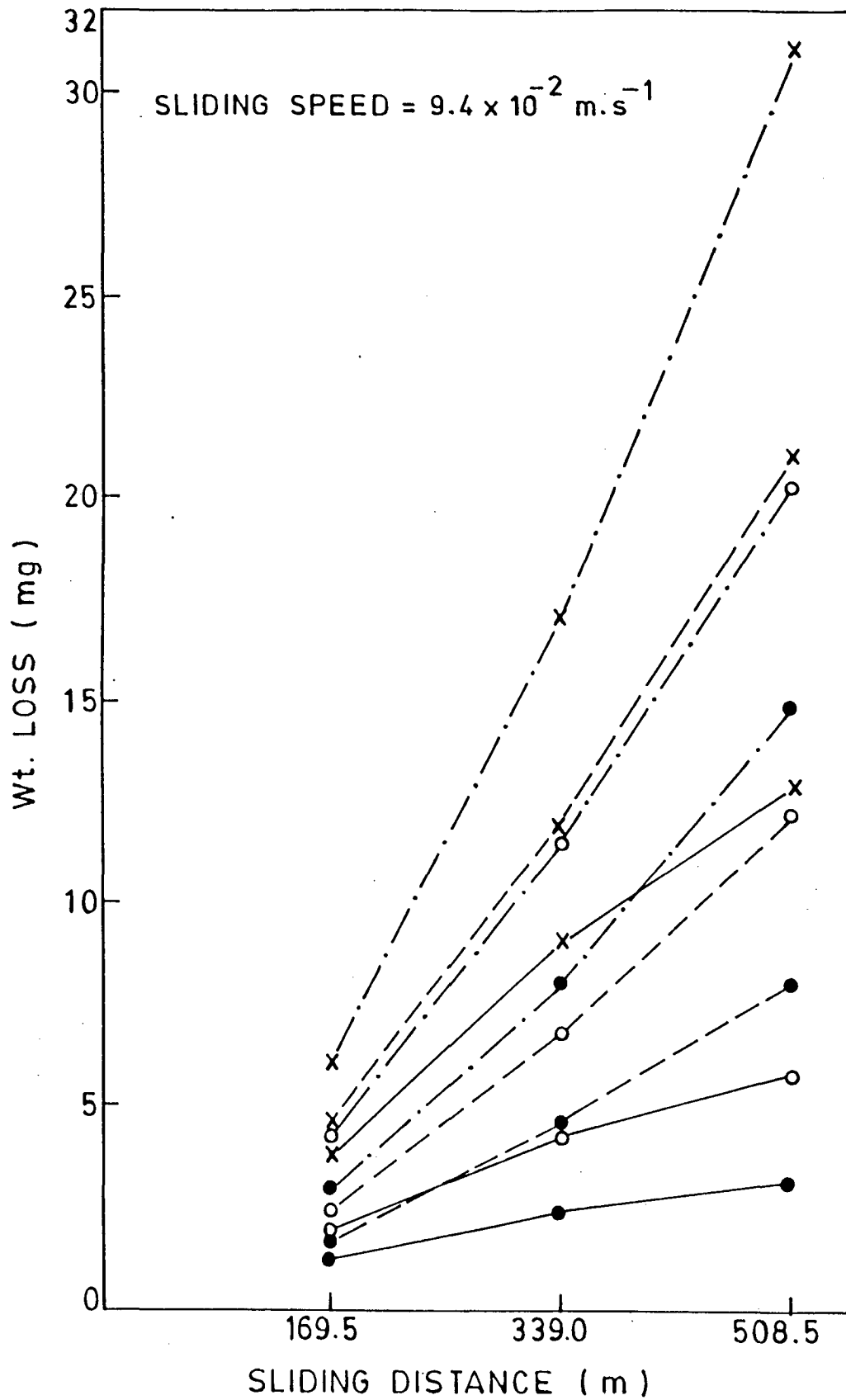


FIG.4.44 Weight loss (mg) plotted as a function of the sliding distance(m) for composite No.1(x), composite No.2(o), and composite No.3(●) at a sliding speed of  $9.4 \times 10^{-2} \text{ m.sec}^{-1}$  and three different bearing loads namely: 500 gms(—), 1000gms.(---) and 1500 gms.(-.-).

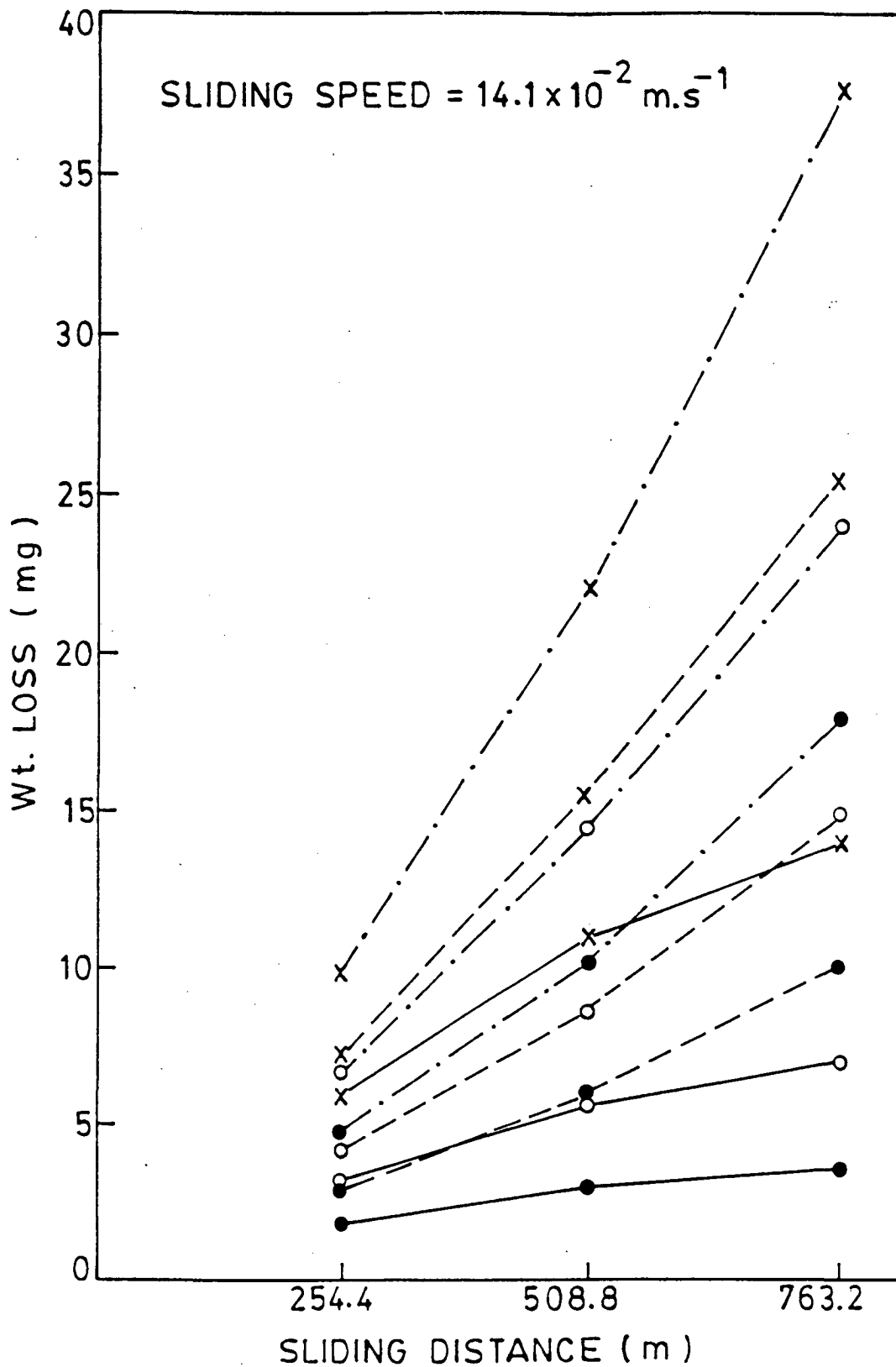


FIG.4.45 Weight loss (mg) plotted as a function of the sliding distance (m) for composite No.1(x), composite No.2(o), and composite No.3(●) at a sliding speed of  $14.1 \times 10^{-2} \text{ m.sec}^{-1}$  and three different bearing loads namely: 500 gms. (—), 1000 gms. (---) and 1500 gms. (-.-).

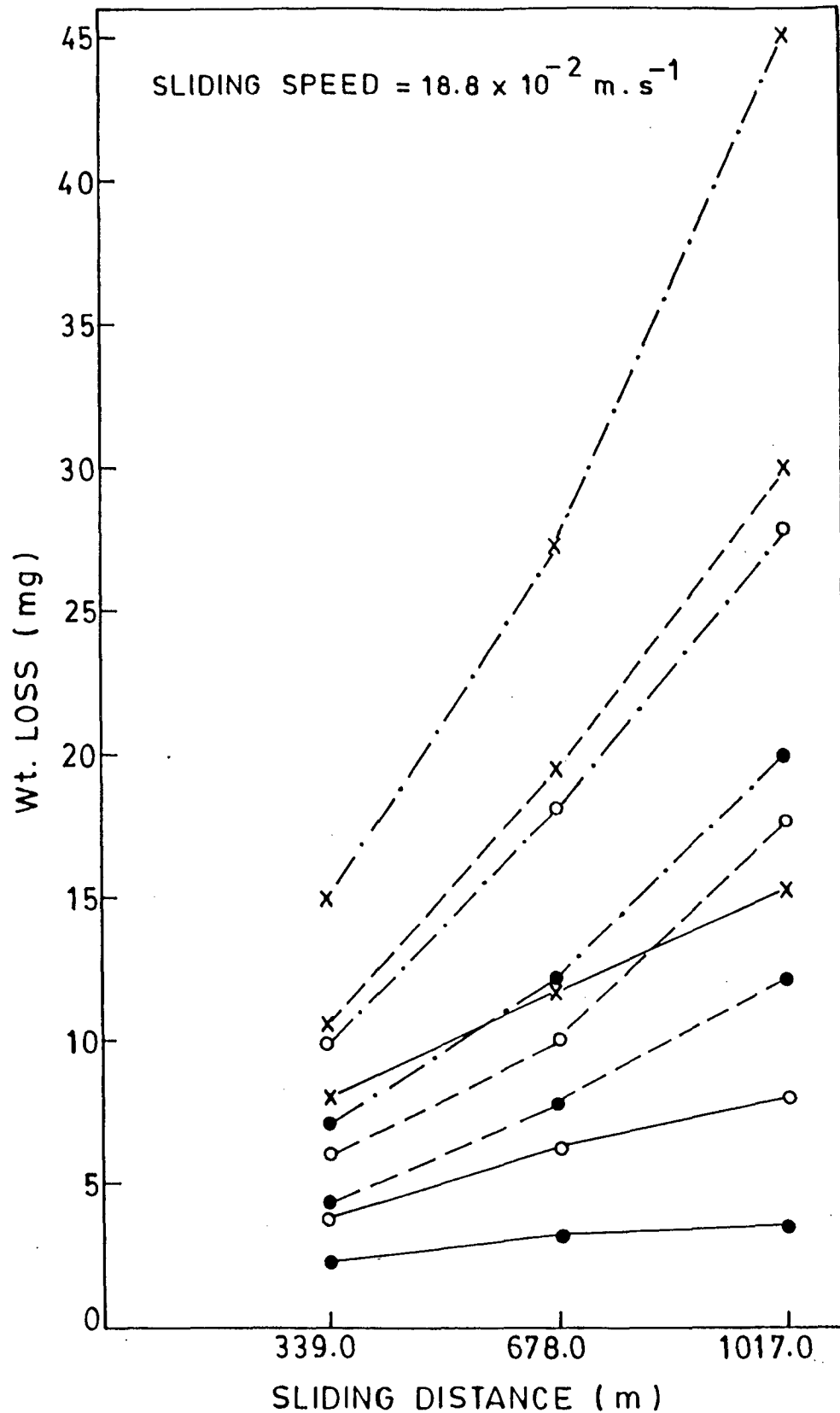


FIG. 4.46 Weight loss (mg) plotted as a function of the sliding distance (m) for composite No.1(x), composite No.2(o), and composite No.3(●) at a sliding speed of  $18.8 \times 10^{-2} \text{ m. sec}^{-1}$  and three different bearing loads namely: 500 gms. (—), 1000 gms. (---) and 1500 gms. (-.-).



maximum period of 90 minutes only. It is for this reason that different levels of sliding distances can be seen to be plotted in Fig.Nos.4.44, 4.45 and 4.46. However, inspite of this limitation, each curve shows almost identical characteristics with respect to the influence of sliding distance on the weight loss during wear. An attempt has been made to plot the results pertaining to the three composites under investigation at all the three bearing loads employed.

It can be seen from the results that in general, composite No.1 undergoes maximum amount of wear under all possible variations of experimental conditions. Also it is apparent from the results that composite No.3 displays minimum amount of wear compared with composite No.2 and 1 under different test conditions. It can be seen from Fig.4.44 that composite No.3 undergoes a wear of only 3.42 mg at 500 gm bearing load even though the wear pin had traversed a distance of 508.5m while composite No.1 under similar condition of bearing load shows a weight loss of 3.72 mg at the minimum sliding distance of 169.5m.

At the corresponding sliding distance of 508.5m and 500 gm bearing load, the composite No.1 shows a weight loss of 12.82 mg which is nearly 4 times the amount of wear undergone by composite No.3. Similar features can be noted from Fig.4.45 and Fig.4.46 plotted at progressively increasing sliding speeds. These curves serve the purpose of comparing the practical performance of the three composites under varying experimental conditions. Similar curves were plotted by other investigators also to bring about the distinct differences between the performances of an ordinary

matrix and the matrix stiffened by some reinforcing constituents. For example, the results of Hosking et.al. [62] shown in Fig.4.47 display how the performance of 2014 alloy stiffened with 20 wt.%(16  $\mu\text{m}$ ) SiC particles is superior to 2024 alloy reinforced with 20 wt.%(16  $\mu\text{m}$ )  $\text{Al}_2\text{O}_3$  particles. In a similar attempt, Yang and Chung [157] compare the performance of different composite materials as a function of sliding distance in Fig.4.48. In another meaningful study, Fukunaga [88] has also compared the performance of a number of composites as a function of the sliding distance (Fig.4.49). Fukunaga has called this curve as "wear progressive curve" and his results are plotted for a sliding speed of  $1 \text{ m}\cdot\text{sec}^{-1}$  and normal bearing load of 4.9N and as expected, all the ceramic fibre reinforced composites display excellent wear resistance compared to ordinary brass employed in his set of experiments. At the same time, the wear resistance of fibre reinforced composites increased with progressive increase in the volume fraction of fibres, which will be entirely expected.

It is indeed extremely difficult to compare the results of present study with the finding of other workers, although the trend of results obtained in case of present composites bear a striking similarity with the findings of other workers [62,88,157]. It is mainly because of the following constraints that an accurate comparison of results becomes difficult:

a) The experimental rig and the procedure adopted in each case is different in its details.

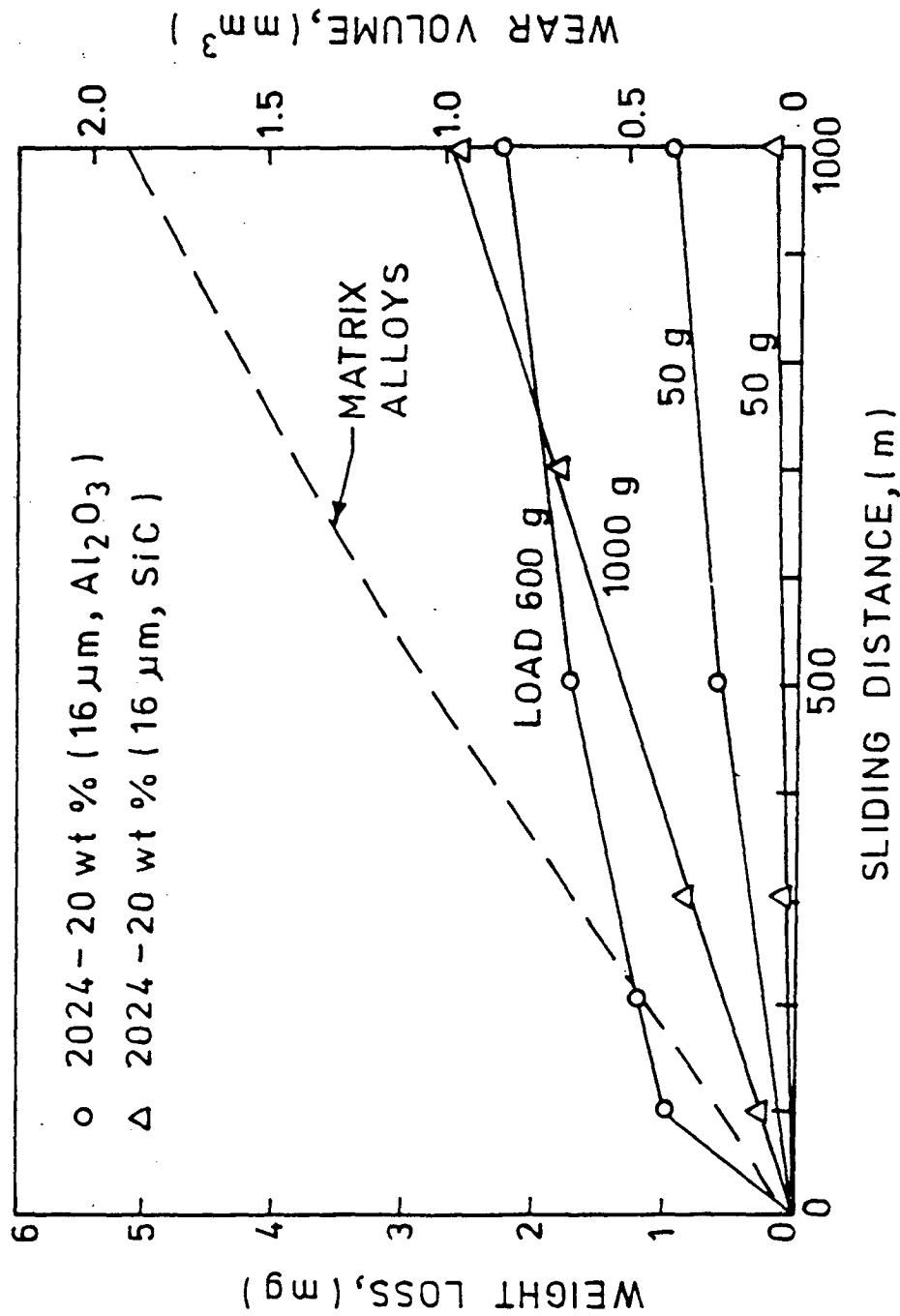


FIG.4.47 Comparison of the wear behaviour of composites containing SiC and Al<sub>2</sub>O<sub>3</sub> particles. (Ref.62)

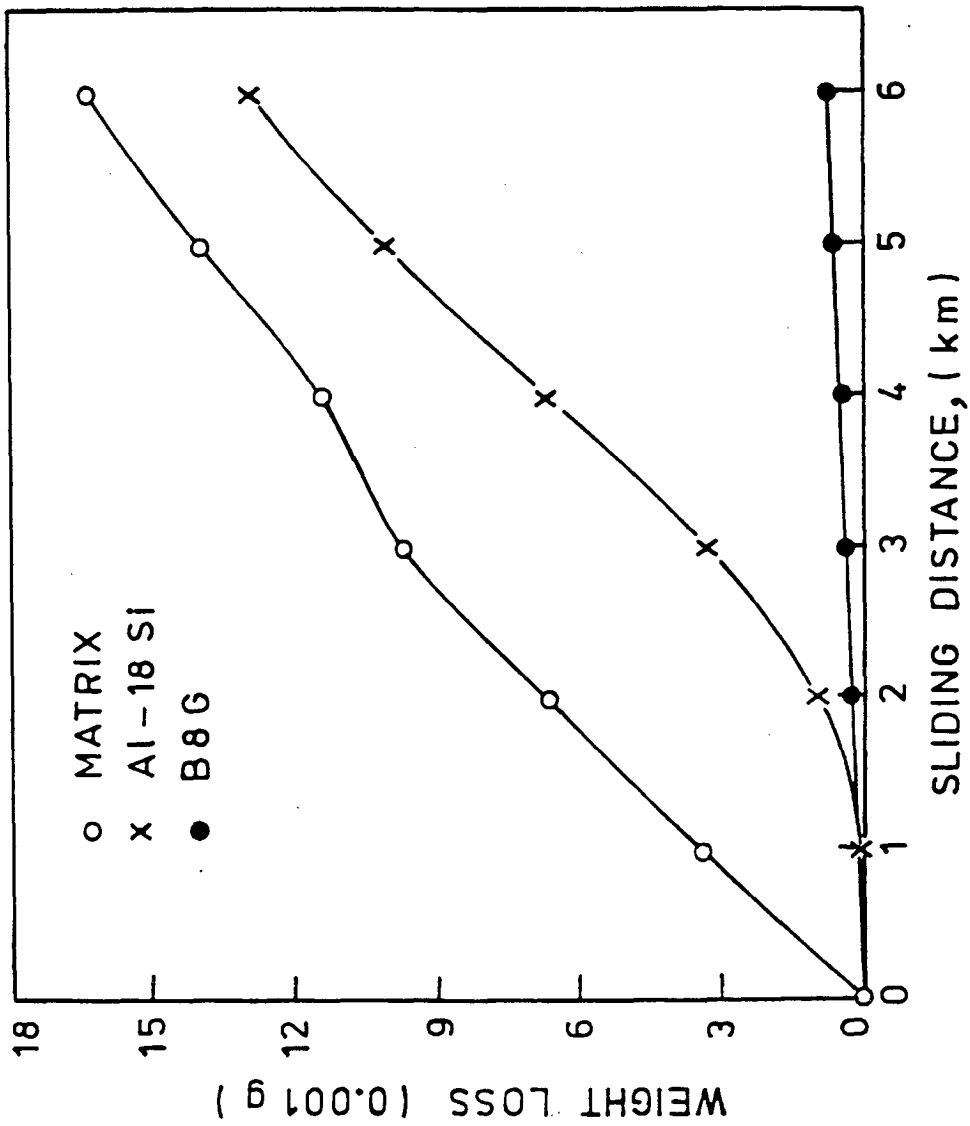


FIG.4.48 Wear weight loss vs. sliding distance of the matrix, Al-18 Si alloy and B8G (8wt% bauxite and 3wt% uncoated graphite dispersed in Al-12Si-1.4Cu-1.3Mg a base alloy) composite. (Ref.157)

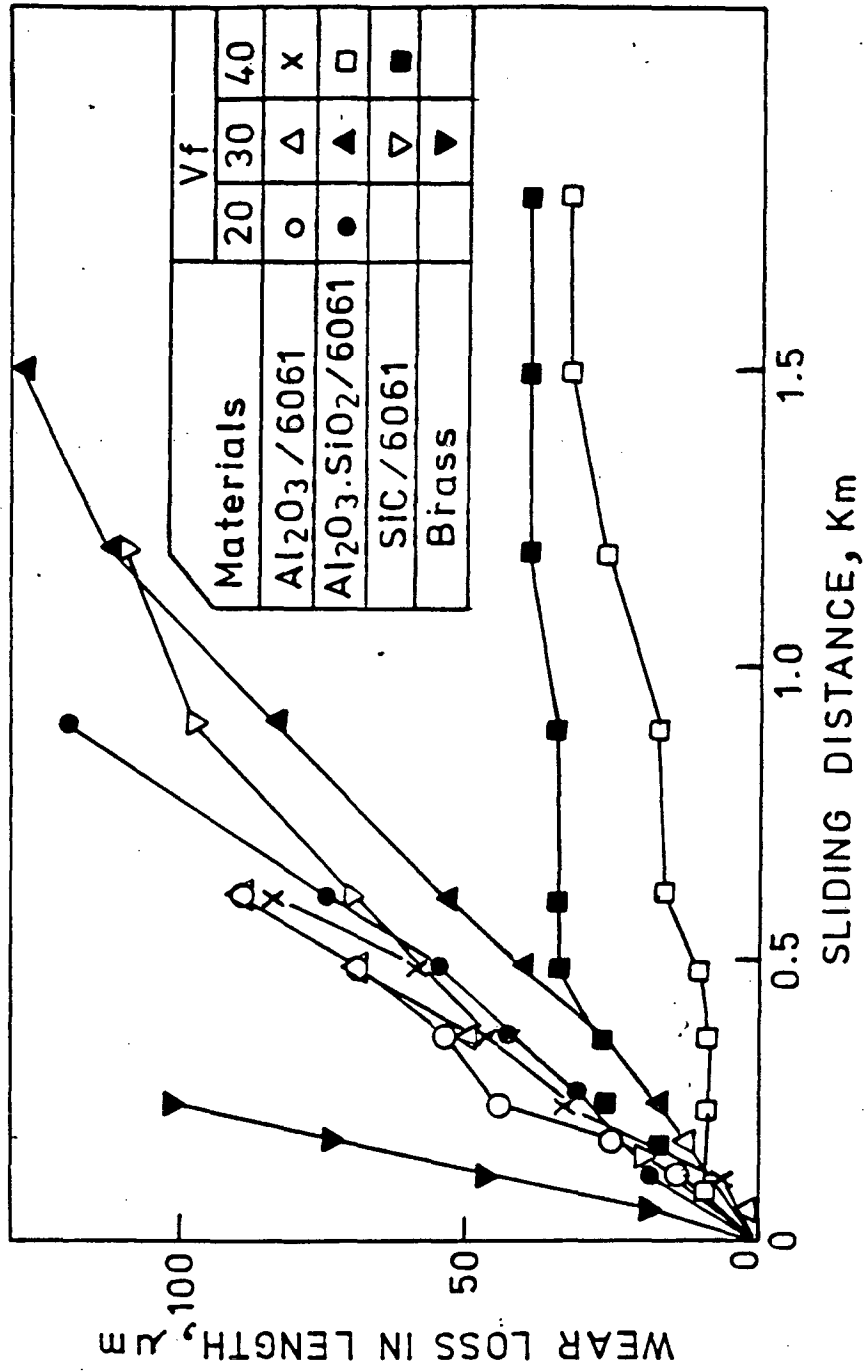


FIG.4.49 Wear progressive curves of ceramic fibre-reinforced aluminium alloy composites (load=4.9 N, speed = 1 m.sec<sup>-1</sup>). (Ref.88)

b) The range of bearing loads, the sliding speeds, and the track lengths employed in each case are widely different.

Nevertheless, if the results of present study are compared with the findings of Hosking et.al.[62], Fig.4.47, it can be seen that the wear behaviour of 2024-20 wt%(16  $\mu\text{m}$ )  $\text{Al}_2\text{O}_3$  composite is superior than the behaviour of composite No.3 (of present investigation). 2024-20 wt%(16  $\mu\text{m}$ )  $\text{Al}_2\text{O}_3$  composite shows a weight loss of nearly 1.8 mg at 600 gm bearing load and 500 meters track length. In comparison, composite No.3 displays a weight loss of 3.4 mg (Table-4.10) at 500 gm bearing load and a track length of 508.5 meters. The sliding speed was nearly identical in both the cases. The superior wear resistance displayed by 2024-20 wt%(16  $\mu\text{m}$ )  $\text{Al}_2\text{O}_3$  composite as against composite No.3 can be attributed to a number of reasons. Firstly, it may be because of a very small area of contact between the wear counterface surface and the wear pin since in this case Hosking et.al. [62] employed a steel ball to rub against the composite specimen of 80 mm dia and 2.4 mm thickness and secondly because a considerably higher amount of  $\text{Al}_2\text{O}_3$  particles of a fixed size (20 wt%, 16  $\mu\text{m}$  average size) were dispersed in 2024 alloy. As against the above case, only 12-13% $V_f$  retention of  $\text{Al}_2\text{O}_3$  was obtained in composite No.3. Also, the matrix of this composite was commercially pure aluminium and not an alloy. As such, 2014-20 wt%(16  $\mu\text{m}$ )  $\text{Al}_2\text{O}_3$  composite would be expected to be much harder and stronger than composite No.3. This factor plus a comparatively smaller area of contact at the wear interface are probably responsible for a comparatively lower

weight loss obtained in the composite investigated by Hosking et.al. [62]. These comparisons, however, should be taken with caution as experimental conditions and the strategy adopted by different workers are widely different from each other. Another reason why these comparisons are difficult to be made is also because of varying methods adopted by different workers to represent their weight loss/wear rate data. This particular parameter of material loss during wear is variously represented as mg., loss in length in terms of  $\mu\text{m}$ , loss in volume in terms of c.c. etc. For accurate comparisons, therefore, exactly identical experimental conditions should be available, which is rarely the case with available scientific literature.

#### 4.4.5 INFLUENCE OF SQUEEZE PRESSURE ON THE WEAR BEHAVIOUR

The concluding result of present study is shown in Fig.4.50 in which wear behaviour of composite Nos. 1,2 and 3 is compared under three different experimental conditions. It is apparent from the results that wear resistance of Al- $\text{Al}_2\text{O}_3$ -MgO particulate MMCs progressively improves as the degree of squeeze pressure applied during the fabrication of composites is systematically raised in steps. It would, therefore, be expected that the wear resistance of these composites would improve further if the degree of squeeze pressure is taken to still higher levels such as 160 to 240 MPa. At the same time, it can be surmised from the above observations that the wear resistance of Al- $\text{Al}_2\text{O}_3$ -MgO particulate MMCs would improve further if the  $\%V_f$  retention of  $\text{Al}_2\text{O}_3$  in the composite is further raised to higher levels such as 20-22%. It would be worth extending the

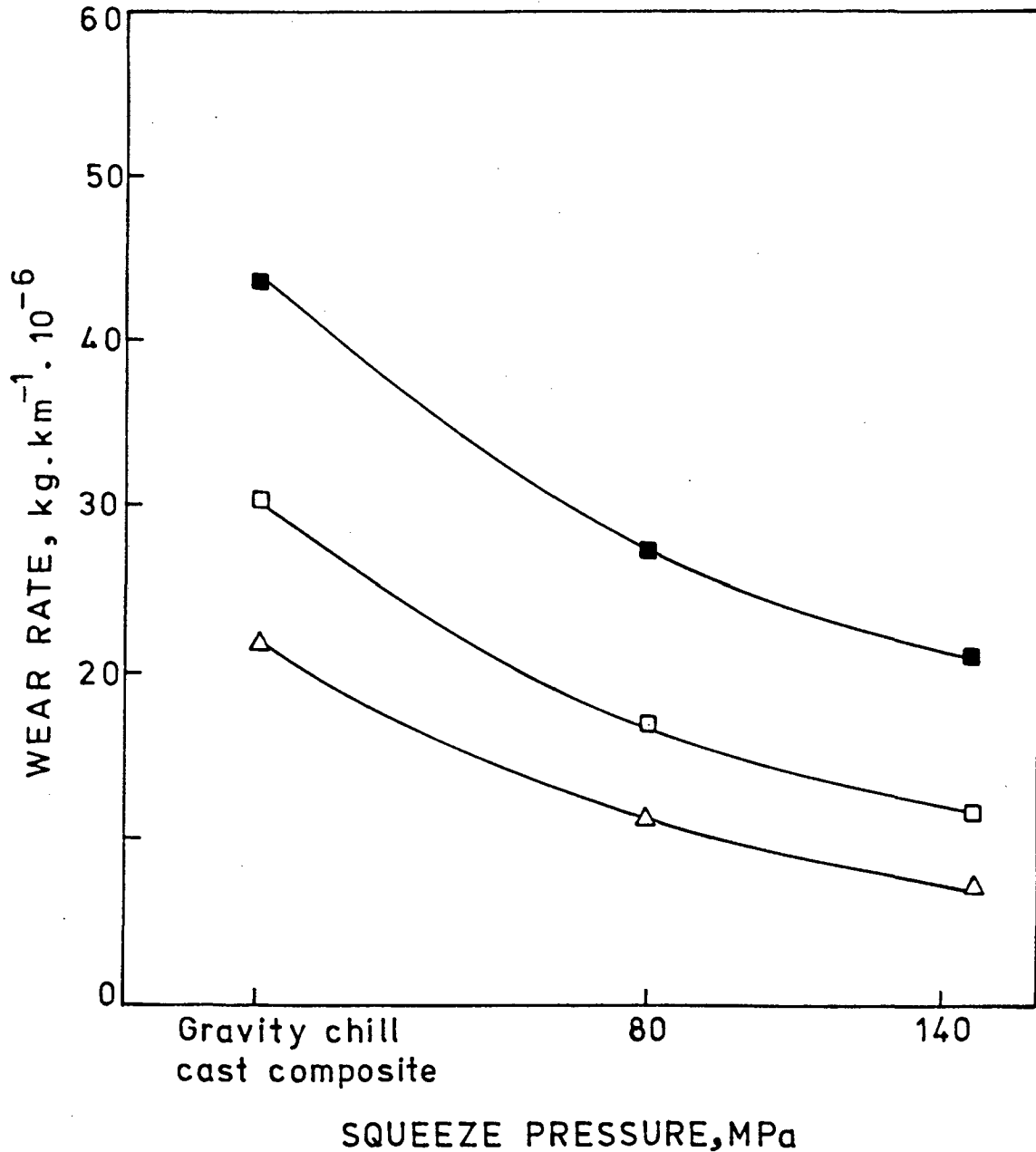


FIG.4.50 Wear rate shown as a function of the degree of squeeze pressure applied during the fabrication of composites under three different conditions of wear;  
 (△) - Load=500gms, sliding speed= $9.4 \text{ m} \cdot \text{sec}^{-1} \cdot 10^{-2}$ , track length=169.5 m.  
 (□) - Load=1000gms, sliding speed= $14.1 \text{ m} \cdot \text{sec}^{-1} \cdot 10^{-2}$ , track length=508.8 m.  
 (■) - Load=1500gms, sliding speed= $18.8 \text{ m} \cdot \text{sec}^{-1} \cdot 10^{-2}$ , track length=1017 m.



present study in the above direction.

A similar improvement in the wear behaviour of Al-Si alloys has been reported by a number of workers [123-126, 130, 178, 179] when the Si content in the alloy is gradually raised to near eutectic level. The wear resistance of Al and Al-Si alloy is reported to be improved with progressive addition of  $\text{Al}_2\text{O}_3$  particles to the matrix [44]. In a similar kind of study the wear resistance of 2024 alloy was shown to improve progressively when increasing size and quantity of  $\text{Al}_2\text{O}_3$  particles were added to the matrix. Also, in this study, SiC particles were shown to impart greater wear resistance to 2014 alloy compared with 2024 alloy reinforced with  $\text{Al}_2\text{O}_3$  particles [62]. In a relatively recent study, Yang and Chung [157] demonstrated that with increasing volume fraction of hard Bauxite particles, the wear resistance of Al-12 Si-1.4 Cu-1.3 Mg matrix alloy progressively improved.

An examination of above results reveals that there can be two approaches to improve the wear resistance of matrix alloy. One of these can be to introduce hard, ceramic particles/discontinuous fibres in the matrix alloy in optimum amount and size. The second approach can be to obtain a strong, tough, densified, porosity free and grain refined matrix through the process of squeeze casting or liquid forging. The present class of Al- $\text{Al}_2\text{O}_3$ -MgO MMCs display a yet another approach in which a fixed level of dispersion of hard ceramic  $\text{Al}_2\text{O}_3$  particles is obtained through the liquid metallurgy route and then subsequently the stirred slurry is squeezed between 80 and 140

MPa to obtain a densified, tough and grain refined composite. The procedure adopted in the present case, therefore, represents a combination of the two strategies mentioned above. In this particular approach, if the  $\%V_f$  retention of  $Al_2O_3$  is progressively raised and if the degree of squeeze pressure applied is taken to still higher levels such as 160 to 240 MPa, much better quality of composites can be expected to be produced with far superior wear resistant properties. The wear resistance of these composites can further be improved if the matrix of composites is changed from the existing ordinary aluminium to some suitable high strength alloy such as 2024 or 2014.

The above class of composites would thus have the combined advantage of both the hard ceramic particles as well as a grain refined and densified base matrix in improving the wear resistance of composites. A grain refined and densified base matrix displays superior wear resistance basically because fine grained structure is more difficult to deform owing to piling up of dislocations along the grain boundaries [183]. This is the basic reason why the strength, toughness and ductility of squeezed composites simultaneously improve with progressive increase in the degree of squeeze pressure applied during the fabrication of such composites [169-172, 175]. Basically, grain boundaries provide obstacles to a free movement of dislocations. As the orientation of the crystals on either side of a grain boundary is different and random, a dislocation moving on a common slip plane in one crystal can rarely move onto a similar slip plane in the adjacent crystal. So, the dislocations are

stopped by a grain boundary and pile up against it [183]. And greater is the surface area of grain boundaries, as is the case with fine grained structure, the greater will be extent of piled up dislocations along grain boundaries and therefore, harder will be the structure and the more difficult it will be to deform such a structure.

Interestingly again this particular route of squeeze casting can be successfully applied for the manufacture of strong and tough 'near net shape' castings with excellent wear resistant properties, where machining can also be minimised. This aspect is important basically because the machining of composites containing hard ceramic particles larger than 50  $\mu\text{m}$  is reported to be difficult even when diamond or nitride edge tools are employed [157].

It can be seen from the results of present investigation that the overbearing factor influencing the wear behaviour of squeezed composites is the bearing load. Sliding speed and sliding distance have relatively little influence. The effect of degree of squeeze pressure applied on the wear rate of composites becomes more pronounced as the bearing load is systematically raised from 500 to 1500 gm. At 500 gm bearing load, composite No.1 shows a wear rate of  $21.9 \text{ kg.km}^{-1} \times 10^{-6}$ , while composite No.3 shows a wear rate of only  $7.7 \text{ kg.km}^{-1} \times 10^{-6}$  under exactly identical conditions of slowest sliding speed ( $9.4 \text{ m.sec}^{-1} \times 10^{-2}$ ) and the smallest track length traversed (169.5m). The above comparison shows that the wear rate of composite No.3 is lower by a margin of  $14.2 \text{ kg.km}^{-1} \times 10^{-6}$

compared to composite No.1. This difference magnifies to 18.4 and  $23 \text{ kg.km}^{-1} \times 10^{-6}$  at 1000 gm and 1500 gm bearing loads respectively although the sliding speeds and track length traversed in the two cases mentioned above progressively increased (the sliding speed and track length respectively in the two cases are:  $14.1 \text{ m. sec}^{-1} \times 10^{-2}$ , 508.5m and  $18.8 \text{ m. sec}^{-1} \times 10^{-2}$ , 1017m). These results suggest that composite No.3 is not as sensitive to progressively increasing bearing loads (from 500 gm to 1500 gms) as is composite No.1. This is primarily because, the matrix of composite No.3 is relatively more dense, strong & grain refined and therefore material removal during wear in this particular case is relatively more difficult compared to composite No.1 even though the bearing load is increased in steps from 500 to 1500 gms. It is basically because of this reason that the performance of composite No.3 is the best under all circumstances of wear conditions.

Referring to the data plotted in Fig.4.50, it can be seen that the influence of the degree of squeeze pressure applied on the wear behaviour of composites under three different wear conditions (enumerated above) is nearly identical. As discussed above and as also apparent from Fig.4.50, gravity chill cast composite (composite No.1) exhibits maximum amount of wear followed by composite No.2 (80 MPa, ambient die temperature) and then composite No.3 (140 MPa, ambient die temperature). If the difference between the maximum and minimum wear rates of different composites is computed (at 1500 gms and 500 gms bearing loads respectively), it can be seen that composite No.1 shows

maximum difference ( $44.1 - 21.9 = 22.20 \text{ kg.km}^{-1} \times 10^{-6}$ ). This data for composite No.2 can be seen to be 16.3 ( $27.5 - 11.2 = 16.3 \text{ kg.km}^{-1} \times 10^{-6}$ ) and it further decreases to 13.4 ( $21.1 - 7.7 = 13.4 \text{ kg.km}^{-1} \times 10^{-6}$ ) in case of composite No.3. An analysis of this data shows that composite No.1 is most sensitive to an increase in bearing load, and other corresponding wear conditions. But as the composite is squeezed at 80 and 140 MPa, this sensitivity progressively decreases. The net objective of this analysis is to show that as the degree of squeeze pressure is systematically raised, the composite becomes more and more wear resistant.

A quantitative comparison of the wear data obtained in the present work with the findings of other workers particularly with regard to the influence of squeeze pressure on the wear behaviour of composites is difficult to be made as precise data on this aspect is really scarce. Some data on the wear behaviour of squeezed composites no doubts is available. But the problem with such cases is that the composite has been prepared at a fixed squeezed pressure and its wear behaviour has been evaluated under varying experimental conditions. For example, Fukunaga [88] prepared 6061-discontinuous  $\text{Al}_2\text{O}_3$  fibre and alumina-silicate fibre reinforced composites at 49 MPa using the fibre-preform temperature of  $550^\circ\text{C}$  and then evaluated the wear behaviour of these composites under dry sliding conditions. Similarly, Hosking et.al. [62] prepared 2024- $\text{Al}_2\text{O}_3$  and 2014-SiC reinforced particulate composites at a squeeze pressure of 200 MPa. Moreover, the composites prepared by Hosking et.al. were of the type of high volume fraction dual layered composites. In a

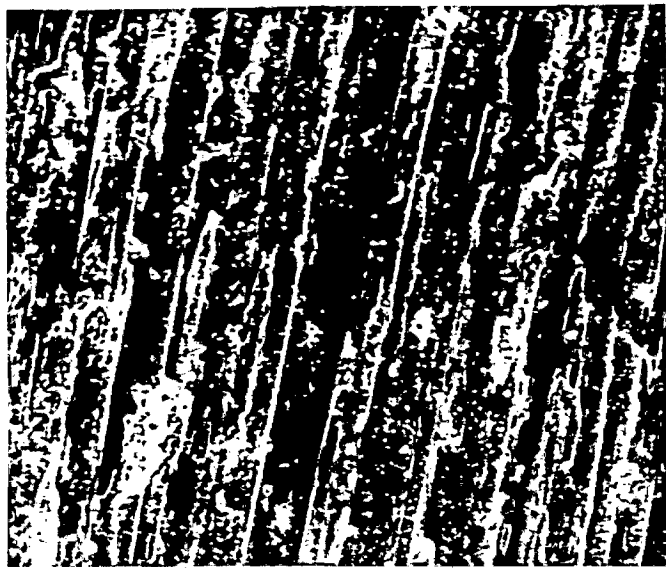
similar kind of study, Verma and Dorcic [7] have compared the wear properties of three different materials namely A206-T<sub>7</sub> aluminium alloy reinforced with an unknown reticulated ceramic foam, aluminium alloy A206 reinforced with discontinuous fibres of Al<sub>2</sub>O<sub>3</sub> and SiO<sub>2</sub> and induction hardened AISI 4315 alloy steel. They have shown in this study that the abrasive wear resistance of Al<sub>2</sub>O<sub>3</sub>-SiO<sub>2</sub> fibre reinforced metal matrix composites is comparable with the behaviour of induction hardened AISI 4315 alloy steel. But the exact pressure at which the above fibre reinforced composites were prepared is not mentioned in their work. It is thus apparent from the above examples that firstly, the above investigators did not study the influence of varying squeeze pressure on the wear behaviour of resulting composites. And secondly, the reinforcing medium, the matrix employed and the method of preparation of composites is different from each case. Under these circumstances the results of present study cannot be compared with the findings of above workers.

But it can safely be concluded from the results of present study that applying a higher squeeze pressure during the fabrication of particulate MMCs can be a possible means of improving the wear resistance of such composites. The wear resistance of squeezed Al-Al<sub>2</sub>O<sub>3</sub>-MgO particulate composites can be improved further if in addition to the above, the matrix of composite is changed to an alloy responding to heat treatment, and if the %V<sub>f</sub> retention of Al<sub>2</sub>O<sub>3</sub> is further raised to 20 to 22%. Also, as suggested previously, the squeeze pressure can also be taken to higher levels such as 160 to 240 MPa. The sum

total of all these steps would result in the preparation of a composite with distinctly superior wear resistance properties.

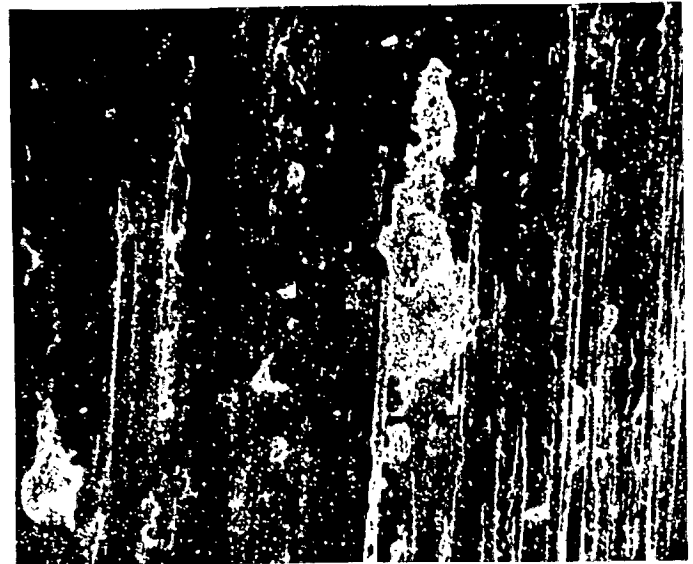
#### 4.4.6 TEXTURE OF WORN SURFACE AND THE DEBRIS MATERIAL

An overall view of the texture of the worn surface of composites is shown in Figs.4.51, 4.52 and 4.53. For example, a typical V grooved texture of the worn surface of composite No.1 at 500 gm load,  $18.8 \text{ m sec}^{-1} \times 10^{-2}$  sliding speed and a track length of 1017 meter is shown in the SEM pictures in Fig.4.51(a-d). Other features relating to the worn surface at comparatively higher magnification are shown in Fig.4.52(a-d). Typical SEM pictures shown in Fig.4.53(a and b) depict how material is removed on the edge of the wear pin. SEM pictures shown in Fig.4.51(a and b) typically depict a combination of adhesive cum abrasive wear processes in which the latter seems to be predominant. It can be seen from Fig.4.51(a and b) that in addition to the presence of usual V grooves, large patches of detached debris material can still be seen adhering to the worn surface. This is typically indicative of a combination of both the adhesive as well as abrasive processes occurring simultaneously in the wear pin. On a closer examination it was found that these patches (small and big) adhering to the worn surface consisted of an assemblage of fragmented pieces of the matrix. Also, this fragmented matrix material was in the process of being dislodged from its original position. When these fragmented pieces are dislodged in stages they tend to form the debris material. Features shown in Fig.4.51(a and b) were commonly observed in case of all the composites. In addition to



a

x80



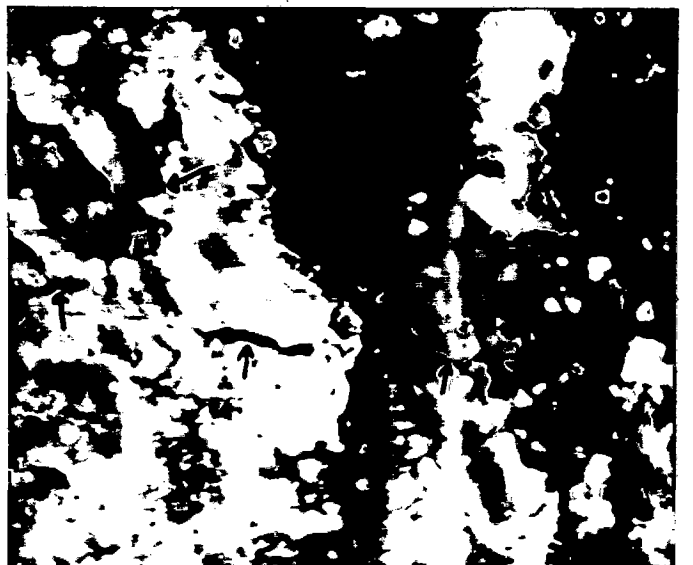
b

x80



c

x320



d

x1250

FIG.4.51 SEM pictures of the worn surface of composite No.1 under 500gm bearing load,  $18.8 \text{ m} \cdot \text{sec}^{-1} \times 10^{-2}$  sliding speed and 1017 m track length.

(a) and (b) show typical scoring marks, grooves and worn patches adhering to the worn surface, (c) and (d) showing grooved worn surface littered with fragmented fine debris material. Note numerous wide and deep tracks occurring in the displaced material on the ridge of grooves. Some of these cracks are marked by arrows.



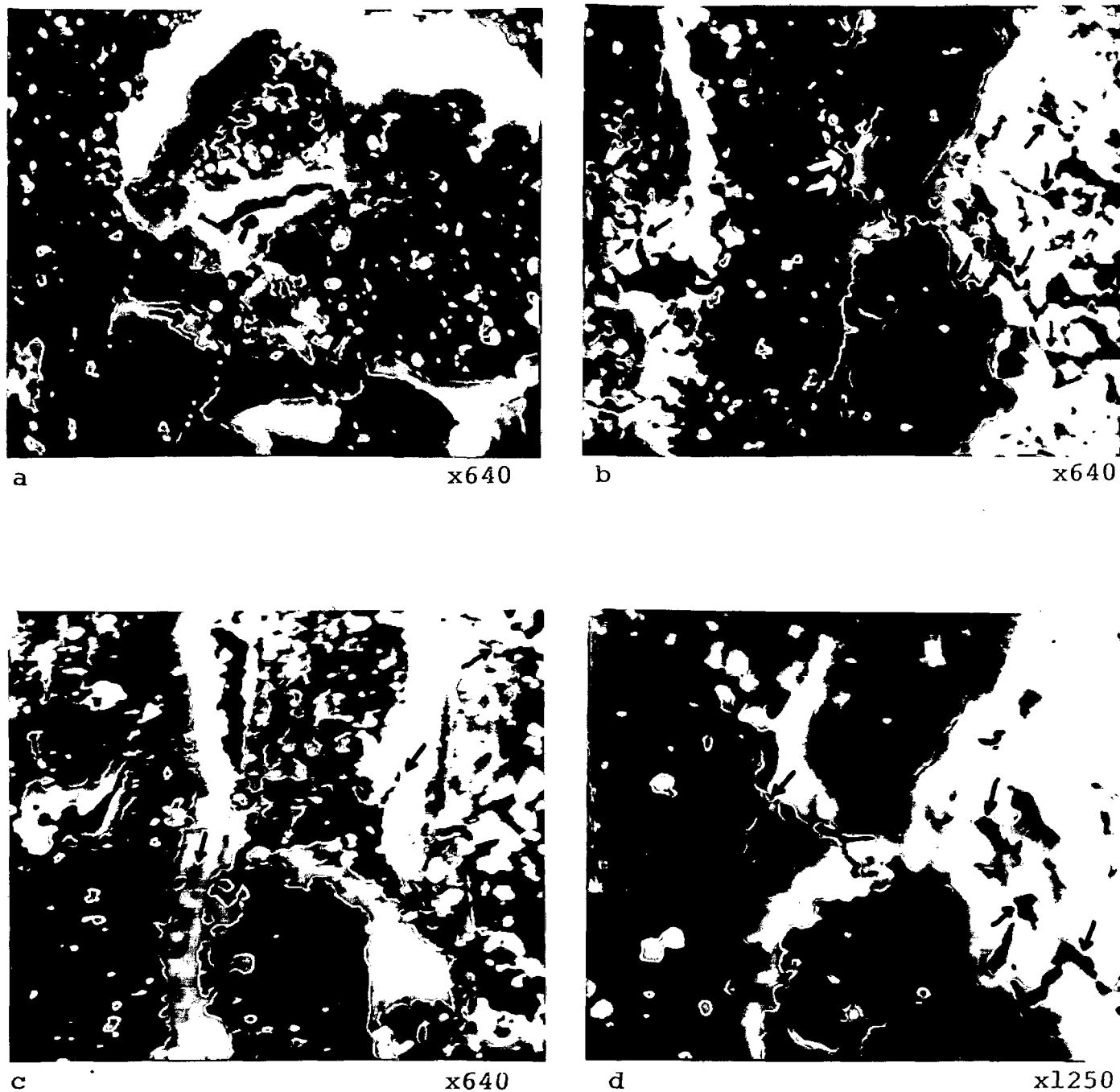
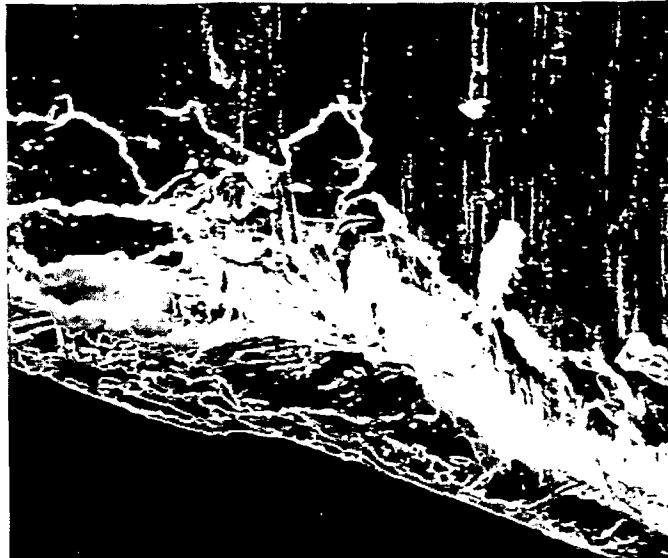
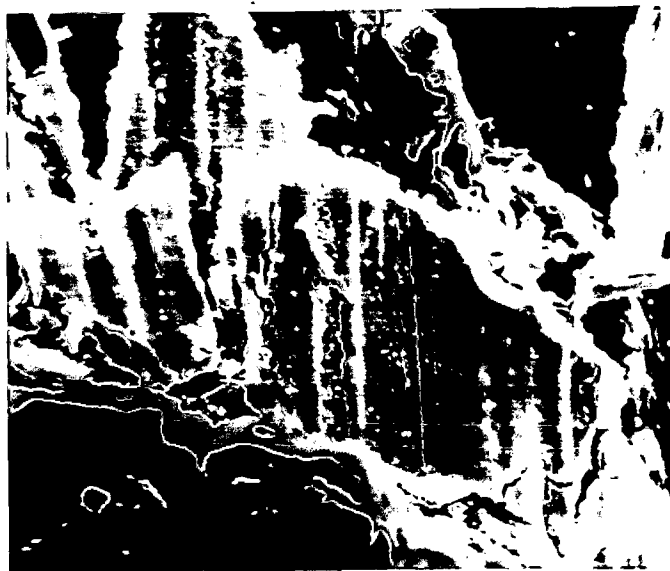


FIG.4.52 SEM pictures showing the details of the worn surface. (a) patches of matrix material scooped out from the grooves undergoing fragmentation through the process of cracks formation. Some of these cracks are marked by arrows, (b) SEM picture showing the special features of cracks emanating from the surface of grooves to the displaced materials on the edges of these grooves. Also, numerous cracks (marked by arrows) can be seen developing into the displaced material on both the edges of the grooves, (c) and (d) SEM pictures showing similar features as mentioned above.



a

x80



b

x80

**FIG.4.53** SEM pictures showing the fracture and removal of matrix material close to the edge of the wear pin. (a) Note the partially sheared material still adhering to the edge of the wear pin because of excellent ductility of composite material, (b) Note typical scoring marks on the individual sheared and partially fragmented pieces. Numerous cracks can be seen developing in these fragmented pieces.

the above features, the entire surface of wear pin was generally seen covered with deep grooves which is indicative of abrasive kind of wear taking place in most specimens [118]. These features observed in the present set of experiments can be attributed to the fact that minimum load applied was as high as 500 gm, while it is well known that for observing adhesive wear process predominantly, one has to move to much smaller loads such as 50 gm [62, 124, 143, 182]. As suggested by Yang and Chung [157], the hard  $\text{Al}_2\text{O}_3$  particles present in the composite first scratch the steel disc and then the rough surface of the steel disc scratches the composite surface giving rise to the formation of deep V grooves. It is also possible that the dislodged hard  $\text{Al}_2\text{O}_3$  particles and the work hardened debris material rolling between the surfaces of counterface steel disc and the wear pin might have resulted in the formation of these grooves. Under these circumstances, the material is removed through the process of abrasive wear. Under the present set of experimental conditions of bearing load, sliding speed and track length, the features mentioned above were commonly observed.

The wear track grooves were often seen littered with fragmented small debris particles [Fig.4.51(c and d), Fig.4.52(a-d)]. Also, on both the edges of V-grooves a raised metal portion or a kind of embankment could be seen all along the length of this groove [Fig.4.51(c,d), Fig.4.52(c)]. This material seen on the embankment was obviously scooped out from the grooves during the process of wear. Since this material will be slightly raised compared to the depth of groove, it will be

the first material to undergo the process of work hardening during further exposure to the rubbing process. As such, this material on the embankment would be expected to undergo further fragmentation through the process of repeated work hardening and generation of cracks within the body of this material. On a closer examination of such locations by the SEM it was found that the sequence of happenings was actually so as mentioned above. An evidence of this sequence of events can be clearly seen in SEM pictures shown in Figs.4.51(d) and 4.52(a-d). It can be seen from these SEM pictures that several deep cracks have already developed in the displaced material and that this material is already in the final stage of fragmentation. Many of these cracks have been marked by arrows in the SEM pictures referred to above. In addition to the above features it can be seen that wide cracks are also present in the base of these grooves (location marked by double arrows in Fig.4.52-b). From the width of the cracks, it can be surmised that perhaps these cracks had developed somewhere deeper in the subsurface below and had finally opened up at the surface of these grooves. This aspect of nucleation and growth of cracks in the subsurface damage is dealt with in detail in subsequent section. However, it is apparent from these SEM pictures that due to the prevailing wear conditions, the metal layer immediately below the grooves would have been work hardened upto a certain finite depth. It appears, therefore, that the material scooped out from the grooves is already in a state of partial fragmentation because of the presence of cracks. Upon further work hardening as mentioned above, the existing cracks propagate further presenting a picture

of almost interconnected network of cracks. At this stage, the body of this material on the embankment appears just loosely knit or it can be said that this material is now almost ready to fall apart. With some further application of wear stresses, this loosely knit body of material actually falls apart and gives rise to the generation of debris materials. This debris material may consist of fine fragmented particles, tiny chips and foils in few cases. Referring to the SEM pictures shown in Fig.4.53(a and b), it can be seen how the worn material is broken and removed close to the edge of the wear pin. The fragmented material still adhering to the edge of the wear pin can be seen displaying scoring marks and cracks on the surface of individual fragmented pieces. Fig.4.53(b) shows these features clearly.

Optical pictures shown in Fig.4.54(a,b) display the morphology of smeared material onto the surface of counterface steel disc. As mentioned earlier the wear pin material was smeared onto the surface of counterface steel disc in the early stages of the start of wear experiments. This smeared material forms a black coloured ring on the surface of steel disc. No effort was made to remove this smeared material and the wear experiments were allowed to continue for a predetermined length of time. This situation actually represents a three body interaction in the present set of experiments. During the progress of wear run, part of these seizure patches could be transferred onto the surface of wear pin and in later stages may be transferred back to the surface of counterface steel disc. An examination of these seizure patches (Fig.4.54,a-b) shows that it

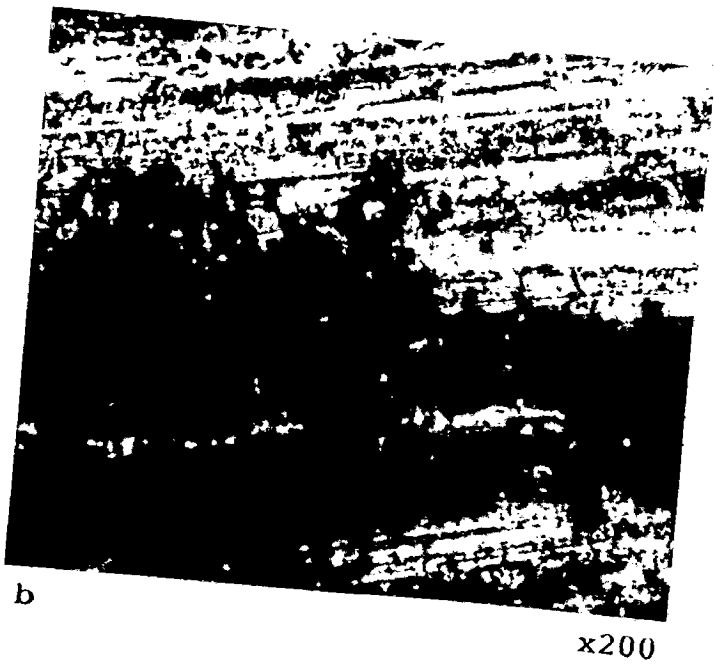
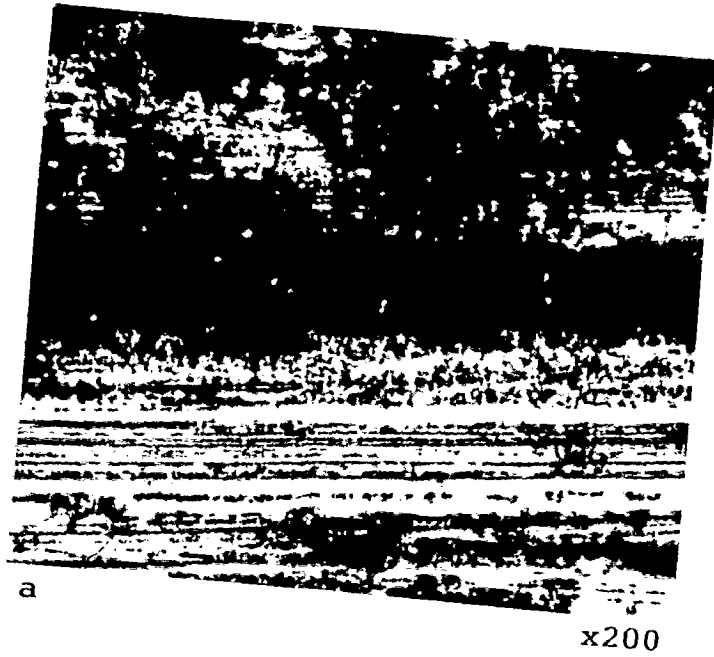


FIG.4.54 Optical pictures showing the morphology of smeared material onto the surface of counter face steel disc. Material in these seizure patches can be seen to be in a state of complete fragmentation. Fine debris particles are filled into the grooves of the counterface steel disc and can be seen coagulated.

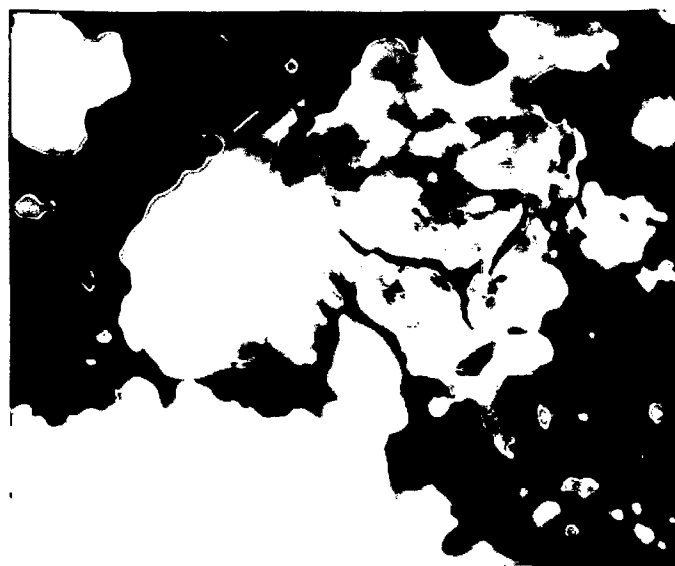
consists of loose debris particles adhering to the surface of counterface steel disc. These patches appear to be in state of almost complete fragmentation. As the wear process continues, these loose particles in the seizure patches ultimately give rise to the generation of fine coagulated debris particles. These seizure patches seem to be almost uniformly distributed in the smeared material forming a black coloured ring as mentioned above.

A detailed examination of the morphology of the debris particles by the SEM is presented in Figs.4.55 and 4.56. A general view of the morphology of collected debris particles is shown in Fig.4.55(a). It can be seen from this picture that a number of foils, fine particles, and agglomerate of fine particles and chips are present in this lot. A closer examination of individual particles reveal interesting features. For example, a SEM picture shown in Fig.4.55(b) presents the details of a dislodged platelet, which has undergone fracture at several locations but its overall configuration is still intact. Fig.4.55-c shows a typical chip, which has been sheared further along its lower surface but the sheared piece is still intact and connected with the main body of the chip. Fig.4.56(a) shows a slightly different morphology of the dislodged chip. It can be seen that this chip has further been fragmented all along its length. It can be seen that wide cracks have been developed in the body of this chip and are running almost all along its total length. It can therefore be seen that even these individual chips are in a state of severe fragmentation. Fig.4.56(b) shows a platelet with similar features as discussed in case of



a

x160



b

x2500



c

x640

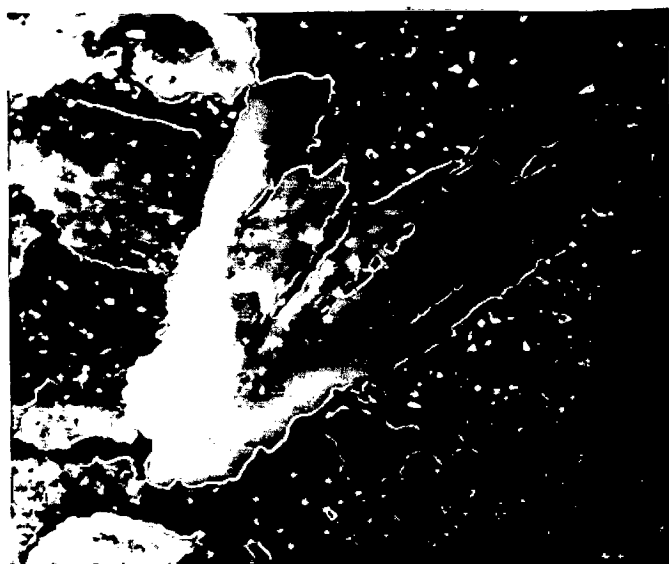
FIG.4.55 SEM pictures of debris material produced during wear experiments.

(a) showing the presence of laminates, foils and thin long chips in the aggregate of debris material,

(b) a foil kind of debris material undergoing further fragmentation,

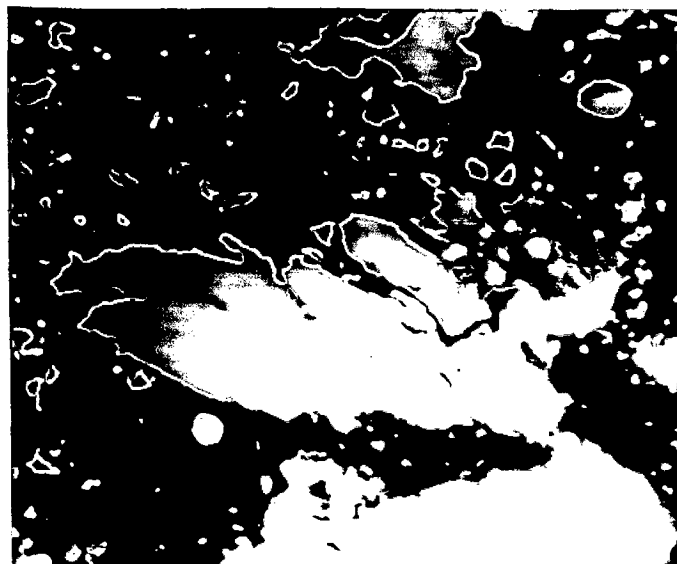
(c) a laminate also undergoing further fragmentation along its lower surface. A number of smaller and approximately spherical debris pieces can also be seen in the picture. These particles appear to be the result of coagulation of several smaller particles into a single nearly spherical aggregates.





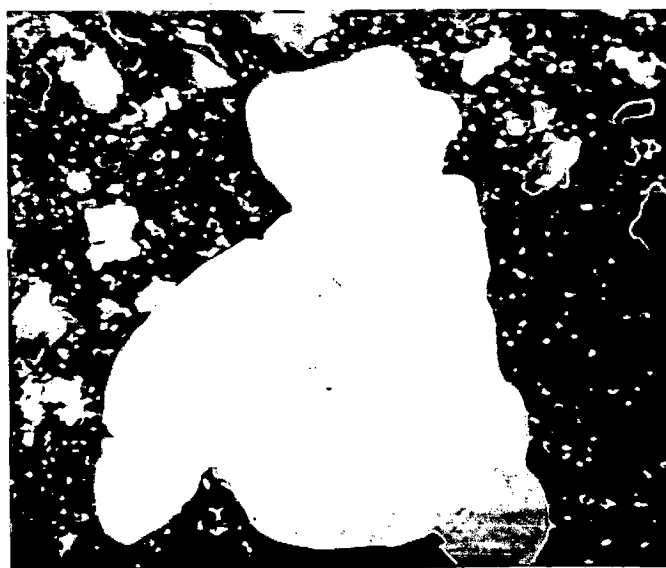
a

x1250



b

x1250



c

x640

**FIG.4.56** SEIs of some other typical debris particles. (a) showing a thin long chip in the process of severe fragmentation. Note the presence of several deep cracks all along the length of this chip, (b) a laminate in the process of further fragmentation, (c) a rare thin foil laminate. Presence of fine cracks in the central region of this foil can be seen. In some instances these cracks can be seen developing from the central region to the periphery of these foils.

platelets shown in Fig.4.55(b). In addition, it can be seen from Fig.4.56(b) that very tiny particles are visible in a state of agglomerated pieces. Simultaneously several small individual pieces can also be seen in this picture. Fig.4.56(c) shows a typical foil. If the central area of the surface of this foil is examined carefully, it can be seen that this area is in the process of further fragmentation as a number of fine cracks can be seen propagating towards the surface of this foil. In many instances, this foil can be seen punctuated with larger number of wider cracks indicating that the foil is in a state of severe fragmentation.

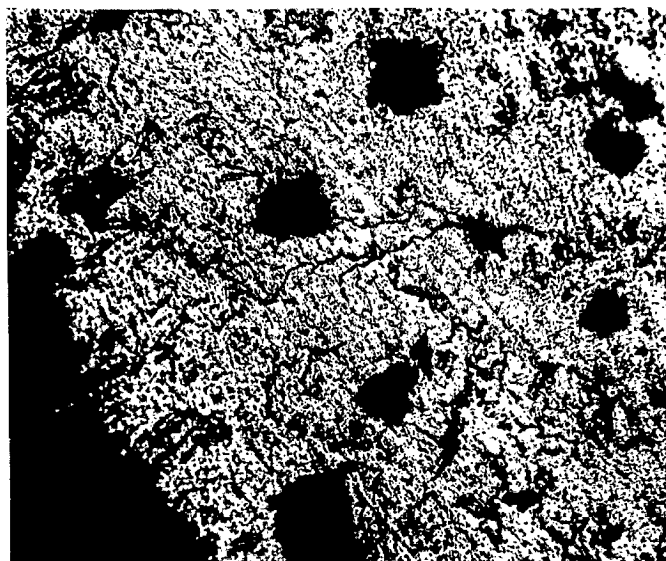
The morphology of a variety of debris particles discussed above is indicative of the wear mechanisms operative during the actual wear process of present class of composites. The presence of coagulated fine debris particles are indicative of the fact that adhesive wear process has played some role during the overall wear of composites. The presence of chips and platelets in the debris aggregate is indicative of the possibility that these particles were produced as a result of the abrasive mode of wear. As discussed earlier, the hard  $Al_2O_3$  particles first scratch the surface of counterface steel disc and then the rough surface of steel disc scratches the surface of wear pin. This is the basic mechanism through which deep grooves or track marks are produced on the surface of wear pin. During the formation of track marks or 'V'grooves, these elongated chips must have been produced. But these elongated chips continue to roll for some time between the two rubbing surfaces of

counterface steel disc and the wear pin and thus are fragmented further. By the time these chips slip out of the rubbing surfaces, they are considerably worked upon and are therefore full of cracks at many locations. But obviously, these chips are the product of scoring marks visible on the wear pin. Similar features were noted by Pramila Bai, Dwarakadasa and Biswas [184] in their study of LM-13-graphite particulate composites. Also, Yang and Chung [157] and Hosking et.al. [62] noted similar features while studying the wear behaviour of the respective particulate composite systems developed by them. The presence of several foils in the debris material clearly points to the possibility that the 'Delamination process' was the probable mechanism through which material removal had occurred in the present class of composites. As proposed by Suh and coworkers [127], all the materials which undergo plastic deformation to a finite depth, undergo wear through a process of 'delamination'.

#### 4.4.7 SUB-SURFACE DAMAGE

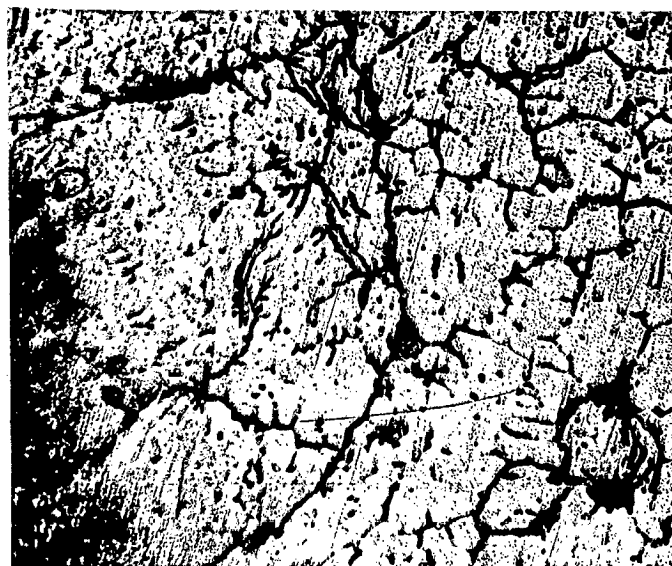
Sub-surface damage in the present class of composites was studied with the help of optical and SEM examination of oblique section and micro hardness measurements along this tapered polished surface. Results of this study are presented in Figs.4.57 and 4.58.

It can be noted from the optical pictures shown in Fig.4.57(a & b) that a kind of delta pattern of cracks exist in the subsurface region just underneath the wear tracks. These cracks initiate at the interface of wear tracks and the



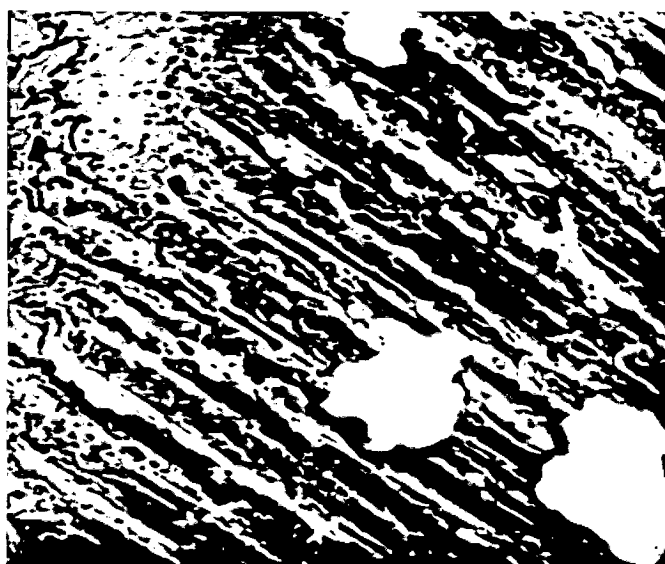
a

x160



b

x160



c

x160

FIG.4.57 (a) and (b) optical pictures showing the microstructures of oblique section exhibiting the presence of river delta pattern of cracks in the work hardened region immediately below the worn surfaces. A dark portion in the extreme left corner region shows the edge of the grooved worn surface. It can be seen that these cracks finally dissipate into the worn surface mentioned above. It is also noteworthy that dispersed  $\text{Al}_2\text{O}_3$  particles are firmly bonded to the base matrix, .

(c) SEM picture showing grooved wear track and scooped out matrix material on the ridges of these grooves and  $\text{Al}_2\text{O}_3$  particles firmly bonded and still present on the grooved track and not dislodged.

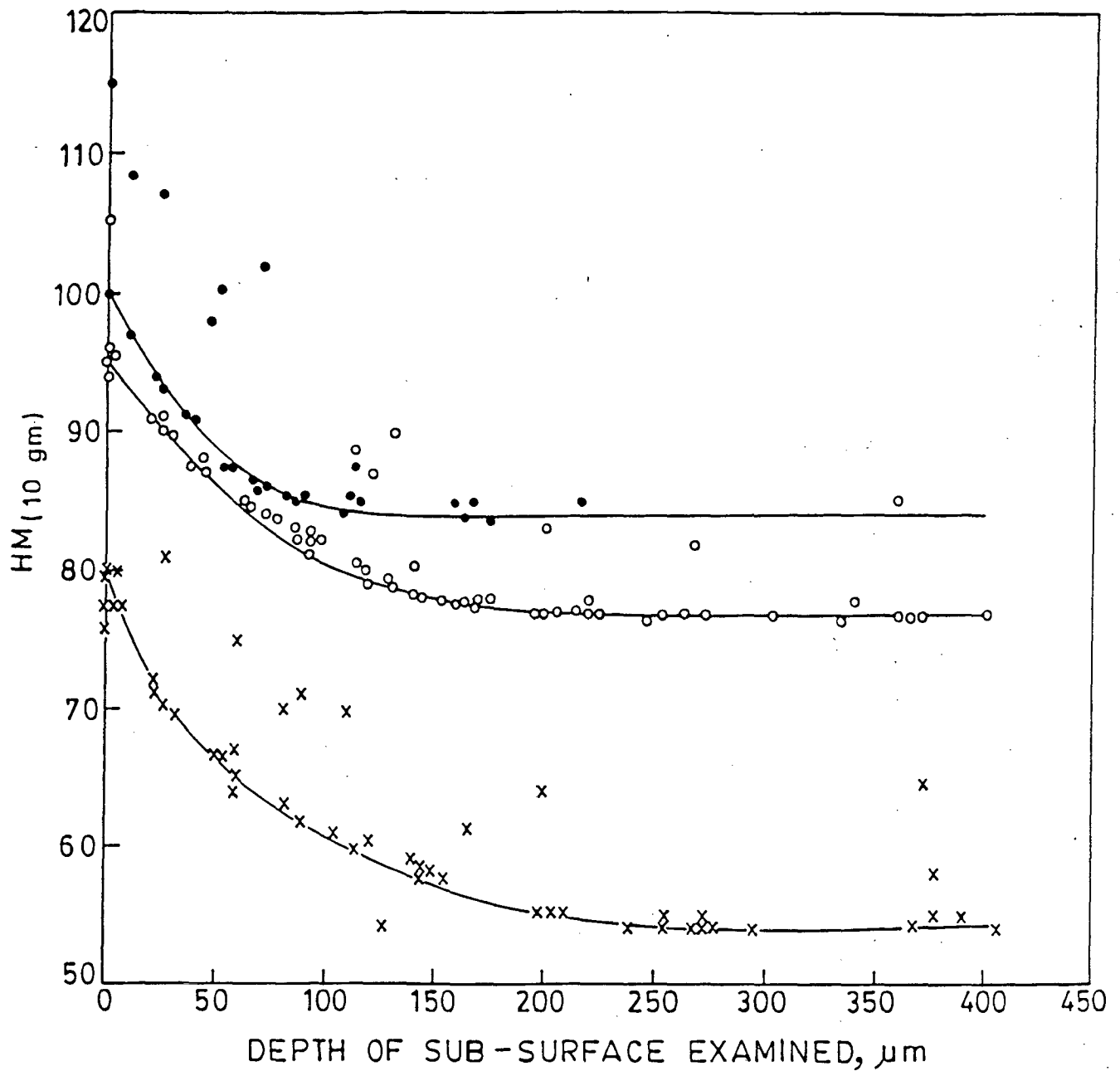


FIG.4.58 Microhardness ( $HM_{10gms.}$ ) plotted as a function of the depth of subsurface region immediately below the worn surface. (x)- Composite No.1, the depth of work hardened region is approx. 250  $\mu m$ , (o) - composite No.2, depth of work hardened region is 200  $\mu m$ , and (●)-Composite No.3, depth of work hardened region, approx. 125  $\mu m$ .

subsurface region just underneath and then progress downwards in the work hardened sub-surface region. The above interface is a most likely location where cracks would initiate primarily because the hardness of metal layer at this location is the highest [Fig.4.58] and secondly because the stress concentration in this particular layer will also be the highest [131]. It was shown by Pramila Bai, Dwarakadasa and Biswas [130] that the friction force between the rubbing surfaces increases with sliding distance until it reaches a stable value. At this stage, the subsurface region is subjected to plastic strain to a considerable but stable depth. And Ruff [131] showed that this strain has a maximum value near the worn surface and decreases with subsurface depth until it is zero in the undisturbed subsurface region. Also it was postulated by Bill and Wisander [185] that the high stacking fault energy of aluminium is responsible for intense plastic strain extending to a considerable depth below the wear surface ultimately resulting in fracture and transfer of material to the harder rubbing surface. Similar features can be noted on the SEM picture of the tapered section shown in Fig.4.57(c). It is noteworthy that  $Al_2O_3$  particles are still intact on the wear track surface and not pulled out even during the process of wear, (Fig.4.57-c). This implies that the  $Al_2O_3$  particles are firmly bonded with the base matrix. In this situation, the hard  $Al_2O_3$  particles will scratch the steel counterface disc surface. But ultimately these  $Al_2O_3$  particles will be dislodged from the composite matrix after the neighbouring matrix material has been worn out considerably. The presence of cracks in the subsurface region as shown in

Figs.4.57(a and b) point to the possibility that perhaps the 'delamination process' as proposed by Suh and coworkers [127] is the predominant mechanism through which material removal occurs in the present class of composites.

Results of microhardness measurements shown in Fig.4.58 for the three composites under investigation also clearly confirm that the subsurface region undergoes work hardening upto a measurable depth due to the process of wear. It is apparent from the results that surface layer immediately below the worn surface has undergone maximum amount of work hardening, which would be expected also. This degree of work hardening then tapers off as deeper layers of subsurface region are approached till ultimately the unaffected base matrix is encountered during microhardness measurements. The depth of this work hardened zone in case of different composites is found to be between 125 to 250  $\mu\text{m}$ . It is noteworthy that composite No.3 develops maximum hardness at the interface (subsurface layer immediately below the worn surface) followed by composites No.2 and 1. It is basically because of this reason that the wear rates obtained for the three composites under different experimental conditions are just in the reverse order. The depth of work hardened region in case of composite No.3 is the least (125  $\mu\text{m}$ ), followed by composite No.2 ( 200  $\mu\text{m}$ ), and then composite No.1 ( 250  $\mu\text{m}$ ). It is basically because the finer the grain size of base matrix the more difficult it is to deform [183]. It is apparent from the results shown in Figs.4.7 and 4.8 that composite No.3 displays maximum level of densification and grain refinement as against composite No.2 and

1. Because of these inherent properties, composite No.3 displays also the highest hardness followed by composite No.2 and 1. Automatically, therefore, composite No.3 displays least depth of work hardened region and highest wear resistance compared to composite No.2 and 1.



## CHAPTER - 5

## SUMMARY OF CONCLUSIONS AND SUGGESTIONS FOR FUTURE STUDIES

## 5.1 CONCLUSIONS

The following conclusions were arrived at from present investigations:

1. Standard 'MgO Coating' technique developed earlier for the preparation of Al-Al<sub>2</sub>O<sub>3</sub>-MgO cast particulate composites needs to be modified for application under humid environmental conditions. Proper degassing of melt by fully dried hexachloroethane tablets followed by Mg plunging to the tune of 0.5% of the melt was found essential to incorporate Al<sub>2</sub>O<sub>3</sub> particles in the stirred slurry. Also, proper h/H ratio (0.81) and adequate d/D ratio (0.60) must be maintained during the creation of vortex to result in optimum retention of Al<sub>2</sub>O<sub>3</sub> in the melt.

2. The modified 'MgO Coating' technique results in almost uniform retention of Al<sub>2</sub>O<sub>3</sub> particles in the base matrix of gravity chill cast composites. These particles were observed to be nicely bonded with the base matrix. Nearly 12 to 13%V<sub>f</sub> retention of Al<sub>2</sub>O<sub>3</sub> was obtained in the matrix at the level of 10 wt% total (Al<sub>2</sub>O<sub>3</sub>+MgO) powder mixture addition containing 15% MgO. But at many locations, the Al<sub>2</sub>O<sub>3</sub> particles were seen coagulated forming different morphologies like clusters, comets and chain like formations etc.

3. The gravity chill cast composites prepared by vortex liquid metallurgy route mentioned above were found to suffer from considerable amount of gas porosity and interdendritic unfed regions. These defects result in premature failure of composites under tensions. Thus, in case of gravity chill cast composites, the full potential of composites in terms of the mechanical properties achievable is never realised in actual practice. These composites were also found to be coarse grained and poor in Vicker's hardness as well as microhardness. Also, the density of these composites was found to be the poorest mainly because of the presence of large sized voids in the cast structure.

4. Squeezing the stirred slurry in the pressure range of 80 to 140 MPa uniformly improves the properties of Al-Al<sub>2</sub>O<sub>3</sub>-MgO particulate composites. Compared to the density of gravity chill cast composite, the density of composite squeezed at 140 MPa and ambient die temperature is increased by 3.681%, signifying a proportionate decrease in the porosity of the squeezed composite. The squeeze casting uniformly improves Vicker's hardness (HV<sub>5</sub>), microhardness (HM<sub>5gm</sub>), and mean dendritic arm spacing of composites. The composite squeezed at 140 MPa and ambient die temperature displays the maximum amount of grain refinement, Vicker's hardness and the microhardness of the base matrix. At a given squeeze pressure, however, the above properties deteriorate uniformly as the die temperature is systematically raised. The squeezed composites display more uniform distribution of Al<sub>2</sub>O<sub>3</sub> particles in the base matrix as against ordinary gravity chill cast composites and the incidence of coagulation of Al<sub>2</sub>O<sub>3</sub> particles was

also observed to be minimum.

5. Experimental evidence shows that submicron MgO particles cause dispersion strengthening of the base matrix. Although these particles show a tendency for segregation towards the grain boundaries but the overall dispersion strengthening effect obtained is excellent. Because the inherent nature of these particles is different, they will not be expected to show any tendency for coagulation at elevated temperature as is the case with usual process of ageing. Therefore, these particles will contribute positively to the performance of squeezed Al-Al<sub>2</sub>O<sub>3</sub>-MgO particulate composites at elevated temperature particularly.

6. EPMA examination of the reacted layer around Al<sub>2</sub>O<sub>3</sub> particles showed that Mg tends to concentrate at the particle/matrix interface and that the MgO content in the reacted layer at this interface is also maximum. It was concluded from these studies that MgO forms an integral part of the reacted layer. This reacted layer is likely to be a MgAl<sub>2</sub>O<sub>4</sub> spinel.

7. The gravity chill cast composites undergo premature failure and thus exhibit poor strength, ductility and semiductile to brittle kind of fracture features. Upon squeezing, the tensile properties of the composites progressively improve. The best tensile properties are exhibited by a composite squeezed at 140 MPa and ambient die temperature. Relevant properties of this composite are; UTS-207.9 MN.m<sup>-2</sup>, 0.2% offset Y.S. - 119.5 MN.m<sup>-2</sup>, % elongation - 13.3 and % reduction in C.S. area - 12.8. Compared to the properties of gravity chill cast composite, the UTS of above

squeezed composite is higher by 53%. But what is even more significant is the fact that the ductility of the squeezed composite indicated by % elongation is higher by 133%. Increasing the die temperature deteriorates the UTS of the composite for a fixed squeeze pressure applied but slightly improves the % elongation. Therefore, squeezing the stirred slurry improves not only the UTS but also the ductility of the composite simultaneously. Squeezing the stirred slurry in the pressure range of 160 to 240 MPa is likely to improve the properties of composites further.

8. Squeezing the stirred slurry in the pressure range of 80 to 140 MPa also brings about a distinct improvement in the performance of the composites particularly with regard to their tensile properties at elevated temperatures. Again, the best properties are displayed by a composite squeezed at 140 MPa and ambient die temperature upto 300°C (573K) test temperature. The UTS of above composite is higher by 52% at 100°C (373K) test temperature compared to ordinary gravity chill cast composite. This figure improves to 161% and 162% at 200°C (473K) and 300°C (573K) test temperatures respectively. This implies that the above composite retains about 72% of its ambient UTS value at 573 K test temperature, while the gravity chill cast composite retains only 44% of its ambient UTS value at the same test temperature. The same squeezed composite retains  $160.4 \text{ MN.m}^{-2}$  UTS value at 300°C while the gravity chill cast composite retains only  $61.1 \text{ MN.m}^{-2}$  UTS at the same test temperature.

9. Results pertaining to 0.2% offset YS values of the squeezed composite at different test temperatures are more encouraging. This is important basically because 0.2% offset YS values are employed as the design criterion for actual engineering components. The squeezed composite (140 MPa and ambient die temperature) retains 94.4% of its ambient YS value at 300°C (573K) test temperature, while the gravity chill cast composite retains only 64.2% of its ambient YS value at the same test temperature. The YS of above squeezed composite is higher by 105% compared to the YS value of gravity chill cast composite at 300°C (573K) test temperature. This implies that the performance of above squeezed composite is superior by a factor of 2.05 compared to ordinary gravity chill cast composite at 300°C test temperature. At 100°C test temperature, the squeezed composite is superior by 53% compared to gravity chill cast composite. Therefore, with progressive increase in test temperature, the performance of above squeezed composite becomes increasingly superior compared with ordinary gravity chill cast composite. The performance of above composites is likely to improve further if the squeeze pressure is taken to still higher levels such as 160 to 240 MPa.

10. A progressively increasing YS/UTS ratio with increasing test temperatures in case of gravity chill cast as well as squeezed composite is indicative of the fact that the performance of the composite progressively improves at elevated test temperatures. The basic difference is that the gravity chill cast composite will undergo failure soon after the 0.2% offset YS is exceeded. It is because such composites undergo premature failure due to the

presence of voids in the cast structure. On the contrary, the squeezed composites will never run this risk because their UTS values are much on the higher side compared to the values of gravity chill cast composites. Therefore, actual components fabricated through the squeeze casting route will be able to perform much better under elevated temperature service conditions.

11. Tensile fracture surfaces of gravity chill cast composites display semiductile to brittle fracture features. These fracture surfaces also typically display the presence of gas porosity and unfed interdendritic regions at many locations. In some instances,  $\text{Al}_2\text{O}_3$  particles could be seen adhering to the walls of these voids pulled and elongated to a long distance under the tensile stress. On the contrary, the squeezed composites displayed fully ductile fracture features. These fracture surfaces were seen punctuated with numerous deep dimples. Typically, the intervening matrix between the walls of individual craters were seen separated from each other through the mode of chisel point or knife edge separation. The average size of these dimples progressively increased as the test temperature was systematically raised. The fracture surfaces of squeezed composites were observed to be virtually free from any voids and unfed interdendritic regions.

12. Increasing degree of squeeze pressure applied during the fabrication of Al- $\text{Al}_2\text{O}_3$ -MgO cast particulate MMCs progressively improves their wear resistance under dry sliding conditions. The wear resistance of above class of composites improves owing to the presence of hard  $\text{Al}_2\text{O}_3$  particles and a strong, tough and grain refined matrix obtained upon squeezing.

13. Composite No. 3 (fabricated at 140 MPa and ambient die temperature) displays highest wear resistance under all conditions of bearing load, sliding speeds and track length. Superiority of this composite improves as the bearing load is increased in steps from 500 gm to 1500 gm. Compared to composite No.1 (ordinary gravity chill cast composite), the wear rate of above composite is lower by  $14.2 \text{ Kg.Km}^{-1} \times 10^{-6}$  at 500 gm load,  $9.4 \text{ m.Sec}^{-1} \times 10^{-2}$  sliding speed and 169.5 m track length. At 1000 and 1500 gm loads, these figures are found to be 18.4 and 23.0 respectively at progressively increasing sliding speeds and track length. These observations lead to the conclusion that progressively increasing degree of squeeze pressure applied during the fabrication of composites, systematically improves their wear resistance under all conditions of dry sliding wear.

14. The phenomenon of work hardening, nucleation, growth and propagation of cracks in the work hardened subsurface region leads to material removal during the process of dry sliding wear. Generally the material removal seems to be occurring according to the mode of the 'delamination process'.

15. The process of dry sliding wear leads to work hardening of subsurface region immediately below the grooved worn surface upto a measurable depth. The microhardness of the sub-surface layer immediately below the worn surface is the highest, signifying maximum amount of work hardening of this layer. This degree of work hardening then tapers off and becomes zero when the deeper undisturbed metal layers are approached. The depth of work hardened region is found to be between 125 to 250  $\mu\text{m}$  in the three

cases of the composites. The depth of work hardened region in case of composite No. 3 is the least (125  $\mu\text{m}$ ), followed by composite No. 2 (200  $\mu\text{m}$ ) and then composite No. 1 (250  $\mu\text{m}$ ). It was found that the wear rate for the three composites mentioned above are just in the reverse order.

16. Examination of the wear track debris material leads to the conclusion that a mixed mode of wear process involving both the adhesive as well as abrasive wear is operative in the present class of composites under the present set of experimental conditions. A transition was noted at 1000 gm bearing load at all the sliding speeds employed. Below 1000 gm bearing load, the adhesive cum abrasive wear seems predominant while beyond 1000 gm bearing load the abrasive wear becomes predominant.

17. Wear resistance of Al-Al<sub>2</sub>O<sub>3</sub>-MgO MMCs can be improved further if a higher %V<sub>f</sub> retention of Al<sub>2</sub>O<sub>3</sub> is attained and if the squeeze pressure is also taken to higher levels (160 to 240 MPa) simultaneously.



## 5.2 SUGGESTIONS FOR FUTURE STUDIES

1. Al-alloys such as 2024, 2014, 6061, 201, 356 etc. may be employed as the base matrix for the preparation of Al alloy-Al<sub>2</sub>O<sub>3</sub>-MgO particulate composites and their properties investigated upto 300°C (573K). This will form an interesting study as most of the above alloys are extensively employed in the industry. Apparently, the properties of above composites would be expected to be superior than ordinary Al-Al<sub>2</sub>O<sub>3</sub>-MgO composites. Also, these composites should also be studied in the heat treated condition. An effort should also be made to incorporate comparatively higher quantities of Al<sub>2</sub>O<sub>3</sub> particles in the above composites. It should perhaps be possible to incorporate upto 20%V<sub>f</sub> of Al<sub>2</sub>O<sub>3</sub> in the composite without much serious problem of coagulation of these particles. With usual precautions of degassing of melt and dehydroxylation of Al<sub>2</sub>O<sub>3</sub> particle surfaces, it should be possible to obtain porosity free composites.

2. In order to achieve fully densified and grain refined composites, it would be interesting to take the squeeze pressure to higher levels such as 160 to 240 MPa. Properties of these composites should be studied in detail and compared with the results of present investigation. Characterising these composites with respect to their behaviour in tension upto 300°C (573K) would form an interesting study. It is proposed that some directional solidification studies should also be carried out with respect to the above composites in order to ascertain a) the segregation pattern of Al<sub>2</sub>O<sub>3</sub> and sub-micron MgO particles and b) the heat

transfer rates across the walls of die and plunger and the liquid slurry in contact with these surfaces. The pressurised feeding conditions should also be simulated and the above factors studied in detail. The variation in the die temperature and the wall thickness of die should be taken as important variables in the above investigations. As a result of these studies, a closer control of the squeeze casting process would be possible.

3. An attempt should be made to fabricate some engineering components with relatively simple geometries out of the composites mentioned above. Also, it would be worth investigating the influence of further processing such as rolling and extrusion of gravity chill cast and squeezed composites on the properties of resulting wrought product.

4. An examination of important properties such as low cycle fatigue, fatigue life, fracture toughness and conventional impact strength of squeezed composites will constitute an interesting study.

5. A study of the properties of squeezed composites with the dispersion of only a specific size of  $\text{Al}_2\text{O}_3$  particles as against a wider size range of  $\text{Al}_2\text{O}_3$  particles employed in the present work would be meaningful. A ceramic filter coupled with squeeze casting operation as employed by Mehrabian and co-workers [62] can be used to obtain a composite with comparatively much higher retention of  $\text{Al}_2\text{O}_3$  particles in the composites.

6. A precise examination of the reacted layer around  $\text{Al}_2\text{O}_3$

particles should be carried out further with the help of proper  $\text{MgAl}_2\text{O}_4$  spinel standard to ascertain the exact composition of this layer. It should be investigated whether the thickness of this layer varies with increasing period of stirring or with varying amounts of Mg employed for plunging. Also, it would be interesting to examine whether the reaction temperature has some effect on the thickness of this layer.

7. Wear behaviour of composite Nos. 1,2 and 3 needs to be investigated under several new conditions. Primarily, the behaviour of these composites should be investigated under the conditions of much lower loads such as 50 and 100 gms and comparatively higher sliding speeds such as 1 to 10  $\text{m}.\text{Sec}^{-1}$ . Also, longer track lengths upto 4 Km should be included in the scope of this study. Also, the wear behaviour of new composites proposed to be fabricated at Sr.No. 1 above should be investigated in detail under dry sliding conditions. In all these cases, an attempt should be made to precisely measure the rise of temperature at the wear interface and also the coefficient of friction should be measured as a function of the track length under a fixed bearing load and the sliding speed. A precise examination of the morphology of debris material generated in the beginning, middle and later stages of wear runs would give a better understanding of the mechanism of material removal at different stages of wear process. This systematic study can be very meaningful and revealing.

## REFERENCES

1. G. Piatti, 'Advances in Composite Materials', Applied Science Publishers Ltd., London, (1978), 12, 15, 16, 62.
2. L.J. Broutman and R.H. Krock, 'Modern Composite Materials', Addison-Wesley Publishing Company, Inc., (1967), 7, 8, 481, 486.
3. L. Holliday, 'Composite Materials', Elsevier Publishing Company, New York, (1966), 66, 68, 83, 221, 290, 292, 453.
4. K.G. Satyanarayana, R.M. Pillai and B.C. Pai, 'Metal Matrix Composites for Aerospace Application - An Overview', Proc. of Seminar on Science and Technology of Composites, Adhesives and Sealants, Bangalore, India, (Sept.28-30,1989), 81.
5. A.J. Clegg, 'Cast Aluminium Composites' Proc. Conf. Aluminium Tech., The Institute of Metals, London, U.K. (11-13 March,1986), 89.1-89.7.
6. Margaret Hunt, 'MMCs For Exotic Needs', Materials Engineering, (April 1989), 53.
7. S.K. Verma and J.L. Dorcic, 'Manufacturing of Composites by Squeeze Casting', Proc. World Materials Congress, Section - Cast Metal Matrix Composites, Chicago, U.S.A., (Sept.24-30,1988), 115.
8. H. Fukunaga, 'Squeeze Casting Processes of Ceramic Fibre Reinforced Metals', Proc. Korea-Japan Metals Symposium on Composite Materials, The Korean Institute of Metals, Seol, Korea, (Nov.10-11,1988), 60.

9. H. Fukunaga, 'Squeeze Casting Processes For Fibre Reinforced Metals and Their Mechanical Properties', Proc. World Materials Congress, Section - Cast Metal Matrix Composites, Chicago, U.S.A., (Sept.24-30,1988), 101.
10. S. Towata and S. Yamada, 'Mechanical Properties of Aluminium Alloys Reinforced with Continuous Silicon Carbide Fibres and Whiskers or Particulates', Trans. Jpn. Inst. Metals, 27(9), (1986), 709.
11. S. Towata, H. Ikuno and S. Yamada, 'Mechanical Properties of Silicon Carbide Fibre Reinforced Aluminium Alloys with Whiskers or Particulates', J. Jpn. Inst. Metals, 51(3), (1987), 248.
12. B.F. Quigley, G.J. Abbaschin and R. Mehrabian, 'A Method For Fabrication of Aluminium - Alumina Composites', Met. Trans. A, 13A, (Jan.1982), 93.
13. A. Munitz, M. Metzger and R. Mehrabian, 'The Interface Phase in Al-Mg/Al<sub>2</sub>O<sub>3</sub> Composites', Met. Trans. A, 10A, (Oct. 1979), 1491.
14. A. Banerji, P.K. Rohatgi and W. Reif, 'Role of Wettability in The Preparation of Metal - Matrix Composites (a Review)', Metallwissenschaft Technik, 38(7), (July 1984), 656.
15. Andreas Mortensen, J.A. Cornie and M.C. Flemings, 'Solidification Processing of Metal - Matrix Composites', Journal of Metals, 40(2), (Feb. 1988), 12.
16. A.A. Das, A.J. Clegg and Zantout, 'Enhancement in the Properties of a Squeeze-Cast Aluminium Magnesium Alloy Containing Delta - Alumina Fibre', Proc. World Materials

- Congress, Section - Cast Metal Matrix Composites, Chicago, U.S.A., (Sept.24-30,1988), 217.
17. A.A. Das, A.J. Clegg, B. Zantout and M.M. Yakoub, 'Solidification Under Pressure: Aluminium and Zinc Alloys Containing Discontinuous SiC Fibre', *ibid*, 139.
  18. B. Zantout, A.A. Das and J.R. Franklin, 'Squeeze Cast Aluminium Composites: Strength at Higher Temperature', *Proc. Conf. The Metallurgy of Light Alloys*, Loughborough Univ., U.K., (March 24-26,1983), 215.
  19. K.G. Kreider, 'Composite Materials', Vol.4, Academic Press, (1974), 1-34 and 38-97.
  20. H.R. Caluser, 'Industrial and Engineering Materials', McGraw Hill, (1975), 381.
  21. K. Kovacova, J. Dille and A. Berghezan, 'Unidirectional Solidification of Ternary Eutectic Al-Ni-Si Alloys', *Composites*, 7(4), (Oct.1976), 249.
  22. W.H.S. Lawson, 'Mechanical Behaviour of Rapidly Solidified Al-Al<sub>2</sub>Cu and Al-Al<sub>3</sub>Ni Composites', *Met. Trans.*, 2, (1971), 2853.
  23. A.W. Tiller, 'Liquid Metals and Solidification', ASM, (1958).
  24. F.D. Lemkey, 'Development of a Second Generation Ductile/Ductile  $\gamma/\gamma'$ - $\alpha$  Eutectic Alloy', *Proc. 3rd. Inter. Symp. on Super Alloys*, (1976), 321.
  25. E.M. Dunn, R.A. Wasson, K.P. Young and M.C. Flemings, 'Growth of In-Situ Composites of Al-Cu-Ni Alloys', *Conf. on In-Situ Composites-II*, New York, (1975).

26. M.M. Farag and M.C. Flemings, 'Structure and Mechanical Behaviour of Al/20%Cu Directionally Solidified Composites', Proc. 2nd Inter. Conf. on Mech. Behaviour of Metals, (1976), 1857.
27. M. Gensamer, Trans. American Society of Metals, 36, (1940), 30.
28. G.S. Ansell and F.V. Lenel, Acta Met., 8, (1960), 612.
29. H.J. Rack and P.W. Niskanen, 'Extrusion of Discontinuous Metal Matrix Composites', Light Metal Age, 42, (Feb. 1984), 9.
30. M. Kiuchi, S. Sugiyama and N. Endo, 'Experimental Study of Metal Forming in Mashy State, VI-Production and Working of Particle Reinforced Clad Metals by Mashy State Process', J. Jpn. Soc. Technol. Plast., 24(274), (Nov. 1983), 1113.
31. P.K. Rohatgi and M.K. Surappa, 'Deformation of Graphite During Hot Extrusion of Cast Aluminium/Silicon/Graphite Particle Composites', Mater. Sci. Engg., 62, (Feb. 1984), 159.
32. E. Yuasa and T. Morooka, 'Hot Extrusion of an Aluminium Composite Containing Dispersed Graphite Particles', J. Jpn. Soc. Technol. Plast., 22(244), (May 1981), 482.
33. M. Kiuchi and S. Sugiyama, 'Production and Mechanical Property of Clad Metals Laminated with Particle Reinforced Composite Metal and Ceramic Powder', Proc. Conf. Mechanical Behaviour of Materials-IV, Stockholm, Swedon, (15-19 Aug., 1983), 1023.
34. K.U. Kainer, H.W. Bergmann and B.L. Mordike, 'Powder Metallurgically Produced Metal - Glass Composites', Powder

- Metallurgy, 26(1), (1984), 30.
35. P.S. Mishra and G.S. Upadhyaya, 'Properties of Sintered Aluminium Dispersed with Titanium and Tungsten Carbides', The Inter. J. Powder Metallurgy and Powder Technology, 11(4), (1975), 129.
  36. E.T. Demisenko, 'Mechanical Properties of Dispersion Strengthened Cu-Al<sub>2</sub>O<sub>3</sub> Materials', Sov. Powder Metall. Met. and Ceram., 19(4), (1980), 265.
  37. P. Sablet de and A. Accary, 'Comparison Between Powder Metallurgy and Competitive Process for the Mass Production of Structural Parts', Powder Metallurgy Int., 9(3), (1977), 131.
  38. H. Schreiner, 'A Comparison of Potential and Limits of Foundry and Sintering Technology', Powder Metallurgy Int., 10(3), (1978), 140.
  39. S. Ray, 'Fabrication of Aluminium - Alumina Particulate Composite by Foundry Technique', M. Tech. Dissertation, Indian Institute of Technology, Kanpur, (India), (1969).
  40. D.N. Williams and J.W. Roberts, Modern Castings, 37, (1960), 81.
  41. R. Mehrabian, R.G. Rick and M.C. Flemings, 'Preparation and Casting of Metal Particulate Non Metal Composites', Met. Trans., 5, (1974), 1899.
  42. R. Mehrabian, A. Sato and M.C. Flemings, 'Cast Composites of Aluminium Alloys', The Light Metals, Vol II, (1975), 177.
  43. P.K. Rohatgi, N. Ranganathan and H.R. Shetty, 'The Use of Metal Coated Refractory Powders to Make Particulate Composites by Infiltration', Composites, 9(3), (July 1978), 153.



44. M.K. Surappa and P.K. Rohatgi, 'Preparation and Properties of Cast Aluminium/Ceramic Particle Composites' J. Mater. Sci., 16(4), (1981), 983.
45. N.I. Deonath and P.K. Rohatgi, 'Cast Aluminium Alloy Composites Containing Copper Coated Ground Mica Particles', J. Mater. Sci., 16(6), (1981), 1599.
46. B.P. Krishnan, M.K. Surappa and P.K. Rohatgi, 'The UPAL Process: A Direct Method of Preparing Cast Aluminium Alloy/Graphite Particle Composites', J. Mater. Sci., 16(5), (1981), 1209.
47. N.I. Abdul Lattef, A.R.I. Khedar and S.K. Goel, 'Preparation of Al-Al<sub>2</sub>O<sub>3</sub>-MgO Cast Particulate Composites Using MgO Coating Technique', J. Mater. Sci. Lett., 4, (1985), 385.
48. N.I. Abdul Lattef, E.S. Dwarakadasa, S.K. Goel and A.R.I. Khedar, 'SEM Study of Fracture in an Al-Al<sub>2</sub>O<sub>3</sub>-MgO Cast Particles Composites', J. Mater. Sci. Lett., 2, (1983), 750.
49. N.I. Abdul Lattef, A.R.I. Khedar and S.K. Goel, 'Microstructure and Mechanical Properties of Al-Al<sub>2</sub>O<sub>3</sub>-MgO Cast Particulate Composites', J. Mater. Sci., 22, (1987), 466.
50. F.A. Badia and P.K. Rohatgi, 'Dispersion of Graphite Particles in Aluminium Castings Through Injection of the Melt', AFS Trans., 77, (1969), 402.
51. C.G. Goetzal, 'Cermets' edited by S.R. Tinkelpough and W.B. Crandell, Reinhold Publishing Corporation, (1960), 73.
52. K. Chandra, S. Ray and D.B. Goel, 'Development of Al-base

- Cast Composites by Internal Oxidation', Proc. Solidification and Casting of Metals, Deptt. of Met. Engg., Univ. of Roorkee, Roorkee, India, (Oct.1984), 21.
53. B.C. Pai and P.K. Rohatgi, 'Cast Graphite Aluminium - A Potential Bearing Alloy', Trans. Indian Institute of Metals, 27,(1974), 97.
  54. F.A. Badia, 'Dispersion of Oxides and Carbides in Al and Zn Alloys', AFS Trans., 79, (1971), 347.
  55. F.A. Badia, D.F. McDonald and J.R. Pearson, 'Graphitic Al-New Method of Production and Some Foundry Characteristics', AFS Trans., 79, (1971), 265.
  56. B.C. Pai and P.K. Rohatgi, J. Mater. Sci. and Engg., 21, (1975), 161.
  57. B.C. Pai, P.K. Rohatgi, K.V. Prabhakar and S. Ray, 'Fabrication of Aluminium - Alumina (Magnesia) Particulate Composites in Foundries Using Magnesium Addition to the Melts', J. Mater. Sci. and Engg., 24, (1976), 31.
  58. S. Ray, 'Fabrication of Particulate Composites by Foundry Techniques', Special Lecture in 292 Continuing Education Course on 'Recent Trends in Solidification of Castings', Unvi. of Roorkee, Roorkee, India, (1979), 1-26.
  59. B.C. Pai and P.K. Rohatgi, 'Production of Cast Aluminium Graphite Particulate Composites Using a Pellet Method', J. Mater. Sci., 13, (1978), 329.
  60. Zhang Zhu, 'A Literature Survey on Fabrication Methods of Cast Reinforced Metal Composites', Proc. World Materials Congress, Section - Cast Metal Matrix Composites, Chicago,

- U.S.A., (Sept. 24-30,1988), 93.
61. A.J. McCoy, R.H. Williams and I.G. Higginbotham, 'Metal/Non-Metal Interfaces - The Wetting of Magnesium Oxide by Aluminium and Other Metals', J. Mater. Sci., 11, (1976), 297.
  62. F.M. Hosking, F. Folgar Portillo, R. Wunderlin and R. Mehrabian, 'Composites of Aluminium Alloys: Fabrication and Wear Behaviour', J. Mater. Sci., 17, (1982), 477.
  63. C.G. Levi, G.J. Abbaschian and R. Mehrabian, 'Interface Interactions During Fabrication of Aluminium Alloy - Fibre Composites', Met. Trans.A, 9A, (1978), 697.
  64. P.K. Ghosh, P.R. Prasad and S. Ray, 'Effect of Porosity on the Strength of Particulate Composites', Z.Metallkunde, Bd.75 (H.12),(1984), 934.
  65. P.K. Ghosh and S. Ray, 'Effect of Porosity and Alumina Content on Mechanical Properties of Compo-Cast Aluminium Alloy - Alumina Particulate Composites', J. Mater. Sci., 21, (1986), 1667.
  66. P.K. Ghosh and S. Ray, 'Effect of Porosity and Alumina Content on the High Temperature Mechanical Properties of Compo-Cast Aluminium Alloy - Alumina Particulate Composites', J. Mater. Sc., 22, (1987), 4077.
  67. V.A. Presnov, 'Physico-Chemical Nature of Bonds Between Dissimilar Materials', Proc. Conf. The Role of Surface Phenomena in Metallurgy, Edited by V.N. Ermenko, Consultants Bureau, N.Y., (1963), 92.
  68. A.P. Levitt, 'Whisker Technology', 1st. ed., Willey Intr.

- Science, New York, (1970), 245.
69. W.A. Weyl, Proc. No.46, ASTM, (1946), 506.
  70. G. Katz, Thin Solid Films, Vol.33, (1976), 99.
  71. A.G. Metcalfe and M.J. Klein, 'Composite Materials', 1st ed., Vol.1, Academic Press, New York, (1974), 125.
  72. S. Nagata, 'Mixing Principles and Applications', John Wiley and Sons, New York, (1975), 250.
  73. J.H. Rushtom and J.Y. Oldshue, Chem. Engg. Progr. Symp. Series, 55(25), (1955), 181.
  74. P.K. Ghosh, S. Ray and P.K. Rohatgi, 'Incorporation of Alumina Particles in Aluminium - Magnesium Alloy by Stirring in Melt', Trans. Jpn. Inst. Metals, 25(6), (1984), 440.
  75. S. Keye, J. Vacuum Sci. Tech., No.11, (1974), 1114.
  76. D. Dixit and V. Agarwal, 'Fabrication of Aluminium Base Composite by Foundry Technique', Trans. Jpn. Inst. Metals, 22(8), (1981), 521.
  77. A. Berghezan, 'Review of Composite Materials', Proc. Conf. Second European Symposium on Material Sciences in Space, Frascati, Italy, (April, 1976), 351.
  78. T. Bewick, 'Squeeze Casting of Aluminium', Foundry Trade Journal (Correspondence Section), 148(3191), (1980), 1200.
  79. V.M. Plyatskii, 'Extrusion Casting', Primary Source, New York, (1965).
  80. G. Welter, Zeitschrift Fur Metallkunde, 9, (1931), 255.
  81. Y. Kaneko, H. Murakami, K. Kuroda and S. Nakazaki, Foundry Trade Journal, 148, (1980), 397.
  82. M.F. McGuire, 'Squeeze Cast Diesel Pistons', Diesel and Gas

- Turbine Progress, (Sept. 1979), 59.
83. R.F. Lynch, R.O. Olley and P.C.J. Gallagher, 'Squeeze Casting of Aluminium', AFS Trans., 83, (1975), 569.
  84. B.W. Howlett, D.C. Minty and C.F. Old, International Conference on Carbon Fibres, their Composites and Applications, London, Paper No.14, (Feb.2-7,1971),1.
  85. K.F. Sahn, Verbunderwerkst Tag., 1, (1974), 269.
  86. S. Suzuki, M. Shiroyangi, H. Matsubara, N. Izawa and N. Kobayashi, Reprint of 52nd Annual Meeting of Japan Society of Light Metals, Nagoya, Japan, (1977), 26.
  87. H. Fukunaga, 'Processing Aspects of Squeeze Casting for Short Fibre Reinforced Metal Matrix Composites', Adv. Materials and Manufacturing Processes, 3(4), (1988), 669.
  88. H. Fukunaga, 'Wear Properties of Discontinuous Ceramic Fibre Reinforced aluminium Alloy', Proc. 6th International Conference on Production Engineering, Osaka, (1987), 673.
  89. J.R. Franklin and A.A. Das, 'Squeeze Casting - a Review of the Status', British Foundryman, 77(3), (1984), 150.
  90. A. Astrop, Machinery and Production Engineering, 139, (Oct.1981), 30.
  91. G. Williams, K.M. Fisher, 'Squeeze Foundry of Aluminium - Alloy Components', Metals Technology, 8, (July 1981), 263.
  92. R.F. Lynch, R.P. Olley and P.C.J. Gallagher, 'Squeeze Casting of Brass and Bronze', AFS Trans., 83, (1975), 561.
  93. G.S. Reddy and G.R.K. Murthy, 'Liquid Forging of an Aluminium Alloy', Trans. Indian Institute of Metals, 31(6), (1976), 484.

94. J.A. Sekhar, G.J. Abbaschian and R. Mehrabian, *Materials Science and Engineering*, 40, (1979), 105.
95. Y. Nishida, H. Matsubara, *The British Foundryman*, 69, (1976), 274.
96. O.G. Epanchintsev, *Russian Casting Production*, (May 1972), 188.
97. R.E. Spear and G.R. Gardener, *AFS Trans.*, 71, (1963), 209.
98. T.N. Lipchin and M.A. Tomsinskaya, *Metalloved Term Obrab Met.*, 10, (Oct.1980), 37.
99. T.N. Lipchin, P.A. Bykov, *Russian Castings Production*, (1973), 109.
100. O.G. Epanchintsev, *Russian Castings Productions*, (1972), 34.
101. A.A. Das and S. Chatterjee, 'Squeeze Casting of an Aluminium Alloy Containing Small Amount of Silicon Carbide Whiskers', *The Metallurgist and Materials Technologist*, (March 1981), 137.
102. S. Chatterjee and A.A. Das, 'Effects of Pressure on the Solidification of Some Commercial Aluminium Base Casting Alloys', *The British Foundryman*, 65, (1972), 420.
103. R.F. Lynch, *United States Patent* 4, 049, 040 issued 20 Sept., 1977.
104. P.N. Bidulya, *Russian Castings Production*, (1964), 396.
105. S. Rajagopal, *J. Applied Metalworking*, 1, (1981), 3.
106. E.J. Stefanides, 'Forging Properties at Casting Costs', *Design News*, 29, (May 1974), 60.
107. W.F. Shaw, T. Watmough, 'Squeeze Casting: A Potential Foundry Process', *Foundry*, 97(10), (Oct.1969), 166.

108. G. Williams, 'Squeeze Form Combines Casting With Forging', Foundry Trade Journal, 156(3278), (1984), 66.
109. S. Ahmed, V. Gopinathan, P. Ramakrishnan, 'Squeeze Casting and Property Evaluation of Alumina Fibre Reinforced Aluminium - Silicon Alloy Matrix Composite', Proc. World Materials Congress, Section - Cast Metal Matrix Composites, Chicago, U.S.A., (Sept.24-30,1988), 149.
110. Toshiro Kobayashi, Masak Yosino, Hiroyoshi Iwanari, Mitsuo Ninomi and Kunji Yamamoto, 'Mechanical Properties of SiC Whisker Reinforced Aluminium Alloys Fabricated by Pressure Casting Method', *ibid*, 205.
111. M.A. Bayoumi and M. Suery, 'Partial Remelting and Forming of Al-Si/SiC Composites in their Mushy Zone', *ibid*, 167.
112. J. Charbonnier, S. Dermarkar, M. Santarini, J. Fages and M. Sabatie, 'High Performance Metal-Matrix Composites Manufactured by Squeeze Casting', *ibid*, 127.
113. Sen-ichi Yamada, Sen-ichi Towata and Hajime Ikuno, 'Mechanical Properties of Aluminium Alloys Reinforced with Continuous Fibres and Dispersoids', *ibid*, 109.
114. Ashish P. Diwanji and Ian W. Hall, 'Effect of Manufacturing Variables on the Structure and Properties of Squeeze Cast C/Al MMCs', *ibid*, 225.
115. Robert J. Sample, Ram B. Bhagat and M.F. Amateau, 'High Pressure Squeeze Casting of Unidirectional Graphite Fibre Reinforced Aluminium Matrix Composites', *ibid*, 179.
116. R.B. Bhagat, M.F. Amateau and J.C. Conway, 'Squeeze Cast Metal Matrix Composites : Evaluation of their Strength,

- Damping Capacity and Corrosion Resistance', *ibid*, 185.
117. U.K. Patent : GB2 129 342A, (1984).
118. E. Rabinowicz, 'Friction and Wear of Materials', John Wiley and Son Inc., New York, (1966), 56, 113-123.
119. A.D. Sarkar, 'Wear of Materials', Pergamon Press, (1978), 3.
120. K. Okabayashi, Y. Nakatani, H. Notani and M. Kawamoto, *J. Jpn. Inst. Light Met.*, 14, (1964), 415.
121. G. Vandelli, *Alluminio*, 37, (1968), 121.
122. A.D. Sarkar, 'Wear', 31, (1975), 331.
123. A.J. Clegg and A.A. Das, 'Wear of a Hypereutectic Aluminium Silicon Alloy', *Wear*, 43, (1977), 367.
124. K. Mohammed Jasim and E.S. Dwarakadasa, 'Wear of Aluminium-Silicon Alloys Under Dry Sliding Conditions', *Trans. Indian Institute of Metals*, 37(5), (Oct.1984), 581.
125. A.D. Sarkar and J. Clarke, 'Wear Characteristics, Friction and Surface Topography Observed in the Dry Sliding of As-Cast and Age Hardening Al-Si Alloys', *Wear*, 75, (1982), 71.
126. Mohammed Jasim Kadhim and E.S. Dwarakadasa, 'Some Studies of Wear of an Al-22 wt.%Si Alloy Under Dry Sliding Conditions', *Wear*, 82, (1982), 377.
127. N.P. Suh, 'An Overview of the Delamination Theory of Wear', *Wear*, 44, (1977), 1.
128. P.K. Rohatgi and B.C. Pai, 'Wear', 28, 1974. 353.
129. A.D. Sarkar and J. Clarke, 'Friction and Wear of Aluminium-Silicon Alloys', *Wear*, 61, (1980), 157.
130. B.N. Pramila Bai, E.S. Dwarakadasa and S.K. Biswas, 'Subsurface Damage in Dry Wear of Al-Si Alloys', *Wear*, 71, (1981), 381.



131. A.W. Ruff, 'Wear', 40, (1976), 59.
132. S. Mohan, V. Agarwala and S. Ray, 'The Effect of Lead Content on the Wear Characteristics of Stir Cast Aluminium - Lead Alloy', Wear, 140, (1990), 83.
133. Yu S. Avramov, V.P. Filonenko, A.P. Gruzlov and A.D. Shlyapin, 'Change of the Structure and Properties of Alloys of Aluminium with Lead in the Process of Plastic Strain', Materials Science and Heat Treatment, 26, (1985), 543.
134. L.F. Mondolfo, 'Aluminium Alloys 1 - Structure and Properties', Butterworths, London, (1976), 50-52, 296, 352.
135. C.S. Sivaramakrishnan, R.K. Mahanti and R. Kumar, 'Studies on Thermal and Wear Behaviour of Al-Si and Al-Si-Cu-Mg Alloys For Bearings', Trans. Indian Institute of Metals, 39(6), (Dec.1986), 643.
136. Sunil Mohan, V. Agarwala and S. Ray, 'Wear Characteristics of Stir Cast Aluminium - Lead Alloys', Z. Metallkunde, Bd. 80(H12), (1989), 904.
137. P.K. Rohatgi and B.C. Pai, J. Lubr. Technol. 101, (1979), 376.
138. B.C. Pai, P.K.Rohatgi and S. Venkatesh, Wear,30,(1974), 117.
139. H. Tokisue and G.J. Abbaschian, Materials Science and Engineering, 34, (1978), 75.
140. S. Biswas, A. Shantaram, N.A.P. Rao, K. Narayanaswamy, P.K. Rohatgi and S.K. Biswas, 'Bearing Performance of Graphite Aluminium Particulate Composite Materials', Tribol. Int., 13(4), (1980), 171.
141. M.K. Surappa, S. Sehan and P.K. Rohatgi, All India Seminar on

- Aluminium, Indian Institute of Metals, New Delhi, India, (Oct.1978).
142. B.P. Krishnan, N. Raman, K. Narayanaswamy and P.K. Rohatgi, Proc. Int. Conf. on Wear of Materials, Dearborn, MI, (April 1979).
143. S.K. Biswas and B.N. Pramila Bai, 'Dry Wear of Al-Graphite Particle Composites', Wear, 68, (1981), 347.
144. M. Suwa, K. Komuro and Ko Seno, J. Jpn. Inst. Met., 40(10), (1976), 1074.
145. E.P. Bowden and D. Tabor, 'Friction and Lubrication in Solids', Oxford Univ. Press : Clarendon Press, Oxford, (1964), 199.
146. V.F. Afanasev, M.A. Parkhomenko, N.I. Semenyuk, V.B. Vishnevskii, M.K. Kovpak and L.V. Zabolotnaya, 'New Materials Based on Silver Synthetic Micas', Fiz. Khim. Mekh. Mater., 5(6), (1970), 680.
147. USSR Patent 209 765 (Jan.26,1968) to V.F. Afanasev, V.B. Vishnevskii, M.K. Kovpak, M.A. Parkhomenko, S.G. Tresvyatskii and N.I. Chernavskaya.
148. French Patent, 2, 031, 657, (1970) to J. Rollet.
149. V.N. Povlikov, A.V. Thachenko, A.D. Kondratenko and S.K. Tresvyatskii, 'Nickel Synthetic Mica Base Ceramets', Sov. Powder Metall. Met. Ceram., 13(10), (Oct. 1974), 808.
150. A. Sato and R. Mehrabian, 'Aluminium Matrix Composites : Fabrication and Properties', Met. Trans. 7B, (Sept.1976), 443.
151. Deo Nath, S.K. Biswas and P.K. Rohatgi, 'Wear Characteristics

- and Bearing Performance of Aluminium - Mica Particulate Composite Material', *Wear*, 60, 1980, 61.
152. D.M. Schuster, M. Skibo and F. Yep, *Journal of Metals*, (Nov.1987), 60.
153. P.K. Rohatgi, B.C. Pai and S.C. Panda, 'Preparation of Cast Aluminium - Silica Particulate Composites', *J. Mater. Sci.*, 14, (1979), 2277.
154. A. Banerji, M.K. Surappa and P.K. Rohatgi, *Met. Trans.*, 14B, (1983), 273.
155. A. Banerji, S.V. Prasad, M.K.Surappa and P.K. Rohatgi, 'Abrasive Wear of Cast Aluminium Alloy - Zircon Particulate Composites', *Wear*, 82, (1982), 141.
156. K.J. Bhansali and R. Mehrabian, 'Abrasive Wear of Aluminium Matrix Composites', *J. Met.*, 34(9), (Sept. 1982), 30.
157. Jingyu Yang and D.D.L. Chung, 'Wear of Bauxite-Particle Reinforced Aluminium Alloys', *Wear*, 135, (1989), 53.
158. J.F. Schontens, *Journal of Metals*, (June 1985), 43.
159. J.C. Bittence, *Met. Prog.*, (July 1987), 45.
160. E.J. Peters, 'Ceramic Fibre Usage in Automotive Composites', Paper Presented at the 3rd IAVD Congress on Vehicle Design and Components, Geneva, Switzerland, (March 1986).
161. E.J. Peters and P. Boymal, 'Ceramic Fibre in Advanced Composites', Paper presented at Impact'85, International Conference on Fibre Developments, Ft. Landerdale, Florida, (March 10-12, 1985).
162. H.T. Angus, 'Cast Iron : Physical and Engineering Properties', BCIRA, Butterworths, IInd ed., (1975).

163. V.T. Cherepin and A.K. Mallik, 'Experimental Techniques in Physical Metallurgy', Asia Publishing House, Bombay, India, (1967), 137.
164. R.W. Heine and K.M. Htun, AFS Trans., 74, (1966), 65.
165. George E. Dieter, 'Mechanical Metallurgy', 2nd Ed., McGraw-Hill International Book Company, (1984), 350.
166. J. Singh, S.K. Goel, V.N.S. Mathur and M.L. Kapoor, 'Initial Experiences with Squeeze Casting of Al-Al<sub>2</sub>O<sub>3</sub>-MgO Particulate Composites Prepared by Modified MgO Coating Technique', Proc. Seminar on Science and Technology of Composites, Adhesives and Sealants, Bangalore (India), (Sept.28-30, 1989), 439.
167. A.K. Gupta, S.N. Tiwari and S.L. Malhotra, 'Techniques For Measuring Hydrogen Content in Aluminium and its Alloys', Jl. Scientific and Industrial Research, 38, (Aug. 1980), 421.
168. J. Singh, S.K. Goel, V.N.S. Mathur and M.L. Kapoor, 'Optical and SEM Observations of Porosity in Gravity and Squeeze Cast Al-Al<sub>2</sub>O<sub>3</sub>-MgO Particulate Composites', Indian Foundry Journal, 36(12), (Dec. 1990), 17.
169. J. Singh, S.K. Goel, V.N.S. Mathur and M.L. Kapoor, 'Role of Squeeze Casting Technique in Achieving Improved Property Performance Levels of Al-Al<sub>2</sub>O<sub>3</sub>-MgO Cast Particulate Composites', AFS Trans., 98, (1990), 115.
170. J. Singh, S.K. Goel, V.N.S. Mathur and M.L. Kapoor, 'Studies on the Behaviour of Squeeze Cast Al-Al<sub>2</sub>O<sub>3</sub>-MgO Particulate Composites Prepared by Modified MgO Coating Technique', Proc. ASM International Conference on 'Advances in Composite Materials', Bombay, India, (Jan.15-18,1990) (In Press).

171. J. Singh, S.K. Goel, V.N.S. Mathur and M.L. Kapoor, 'Mechanical Property Evaluation of Al-Al<sub>2</sub>O<sub>3</sub>-MgO Particulate MMCs upto 300°C (573K) Solidified under Pressure between 80 and 140 MPa', Int. Conf. on Aluminium (INCAL-91), Bangalore, India, (Feb.6-8, 1991) (Accepted).
172. J. Singh, S.K. Goel, V.N.S. Mathur and M.L. Kapoor, 'Development Characterisation of High Quality Al-Al<sub>2</sub>O<sub>3</sub>-MgO Squeeze Cast Particulate MMCs for Elevated Temperature Application upto 573K', The First Metallurgical Symposium of Iran (F-MS1), Shahid Chamran Univ., Ahuag, Iran, (March 9-15, 1991) (Accepted).
173. P.K. Rohatgi, F.M. Yarandi and Y. Liu, 'Influence of Solidification Conditions on Segregation of Aluminium-Silicon Carbide Particle Composites', Proc. World Materials Congress, Section-Cast Metal Matrix Composites, Chicago, U.S.A., (Sept.24-30, 1988), 249.
174. S. Ray, 'Porosity in Foundry Composites Prepared by Vortex Method', *ibid*, 77.
175. J. Singh, S.K. Goel, V.N.S. Mathur and M.L. Kapoor, 'Elevated Temperature Tensile Properties of Squeeze Cast Al-Al<sub>2</sub>O<sub>3</sub>-MgO Particulate MMCs upto 573K', *Jl. Mater. Sci.*, 26, (1991) (In Press).
176. R.S. Yaseen and E.S. Dwarakadasa, 'Wear of Aluminium under Dry Sliding Condition', *Wear*, 84, (1983), 375.
177. R.S. Yaseen, E.S. Dwarakadasa and A.R. Ismail, 'Subsurface Damage During Dry Sliding Wear of Al-Al<sub>3</sub>Ni Eutectic Alloy', *Wear*, 85, (1983), 213.

178. R. Shivanath, P.K. Sengupta and T.S. Eyre, 'Source Book on Wear Control Technology', American Society For Metals, Cleveland, Ohio, (1978).
179. R. Shivanath, P.K. Sengupta and T.S. Eyre, 'Wear of Aluminium - Silicon Alloys', British Foundryman, 70, (1977), 349.
180. J. Singh, S.K. Goel, V.N.S. Mathur and M.L. Kapoor, 'Adhesive Wear Behaviour of Squeeze Cast Al-Al<sub>2</sub>O<sub>3</sub>-Mg Particulate MMCs Under Dry Sliding Conditions', AFS Casting Congress - 1991, Birmingham, AL, U.S.A., (May 5-9,1991) (Accepted).
181. W. Hirst and J.K. Lankaster, Proc. Royal Soc., London, Ser.A, 259, (1960-61), 228.
182. K. Razavizadeh and T.S. Eyre, 'Oxidative Wear of Aluminium Alloys', Wear, 79, (1982), 325.
183. V. Raghvan, 'Materials Science and Engineering' Prentice Hall of India Ltd., New Delhi, (1989), 262-265.
184. B.N. Pramila Bai, E.S. Dwarakadasa and S.K. Biswas, 'Scanning Electron Microscopy Studies of Wear in LM13 and LM13 - Graphite Particulate Composites', Wear, 76, (1982), 211.
185. R.C. Bill and D.W. Wisander, Wear, 41, 1977, 351.

## APPENDIX

## XEROX COPIES OF PUBLISHED RESEARCH PAPERS

1. "Role of Squeeze Casting Technique in Achieving Improved Property Performance Levels of Al-Al<sub>2</sub>O<sub>3</sub>-MgO Cast Particulate Composites", 94th Casting Congress, AFS, April 21-24, 1990, Detroit, MI, USA. AFS Transactions, 98, (1990), 115-122.
2. "Initial Experiences with Squeeze Casting of Al-Al<sub>2</sub>O<sub>3</sub>-MgO Particulate Composites prepared by Modified MgO Coating Technique", Proc. Seminar on "Science and Technology of Composites, Adhesives and Sealants", Sept. 28-30, 1989, Bangalore (India), pp. 439-447.
3. "Optical and SEM Observations of Porosity in Gravity and Squeeze Cast Al-Al<sub>2</sub>O<sub>3</sub>-MgO Particulate Composites", Indian Foundry Journal Vol. XXXVI, No.12, Dec. 1990, 17-23. This paper was also presented in National Seminar on "Alloy Design and Development", March 10-11, 1989, Roorkee (India).
4. "Elevated Temperature Tensile Properties of Squeeze Cast Al-Al<sub>2</sub>O<sub>3</sub>-MgO Particulate MMCs upto 573 K", Journal of Material Science, 26, (1991).

# Role of Squeeze-Casting Technique in Achieving Improved Property Performance Levels of Al-Al<sub>2</sub>O<sub>3</sub>-MgO Cast Particulate MMCs

J. Singh  
S. K. Goel  
V. N. S. Mathur  
M. L. Kapoor  
University of Roorkee  
Roorkee, INDIA

## ABSTRACT

Standard MgO coating technique, developed earlier for the preparation of Al-Al<sub>2</sub>O<sub>3</sub>-MgO cast particle MMCs (metal matrix composites), needs to be modified for application under humid environmental conditions. Modified MgO coating technique results in usual 12 to 13% V<sub>f</sub> retention of Al<sub>2</sub>O<sub>3</sub> in the matrix.

Gravity chill cast composites suffer from considerable amount of gas porosity and interdendritic unfed regions. These defects result in premature failure of composites under tension. Also, such composites display poor ductility and semi-ductile to brittle fracture features. But when the stirred slurry is squeezed in the pressure range of 80 to 140 MPa, the properties uniformly improve. The best properties are displayed by a composite squeezed at 140 MPa and ambient die temperature. The UTS of this composite is higher by 53% compared to gravity chill cast composite, but, significantly, the ductility is higher by 133%. The exact properties of this composite are: UTS and 0.2% offset Y. S.—207.9 and 119.5 MN.m<sup>-2</sup>, respectively, % elongation—13.3%, reduction in C. S. area—12.8. But, increasing the die temperature deteriorates the properties of composites at all squeeze pressures. Squeezed composites display fully ductile fracture features. Properties of these MMCs squeezed in the range of 160 and 220 MPa are being investigated, which are likely to improve greatly.

## INTRODUCTION

Cast particulate MMCs are designed for specific end applications. In the past, a number of ceramic particles such as Al<sub>2</sub>O<sub>3</sub>, graphite, SiC, zircon, mica, illite-clay, shell-char, etc. have been incorporated in aluminum and zinc based alloys using the liquid metallurgy technique.<sup>1-6</sup> Among all these variety of MMCs, Al or Al alloy-Al<sub>2</sub>O<sub>3</sub> composites are known for their excellent high temperature strength and hardness up to around 350C.<sup>4,5</sup> Additionally, these composites also display superior adhesive wear characteristics compared to pure aluminum.<sup>4,5</sup> Al-Al<sub>2</sub>O<sub>3</sub>-MgO cast particulate composites developed and characterized recently, also fall in this broad category of MMCs.<sup>7-11</sup>

It has recently been appreciated that cast particulate MMCs prepared by the Vortex liquid metallurgy route suffer from a considerable amount of porosity. As a result, full potential of the composite in terms of the mechanical properties achievable is not realized in actual practice.<sup>12-15</sup> The role of porosity in influencing the tensile properties of such particulate composites has been investigated recently. The dependence of strength on porosity was shown to be linear in case of Al-4% Mg + Al<sub>2</sub>O<sub>3</sub> particulate composites.<sup>12-15</sup> In another investigation involving Al-Al<sub>2</sub>O<sub>3</sub>-MgO chill cast particulate composites, it was shown that the presence of voids lead to premature failure of the composite and also the fracture features are, at best, semiductile in nature.<sup>16,17</sup> The morphology of voids was studied in this case using optical examination of polished surfaces and the SEM examination of fractured surfaces of tensile specimens. The problem of voids, however, is significant only in those cases where the tensile properties of the composites are of prime interest. Notably, this is precisely the case with Al-Al<sub>2</sub>O<sub>3</sub> and Al-Al<sub>2</sub>O<sub>3</sub>-MgO cast particulate MMCs, as their properties up to 350C are of prime interest in addition to their superior adhesive wear resistance.

In a recent study, squeeze casting or liquid forging of stirred slurry was employed as a possible means of producing near porosity-free composites with possibly much improved property performance levels. It would be expected that squeezing the stirred slurry would result in a densified and grain refined composite with near zero porosity level. The squeeze casting technique has been employed in recent times to a number of other composite systems, metals and alloys with a similar objective in mind.<sup>8,18-20</sup> Also, this technique can be a viable means of producing near net shape actual castings.

Preliminary investigations on Al-Al<sub>2</sub>O<sub>3</sub>-MgO cast particulate composites had revealed that increasing squeeze pressure improves not only the UTS but also the ductility of the composite simultaneously.<sup>17</sup> Results of a subsequent detailed investigation are presented in this paper.

## EXPERIMENTAL

### Preparation of Stirred Slurry Using Modified MgO Coating Technique

The standard MgO coating technique described earlier<sup>7-11</sup> needs to be modified for application under humid environmental conditions. This statement is based on the results of a series of experiments. A systematic development of modified MgO coating technique to suit the special conditions mentioned above has been described fully in earlier publications.<sup>16,17</sup>

Briefly, it was found essential that the well-superheated aluminum melt (about 1100 gms at 860C) be properly degassed using 10 gm fully dried hexachloroethane tablets to decrease the H<sub>2</sub> potential of the bath. This was followed by Mg plunging in the melt. In initial experiments, the quantity of metallic Mg was varied between 0.4 and 0.7% of the melt.<sup>16</sup> But in subsequent squeeze casting experiments, this quantity was fixed at 0.5%. Soon after, a clear vortex is created in the melt using a marine blade impeller of standard dimensions and a fully heat-treated (Al<sub>2</sub>O<sub>3</sub> + MgO) powder mixture containing 15%MgO is added gradually along the walls of the vortex.

The quantity of this powder amounted to 10wt% of the melt except in one case where this quantity was halved (Sr. No. 16, Tables 1 and 2). The objective of heat treating (Al<sub>2</sub>O<sub>3</sub> + MgO) powder mixture at 900C for 2 hr is to fully dehydroxylate the surfaces of dispersoid particles.<sup>4</sup> Also, while adding, the powder mixture is maintained at ≈200C to prevent any moisture pick-up. The melt must



Table 1.  
Some Characteristics of Gravity Chill Cast and Squeezed Commercially Pure Aluminum and Al-Al<sub>2</sub>O<sub>3</sub>-MgO Particulate Composites

| Melt Sr. No. | Material  | Casting Condition | Pressure MPa | Die Temp. °C | Total (Al <sub>2</sub> O <sub>3</sub> + MgO) Powder | %V <sub>i</sub> Retention of Al <sub>2</sub> O <sub>3</sub> | Density in Kerosene Oil gms/cc | % Increment in Density | Mean Dendritic Arm Spacing mm |
|--------------|-----------|-------------------|--------------|--------------|---|---|--------------------------------|------------------------|-------------------------------|
| 1            | Pure Al   | Gravity Cast      | —            | —            | —   | —   | 2.6107                         | —                      | 48                            |
| 2            | Pure Al   | Squeeze Cast      | 110          | RT           | —   | —   | 2.7160                         | 4.030                  | —                             |
| 3            | Composite | Gravity Cast      | 0            | —            | 10  | 12.30   | 2.789                          | —                      | 46                            |
| 4            | -do-      | Squeeze Cast      | 80           | RT           | 10  | 12.40   | 2.8519                         | 1.926*                 | 30                            |
| 5            | -do-      | -do-              | —            | 100          | —   | 11.61   | 2.8521                         | 1.933                  | 34                            |
| 6            | -do-      | -do-              | —            | 200          | —   | 13.83   | 2.8520                         | 1.929                  | 36                            |
| 7            | -do-      | -do-              | 100          | RT           | 10  | 12.90   | 2.8672                         | 2.473                  | 24                            |
| 8            | -do-      | -do-              | —            | 100          | —   | 12.02   | 2.8674                         | 2.480                  | 29                            |
| 9            | -do-      | -do-              | —            | 200          | —   | 13.40   | 2.8670                         | 2.466                  | 32                            |
| 10           | -do-      | -do-              | 120          | RT           | 10  | 12.20   | 2.8843                         | 3.084                  | 19                            |
| 11           | -do-      | -do-              | —            | 100          | —   | 12.30   | 2.8841                         | 3.077                  | 22                            |
| 12           | -do-      | -do-              | —            | 200          | —   | 11.88   | 2.8840                         | 3.074                  | 24                            |
| 13           | -do-      | -do-              | 140          | RT           | 10  | 12.70   | 2.9010                         | 3.681                  | 12                            |
| 14           | -do-      | -do-              | —            | 100          | —   | 11.78   | 2.9008                         | 3.674                  | 16                            |
| 15           | -do-      | -do-              | —            | 200          | —   | 11.99   | 2.9012                         | 3.688                  | 18                            |
| 16           | Composite | Squeeze Cast      | 115          | 200          | 5   | 9.78  | 2.8512                         | 1.901                  | 27                            |

\* Density of chill cast composite taken as the basis for calculations of % increment in the density of squeezed composites.  
Squeezing time—40 secs (each case) Strng started from 860C Pounng temp. of slurry in the die—800C  
Time spent in transferring the melt in the die and placing the same under the hydraulic press for squeezing = 4 to 6 secs.  
RT—Room Temperature

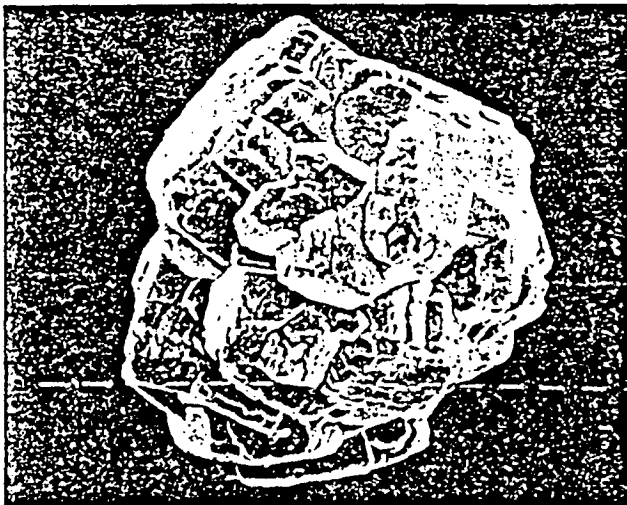
Table 2.  
Room Temperature Mechanical Properties of Gravity Chill Cast and Squeezed Commercially Pure Aluminum and Al-Al<sub>2</sub>O<sub>3</sub>-MgO Particulate Composites

| Melt Sr. No. | Mean Vicker's Hardness HV <sub>0.05</sub> $\bar{x}$ | Mean Micro-Hardness of Base Matrix HM <sub>0.05</sub> $\bar{x}$ | ROOM TEMPERATURE TENSILE PROPERTIES |                                    |              |                          |
|--------------|---|---|-------------------------------------|------------------------------------|--------------|--------------------------|
|              |   |   | U.T.S. MN.m <sup>-2</sup>           | 0.2% Offset Y.S.MN.m <sup>-2</sup> | Elongation % | Reduction in C.S. Area % |
| 1            | 31.60   | 33.8  | 84.0                                | 56.0                               | 19.32        | 19.00                    |
| 2            | 43.38   | 47.6  | 114.3                               | 59.8                               | 24.49        | 21.70                    |
| 3            | 41.83   | 59.6  | 136.3                               | 85.6                               | 5.70         | 5.50                     |
| 4            | 60.90   | 79.9  | 168.1                               | 87.2                               | 7.20         | 6.60                     |
| 5            | 58.50   | 79.1  | 165.0                               | 86.1                               | 8.00         | 7.50                     |
| 6            | 56.30   | 78.9  | 163.0                               | 84.5                               | 10.30        | 10.00                    |
| 7            | 63.64   | 81.6  | 180.3                               | 94.6                               | 8.60         | 8.00                     |
| 8            | 62.20   | 81.0  | 173.2                               | 91.7                               | 9.40         | 8.80                     |
| 9            | 61.00   | 80.8  | 172.1                               | 89.9                               | 11.40        | 19.90                    |
| 10           | 67.76   | 85.1  | 185.9                               | 100.3                              | 10.40        | 9.90                     |
| 11           | 66.10   | 84.8  | 183.3                               | 97.8                               | 11.20        | 10.60                    |
| 12           | 64.00   | 84.5  | 181.8                               | 95.6                               | 13.50        | 13.10                    |
| 13           | 73.18   | 87.2  | 207.9                               | 119.5                              | 13.30        | 12.80                    |
| 14           | 71.00   | 87.0  | 198.6                               | 108.5                              | 13.90        | 13.76                    |
| 15           | 68.30   | 86.9  | 193.3                               | 102.9                              | 16.50        | 16.10                    |
| 16           | 48.50   | 63.5  | 160.3                               | 83.3                               | 7.75         | 7.36                     |

be stirred for about 90 sec to fully incorporate the dispersoid particles into the melt. The total operation of degassing, Mg plunging, and incorporation of powder in the melt consumes nearly 2 minutes. The final stirred slurry is poured at 800C. The experimental procedure described above is termed as modified "MgO coating tech." Figure 1 shows MgO coated and uncoated  $Al_2O_3$  particles, while Figure 2 shows the experimental setup employed in the present work.

### Squeeze Casting of Stirred Slurry

A 60 t semi-automatic hydraulic press was employed to squeeze cast the stirred slurry in alloy cast iron die and plunger to result in the preparation of cylindrical castings of 70 mm dia and 60 mm length (Fig. 2b). A metered quantity of stirred slurry was poured in alloy cast iron die, and the squeezing was carried out in the pressure range of 80 to 140 MPa with regular increment of 20 MPa. The die temperature was varied as ambient, 100 and 200C. Interior die and plunger surfaces were thoroughly dried and dressed with colloidal graphite powder suspended in acetone prior to their use. The entire process of transferring the stirred slurry to the die and then fixing the die and plunger together under the press consumed nearly 4 to 6 seconds. The slurry was squeezed for 40 sec in each case.



(1a)



(1b)

Fig. 1. SEM pictures of (a) uncoated (X640), and (b) MgO-coated  $Al_2O_3$  particle (X1250).

### Mechanical Property Evaluation

Mechanical property performance of squeezed composites was determined in tension at ambient temperature using Monsanto Tensometer type W. Dimensions of a standard tensile specimen employed in the present work are shown in Figure 3. The microhardness of the base matrix of composites ( $HM_{30}$ ) was determined using Leitz Micro Hardness Tester in order to ascertain the influence of the degree of squeezing on the base-matrix. Vickers Hardness ( $HV_0.05$ ) of the composites was also determined to supplement the above observations. Density of composites was determined using Archimedes' principle.

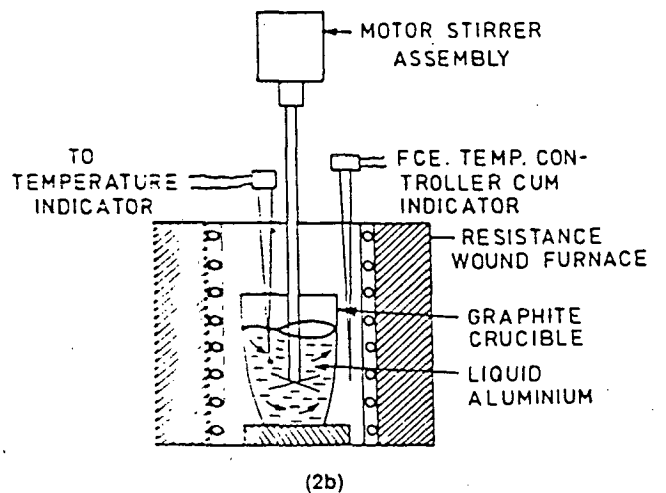
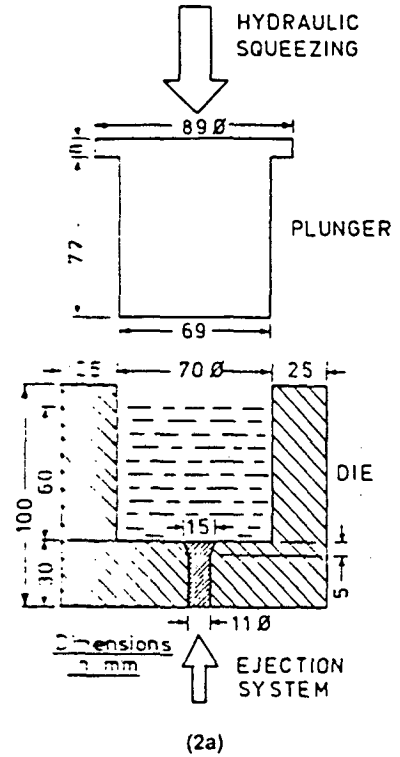


Fig. 2. Schematic diagram showing the experimental set up (a) for preparing the stirred slurry, and (b) for the squeeze casting operation.

### Optical and SEM Observations

Standard quantitative metallography techniques were employed to determine the average %  $V_f$  retention of  $Al_2O_3$  in the composites and their mean dendritic arm spacing in individual cases. These aspects could have direct relationship with the degree of squeeze pressure applied, and the temperature of the die.

Polished surfaces of squeezed composites were examined optically to ascertain the nature of distribution and possibly some segregation of  $Al_2O_3$  particles in the composites. Fractured surfaces of tensile specimens were examined by the SEM to study the nature of the fractures broadly.

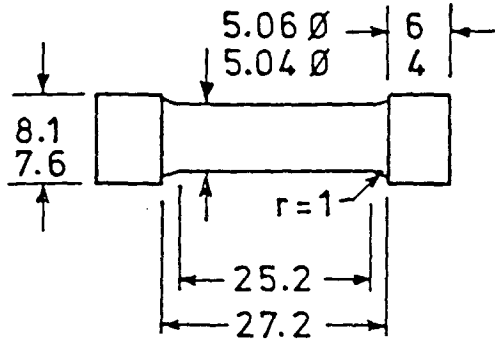
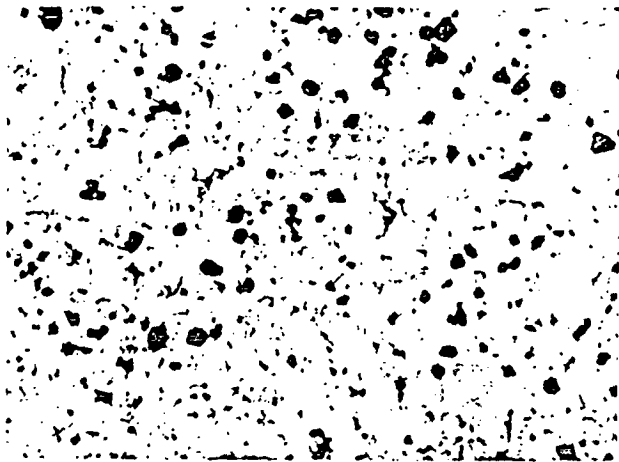


Fig. 3. Schematic diagram of the tensile specimen (dimensions in mm).



(4a)



(4b)

Fig. 4. (a) Optical picture showing uniform distribution of  $Al_2O_3$  particles in the composite (X40); (b) Optical picture showing  $Al_2O_3$  particle nicely bonded with the base matrix (X375).

### RESULTS AND DISCUSSION

#### Role of Modified MgO Coating Technique in Preparation of Stirred Slurry

The conclusion that the standard MgO coating technique needs to be modified for use under humid environmental conditions is based on a series of experiments. The modifications, such as degassing of the melt prior to Mg plunging by 0.5%Mg, must be decreasing the  $H_2$  potential of the bath, resulting in the creation of favorable energy conditions for the incorporation and retention of heat-treated ( $Al_2O_3$  + MgO) particles in the melt. This aspect is being studied in depth and the results will be reported later. The problem of wettability exists only with the  $Al_2O_3$  particles while the submicron MgO particles inherently display good wettability for liquid aluminum.<sup>21,22</sup>

#### PROPERTIES OF SQUEEZED COMPOSITES

The basic objective of squeezing the stirred slurry is to obtain a densified composite with minimum possible porosity levels. In a previous study of polished composite samples and the SEM examination of fractured tensile surfaces, it was shown that gravity chill cast composites suffer from a considerable amount of porosity.<sup>16</sup> These include gas porosity and also the unfed interdendritic solidification contraction regions. Gas porosity has been observed in such composites by others also.<sup>12-15</sup> The net result is that full potential of the composites in terms of the mechanical properties achievable is not realized in actual practice. It would thus be expected that squeezed composites would display much superior property performance levels.

Results of the present study are summarized in Tables 1 and 2 and are plotted in Figures 5-11. The SEM study of the fractured surfaces of tensile specimens is shown in Figures 12-15. Table 1 shows  $\%V_f$  retention of  $Al_2O_3$ , mean dendritic arm spacing and density of composites under different experimental conditions. Table 2 shows mechanical properties of the composites exclusively obtained at an ambient temperature. For the sake of comparison, results pertaining to gravity chill cast and squeezed pure aluminum at 110 MPa and gravity chill cast composite are also included in Tables 1 and 2. A typical case of composite squeezed at 115 MPa where only 5 wt% of total powder mixture ( $Al_2O_3$ +MgO) instead of usual 10% was stirred in the melt is presented at Sr. No. 16 of Tables 1 and 2.

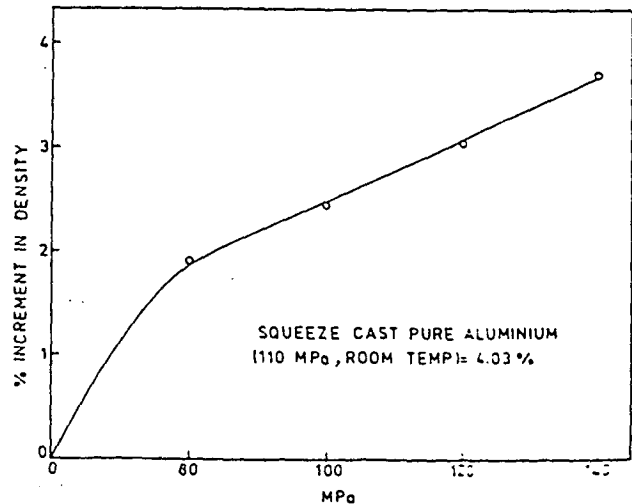


Fig. 5. Percent increment in density of composite shown as a function of the squeeze pressure applied.

Optical pictures of a squeezed composite (140 MPa, ambient die temperature) are shown in Figure 4 (a and b). These pictures display good and uniform retention of  $Al_2O_3$  in aluminum-base matrix. The  $Al_2O_3$  particles can be seen nicely bonded with the base-matrix (Fig. 4b). Coagulation of some  $Al_2O_3$  particles, which is a characteristic feature of particulate composites prepared by the Vortex liquid metallurgy route, can also be seen in the photomicrograph. The presence of some second phase constituents that can be seen in the picture is due to the impurities present in commercially pure aluminum.<sup>23</sup>

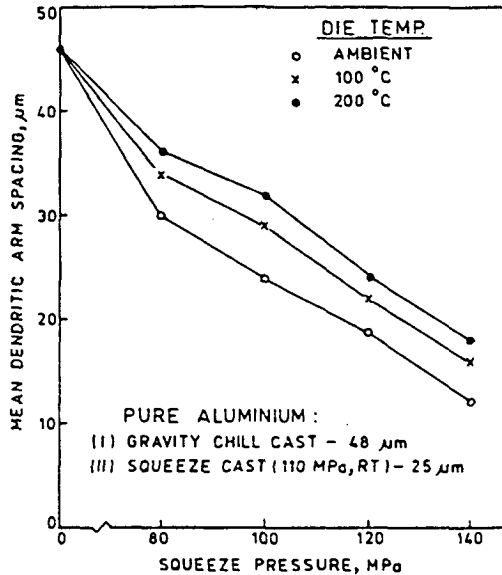


Fig. 6. Variation in mean dendritic arm spacing of composite obtained at three different die temperatures shown as a function of the squeeze pressure applied.

### Effect of Squeeze Pressure on %V<sub>r</sub>, Retention of $Al_2O_3$ , density, and Mean Dendritic Arm Spacing of Composites (Table 1)

It can be seen from the results that %V<sub>r</sub> retention of  $Al_2O_3$  in the composites is not materially influenced by either the die temperature or the degree of squeeze pressure applied. It is because this factor is influenced by only the MgO content of total powder mixture and the net amount of this powder mixture stirred in the melt. This is apparent from the results of heat No. 16, where only 5% of total powder

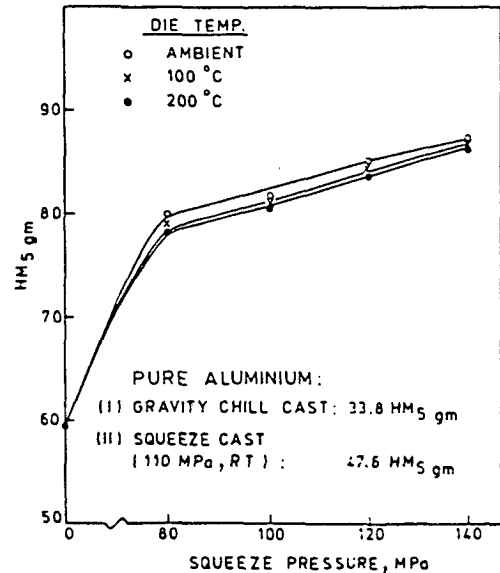


Fig. 8. Microhardness of the base matrix obtained at three different die temperatures shown as a function of the squeeze pressure applied.

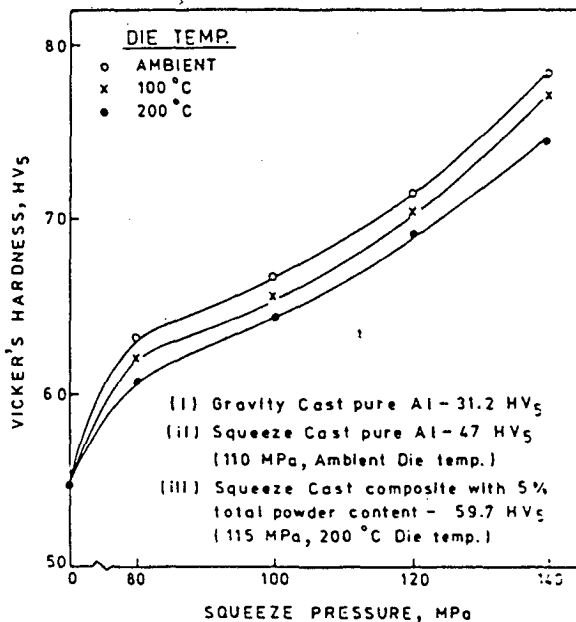


Fig. 7. Vickers hardness of composites obtained at three different die temperatures shown as a function of the squeeze pressure applied.

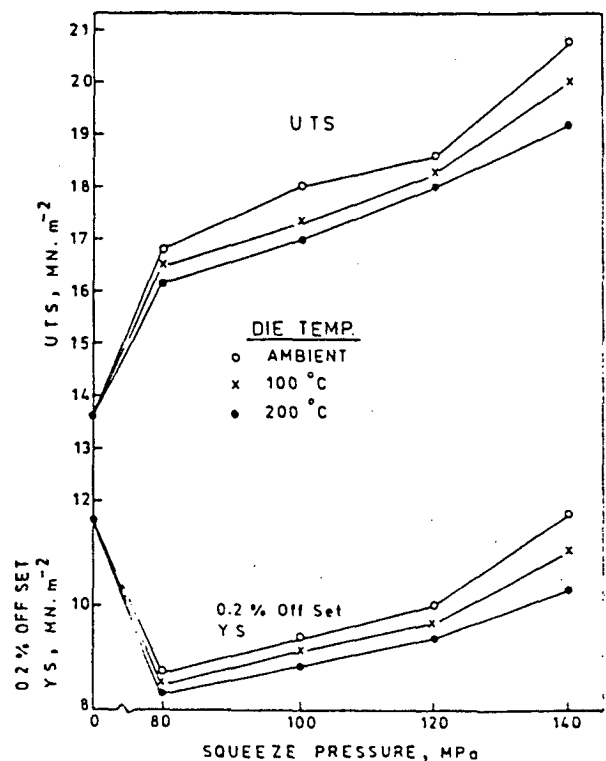


Fig. 9. UTS and 0.20% offset Y.S. data of composites at different die temperatures shown as a function of the squeeze-pressure applied.

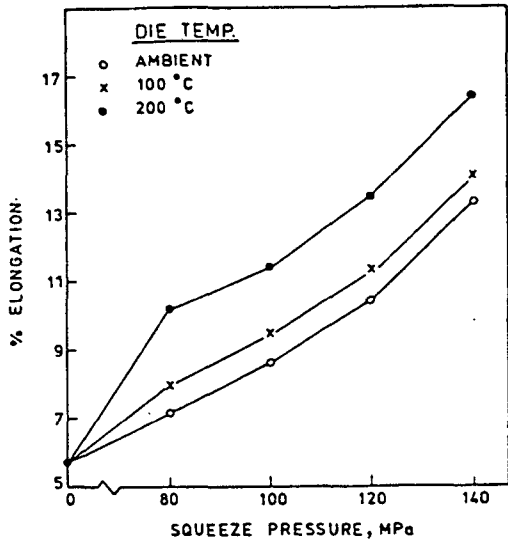


Fig. 10. Percent elongation of composites shown as a function of the squeeze pressure applied and the die temperature.

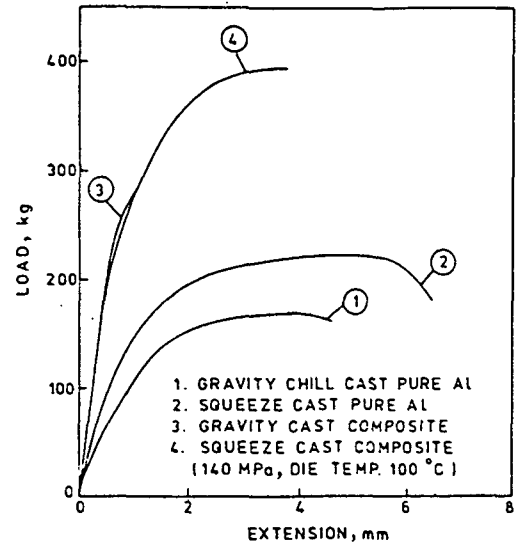


Fig. 11. A typical load-extension plot obtained in different cases of gravity chill cast and squeezed pure aluminum and composites.



Fig. 12. SEM picture of a tensile fracture surface of gravity chill cast composite showing the presence of large sized voids, pulled and enlarged under tension. (X320).



Fig. 13. SEM picture of a tensile fracture surface of gravity chill cast composite showing the presence of interdendritic solidification construction areas. Note the dendritic arms jetting out into the void space. (X640)

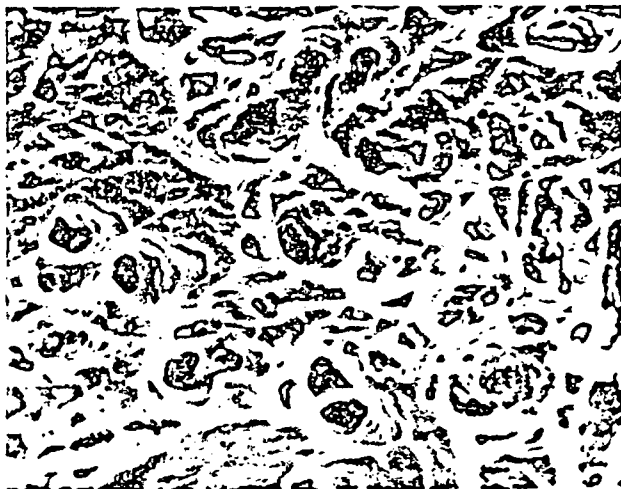


Fig. 14. SEM picture of the tensile fracture surface of the composite squeezed at 140 MPa and ambient die temperature, showing the presence of deep dimples, characteristic of a ductile fracture. (X320).



Fig. 15. SEM picture showing knife-edge separation of the base-matrix of squeezed composite (140 MPa, ambient die temperature) characteristic of a ductile fracture. (X1250)

mixture containing 15% MgO was stirred in the melt. Based on the results of an earlier investigation,<sup>9-11</sup> only 10% total powder mixture containing 15% MgO was added uniformly to all the melts employed for subsequent squeeze casting operations.

The process of squeeze casting would naturally result in densifying the composites. This is extremely important in the sense that it signifies a proportionate decrease in the level of porosity existing in the composites. It can be seen that the density of composites progressively increases as the squeeze pressure applied is increased in steps. There is a jump of 1.926% in the density of composite when the slurry is squeezed at 80 MPa. For these calculations, the density of gravity chill composite is taken as the reference point. This increment in density becomes significant only when the level of squeeze pressure is taken to the next higher step. The influence of die temperature on this factor appears to be negligible. The increment in density finally rises to 3.688% at 140 MPa squeeze pressure. It would naturally be expected that the composite can be densified even further by taking the squeeze pressure to still higher levels such as 160 to 220 MPa. Work in this region of squeeze pressure is under way and the results will be reported in near future. There must, however, be a limit to densifying the composites, and this level must be close to the theoretical density of this composite system. The relationship between % increment in density and the squeeze pressure can be seen to be linear in the region of 80 to 140 MPa (Fig. 5), but beyond this region up to 220 MPa, this tendency would be expected to taper off giving rise to an overall parabolic behavior pattern.

As a consequence of the densification of composites, the porosity existing in the composite would be expected to decrease proportionately. Squeezing the stirred slurry would result in distinctly the following effects:

- 1) A drastic decrease in the formation of gas porosity precipitate during solidification under high pressure.
- 2) Plugging of interdendritic unfed areas due to pressurized feeding.
- 3) Press forging of the composite at just below the solidus temperature for a limited period of time during the later stages of squeezing operation leading to some degree of grain refinement.

Another consequence of squeeze casting is the attainment of refined grain structure in the cast product. Results of this study are plotted in Figure 6. The effect of die temperature on this parameter is also entirely on the expected lines. It would, thus, appear that the composites squeezed at ambient die temperature would display the best mechanical properties.

### Effect of Squeeze Pressure on Mechanical Properties of the Composites

Results of this study are summarized in Table 2 and plotted in Figures 7-10. It can be seen from the results that the process of squeeze casting brings about an overall improvement in the mechanical properties of composites. As the squeeze pressure is increased in steps, the hardness, UTS, 0.2% offset Y.S. and elongation also improve in steps. This improvement in the properties of composites can be directly attributed to an improved level of densification of composites, a higher hardness and some degree of grain refinement obtained as a result of increasing squeeze pressure. Slight lowering of tensile properties at progressively increasing die temperature is entirely expected. It is because the factors such as hardness and dendritic arm spacing, which influence the tensile properties, progressively lower with increasing die temperature.

It can be seen that the Vickers Hardness ( $HV_0.05$ ) of the composite progressively improves as the squeeze pressure is systematically raised (Fig. 7). The effect of higher die temperatures, such as 100 and 200C, is to proportionately decrease the hardness attained, which is entirely expected. The microhardness data ( $HM_{0.05}$ ) plotted in Figure 8 also shows the same trend. It can be seen that these data are fully supported by the density data discussed earlier.

While referring to the data recorded in Table 2 and also shown in Figure 8, it can be seen that the microhardness of the base matrix of gravity chill cast composite improves by about 76% compared to the microhardness of gravity chill cast pure aluminum. This is attributed to the dispersion strengthening of the base matrix of composite by submicron MgO particles.<sup>9-11</sup> These particles may also show a tendency for segregation towards the grain boundaries or also in interdendritic regions.<sup>9-11,24</sup>

The level of densification of composite, obtained by a certain degree of squeeze pressure applied, is a single vital factor, which regulates the tensile properties of the composites. This is because the level of densification controls other factors such as the amount of porosity, hardness, and dendritic arm spacing, which indirectly influence the tensile behavior of the composites. It is because of this single vital factor that not only the UTS, but also the ductility of the composite indicated by elongation progressively improves as the squeeze pressure applied is systematically raised in steps (Figs. 9 and 10).

It can be seen from the data recorded in Table 2 that the UTS of the composite improves from 168  $MN.m^{-2}$  at 80 MPa and ambient die temperature to 207.9  $MN.m^{-2}$  at 140 MPa and ambient die temperature, signifying an improvement of  $\approx 24\%$ . Compared to the properties of the gravity chill cast composite, this improvement is  $\approx 53\%$ . But what is more significant is that % elongation of the squeezed composite at 140 MPa and ambient die temperature is higher by  $\approx 85\%$ , compared to the composite squeezed at 80 MPa and ambient die temperature. This figure is  $\approx 133\%$  compared to the gravity chill cast composite. This ductile behavior of the composite can be directly attributed to a near absence of porosity in squeezed composites and some grain refinement obtained at 140 MPa.

A typical load-extension plot is shown in Figure 11, where different cases of gravity chill cast and squeezed pure aluminum and composite are depicted. It can be seen that gravity chill cast composites undergo premature failure although the nature of the plot in this case up to the point of failure is similar to the one of squeezed composite. This behavior may be attributed to the presence of large amounts of porosity in gravity chill cast composites. The experience of other investigators is similar, though the composite system involved and the preparation technique are different.<sup>12-15</sup>

### Role of Squeeze Pressure in Influencing Tensile Fracture Features of Composites

Detailed examination of the fractured surfaces of tensile specimens by the SEM revealed that gravity chill cast composites exhibit semi-ductile fracture features. The fractured surface was seen punctuated with a large number of locations where void spaces pulled to a long distance under tensile stress could be seen. Such a typical SEM picture is shown in Figure 12. Another interesting feature of these fractured surfaces was the presence of unfed interdendritic regions. These locations are characterized by the presence of protruding dendritic arms in the unfed void space pulled apart under the tensile stress (Fig. 13). Such characteristic features were also observed during an earlier study of the fractured surfaces of gravity chill cast

Al-Al<sub>2</sub>O<sub>3</sub>-MgO particulate composites.<sup>16,17</sup> The presence of these features, however, lead to premature failure of gravity chill cast composites. This failure is because the defects, like gas porosity and interdendritic unfed regions, present great amounts of discontinuity in the cast structure.

On the contrary, the fracture features of the squeezed composite shown in Figures 14 and 15 are fully ductile in nature. These observations indirectly support the ductility data recorded in Table 2. The entire fracture surface of squeezed composites is characterized by the presence of deep dimples with extensive deformation markings along the walls of individual craters. Notably, individual dimples are very deep signifying that the matrix was pulled to a long distance before final fracture. This kind of fracture is produced by the coalescence of voids under the tensile stress. A considerable amount of energy is spent in this process of particle matrix interface decohesion, formation of micro voids and void-sheets, ultimately leading to the formation of voids, which are enlarged under the tensile-stress as the matrix is undergoing deformation. The intervening matrix between the voids so created separates out in the present case through a mode of chisel-point or knife-edge separation at the point of fracture (Fig. 15). This is indicative of an excellent ductility displayed by the squeezed composite. Because of the reasons mentioned above, the matrix takes considerable amount of stress before final fracture. This is the basic reason why squeezed composites display much superior UTS as well as % elongation compared to gravity chill cast composites. As the squeeze pressure is progressively increased, the void space progressively decreases, and therefore, the resulting composites display increasingly superior ductile behavior.

## CONCLUSIONS

1. Standard MgO coating techniques of preparing Al-Al<sub>2</sub>O<sub>3</sub>-MgO cast particulate composite need to be modified for application under humid environmental conditions.

2. Gravity chill cast composites prepared by the vortex liquid metallurgy route suffer from a considerable amount of gas porosity and interdendritic unfed regions. These defects result in premature failure of composites under tension. Thus, the full potential of the composite in terms of the mechanical properties achievable is not realized in actual practice.

3. Squeezing the stirred slurry in the pressure range of 80 to 140 MPa uniformly improves the properties of composite. Compared to the gravity chill cast composite, the density of composite squeezed at 140 MPa and ambient die temperature is increased by 3.681%, signifying a proportionate decrease in the porosity of the squeezed composite. The squeeze casting uniformly improves hardness (HV<sub>0.05</sub>), microhardness (HM<sub>0.05</sub>), and mean dendritic arm spacing of composites. At a given squeeze pressure, however, the above properties deteriorate with increasing die temperature.

4. The best tensile properties are exhibited by a composite squeezed at 140 MPa and ambient die temperature. Relevant properties of this composite are: UTS—207.9 MN.m<sup>-2</sup>, 0.2% off-set Y.S.—119.5 MN.m<sup>-2</sup>, % elongation—13.3, and % reduction in C.S. area—12.8. Compared to the properties of the gravity chill cast composite, the UTS of the above squeezed composite is higher by 53%. But what is more significant is that the ductility of the squeezed composite indicated by % elongation is higher by =133%. Increasing die temperature deteriorates the UTS for a fixed squeeze pressure, but slightly improves the % elongation. Squeezing the stirred slurry in the pressure range of 140 to 220 MPa is likely to improve the properties of composite further.

5. Fracture features of the composite undergo a major change upon squeezing. The composite squeezed at 140 MPa and ambient die temperature displays fully ductile fracture features, while the gravity chill cast composite displays, at best, semi-ductile fracture features.

## ACKNOWLEDGMENT

The authors would like to express their thanks to the University Grants Commission for extending financial support to Mr. Jag Pal Singh, SRF, during the course of this investigation.

## REFERENCES

1. P. K. Rohatgi, N. Ranganathan, and H. R. Shetty; *Composites*, 9, Nr 3, pp 153-156 (1978).
2. B. C. Pai and P. K. Rohatgi; *J. Mater. Sci.*, 13, pp 329-335 (1978).
3. S. Biswas, U. Srinivasa, S. Seshan, and P. K. Rohatgi; *AFS Transactions*, vol 71, pp 159-166 (1980).
4. M. K. Surappa and P. K. Rohatgi; *J. Mater. Sci.*, 16, pp 983-993 (1981).
5. F. M. Hosking, F. F. Portillo, R. Wunderlin, and R. Mehrabian; *J. Mater. Sci.*, 17, pp 477-498 (1982).
6. A. Banerjee and P. K. Rohatgi; *J. Mater. Sci.*, 17, pp 335-342 (1982).
7. B. F. Quigley, G. J. Abbaschian, R. Wunderlin, and R. Mehrabian; *Metall. Trans.* 13A, pp 93-100 (1982).
8. Z. Zhu; *Proc. World Materials Congress: Cast Metal Matrix Composites*, Chicago, USA, pp 93-99 (Sep 24-30 1988).
9. N. Izzet, E. S. Dwarkadasa, S. K. Goel, and A. Razzaq Ismail; *J. Mater. Sci. Lett.*, 2, pp 750-752 (1983).
10. N. I. Abdul-Lattef, A. R. I. Khedar, and S. K. Goel; *J. Mater. Sci. Lett.*, 4, pp 385-388 (1985).
11. N. I. Abdul-Lattef, A. R. I. Khedar, and S. K. Goel; *J. Mater. Sci.*, 22, pp 466-472 (1987).
12. P. K. Ghosh, P. R. Prasad, and S. Ray; *Z. Metallkunde*, 75, H-12, pp 934-937 (1984).
13. P. K. Ghosh and S. Ray; *J. Mater. Sci.*, 21, pp 1667-1674 (1986).
14. P. K. Ghosh and S. Ray; *J. Mater. Sci.*, 22, pp 4077-4086 (1987).
15. S. Ray; *Proc. World Materials Congress, Cast Metal Matrix Composites*, Chicago, USA, pp 77-80 (Sep 24-30, 1988).
16. J. Singh, S. K. Goel, V. N. S. Mathur, and M. L. Kapoor; *Proc. Conf. on "Alloy Design and Development"*, Univ. of Roorkee, India (Mar 10-11 1989).
17. J. Singh, S. K. Goel, V. N. S. Mathur, and M. L. Kapoor; *Proc. Conf. on "Science and Technology of Composites, Adhesives and Sealants"* Bangalore, India (Sep 28-30 1989).
18. B. Zantout, A. A. Das, and J. R. Franklin; *Proc. Conf. on "The Metallurgy of Light Alloys"*, Loughborough Univ., U.K., pp 215-221 (Mar 24-26 1983).
19. A. J. Clegg; *Proc. Conf. on "Aluminum Tech, 86"*, The Institute of Metals, London, U.K., pp 89.1-89.7 (Mar 11-13 1986).
20. S. K. Verma and J. L. Dorcic; *Proc. World Materials Congress Cast Metal Matrix Composites*, Chicago, USA, pp 115-126 (Sep 24-30 1988).
21. A. Banerji, P. K. Rohatgi, and W. Reif; *Metal Wissenschaft Technik*, 7, pp 656-661 (July 1984).
22. A. J. Meevov, R. H. Williams, and I. G. Higginbotham; *J. Mater. Sci.* 11, pp 297-302 (1976).
23. L. F. Mondolfo; *Aluminum Alloys Structure and Properties*, Butterworths, London-Boston, Chap 1, Sec 2, pp 50-52.
24. P. K. Rohatgi, F. M. Yarandi, and Y. Liu; *Proc. World Materials Congress: Cast Metal Matrix Composites*, Chicago, USA, pp 249-255 (Sep 24-30 1988).



जवाहरलाल नेहरू  
जन्मशती

JAWAHARLAL NEHRU  
CENTENARY

1889 *JN* 1989

JAWAHARLAL NEHRU CENTENARY CELEBRATIONS  
SCIENCE AND TECHNOLOGY SEMINAR SERIES

PROCEEDINGS OF SEMINAR  
ON  
SCIENCE AND TECHNOLOGY OF  
COMPOSITES, ADHESIVES AND SEALANTS

September 28-30, 1989  
Hotel Ashok, Bangalore, India



INDIAN SOCIETY  
FOR ADVANCEMENT  
OF MATERIALS &  
PROCESS  
ENGINEERING



HINDUSTAN  
AERONAUTICS LIMITED  
BANGALORE



THE INSTITUTION  
OF ENGINEERS  
(INDIA)  
(BANGALORE CHAPTER)



INITIAL EXPERIENCES WITH SQUEEZE CASTING OF Al-Al<sub>2</sub>O<sub>3</sub>-MgO PARTICULATE  
COMPOSITES PREPARED BY MODIFIED MgO COATING TECHNIQUE

Jagpal Singh\*, S.K.Goel\*\*, V.N.S.Mathur\*\* and M.L.Kapoor\*\*

\*SRF, Deptt. of Met. Engg., University of Roorkee, Roorkee

\*\*Professors, Deptt. of Met. Engg., University of Roorkee, Roorkee.

ABSTRACT

Modified 'MgO Coating technique' is essential to be used under humid environmental conditions for the preparation of Al-Al<sub>2</sub>O<sub>3</sub>-MgO cast particulate composites. Such gravity chill cast composites suffer from considerable amount of porosity and interdendritic solidification contraction areas. Squeeze casting or liquid forging the stirred slurry can be an effective means of producing dense and near porosity free composites. Squeezing the above composites has been attempted in the pressure range of 80 to 140 MPa in the present work. It has been observed that the density, hardness and the tensile properties of the composites uniformly improve as the squeeze pressure is systematically increased in steps of 20 MPa. The composite liquid forged at 140 MPa shows 207.9 MN.m<sup>-2</sup> UTS, 119.5 MN.m<sup>-2</sup> 0.2% offset Y.S., 13.3% elongation and 12.8% reduction in C.S. area. The UTS of this composite is higher by  $\approx$  53% and the ductility represented by per cent elongation is improved by  $\approx$  133% compared to gravity chill cast composite. It is expected that still better properties of the composite can be achieved if the squeeze pressure is taken to higher levels such as 180, 200 or 220 MPa.

INTRODUCTION

Metal - non metal cast particulate composites are designed for specific end applications. A number of ceramic particles such as Al<sub>2</sub>O<sub>3</sub>, graphite, silicon - carbide, sircon, mica, illite clay, shell - char etc. have been incorporated in aluminium copper and zinc based alloys using liquid metallurgy techniques for the purpose [1-6]. Among all these composites, Al-Al<sub>2</sub>O<sub>3</sub> and aluminium alloy-Al<sub>2</sub>O<sub>3</sub> composites are designed for comparatively superior high temperature performance upto around 350°C. Actually, these composites are known to possess excellent high temperature hardness and strength upto 350°C [3,4]. And their adhesive wear characteristics are also found to be superior than aluminium [3,6]. As such, these composites can be put to high temperature and wear resistant applications.

The basic problems associated with the 'Liquid - metallurgy' technique of fabricating these composites are: poor wettability of dispersoid particles, their non-uniform

dispersion in the base matrix, coagulation of dispersoid particles and the occurrence of considerable amount of porosity in the composite. All other problems except porosity have been tackled in a number of ways [1,9]. In fact, porosity is a serious problem with cast particulate composites, which does not allow their full potential to be realised in terms of their mechanical properties. In recent studies [10,12], an attempt has been made to quantify the effect of porosity on the mechanical properties of compocast aluminium alloy Al<sub>2</sub>O<sub>3</sub> particulate composites. One possible way of drastically reducing porosity levels to bare minimum is to liquid forge or 'Squeeze cast' the stirred slurry in the pressure range of 80 to 200 MPa. Also this technique can be an effective means of producing critical engineering components with much superior property levels.

'MgO coating' technique of fabricating Al-Al<sub>2</sub>O<sub>3</sub>-MgO cast particulate composites and their special microstructural and mechanical property features were reported earlier [13-

15]. This technique was found to result in the fabrication of a new class of composites with excellent elevated temperature tensile properties upto 250°C (523°K) [15].

Recent investigations [16], however, have revealed that the standard MgO coating technique need to be modified if a fair amount of retention of  $Al_2O_3$  particles is to be achieved under humid environmental conditions. Details of the 'modified MgO coating' technique have been reported recently [16].

In this recent present work, an effort has been made to liquid forge or squeeze cast the stirred slurry prepared by 'modified MgO coating' technique in the pressure range of 80 to 140 MPa. Results of a preliminary investigation on the physical and mechanical properties of composites and their related microstructures are reported in this paper.

#### EXPERIMENTAL

'Modified MgO coating' technique and 'Vortex liquid metallurgy' route was adopted for the preparation of the stirred slurry for subsequent squeeze-casting operations. Basic details of the 'modified MgO coating' techniques are outlined below.

About 1100 gms of commercially pure Aluminium melt (99.7 % purity) was well superheated to 860°C and then degassed by 10 gm fully dried hexachloroethane tablet. The commercially pure aluminium was found to contain 0.224% iron and 0.019% Si as the chief impurities. After the bath was thoroughly cleaned, Mg plunging was commenced. In the initial experiments, the amount of Mg employed for the purpose was varied from 0.4 to 0.7% in regular increments of 0.1%. After the data from these experiments was available, Mg plunging to the tune of 0.5% was fixed for all subsequent squeeze casting experiments. Importantly, liquid melt degassing followed by Mg plunging was carried out in quick succession one after the other just prior to the creation of vortex and the addition of  $Al_2O_3 + MgO$  powder along the walls of

vortex. The surfaces of  $Al_2O_3$  and MgO powder were thoroughly dehydroxylated at 900°C for 2 hours and then cooled in a dessicator prior to their mixing in a blender for over 45 minutes. The blended  $Al_2O_3 + MgO$  powder contained 15% MgO in each case. The amount of this powder added to the melt for the creation of stirred slurry amounted to 10 wt.% of the melt in each case. The stirred slurry could then be either chill cast or liquid forged. The stirring was required to be continued for nearly 90 secs to fully incorporate the powder in the melt. As mentioned above, the temperature of the melt at the start of the operation was maintained at 860°C and the final stirred slurry was poured at 800°C. The experimental set up used in the present investigation is shown in Fig. 1.

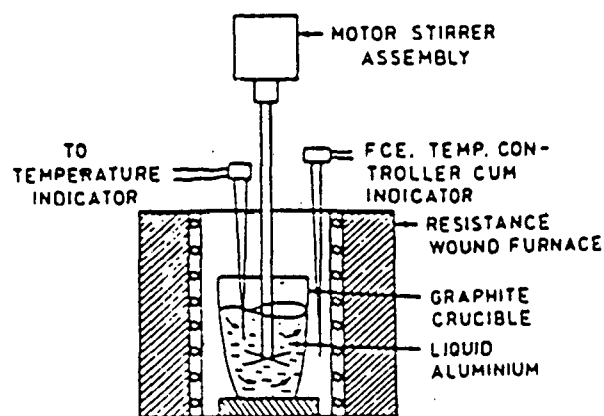


Fig. 1 : Schematic diagram showing experimental set up

Chill-cast cylindrical castings of 40 mm O.D. and 125 mm length were obtained from the above slurry. Also a metered quantity of this slurry was poured in alloy cast iron die and plunger and quickly squeezed by a 60 t semi-automatic hydraulic press in the pressure range of 80 to 140 MPa with regular increment of 20 MPa. In all these squeeze casting experiments, only cold die and plunger was employed. About 4 to 6 secs were spent in the process of transferring the slurry to the die and then fixing the die and plunger together under the press for squeezing. Then the slurry was squeezed at various pressures for 40 secs in each case. Cylindrical squeeze

cast products of 70 mm dia and 60 mm length were obtained this way.

The above chill and squeeze cast composites were examined for their microstructural features using standard metallographic techniques. Tensile properties of the composites were determined using Monsanto Tensometer type W. The fractured surfaces of tensile specimens were examined by the SEM with a view to ascertaining the nature and mechanism of fracture in these composites. The composites were further characterised by estimating other properties such as density, Hm of the base matrix,  $HV_5$  and %  $V_f$  retention of  $Al_2O_3$  using standard experimental techniques.

## RESULTS AND DISCUSSION

### Modified MgO Coating Technique

Properties of the composites prepared by above technique with varying percentages of Mg plunging are recorded in Table-1.

It can be seen from the results that %  $V_f$  retention of  $Al_2O_3$  increases only slightly as the amount of Mg plunging is increased in steps. There is virtually no material change in the micro hardness of the base matrix although the density of the composites improves marginally. Similarly, there is no material change in the tensile characteristics of the composites upto 0.6% Mg plunging, but beyond that, some noticeable improvement was recorded. It may be mentioned that in subsequent squeeze-casting experiments, the Mg plunging was maintained at the level of 0.5% only.

As reported earlier [16], the standard 'MgO coating' technique [14] had to be modified to suit humid environmental conditions as existing in this region. It is apparent from the results shown in Table-1, that the 'modified MgO coating' technique is adequate to result in usual %  $V_f$  retention of  $Al_2O_3$  in the composite, as observed in previous investigations [14,15]. Compared to the 'Mg plunging method' developed earlier [3,9], the amount of Mg needed by 'modified MgO coating' techni-

que is just only 12 to 16%.

It is believed that degassing of melt by hexachloroethane and its subsequent treatment by metallic Mg brings down the oxygen and hydrogen potential of the bath, which makes energy conditions favourable for the incorporation of  $Al_2O_3$  in the melt. It is because in earlier experiments, when these precautions were not observed, practically very few  $Al_2O_3$  particles were retained in the melt even though the mixture of  $Al_2O_3 + MgO$  particles was thoroughly dehydroxylated at 900°C for 2 hours. However, this aspect is being studied exclusively in detail and the results will be reported later.

### SQUEEZE CASTING OF THE COMPOSITES

Results pertaining to this study are recorded in Table-2. For the sake of comparison, results pertaining to chill cast and subsequent pure aluminium (110 MPa) and chill cast composite are also included in the table.

It is apparent from the results that the process of liquid forging brings about an overall improvement in the performance of the composites. In a previous study [16], it was shown through a detailed study of the optical pictures of polished specimens and the SEM pictures of the fractured surfaces of tensile specimen that chill cast composites suffer from considerable amount of porosity and unfed interdendritic solidification contraction areas. In a way, these features are an integral part of chill cast composites. The problem is further magnified due to the use of liquid metallurgy route as a basic technique for the preparation of the composites. So long as these defects exist in cast particulate composites, their full potential in terms of the mechanical properties achievable can never be realised. In this respect, squeeze casting can be an effective means of producing near porosity free composites. Two photomicrographs of the composite squeeze at 140 MPa are shown in Fig. 2. It can be seen from these pictures that although the composite is relatively free from porosity, but the structure is characterised by the presence of

Table 1 : Characteristics of composites prepared by 'Modified MgO-Coating' technique

| Sl. | % Mg Plung-<br>ing in liq.<br>Al | % V <sub>f</sub> reten-<br>tion of Al <sub>2</sub> O <sub>3</sub><br>in composite | Micro hard-<br>ness of Matrix<br>H <sub>M</sub> kgs/mm <sup>2</sup> | Density in<br>kerosene<br>oil,<br>gms/cc | Mechanical Properties     |   |                      |                                       |        |      |      |
|-----|----------------------------------|---|---|--|---------------------------|---|----------------------|---------------------------------------|--------|------|------|
|     |                                  |   |   |  | UTS<br>MN.m <sup>-2</sup> | 0.2% offset<br>Y.S.<br>MN.m <sup>-2</sup> | Elonga-<br>tion<br>% | Red <sup>n</sup> in<br>C.S. area<br>% |        |      |      |
| 1   | 2                                | 3   | 4   | 5  | 6                         | 7   | 8                    | 9                                     |        |      |      |
| 1   | 0.4                              | 11.61   | (U)   | 62.96                                    | (U)                       | 2.7882                                    | (U)                  | 137.7                                 | 114.45 | 5.7  | 4.0  |
|     |                                  | 11.12   | (B)   | 63.59                                    | (B)                       | 2.7791                                    | (B)                  |                                       |        |      |      |
| 2   | 0.5                              | 12.599  | (U)   | 62.89                                    | (U)                       | 2.809                                     | (U)                  | 137.8                                 | 115.6  | 5.7  | 5.5  |
|     |                                  | 11.98   | (B)   | 63.11                                    | (B)                       | 2.795                                     | (B)                  |                                       |        |      |      |
| 3   | 0.6                              | 13.4  | (U)   | 61.27                                    | (U)                       | 2.8194                                    | (U)                  | 137.25                                | 117.1  | 5.85 | 5.7  |
|     |                                  | 13.135  | (B)   | 63.1                                     | (B)                       | 2.8129                                    | (B)                  |                                       |        |      |      |
| 4   | 0.7                              | 14.259  | (U)   | 61.51                                    | (U)                       | 2.8400                                    | (U)                  | 144.1                                 | 118.4  | 6.32 | 6.25 |
|     |                                  | 13.825  | (B)   | 60.54                                    | (B)                       | 2.8301                                    | (B)                  |                                       |        |      |      |

Remarks : (a) Total powder mixture (Al<sub>2</sub>O<sub>3</sub> + MgO) containing 15% MgO added to the melt = 10 wt. %  
 (b) Sample taken from the top portion of cylindrical casting is denoted by (U) and that from the bottom portion by (B).

Table 2 : Properties of gravity chill cast and squeezed commercially pure aluminium and the composite.

| Sl. | Material       | Squeeze<br>pressure<br>MPa | % V <sub>f</sub> reten-<br>tion of<br>Al <sub>2</sub> O <sub>3</sub> | Density in<br>kerosene<br>oil<br>gms/cc | % Increment<br>in density | Vicker's Hardness<br>H <sub>V5</sub> |           |          | Microhardness of Base<br>matrix H <sub>M5</sub> gm |           |          |
|-----|----------------|----------------------------|--|---|---------------------------|--------------------------------------|-----------|----------|--|-----------|----------|
|     |                |                            |  |   |                           | Range                                | $\bar{x}$ | $\sigma$ | Range  | $\bar{x}$ | $\sigma$ |
| 1   | 2              | 3                          | 4  | 5                                       | 6                         | 7                                    | 8         | 9        | 10   | 11        | 12       |
| 1.  | Pure Aluminium | Nil                        | Nil  | 2.6107                                  |                           | 30.9-34.0                            | 31.6      | 1.11     | 31.5-35.8  | 33.8      | 1.49     |
| 2.  | Pure Aluminium | 110                        | Nil  | 2.716                                   | 4.033                     | 40.0-48.6                            | 43.38     | 2.62     | 45.6-50.1  | 47.6      | 1.63     |
| 3.  | Composite      | Nil                        | 12.3   | 2.798                                   | -                         | 40.0-44.6                            | 41.83     | 1.81     | 50.6-63.8  | 59.5      | 4.23     |
| 4.  | Composite      | 80                         | 12.4   | 2.8519                                  | 1.926                     | 54.4-64.6                            | 60.9      | 3.20     | 70.4-86.7  | 79.9      | 4.94     |
| 5.  | Composite      | 100                        | 12.9   | 2.8672                                  | 0.536                     | 58.2-69.2                            | 63.64     | 3.18     | 73.6-87.9  | 81.6      | 4.79     |
| 6.  | Composite      | 120                        | 12.2   | 2.8843                                  | 0.596                     | 59.8-72.0                            | 67.76     | 4.44     | 75.3-88.0  | 85.1      | 3.43     |
| 7.  | Composite      | 140                        | 12.7   | 2.9010                                  | 0.579                     | 67.4-78.6                            | 73.18     | 4.14     | 77.6-90.4  | 87.2      | 04       |

Table 2 : Contd...

| Sl. | Material       | Mechanical Properties    |                     |              |                                       | Casting condition  |
|-----|----------------|--------------------------|---------------------|--------------|---------------------------------------|--------------------|
|     |                | UTS<br>MN/m <sup>2</sup> | 0.2% Offset<br>Y.S. | % Elongation | Red <sup>n</sup> in<br>C.S. area<br>% |                    |
| 13  | 14             | 15                       | 16                  | 17           |                                       |                    |
| 1.  | Pure Aluminium | 85.5                     | 53.4                | 18.7         | 18.1                                  | Gravity chill cast |
| 2.  | Pure Aluminium | 114.3                    | 59.8                | 24.49        | 21.7                                  | Squeeze cast       |
| 3.  | Composite      | 136.3                    | 115.6               | 5.7          | 5.5                                   | Gravity chill cast |
| 4.  | Composite      | 168.1                    | 87.1                | 7.2          | 6.65                                  | Squeeze cast       |
| 5.  | Composite      | 180.3                    | 94.6                | 8.6          | 8.00                                  | Squeeze cast       |
| 6.  | Composite      | 185.9                    | 100.3               | 10.4         | 9.9                                   | Squeeze cast       |
| 7.  | Composite      | 207.9                    | 119.5               | 13.3         | 12.8                                  | Squeeze cast       |

Remarks : (a) Stirred slurry gravity/squeeze cast in alloy cast iron dies.  
 (b) Only cold die and plunger employed for squeeze casting the composite.